THE UNIVERSITY
of EDINBURGH

Dispersive Hydrodynamics in a Non-local Non-linear Medium

Saleh Ahmad Baqer

Doctor of Philosophy
University of Edinburgh
2020

To Jaber
for his unfailing support and motivation in my entire life

Abstract

Dispersive shock wave (DSW), sometimes referred to as an undular bore in fluid mechanics, is a non-linear dispersive wave phenomenon which arises in non-linear dispersive media for which viscosity effects are negligible or non-existent. It is generated when physical quantities, such as fluid pressure, density, temperature and electromagnetic wave intensity, undergo rapid variations as time evolves. Its structure is a non-stationary modulated wavetrain which links two distinct physical states. DSW's occurrence in nature is quite omnipresent in classical/quantum fluids and non-linear optics.

The main purpose of this thesis is to fully analyse all regimes for DSW propagation in the non-linear optical medium of a nematic liquid crystal in the defocusing regime. These DSWs are generated from step initial conditions for the intensity of the optical field and are resonant in that linear diffractive waves (termed dispersive waves in the context of fluid mechanics) are in resonance with the DSW, leading to a resonant wavetrain propagating ahead of it. It is found that there are six hydrodynamic regimes, which are distinct and require different solution methods. In previous studies, a reductive nematic Korteweg-de Vries equation and gas dynamic shock wave theory were used to understand all nematic dispersive hydrodynamics, which do not yield solutions in full agreement with numerical solutions. Indeed, the standard DSW structure disappears and a "Whitham shock" emerges for sufficiently large initial jumps. Asymptotic theory, approximate methods or Whitham's modulation theory are used to find solutions for these resonant DSWs in a given regime. It is found that for small initial intensity jumps, the resonant wavetrain is unstable, but that it stabilises above a critical jump height. It is additionally found that the DSW is unstable, except for small jump heights for which there is no resonance and large jump heights for which there is no standard DSW structure. The theoretical solutions are found to be in excellent agreement with numerical solutions of the nematic equations in all hydrodynamic regimes.

Acknowledgement

Professor Noel F. Smyth, my supervisor and mentor, I am not sure from where to start in acknowledging you for all what you have done for me during my PhD study period. I have been procrastinating writing the acknowledgment part of my thesis because I always find myself out of words when it comes to thanking you. I have reached the end of writing my thesis, so I shall do my best and be brief! I would like first to thank you for introducing me to the wonderful field of physical applied mathematics of non-linear dispersive wave theory. I am happy that you have set me working on a research project that lies in the interface of theoretical and computational applied mathematics. I still remember the first day when I arrived in Edinburgh with no sufficient computational and perturbation/asymptotics backgrounds as my previous degrees were too purely oriented. I am very thankful for your patience, especially in the first and second years of my PhD where you gave me time with no pressure to learn new topics that I have not studied before through taking excellent courses offered by the School of Mathematics in parallel with my research. I am also thankful for your extreme patience when I ask very elementary questions in the "physical" concepts of wave theory. Thank you for being always there whenever I have a lot of questions or need help in general. I am glad that I have collaborated with a real scientist and researcher whose level of knowledge is bottomless and whose applied mathematical understanding and intuition are extremely deep. I wish I have some of them. I could not ask for a kinder and better PhD supervisor than you. It has been a full privilege and honour to work with one of the notable students of the father of non-linear dispersive wave theory who wrote the academic bible "*Linear and Non-linear Waves,*" Gerald B. Whitham, FRS, (1927–2014). Last but not least, I am grateful for the time you spent reviewing my thesis.

My PhD study was comprehensively funded by Kuwait University (KU). I am sincerely grateful for their trust by supporting me with such a scholarship. I am looking forward to returning back there and serving them academically. Within the environment of KU, I was very lucky to be motivated and supported by doctors Haidar Khajah, Ismail Taqi, Abdullah Al-Shammari, Hamid Said, Salem Al-Yaqoob, Ali Bumajdad, Lyubomir Boyadjiev, Hani Farran, Michael Johnson and Ali Dashti. I am particularly indebted to Haidar Khajah who was, and still is, a driving force and a source of inspiration. I have warm memories in his office which was always open for various scientific discussions. It was totally a suitable platform for intellectual enrichment. I would like to thank Abeer Al-Sanad, from the office of the vice president for academic affairs at KU, and Halal Mohammed, from Kuwait cultural office in London, for their valuable assistance in administrative issues.

During my PhD study, I had the opportunity to meet excellent researchers and high caliber people in non-linear waves, in no particular order: doctors Patrick Sprenger, Daniel Ratliff, Gennady El, Mark Hoefer, Gaetano Assanto, Timothy Marchant, Panayotis Panayotaros, Bryan Tope, Rosa Maria Vargas and Cassandra Khan. I have enjoyed

chatting with all of them. I am thankful to Yik Keung Ying (Tony) for being such a friendly and nice office-mate. I would like to thank my examiners doctor Benjamin Goddard and professor Gennady El for their insightful comments and corrections that improved my thesis.

Al-Ferri and Ahmado, my friends. Thanks for being part of my life. I fondly remember our gatherings, especially the video game sessions where I was introduced to the world of survival horror. What a big mistake to follow you in playing this category of video games! Ahmado, you are a super-duper amazing and adorable friend that any sound person could ask for in his life. Thank you for motivating me to continue my academic study. I always feel so sheepish when I remember your unmatched hospitality that you have given me at your home. Many thanks for everything. Al-Ferri, it is so hard to find a friend like you in this life. I am appreciative of your unwavering questions about me. Your tenacious stimulation, since the first time I have known you, means a lot to me. Thank you so much. Big shout out to my boys Ali Shaiban, Mohammad Banyan and doctors Ali Al-Lawati, Mohammad Al-Balushi, Hussain Al-Qattan for the encouragement and the good times.

I am genuinely grateful to my family for their extreme patience, faith and understanding of the stress and pressure of postgraduate studies. In particular, I am immensely indebted to my brother Jaber Baqer for his endless support and encouragement in my whole life. Thanks for your constant care, love, and kindness. Thank you for being all ears and there when I am down. I love you and always will. This thesis is dedicated to you.

Contents

List of Abbreviations

ODE : Ordinary Differential Equation

PDE : Partial Differential Equation

NLC : Nematic Liquid Crystal

KdV : Korteweg-de Vries

CS : Calogero-Sutherland

FPUT : Fermi-Pasta-Ulam-Tsingou

NLS : Non-linear Schrödinger

BEC : Bose-Einstein Condensate

KdV5 : 5^{th} Order Korteweg-de Vries with Zero 3^{rd} Order Dispersion

IST : Inverse Scattering Transform

FFT : Fast Fourier Transform

IFFT : Inverse Fast Fourier Transform

RK4 : Runge-Kutte Method of Fourth Order Accuracy

VSW : Viscous Shock Wave

WKBJ: Wentzel-Kramers-Brillouin-Jeffreys

DSW : Dispersive Shock Wave

PDSW : Perturbed Dispersive Shock Wave

RDSW : Radiating Dispersive Shock Wave

CDSW : Crossover Dispersive Shock Wave

TDSW : Travelling Dispersive Shock Wave

VDSW : Vacuum Dispersive Shock Wave

List of Figures

List of Tables

Chapter 1

Physical and Mathematical Backgrounds

1.1 Nematic Liquid Crystals and Non-linear Optics

The discovery of liquid crystals dates back to the 19^{th} century. It is ascribed to the moment when Frederick Reinitzer, an Austrian chemist, heated a solid sample of cholesteryl benzoate in his lab to investigate the sample's chemical and physical properties. During his experiment, Reinitzer found that the sample manifested two different melting points, unlike any other organic compounds [2]. At temperatures around 145 °C, he observed that the sample changed into a peculiar hazy liquid and then became a normal transparent liquid at higher temperatures. That foggy liquid was understood to be a new state of matter by the German physicist Otto Lehmann. Lehmann named this intermediate phase which lies between the solid and liquid (isotropic) states a liquid crystal [3]. Scientific experiments then found that molecules of liquid crystals are long, thin, ellipsoid-shape and of moderate-size with a rigid centre allowing them to maintain their forms [4]. They are also easily polarisable molecules, so they form strong dipoles after being exposed to an electric field [4, 5]. The main reason for this is the fact that liquid crystals consist of complex organic molecules which are based on aromatic elements (benzene rings) as their functional groups. A benzene group has a number of electrons that are free to move relatively [4]. Therefore, when a liquid crystal is exposed to a polarised electromagnetic wave, these electrons delocalise and a dipole moment in each of the molecules is generated. The application of liquid crystals in today's modern technology is quite ubiquitous. For example, they are used in TVs, computer monitors, electronic watches, medical thermometers, optical imaging equipment et cetera.

The molecules of liquid crystals exist in different natural arrangements: positional or orientational order [4]. The positional order refers to regular distances between the molecules, whilst orientational order indicates a common averaged direction. The types of molecular organisation play a key role when it comes to classifying the phases of liquid crystals, as we shall see shortly. There is a another kind of molecular arrangement, the so-called bond-orientational arrangement, which represents a line attaching the centres of closest-neighbour molecules without a uniform spacing condition, but this is outside the scope of the present work so we will not deal with it further. Liquid crystals possess a high level of orientational alignment because of strong intermolecular forces, but a low positional order. As a result of this, they exhibit anisotropic features. Their molecules tend to self-align themselves and point in one particular direction represented by a unit vector known as the molecular director $\hat{n}$, as shown in Figure 1.1(a). The orientational

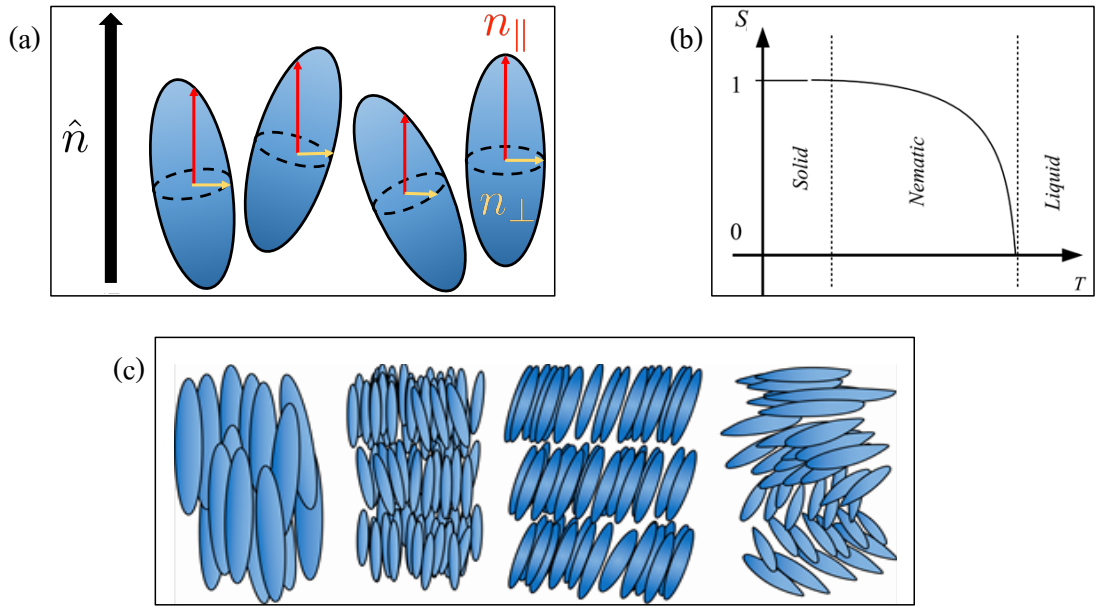

Figure 1.1: Thermotropic liquid crystals and properties. (a) Collection of liquid crystal's molecules oriented averagely towards the director unit vector $\hat{n}$. The parallel and orthogonal refractive indices are illustrated by $n_{||}$ (red arrow) and $n_{\perp}$ (yellow arrow). (b) Phase transitions from solid to nematic liquid crystal and then to liquid are shown in terms of the order parameter S as a function of the temperature T. Courtesy of Gaetano Assanto et al [6]. (c) From left to right: nematic, smectic A, smectic B and chiral liquid crystals structures. This image was retrieved from the URL https://www.medicinescomplete.com/mc/rem/2012/cf-fig-26-50.png. (Online version in colour.)

order is described in terms of the molecular director and another parameter termed the order parameter S. This parameter S shows how much molecular ordering exists on scale 0 to 1 and it is given by the mathematical expression

$$S = \frac{1}{2}\left\{3\left\langle \cos^2\gamma \right\rangle - 1\right\}, \tag{1.1}$$

where γ is the angle between the director and the long molecular axis; the bracket <> denotes the average taken over the total solid angle γ [6]. The order parameter usually depends on temperature T as most of the liquid crystals are thermometric media, a phase that will be discussed below. In Figure 1.1(b), the order parameter of a solid is given by $S(0) = 1$ and as the temperature T rises, it vanishes to zero, at which the state is a liquid.

In general, liquid crystals are categorised into three categories: thermotropic, lyotropic and metallotropic. Thermotropic is a phase of matter for which orientational and positional orders depend on the temperature only. In contrast, lyotropic is a state of matter for which the order depends on both the temperature and the concentration of the liquid crystal in a solvent such as water. The last category of the liquid crystals, metallotropic, consists of organic and inorganic molecules, and the order in this case is governed by the ratio between these different molecules together with the temperature and the concentration. Most liquid crystals are thermotropic materials and have uniaxial molecular arrangements. This thesis is related to this kind of liquid crystals. Based

on the geometry of the molecular arrangements, the thermotropic phase is divided into three sub-categories, as presented in Figure 1.1(c):

- **Nematic phase**. A nematic liquid crystal is characterised by its elongated and rod-like molecules, therefore its name as nematic which comes from the ancient Greek word for thread. Nematic molecules have no positional order because their ends are not aligned with one another. However, due to the intermolecular forces, they tend to retain an alignment parallel to the molecular director $\hat{n}$.

- **Smectic phase**. This phase takes place at lower temperatures than the nematic phase. Its molecules are in fact nematic, but with the molecules packed into layers. In smectic A, the long molecular axes are orthogonal, or slightly orthogonal, to the layer planes, while in smectic B, the axes are inclined with respect to the planes.

- **Chiral phase.** Chiral molecules are nematic and grouped in layers similar to the smectic phase. Nonetheless, the axis of each molecule is oriented parallel to its neighbours within the same layer. Moreover, the director's angle in each layer rotates from one level to the next, forming a helical pattern.

In this thesis, we are only interested in the nematic phase of thermotropic liquid crystals. In particular, we are concerned with how the nematic molecules respond to an applied, linearly-polarised, coherent light wave. Therefore, we shall now discuss the optical properties of nematic liquid crystals and describe the interactions between nematic materials and linearly-polarised electromagnetic waves.

In optics, the term polarisation has two meanings. Sometimes it refers to dipole moment (dipoles are molecules that contain a pair of positive and negative equal-magnitude charges with a slight separation distance) per unit volume, and is given by the product between the electric charge q and the separation distance d from the negative charge to the positive one:

$$P = Nqd, \tag{1.2}$$

where N is the number of the dipoles [9, 10]. On the other hand, the same term is used to describe the polarisation of light, which is the direction of the electric field in an electromagnetic wave. Electromagnetic waves can be linearly, circularly or elliptically polarised [9, 10]. Here, we are only concerned with the linear polarisation case. Liquid crystals either consist of permanent dipoles or unpolarised molecules [4]. Those which are unpolarised become polarised under the application of an electric field. The dipoles are either along or across the long molecular axes. When they are parallel, or nearly parallel, to the long molecular axes, the molecules tend to align with the electric field direction and are perturbed from their equilibrium positions at a particular angle due to the generated dipolar torque which is balanced with the elastic intermolecular forces of liquid crystals [4, 6]. Otherwise, they tend to orient normally to the electric field direction. This property is often referred to as reorientation. Such a molecular rotation does not occur unless the power of the induced electric field is high enough. The reason for this is that nematic liquid crystals are highly elastic media. A minimum electric field is required to initiate this rotation and overcome the elastic intermolecular forces. This minimum electric field is termed Fréedericksz threshold [4, 6]. Below this threshold, the director remains unrotated. The deformation of the director undergoes three possible distinct geometries: splay, twist and bend, see e.g. [5, 6] for further details.

The nematic molecules respond to the electric field collectively, which causes either a uniform or non-uniform modification in the structure of the molecular director depending upon the intensity of the electric field. If the electric field strength is extremely high, some undesired physical effects and irreversible optical damages take place, such as local heating which can destroy the nematic phase. Beside the reorientational property, nematic liquid crystals are typically saturable materials. This means that when the initial long molecular axes are parallel to the applied electric field direction, the molecular director is not displaced. Nematic liquid crystals are also non-local media; in the sense that the response of the nematic to the optical forcing extends beyond the waist of the optical beam [5, 6, 7, 8].

Now let us consider some important linear and non-linear optical effects, such as linear/non-linear diffraction (dispersion), non-linear self-focusing and self-trapping. Basically, the difference between linear and non-linear optics is that the first is a field of physics that studies the interaction between matter and light waves of weak intensities, while the latter is concerned with the interplay between matter and light waves of strong intensities. In linear regimes, a polarised light beam spreads over a targeted optical medium and its size gets gradually wider than the original size of the beam as it propagates. This classical linear effect is called linear optical diffraction (spatial spreading waves) or dispersion (temporal spreading waves). However, in non-linear regimes, the situation is much more complicated. The light beam may diffract, self-focus (it focuses upon itself without the aid of any additional tools such as a lens) or self-trap (confines itself and travels steadily without the aid of any extra optical tools) depending on the natural properties of the optical medium plus the strength of the intensity of the light beam, see e.g. Figure 1.5 in Section 1.3. The radical transition from linear to non-linear optics is ascribed to John Kerr, a British physicist. Kerr launched a linearly polarised light beam through an optical material and kept raising the beam's intensity until he discovered two new optical features.

First, the refractive index of a solid or liquid does not only depend on the induced optical wavelength, it could also depend on the optical wave's intensity. A traditional example for this is the refractive index of fused silica for which the refractive index is given by [9]

$$n(\lambda, I) = n_0(\lambda) + n_2 I, \tag{1.3}$$

with n_0 the low intensity (linear) index, n_2 the non-linear index (Kerr coefficient) and I the beam's intensity. Another example that is relevant to the work of this thesis is nematic liquid crystals. It has been found that their non-linear refractive index depends on the molecular rotational angle γ generated by a linearly-polarised light beam [5, 6, 11], namely,

$$n_e(\gamma) = \frac{n_{\parallel} n_o}{\sqrt{n_{\parallel}^2 \cos^2(\gamma) + n_o^2 \sin^2(\gamma)}}, \tag{1.4}$$

where $n_o = n_{\perp}$ is the linear refractive index for a so-called ordinary beam, which will be defined shortly. Here, $n_{\parallel}$ is the refractive index that is parallel to the nematic director $\hat{n}$. It is measured by a linear-polarised electric field that is parallel to the nematic director. On the other side, $n_{\perp}$ is the refractive index that is perpendicular to the nematic director $\hat{n}$. It is measured by a linear-polarised electric field that is perpendicular to the nematic director. Figure 1.1(a) demonstrates these two different refractive indices. In nematic liquid crystals, $n_{||} > n_{\perp}$ always [6]. As we can see, there are two distinct kinds of refractive indices: ordinary refractive index n_o and

extraordinary refractive index denoted by n_e. This is because nematic liquid crystals are birefringent materials, in particular uniaixal materials [6]. Therefore, the light beam splits into two eigenmodes [1, 4, 6]. One is non-dispersive (an ordinary beam associated with the refractive index n_o) and the another one is dispersive (an extraordinary beam associated with the refractive index n_e).

Second, as opposed to linear media in which the response of the polarisation to the electric field E is linear [9, 10], i.e.,

$$P_L = \varepsilon_0 \chi^{(1)} E, \tag{1.5}$$

where ε_0 is the vacuum permittivity and $\chi^{(1)}$ is the linear electric susceptibility of the material, the polarisation responds non-linearly to the electric field in non-linear materials. As the electric field of the optical beam increases, the polarisation increases sequentially. However, this action does not continue indefinitely. As the optical field grows to be very large, the magnitude of the field itself starts to become on the magnitude of the electric fields between the atoms in the materials. When this process takes place, the materials themselves become "slightly" altered and the optical behaviour is no longer linear. Instead, it starts to become weakly non-linear. Mathematically, this can be given as a Taylor expansion in the electric field E [9, 10],

$$P = \varepsilon_0 \left\{ \chi^{(1)} E + \chi^{(2)} E^2 + \chi^{(3)} E^3 ... \right\} = P_L + P_{NL}, \tag{1.6}$$

where the $\chi^{(i)}$s are the $i-$th order electric susceptibilities.

The last thing we need to discuss in this section is the optical self-trapping property of nematic liquid crystals. This is probably the most important optical feature of nematic materials. For any non-linear optical media, there are two types of self-trapped waves that can occur: bright and dark self-trapped waves. In general, when an intense laser beam penetrates a nematic cell, the self-focusing and dispersion effects balance each other to result in a bright self-confined beam propagating through the cell without any change in its form. The laser beam's intensity in this case is of peak shape [6]. This kind of wave is called a bright optical solitary wave. However, in a doped nematic cell, which will be discussed in Section 1.3, the beam may confine as a dark self-confined region travelling in the crystal and the beam's intensity becomes of dip shape [6, 58]. This self-confined beam with an intensity dip is termed a dark solitary wave. Prior to presenting a laboratory experimental set-up that shows how these classes of nematic waves can be produced, we give a brief introduction of solitary waves and their historic developments.

1.2 Solitary Waves and Solitons

The first observation of solitary waves, in the context of water waves, was made by John Scott Russell, who was a British civil engineer and naval architect living in the 19^{th} century. In the year of 1834 he was riding on a horse and pursuing a horse-drawn boat in the narrow Union Canal which connects Edinburgh and Glasgow. Russell's pursuit of that boat was not without motivation. At that time he was carrying out experiments to design the optimal shape of a canal boat. When the boat accidentally stopped moving, presumably because of an obstacle it encountered, he recognised the development of a peculiar and unique wave that was propagating behind the boat. That wave featured properties that were not expected by the community of scientists

at that time. Those properties are:

- Contrary to classical (linear) waves which were believed to be of an oscillatory type only, Russell's wave was a travelling single hump, i.e., a localised wave, propagating on the surface of the canal.
- The wave was observed to maintain its form without any deformation over large distances and long times, which is a manifestation of its robustness against natural perturbations caused by the uneven canal floor.

Since then, Russell termed this unprecedented wave phenomenon a "wave of translation" and started to recreate it experimentally in his 30 ft wave tank that he had built in the backyard of his home. After several experimental trials that lasted over a period of 10 years, he succeeded in simulating that translating wave in his tank and immediately reported his discovery in the 14^{th} meeting of the British Association for the Advancement of Science. Russell explained his finding in his famous report [12] in the following way:

"... I was observing the motion of a boat which was rapidly drawn along a narrow channel by a pair of horses, when the boat suddenly stopped not so the mass of water in the channel which it had put in motion; it accumulated round the prow of the vessel in a state of violent agitation, then suddenly leaving it behind, rolled forward with great velocity, assuming the form of a large solitary elevation, a rounded, smooth and well-defined heap of water, which continued its course along the channel apparently without change of form or diminution of speed. I followed it on horseback, and overtook it still rolling on at a rate of some eight or nine miles an hour, preserving its original figure some thirty feet long and a foot to a foot and a half in height. Its height gradually diminished, and after a chase of one or two miles I lost it in the windings of the channel. Such, in the month of August 1834, was my first chance interview with that singular and beautiful phenomenon which I have called the Wave of Translation ..."

After the discovery and the experiments of Russell on solitary waves, George Airy believed that the theoretical solution for a solitary wave can be deduced from linear wave theory [13]. He thought that the dynamics of shallow water waves, such as canal waves, are fully governed by the linear hyperbolic partial differential equation (PDE), known as the wave equation [1, 99],

$$\frac{\partial^2 u}{\partial t^2} - c^2 \frac{\partial^2 u}{\partial x^2} = 0, \tag{1.7}$$

where $c = \sqrt{gh}$. The variable u is related to the water wave elevation from the fluid equilibrium surface. The parameter c is the linear shallow water wave velocity and is given in terms of the gravitational acceleration g and the water depth h. Indeed, the linear wave equation (1.7) admits a solitary wave solution, the so-called d'Alembert solution [1, 99], of the form

$$u(x,t) = f(x + \sqrt{gh}t) + g(x - \sqrt{gh}t) \tag{1.8}$$

for any real-valued, smooth functions f and g such that f and g approach one constant asymptotic state as $x \to \pm\infty$, for instance, $\text{sech}^2(x \pm \sqrt{gh}t)$. Although Airy was correct in the interpretation that the sech^2 solution exhibits the form of a solitary wave, it is because the general form of a solution of the linear wave equation (1.7) is generic enough

to encompass any such solution. Moreover, modelling shallow water waves by using the linear wave equation (1.7) disagrees with non-linear shallow water wave theory [1] in that the wave velocity c does not depend on the wave amplitude. George Stokes, on the other hand, did not agree with Russell's solitary wave as he believed that gravity water waves are dispersive waves and the only permanent form of waves that could possibly exist is sinusoidal waves (Fourier modes).

Russell's observation at that time did not stand on a strong theoretical basis and it lacked a mathematical background. Consequently, his finding was not taken seriously among the applied mathematics and physics communities. However, after more than 20 years, John Boussinesq [14] and Lord Rayleigh [15], independently, felt that what prohibited the theoretical prediction of the solitary wave, that is Russell's wave, was the neglect of non-linearity to which could balance dispersion. In other words, and in general, the root reason behind the formation of solitary waves is a balance between a linear effect, causing the waves to disperse, and a non-linear effect, causing the waves to steepen and then break. Indeed, with the supposition of an incompressible and inviscid fluid and weakly non-linear profile long waves (shallow water), Boussinesq formulated a mathematical model that describes what Russell observed. His equation admits a localised wave solution, with a sech^2, that vanishes in the limit $|x| \to \infty$. The resulting Boussinesq equation is a bi-directional, non-linear, dispersive wave equation, given in normalised form [14, 16]

$$\frac{\partial^2 u}{\partial t^2} - \frac{\partial^2 u}{\partial x^2} - \underbrace{3\frac{\partial^2 u^2}{\partial x^2}}_{\text{Non-linearity}} - \underbrace{\frac{\partial^4 u}{\partial x^4}}_{\text{Dispersion}} = 0. \tag{1.9}$$

The linear dispersion relation exhibits right-running and left-running waves, on that it is a bi-directional equation. Rayleigh's approach to justify Russell's wave of translation was different and much more direct than Boussinesq's method. Of course, the conclusion was the same, the reader can refer to e.g. [15] for further details. Rayleigh was not aware of Boussinesq's work at that time, but he became familiar with it eventually. He finished his article [15] with the following remark:

"I have lately seen a memoir by M. Boussinesq, Comptes Rendus, Vol. LXXII, in which is contained a theory of the solitary wave very similar to that of this paper. So as far as our results are common, the credit of priority belongs of course to M. Boussinesq."

There was now a mathematical verification that waves can exist with a non-oscillatory shape, consistent with Russell's observation and experiments. Yet, it was still believed that oscillatory waves only exist in linear regimes. Korteweg and de Vries, however, in 1895 realised that Boussinesq and Rayleigh deduced their theoretical solutions under the single assumption that the shallow water wave decays at $\pm\infty$. Before extending this assumption, and for the sake of simplicity, they first considered wave solutions propagating to the right direction only. This led to the following uni-directional, non-linear, dispersive wave equation [17]

$$\frac{\partial u}{\partial t} + \underbrace{6u\frac{\partial u}{\partial x}}_{\text{Non-linearity}} + \underbrace{\frac{\partial^3 u}{\partial x^3}}_{\text{Dispersion}} = 0, \tag{1.10}$$

which is known as Korteweg-de Vries (KdV) equation and can be deduced from the

Boussinesq equation (1.9) [1]. Then, instead of seeking a wave like solitary wave they sought a general travelling periodic wavetrain, say, $u = u(x - Vt)$ where V is the phase velocity, and solved the resulting non-linear ordinary differential equation (ODE). The general solution was found as a periodic wavetrain in terms of the Jacobian elliptic function cn and it is analogous to the cosinusoidal solution of the linear equation (1.7), hence it is named a cnoidal wave. Some contemporary books [19] and research papers [18, 20], though, tend to prefer to represent this periodic wavetrain in terms of the Jacobian elliptic function dn instead of cn. Similarly, it is called dnoidal waves and can be expressed as [18, 19, 20]

$$u(x,t) = \bar{u} + \frac{2a}{m}\,\mathrm{dn}^2\left(\sqrt{\frac{a}{m}}\,\{x - V_p t\}\,; m\right) - \frac{2a}{m}\frac{E(m)}{K(m)}. \tag{1.11}$$

Here, a, m, $\bar{u}$, $K(m)$ and $E(m)$ being the amplitude, the modulus squared parameter of elliptic integrals, the wave mean and the complete elliptic integrals of first and second kinds, respectively. The phase velocity satisfies

$$V_p = 6\bar{u} + 4a\left\{\frac{2}{m} - 1\right\} - \frac{12a}{m}\frac{E(m)}{K(m)}. \tag{1.12}$$

In the infinite-wavelength asymptotic limit, associated with $m \to 1$, this solution reduces to the solitary wave solution which is known from the work of Boussinesq and Rayleigh, namely,

$$u(x,t) = \bar{u} + a_s\,\mathrm{sech}^2\left(\sqrt{\frac{a_s}{2}}\,\{x - V_s t\}\right), \tag{1.13}$$

where $a_s = 2a$ is the soliton's amplitude and $V_s = 6\bar{u} + 2a_s$ is its velocity. In the linear limit, with $0 < a \ll 1$ and $m \to 0$, the dnoidal wavetrain (1.11) simplifies to classical cosine waves. After using some Jacobian elliptic functions identities [21] we get

$$u(x,t) = \bar{u} + a\cos\left(2\sqrt{\frac{a}{m}}\,\{x - V_p t\}\right) + \mathcal{O}(a). \tag{1.14}$$

Some connections between steady dnoidal, solitary and harmonic waves, depending on the values of a, $\bar{u}$, m and t, are given in Figure 1.2(b). This major contribution from Korteweg and de Vries showed that periodic wavetrains are possible in non-linear regimes. In this regard their work is considered to be far more general than the previous mathematical contributions. Figure 1.3 shows some examples of solitary and cnoidal waves occurring in fluids.

After that, the research on non-linear dispersive waves was not extremely active and went through a long period of dormancy until around the mid of the 20^{th} century. In 1965, Zabusky and Kruskal [22] solved the KdV equation (1.10) with periodic boundary conditions and a harmonic initial condition numerically, in particular $u(x,0) = 10\cos\pi x$ on the spatial domain $[0,2]$, and they discovered something remarkable. First, they noticed that the initial cosinusoidal wave began to steepen until it arrived at a breaking point, that is, a point at which a slope is nearly vertical. Second, prior to the occurrence of breaking, small waves were generated behind the shock-like structure. These waves started growing gradually. As this growth was occurring, the collection of waves spread over the whole spatial domain and formed a group of solitary waves, each of them propagating with a distinct velocity. Afterwards, as the time advanced, these solitary waves started to interact with each other due to the imposed periodic boundary conditions. The most important and astonishing thing that was discovered in this

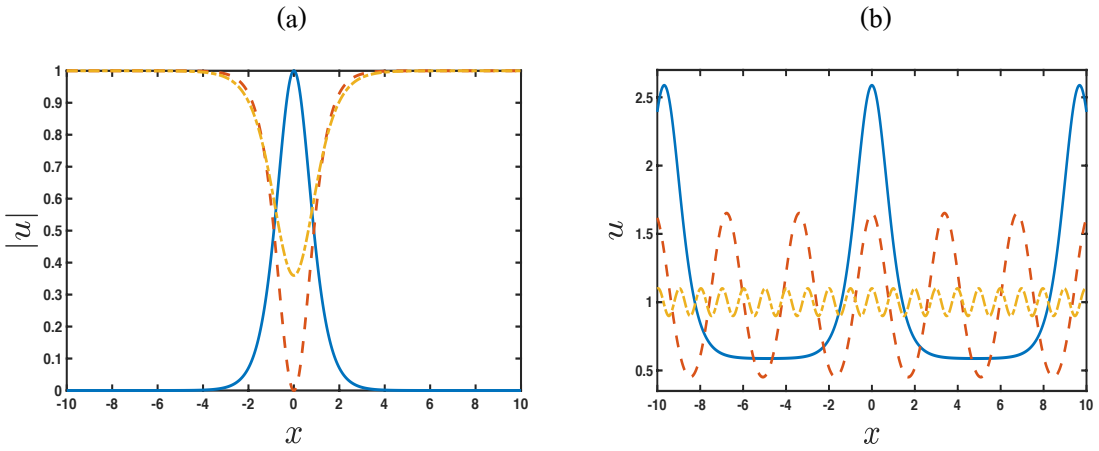

Figure 1.2: Steady dnoidal waves and solitons at $t = 0$. (a) Bright soliton: (blue) solid line; black soliton with $A = 0$ and $B = 1$: (orange) dashed line; gray soliton with $A = 0.6$ and $B = 0.8$: (yellow) dash-dot line. The parameter a_s was chosen 1.0 in the expressions (1.19) and (1.20). (b) dnoidal waves approaching the solitary wave limit with $m = 0.999$, $\bar{u} = 1$ and $a = 1.0$: (blue) solid line; dnoidal waves with $m = 0.5$, $\bar{u} = 1$ and $a = 0.6$: (orange) dashed line; dnoidal waves approaching the linear waves limit with $m = 0.01$, $\bar{u} = 1$ and $a = 0.1$: (yellow) dash-dot line. (Online version in colour.)

numerical study was the clean interactions between the KdV solitary waves. By a clean interaction we mean that the interacting solitary waves survived the collision with no change in shape and speed. The only effect that the collision left behind was a phase shift, namely, a shift in the position of the contributing solitary waves [22]. This collision resembles a typical elastic collision between solid particles. Because of this particle-like behaviour possessed by solitary waves, Zabusky and Kruskal coined these waves "solitons." The motivation that drove Zabusky and Kruskal to undertake this numerical research project is connected with the FPUT problem [24], an abbreviation that stands for Fermi-Pasta-Ulam-Tsingou. In 1955, right after the emergence of one of the first fast computers at Los Alamos, called Maniac I, Fermi had an idea to test an unproven hypothesis in statistical mechanics which says that, in simple words, after a long time the energy of a system is spread equally among all modes. This hypothesis is often referred to as energy equipartition [23]. He and his collaborators tested this hypothesis by studying numerically a mass-spring system in which the restoring force is a non-linear function of the displacement from an equilibrium position (non-linear mass-spring problem), which is a model of atoms in a crystal. At the beginning, they expected to see a gradual and continuous transfer of energy from the first mode to the higher ones. Instead, after leaving the numerical code to run for a long time, they noticed that the energy only increased from the first mode to few more modes, about five modes, and then it recurred to its original value, which was in the first mode and kept going in this pattern until the end of the numerical simulation. Their system exhibited a periodic behaviour rather than an ergodic one. Fermi and his co-workers did not have a theoretical explanation for this surprising result, but the work of Zabusky and Kruskal provided an excellent illustration. In the continuum and long-wave limits, Fermi's equations that govern the dynamics of the non-linear mass-spring system can be reduced to a KdV equation like (1.10), as shown in [22, 25, 26]. From this, we understand that the initial condition in the FPUT problem gives rise to a certain

number of solitons. Hence, the energy excitation is in the first few modes, with clean interactions between them, thus the observed energy recurrence.

Two years after the discovery of solitons, Gardener, Greene, Kruskal and Miura developed a new method that solves the KdV initial value problem exactly [28]. This method is known as the inverse scattering transform (IST) and was the first general method that solves non-linear PDEs. It is the non-linear analog of a standard Fourier transform used to solve linear PDEs. The point spectrum of the KdV scattering problem was found to correspond to solitons [1, 27, 28, 26]. Subsequently, it was realised in general that clean interactions between solitons is a direct consequence of having an inverse scattering solution. In other words, if an equation, or system of equations, is exactly solvable, possesses an inverse scattering solution and has an infinite number of conservation laws, then it is guaranteed that its solitary waves interact elastically with each other. An equation that has this property is said to be an "integrable equation." Solitary waves are called solitons in this case. With this background, the different terms soliton and solitary wave emerge. Every soliton is a solitary wave, but not the converse. An example of a system of equations that has solitary wave solutions, but their collision is not clean, is the nematic system of equations (2.19) and (2.20), which is the main mathematical model in this thesis, see e.g. [30, 31, 32, 33]. That is why we will use the term solitary wave rather than soliton when it comes to studying these equations; they form a non-integrable system.

As the research area of non-linear dispersive waves has developed, many non-linear dispersive PDEs other than KdV equation were found to be integrable and admit soliton and cnoidal wave solutions. For instance, the modified KdV equation [29], the non-linear Schrödinger (NLS) equation [36], the sine-Gordon equation [37], the Kadomtsev-Petviashvili equation [26, 27], the Benjamin-Ono equation [38], the Gardner equation [39] et al. A wide list of similar equations can be found in e.g. [40]. The non-linear wave equation that we shall focus on is the NLS equation because the mathematical model in this thesis reduces to the NLS equation in one limit, as see in Section 2.1. The NLS equation has a huge array of applications as it naturally arises in non-linear optics [41, 42, 43, 44], fluid mechanics (deep water waves) [45, 46, 47] and plasma physics [48, 49]. Sometimes it is referred to as the Gross-Pitaevski equation, after Gross and Pitaevski who deduced it in the context of Bose-Einstein condensates (BECs) [50, 51, 52]. There are two versions of the NLS equation: focusing and defocusing equations.

In dimensionless form, the focusing NLS equation is

$$i\frac{\partial u}{\partial t} + \underbrace{\frac{1}{2}\frac{\partial^2 u}{\partial x^2}}_{\text{Dispersion}} + \underbrace{|u|^2 u}_{\text{+ve Non-linearity}} = 0, \tag{1.15}$$

and has a soliton solution of the form [35]

$$u(x,t) = a_s \operatorname{sech}\left(a_s\left\{x - V_s t\right\}\right) e^{i(kx-\omega t)}, \tag{1.16}$$

where a_s, V_s, k and ω are the soliton amplitude, the soliton velocity, the wavenumber and frequency of the carrier plane wave (background wave), in order. Here, the soliton velocity satisfies $V_s = k$ and the frequency ω is provided by the linear dispersion relation $\omega = k^2/2 - a_s$. A well-known application of the focusing NLS equation in fluid mechanics is the explanation that it provides for the evolution of the deep water wave modulational instability which is known as Benjamin-Feir instability, see [19, 25] for

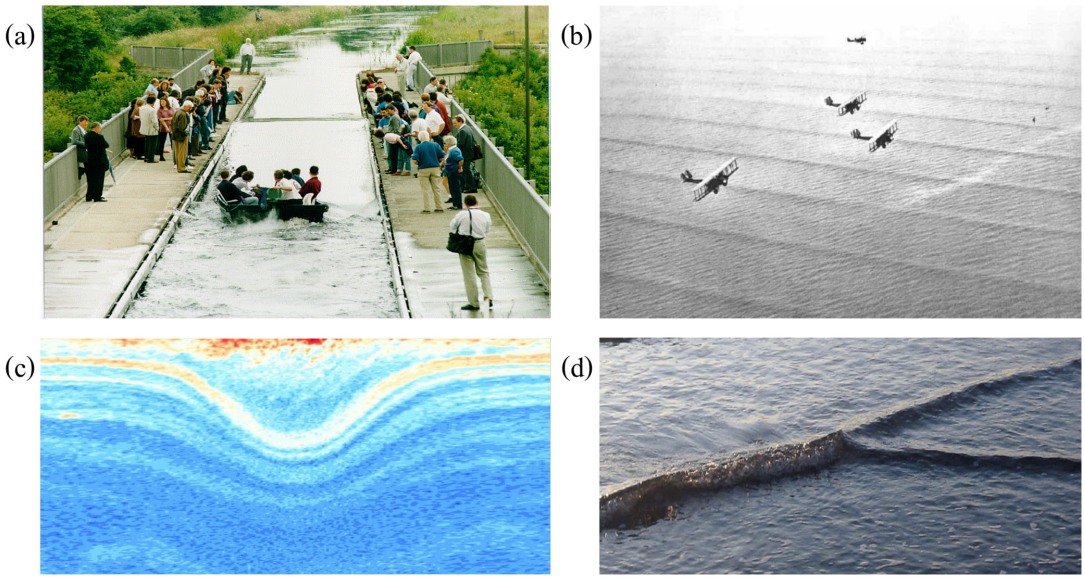

Figure 1.3: Solitary and cnoidal waves in fluids. (a) Russell's solitary wave in the Union Canal recreated by a group of scientists who gathered in a non-linear waves conference that took place at Heriot-Watt University in 1995. The soliton, appearing as a hump wave, is ahead of the boat. This image was retrieved from the URL https://www.ma.hw.ac.uk/solitons/soliton1.html. (b) Cnoidal waves in the Panama Coast, Central America, taken in 1933. Image source: National Geographic Magazine, Volume 63. (c) Echogram of a large internal (dark) solitary wave in the Saguenay Fjord, Canada, taken in 2016. Courtesy of Daniel Bourgault et al [169]. (d) An interaction (Y-type interaction) between two solitons in Nuevo Vallarta, Mexico, taken in 2012. Courtesy of Mark Ablowitz et al [170]. (Online version in colour.)

detailed discussion. In the other hand, the defocusing NLS equation is given by

$$i\frac{\partial u}{\partial t} + \underbrace{\frac{1}{2}\frac{\partial^2 u}{\partial x^2}}_{\text{Dispersion}} - \underbrace{|u|^2 u}_{\text{-ve Non-linearity}} = 0, \tag{1.17}$$

and its soliton solution is [34]

$$u(x,t) = a_s \left\{B \tanh\left(a_s B \left\{x - V_s t\right\}\right) + iA\right\} e^{i(kx-\omega t)}, \tag{1.18}$$

where $V_s = a_s A + k$ and $\omega = k^2/2 + a_s$. The constants A and B are connected through the relation $A^2 + B^2 = 1$. The defocusing soliton solution (1.18) admits two types of soliton solutions, known as black and gray solitons. The black soliton corresponds to the case when $A = 0$ and $B = 1$, while the latter one is associated with the case when $A, B \neq 0$. Note that in the theory of hydrodynamics, the defocusing NLS equation appears as a system of dispersive Euler equations for compressible gas dynamics, see Section 2.1 for further illustration.

The nomenclature focusing and defocusing originates from non-linear optics. In practice, that is in an experimental setting, when a light wave propagates through an optical medium, the light wave intensity $I = |u|^2$ is the physical quantity that is actually measured inside the medium, not the complex electric field u. When this medium is a focusing one, the refractive index increases with I, so that the beam

self-focuses, forming a bright region. This bright region is called a bright soliton and mathematically is given by

$$I = a_s^2 \operatorname{sech}^2 \left(a_s \left\{ x - V_s t \right\} \right). \tag{1.19}$$

Bright solitons can be used as information carrier waves (optical bits), for instance, in optical fibers. This is one of several advantages they have in real-life applications, the references [41, 42, 43, 44] provides wide benefits obtained from this kind of optical solitons. On the other hand, when the medium is of defocusing type, the refractive index decreases with the intensity rather than increases, resulting in a dark self-confined region. This dark region is coined a dark soliton and mathematically is given by

$$I = a_s^2 \left\{ B^2 \tanh^2 \left(a_s B \left\{ x - V_s t \right\} \right) + A^2 \right\}. \tag{1.20}$$

Such a soliton demands optical fibers to have a non-zero optical background, i.e., to be continuously flooded with light while the dark soliton propagates back and forth. For this and other reasons dark solitons are not practical in optical fiber communications. However, they have been observed in experiments [53, 58]. Figure 1.2(a) displays the intensity profiles of the bright (1.19) and black/gray (1.20) steady solitons. The bright soliton intensity is similar to Russell's water wave, i.e., a hump, whereas the dark (gray) counterpart takes the form of a flipped hump that drops to $x = 0$ ($x \neq 0$). The resemblance between wave phenomena occurring in optics and fluids is generally deep. In the same way bright and dark solitons arise in optical materials, they also do in deep water waves. As for black/gray solitons, it may sound strange that water waves in the form of a flipped, well-defined lump are possible to exist, but this has been observed by a group of scientists at École Centrale Marseille in a wave tank experiment. Travelling waves of dipping amplitudes occurring within the water in the tank were detected, see [54] for details. These waves are called "internal solitary waves" and their existence in oceans is ubiquitous, one clear illustration of this is depicted in Figure 1.3(c). They are produced when the interface between the fluid layers is perturbed, such as when tidal flow passes over rough ocean floors, ridges, or other obstacles. In addition to these types of solitons, there are several others such as breathers [55], gap solitons [56], vortex solitons [27, 57], etc. These waves are outside the scope of this thesis, so we will not discuss them further.

We have given so far a brief introduction to solitary waves, nematic liquid crystals and their basic physical properties. We are ready now to present an experimental set-up that generates bright or dark solitary wave in nematic liquid crystals.

1.3 Experimental Set-up

As in Figure 1.4, let us consider the propagation of a coherent, linearly-polarised light beam from a laser, such as Argon laser, through an optical cell filled with a nematic liquid crystal, a typical type which is used is the commercial mixture E7 [6]. Suppose that the light propagates in the direction Z down to the cell with the laser beam being polarised in the X direction. The Y coordinate then closes the coordinate system as depicted in the figure. Typically, the physical cell dimensions are 200 μm×30 μm×1 mm [6]. Two parallel slides of glass are used to trap this nematic cell and separated by a distance. In addition, a third glass plate is deployed to seal the cell's entrance as shown in the figure. The role of this additional glass is to avoid the formation of an undesired meniscus at the interface of air and the nematic liquid crystal. A meniscus

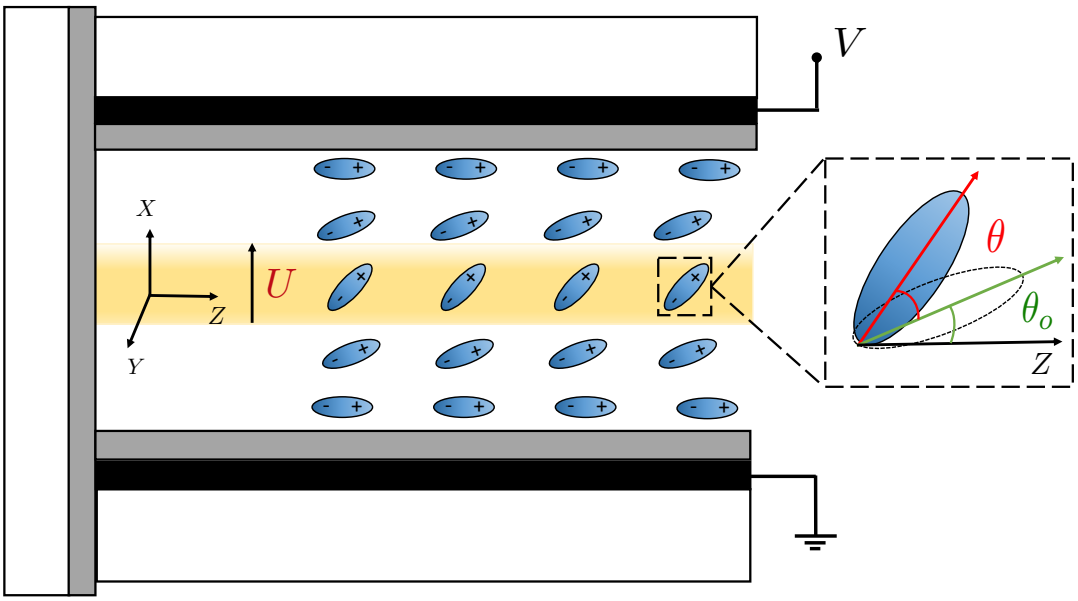

Figure 1.4: Experimental design of an optical apparatus. A generated bright solitary wave (yellow region), nematicon, by a linear-polarised light wave U propagating through a cell filled with a focusing nematic liquid crystal. The light wave is linearly polarised in the direction X. Two thin electrodes, creating dipole moments, and anchoring films are attached. They are shown by (black) and (gray) regions, respectively. The nematic molecules which are located at the boundaries are held tightly by the virtue of the anchoring films. The far right inset (black) dashed box exhibits angular positions of a nematic molecule with respect to the direction of the propagation Z before and after releasing the light wave through the nematic cell. (Online version in colour.)

could change the polarisation and phase distribution of the input laser beam. There is an external static electric field E that is applied across the cell through a voltage source V and produced from a pair of attached thin film electrodes. Such an electric field creates dipoles in the nematic molecules, realigns them towards the direction of the polarisation and pre-tilts them at an angle θ_0 with respect to the direction of the propagation, as shown in the figure. There is also a pair of polymer anchoring films deposited on the internal surfaces of the electrodes. Their role is to anchor the molecules at the boundaries at $\theta_0 \ll \pi/2$ and prevent defects in the orientation of the molecular director. One of the main complexities of the nematic medium is that if its molecules are initially aligned with their director orthogonal to the electric field U, then the optical Fréedericksz threshold exist. Therefore, a minimum static electric field E is required to overcome the elastic intermolecular forces and enable the molecular rotation θ. For this reason, the voltage source is used at specific amount of voltage with a low frequency, for example, $V = 0.8$ V with frequency 1 kHZ [6, 7]. Otherwise, the nematic molecules will not experience the rotation θ. The optical power of the launched light beam is adjusted at milliwatt levels at a wavelength typically in the near infrared, for instance, 2 mW at wavelength 514 nm [6, 7]. High optical power yields excessive heating which can cause the medium to change its state out of the nematic. With this background and experimental settings, the following are observed:

- The director's configuration is uniformly reoriented and planarly aligned.
- An additional optical, rotational angle θ is induced in the molecules from the

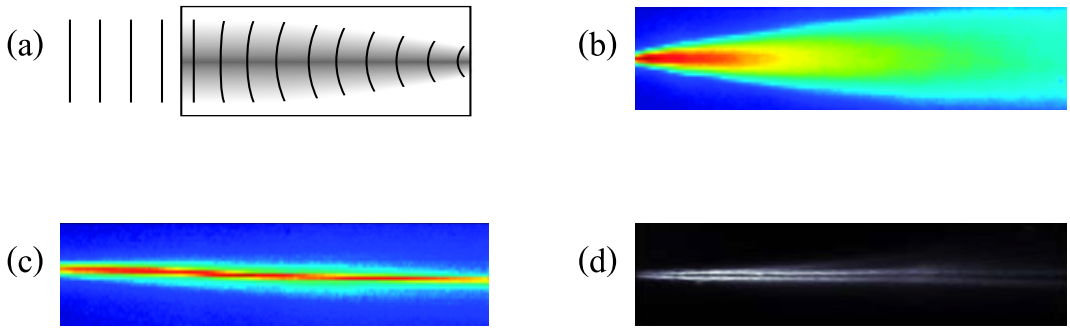

Figure 1.5: Optical properties and experimental formations of a laser beam travelling through different optical media. (a) Illustration of the self-focusing property generated by increasing the power of a laser beam propagating in a Kerr medium. Courtesy of Geoffrey New [9]. (b) Linear diffracting wave in a nematic liquid crystal that results when the optical power of a laser beam is less than a minimum milliwatt, such as 2 mW. Courtesy of Gaetan Assanto et al [7]. (c) Bright nematicon generated when the optical power of a laser beam is 2 mW. Courtesy of Gaetano Assanto et al [7]. (d) Dark nematicon obtained when an azo dye is added to the nematic cell. The minimum optical power to create this dark nematicon was found to be of magnitude 4 mW. Courtesy of Gaetano Assanto et al [6]. (Online version in colour.)

pre-titled position θ_0.

- In general, the light beam tends to self-focus due to the effect of non-linearity (Kerr effect). However, the basic saturation and non-locality properties of nematic liquid crystals do not allow the self-focusing to continue to dominate the diffraction. Instead, the self-focusing and diffraction balance each other, resulting in an intense and undistorted bright self-confined beam, which is a bright nematic solitary wave, see Figure 1.5(c). This wave is often found in the literature by an alternative name, bright "nematicon." The term nematicon refers to a spatial optical solitary wave propagating through a nematic liquid crystal in the "time-like" direction Z.

- When the power of the optical beam is reduced below a minimum level, such as 2 mW [6, 7], the molecules still undergo an extra rotation, but the induced laser beam self-diffracts rather than self-confines, as seen in Figure 1.5(b). We are not interested in this linear behaviour.

Although a nematic liquid crystal is usually a focusing medium; that is it produces a bright nematicon from a milliwatt laser beam and the refractive index increases with intensity, it has been found that the addition of small amounts of an azo dye (an organic chemical compound) to the nematic liquid crystal modifies the medium's response. The nematic becomes a self-defocusing medium instead [58]. By way of explanation, when a light beam propagates through a cell with an azo dye doped nematic, the light diffracts (defocuses) in the entire cell and, most importantly, it leaves in the middle a dark self-confined region with reduced light, as illustrated in Figure 1.5 (d). This dark portion is a dark nematic solitary wave, or dark nematicon.

The addition of an azo dye is necessary when it comes to studying nematic dispersive shock waves (DSWs). Nematic DSWs are created when abrupt changes in the optical

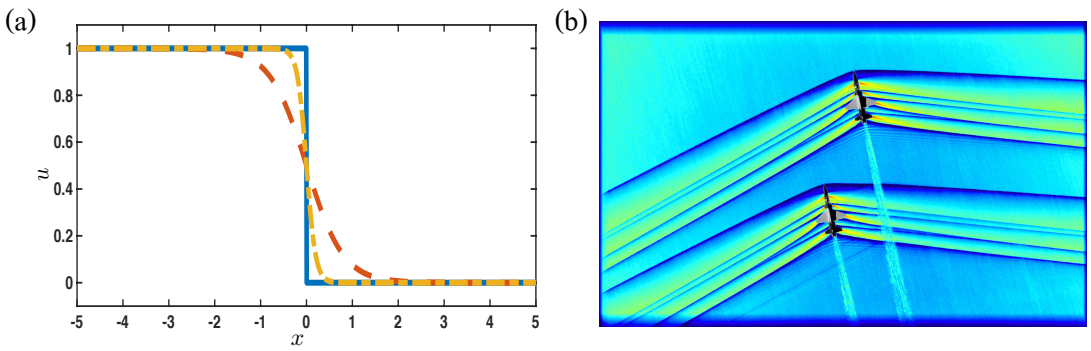

Figure 1.6: Mathematical and physical formations of VSWs. (a) Stationary Hyperbolic tangent profiles given by the expression (1.25) smoothing out a physical singularity which is shown by a (blue) solid line. Here, the (orange) dashed line is a tanh with $\mu_v = 0.2$ and the (yellow) dash-dot line is a tanh with $\mu_v = 0.05$. In the plot, $u_- = 1$ and $u_+ = 0$. (b) Two aircraft flying at speeds faster than the speed of sound in the atmosphere which yield to shock waves travelling away from the planes, resulting in a sonic boom sound. Courtesy of Nasa [110]. (Online version in colour.)

intensity take place, subsequently leading to sudden changes in the nematic molecular response. It has been found that focusing nematic liquid crystals exhibit unstable DSWs [59, 128]. However, the defocusing counterpart manifests stable DSWs [60, 61], especially when the initial rapid changes in the optical intensity are small. We will discuss this later in more details. Unfortunately, unlike other kinds of DSWs occurring in fluid mechanics, BECs and optical fibres, nematic DSWs have been solely investigated numerically and theoretically. No laboratory experiments exist to our knowledge. It is hoped that such experiments can be conducted in the future. This thesis is centred on DSWs in defocusing nematic liquid crystals. It is important then to give an introduction to this type of waves and present the key mathematical tools needed to study them. This will be the subject of the next section.

1.4 Dispersive Shock Waves and Whitham's Averaging Theory

Shock waves are non-linear wave phenomena that generally occur when physical quantities vary rapidly due to the effect of non-linearity [1]. Shock waves arise in a wide range of physical applications. In gas dynamics, a shock wave is generated when the speed of sound is exceeded by an evolving physical quantity, such as fluid velocity, temperature, pressure or density, resulting in supersonic flow. This implies that the Mach number is greater one ($M > 1$), leading to a sonic boom. In shallow water wave theory, on the one hand, a shock wave emerges when a fluid moves with velocity greater than the linear shallow water wave velocity $\sqrt{gh}$, where g is the gravity acceleration constant and h is the water depth. This implies that the Froude number is greater than one ($Fr > 1$), yielding a supercritical flow. Shock waves are also found in other applications related to, e.g., modelling traffic flow and erosion [1, 94, 95, 96, 97, 98]. The most general scalar, one-dimensional mathematical model which has a shock wave solution is the non-linear hyperbolic PDE

$$\frac{\partial u}{\partial t} + \frac{\partial}{\partial x} f(u) = 0. \tag{1.21}$$

The simplest initial condition which will generate a right-propagating shock is the step initial condition

$$u(x,0) = \begin{cases} u_-, & x < x_0 \\ u_+, & x > x_0, \end{cases} \tag{1.22}$$

such that $u_- > u_+$ on assuming that $f'(u) > 0$. This initial condition breaks immediately, forming a shock at x_0. This mathematical problem is called Riemann problem. The variable u is a mathematical quantity that is related to a physical quantity, such as the fluid velocity. The flux function f is a smooth function such that $f''(u) \neq 0$ (a genuine non-linearity condition in hydrodynamics). If $f'(u) < 0$, then a shock wave is formed only when $u_- < u_+$. The shock will travel to the left in this case. The case of $u_- < u_+$ with $f'(u) > 0$ leads to a right-propagating rarefaction wave [1, 99], which is also of concern in this thesis. The formation of shocks is more complicated when $f'(u) > 0$ for some values of u and $f'(u) < 0$ for others. In this case, multiple shocks travelling in different directions can be generated [100]. Since this case is outside the scope of this thesis, it will not be discussed here. A famous example of Riemann problem is the Hopf equation, for which $f(u) = u^2/2$, which leads to the convective derivative present in fluid equations [1].

In a shock wave Riemann problem, when the initial condition breaks immediately, multiple distinct values of a physical quantity are produced at one single position. This could be different fluid density or velocity values at one position x, which is obviously non-physical. In the language of mathematics, the breaking process yields a blow-up in the derivative values; gradient catastrophe [1, 18]. This hydrodynamic singularity must be resolved. The way to resolve this relies fundamentally on the nature of the physical medium. Within our domain of interest and concern, there are media which are viscous, that is, the dispersion effect is very small, as for the flow generated by supersonic aircraft; see Figure 1.6(b) [109, 110], and dispersive, namely, the viscosity effect is almost zero or does not exist, such as quantum fluids and optical materials [111, 112, 113, 115, 119]. In either way, a specific non-zero differential (or integro-differential) operator D_x [18, 86], that contains derivatives of second order or higher in spatial and/or mixed partial derivatives, can be added to equation (1.21)

$$\frac{\partial u}{\partial t} + \frac{\partial}{\partial x} f(u) = D_x(u) \tag{1.23}$$

in order to resolve the shock discontinuity. Shock waves that occur in viscous, sometimes called dissipative, media are called classical or viscous shock waves (VSWs) and the hydrodynamic singularity is overcome by adding derivatives of even order, and of asymptotic limit $\mathcal{O}(\mu_v)$, where μ_v is a parameter that measures the strength of kinematic viscosity and usually this is very small $0 < \mu_v \ll 1$. In fluid dynamics, even order derivative terms in hydrodynamic equations capture viscosity, whilst odd order derivative terms correspond to the effect of dispersion, see [120, 121, 122]. The simplest dissipative hydrodynamic model that manifests a VSW is Burgers' equation, with $f(u) = u^2/2$ and $D_x(u) = \mu_v u_{xx}$,

$$\frac{\partial u}{\partial t} + u\frac{\partial u}{\partial x} = \mu_v \frac{\partial^2 u}{\partial x^2}, \tag{1.24}$$

which is exactly solvable via Cole-Hopf transformation [1]. This simple Riemann prob-

lem admits a travelling wave solution of the form

$$u(x,t) = \frac{u_- + u_+}{2} - \frac{u_- - u_+}{2} \tanh\left(\frac{u_- - u_+}{4\mu_v}\{x - V_{\text{shock}}t\}\right), \tag{1.25}$$

which moves with the shock velocity $V_{\text{shock}} = \{u_- + u_+\}/2$. Figure 1.6(a) shows a non-physical singularity in the fluid velocity smoothed and regularised by the hyperbolic tangent solution (1.25), we can also see the effect of the viscosity in this regularisation process.

In contrast to a compressible flow shock, when viscosity is negligible or non-existent and dispersion dominates, the rapid transition of a shock wave is replaced by an unsteady (continual spatial expansion), non-linear, dispersive, slowly modulating wavetrain to connect the steady, initial rear u_- and front u_+ states, see Figure 1.7. This wavetrain is termed a dispersive shock wave (DSW) because it is the dispersive analogue of a VSW, also well-known as an undular bore in fluid mechanics applications [123]. It should be noted that in fluid mechanics, bores come in two general forms, viscous bores and undular bores [18]. A viscous bore is a steady wave that is formed due to a balance between viscosity and dispersion/non-linearity, so that viscous bores dissipate energy [1, 18, 124]. In comparison, for a DSW, an undular bore, there is no loss and it is an unsteady modulated wave for which the dispersion stops non-linear breaking, as occurs for a gas dynamic shock due to the effect of viscosity. In general, a DSW exists as a multi-scale wavetrain involving two distinct scales: a fast oscillatory scale given by the wave phase, and a slowly varying scale characterised by the amplitude, wavenumber, angular frequency and mean height of the wave envelope. Furthermore, its structure generically has two distinct edges, with a solitary wavetrain at one edge and a linear, dispersive wavetrain at the opposite edge. Each of these boundaries propagates with a different velocity. In this regard, the non-linearity of DSWs are considered to be of strong type.

From a mathematical viewpoint, unlike dissipative hydrodynamics, the non-physical singularity in this situation is regularised by adding an odd order derivative term to equation (1.21) as this results in dispersion. The most classic and simplest mathematical model that combines both non-linear propagation effects and dispersive effects is the KdV equation, with $f(u) = 3u^2$ and $D_x(u) = -\mu_d u_{xxx}$,

$$\frac{\partial u}{\partial t} + u\frac{\partial u}{\partial x} = -\mu_d \frac{\partial^3 u}{\partial x^3}; \ \mu_d > 0. \tag{1.26}$$

Here, μ_d gives the strength of dispersion and it is assumed that it is strictly positive. The Riemann problem for the KdV equation is non-trivial, unlike that for Burgers' equation (1.24). The standard manner to find DSW solutions, giving how the amplitude, wavenumber, velocity and mean height of a DSW evolve with respect to space and time, is Whitham's modulation theory developed in the 1960s, which is based on the method of averaged Lagrangians or averaged conservation laws [1, 82, 83] for non-linear dispersive wave equations. This method is also known as Whitham's averaging theory. It is the basic mathematical tool in the field of dispersive hydrodynamics; the counterpart of dissipative hydrodynamics. Whitham's averaging theory is a powerful method used in physical applied mathematics to analyse both slowly varying linear and, most importantly, non-linear dispersive waves [1]. In general, the method produces a system of equations, termed modulation equations, that describes and governs a slowly varying wavetrain. If this system of modulation equations forms a hyperbolic system (eigenvectors form a basis or eigenvalues are real), then the underlying non-linear pe-

riodic wave is stable. On the other hand, if the modulation equations form an elliptic system (eigenvalues are complex), then the wave is unstable. Note that if the associated eigenvalues with the modulation system are real and distinct, then Whitham modulation equations are "strictly" hyperbolic. Whitham used his modulation theory to give a theoretical explanation for the Benjamin-Feir instability of gravity water waves [84], showing that the modulation equations for gravity water waves are elliptic if the product kh of the depth of the water h and the wavenumber k is above a critical value.

The breakthrough for the theory of DSWs was the realisation that if the modulation equations for a non-linear dispersive wave equation form a hyperbolic system, then an expansion fan solution of these equations corresponds to a DSW. The first DSW solution found was that for the KdV equation [105] based on its previously derived modulation equations [1, 83]. There are two ways to undertake Whitham's averaging theory, either by averaging Lagrangians or by averaging conservation laws for the equations that govern physical systems of interest. The basic steps of modulation theory to reach to a DSW solution can be summarised as follows:

- Find a Lagrangian for the non-linear dispersive wave equation of interest. Alternatively, if one wants to use the conservation laws approach, then Nöther's Theorem can be implemented to find the conservation laws for this equation. Here, it is worth to mention that, for instance, in the physical theory of shock waves, random conservation laws are not accepted and will not lead to valid jump conditions for shocks, so Nöther's Theorem is the physical approach to use. We will come across this case in Section 4.2.

- Average the Lagrangian or the conservation laws over the rapid-scale of the wave, i.e., the period or the phase. This will leave the averaged Lagrangian or the averaged conservation laws in terms of parameters that are slowly varying in space and time.

- Take variations of the averaged Lagrangian with respect to the slowly varying wave parameters. This yields a set of modulation equations which are averaged Euler-Lagrange equations. We note that the equations which are obtained after averaging the conservation laws are the modulation equations themselves.

- Next step, the most challenging step, is to set the modulation equations in Riemann invariant form or a diagonal system of Riemann variables if the modulation equations are hyperbolic. This is always possible for a 2×2 system of modulation equations, but not always achievable for systems whose sizes higher than this (Pfaff's problem) [1].

- Determine when the attained characteristic eigenvalues, namely, the characteristic curves or the non-linear group velocities, are real or imaginary. If the eigenvalues are real (real and distinct), or more generally the eigenvectors form a basis, then the system is hyperbolic (strictly hyperbolic) and we have a stable DSW. Otherwise, if the eigenvalues are imaginary, then we have an unstable DSW due to the modulational instability.

- We now suppose that the modulation equations are hyperbolic. We determine the right characteristic on which the expansion fan solution corresponds to a DSW. Note that in the linear approximation $0 < a \ll 1$, the DSW characteristics reduce to the trailing edge characteristics which move with the linear group velocity, where a is the wave amplitude. If the modulation equations form an elliptic system, then no simple wave solution, corresponding to a DSW, exists.

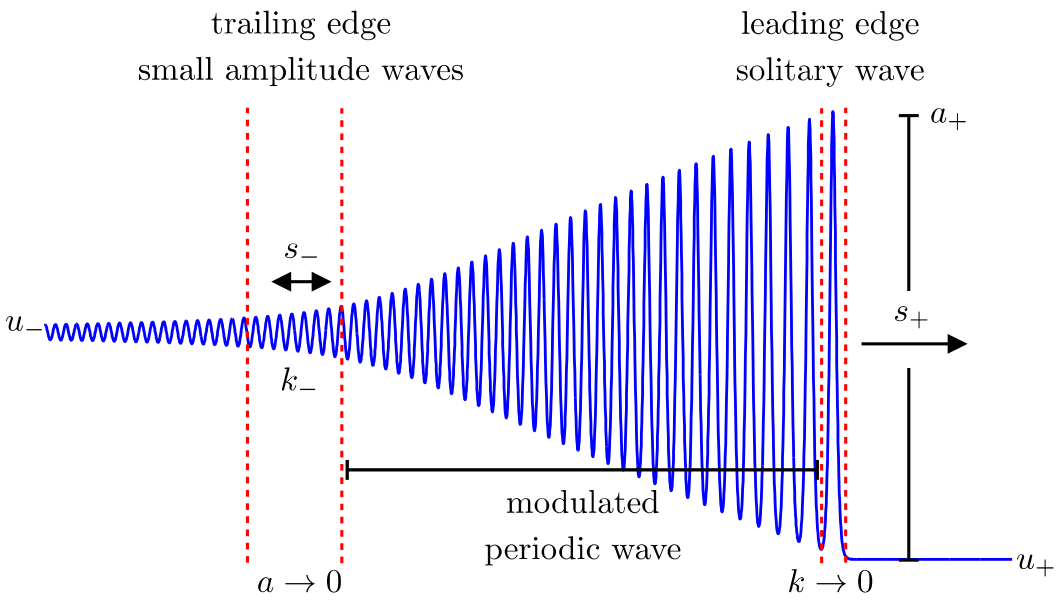

Figure 1.7: Full details of a KdV DSW structure, with positive polarity and positive orientation. The unphysical singularity in the variable u is regularised via a modulated cnoidal wavetrain shown by a (blue) solid profile. The slowly varying amplitude and wavenumber within the DSW are denoted by a and k, respectively. The speed at the trailing edge is given by s_-, whereas the leading edge velocity is given by s_+. Courtesy of Mark Hoefer et al [171]. (Online version in colour.)

Modulation theory is related to the standard method of multiple-scales from perturbation theory, as shown in [1]. Astonishingly, Whitham found that secular terms in the method of multiple-scales which are needed to eliminate unperiodic solutions are exactly the averaged conservation laws obtained from Nöther's theorm or the averaged Euler-Lagrange equations acquired from the method of averaged Lagrangians. This is a main reason why "arbitrary" conservation laws are not physically valid in shock wave theory.

Let us now return to the KdV Riemann problem, equation (1.26) subject to the initial condition (1.22). Following the work of Gurevich and Pitaevskii [105], the KdV equation has the cnoidal (periodic wave) solution

$$u(x,t) = u_- - \{u_- - u_+\}\, m + 2\,\{u_- - u_+\}\, m\, \mathrm{cn}^2\, \frac{K(m)}{\pi\sqrt{\mu_d}}(kx - \omega t), \tag{1.27}$$

where $K(m)$ is the complete elliptic integral of the first kind [21]. In modulation theory, the wave parameters, the amplitude a, wavenumber k, mean height $\bar{u}$, phase velocity V_p, upper u_P and lower u_L parts of the DSW's envelope, are allowed to slowly vary. In the KdV DSW, these parameters are given by [105, 125]

$$a = 2\,\{u_- - u_+\}\, m \quad , \quad \bar{u} = 2u_+ - u_- + \{u_- - u_+\}\left\{2\frac{E(m)}{K(m)} + m\right\}, \tag{1.28}$$

$$k = \frac{\pi}{K(m)}\sqrt{u_- - u_+} \quad , \quad V_p = 2u_- + 4u_+ + 2\,\{u_- - u_+\}\, m, \tag{1.29}$$

$$u_P = u_- + \{u_- - u_+\}\, m \quad , \quad u_L = u_- - \{u_- - u_+\}\, m, \tag{1.30}$$

where $E(m)$ is the complete elliptic integral of the second kind [21]. The characteristic velocities in the KdV Riemann system that correspond to this DSW are, $0 \leq m \leq 1$,

$$\frac{x}{t} = V_p - 4\{u_- - u_+\}\frac{m\{1-m\}K(m)}{E(m) - \{1-m\}K(m)}. \tag{1.31}$$

Thus, the solitary wave (leading) edge, $m \to 1$, moves with the velocity

$$V_s = 4u_- + 2u_+, \tag{1.32}$$

and the linear dispersive wavetrain (trailing) edge, $m \to 0$, propagates with the group velocity

$$c_g = 12u_+ - 6u_-. \tag{1.33}$$

The geometrical structure of the KdV DSW solution (1.27)–(1.28) is illustrated in Figure 1.7. The sign of the dispersion in the KdV equation (1.26) is positive. If this sign is negative, that is,

$$\frac{\partial u}{\partial t} + u\frac{\partial u}{\partial x} = \mu_d \frac{\partial^3 u}{\partial x^3};\ \mu_d > 0, \tag{1.34}$$

then the arrangement of the solitary waves and the linear dispersive waves in the DSW structure flips. The linear dispersive waves locate the leading edge of the DSW and the solitary waves occupy the trailing side. This motivates us to define an orientation for DSWs by introducing a parameter denoted by d [18]. When the solitary waves are at the leading edge of the DSW, then the value of the orientation parameter is defined by $d = 1$, otherwise, $d = -1$. Moreover, the negative sign of the dispersion in the KdV equation (1.34) makes the modulated wavetrain of the DSW dips in the varying mean level $\bar{u}$, rather than elevating about it as in Figure 1.7. This consequence allows us to introduce another new parameter p which determines the polarity of DSWs [18]. If the edge of the solitary wave is an elevation edge, then $p = 1$ and the governing DSW is termed bright DSW, and if it is a depression edge, then $p = -1$ and the dark DSW term is used. Feasible orientations and polarities of DSWs are outlined in Figure 1.8(a). The KdV DSW ($p = -1, d = -1$) given by equation (1.34) is shown in the bottom left corner of Figure 1.8(a).

Remark 1. *Note that the top left and bottom right corners of Figure 1.8(a) are also KdV DSWs. They are associated with the KdV equations (1.26) and (1.34) under the simple transformation $x \to -x$, respectively.*

The type of the DSW exhibited by the defocusing NLS Riemann problem (equation (1.17) subject to an initial jump condition in $|u|$), on the other hand, is notably different than that of the KdV Riemann problem. As time evolves and this initial discontinuity breaks, two distinct waves propagate in opposite directions, with a shelf in-between, as the NLS equation is a bi-directional equation. One wave is a non-dispersive wave (an expansion fan) that moves in the upstream direction and the other wave is a DSW that travels in the downstream direction, with solitary waves at the trailing edge and linear dispersive waves at the leading edge, as depicted in Figure 1.8(b). Thus, the defocusing NLS DSW possesses negative polarity $p = -1$ and negative orientation $d = -1$.

The KdV and defocusing NLS DSWs are stable DSWs due to the hyperbolicity of the associated Whitham modulation equations. In contrast, the focusing NLS Riemann Problem, namely, equation (1.15) subject to an initial jump condition in $|u|$, has Whitham modulation equations which form a strict elliptic system. Hence, its DSW is unstable [59, 128]. In Figure 1.8(c), we recognise that the hydrodynamic singularity is

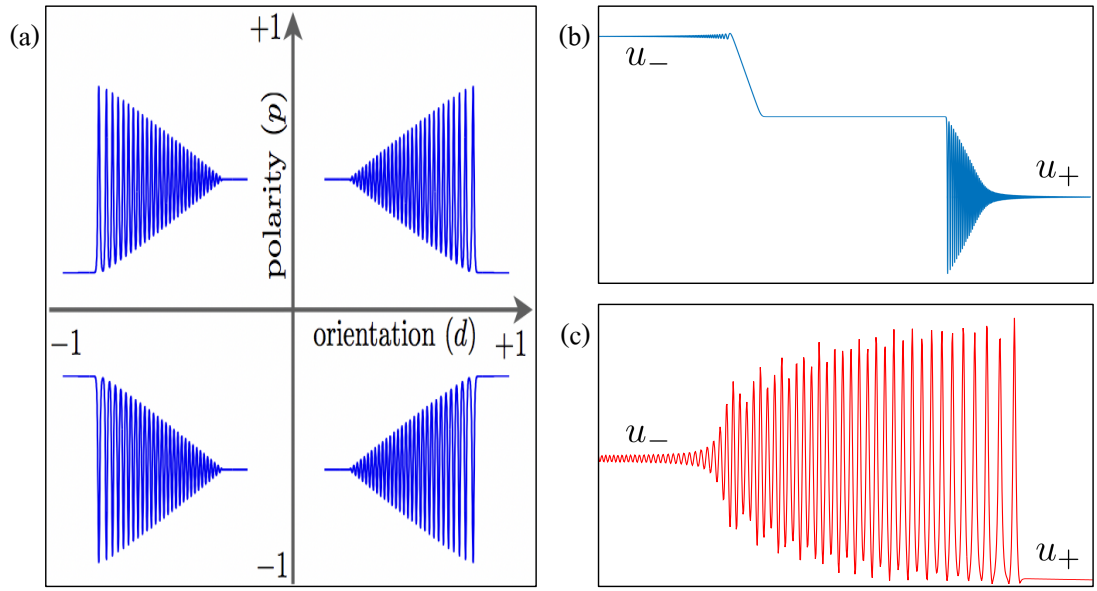

Figure 1.8: Stable and unstable DSW types. (a) Demonstration of the polarities and orientations of standard (KdV and NLS) DSWs. Courtesy of Mark Hoefer et al [18]. (b) Stable DSW as a solution of a "defocusing" NLS Riemann problem. (c) Unstable DSW as a solution of a "focusing" NLS Riemann problem. Courtesy of Noel F. Smyth et al. [59].

regularised by an unstable modulated wavetrain, namely, an unstable bright-like DSW with $p = 1$ and $d = 1$ connecting the initial stationary levels $|u| = u_-$ and $|u| = u_+$ together.

As mentioned previously, the most difficult step in modulation theory is the ability to set modulation equations in Riemann invariant form or a diagonal system of Riemann variables. Because the concepts of Riemann invariant and Riemann variable appear a lot in this thesis, let us briefly introduce their definitions. Consider a system of one dimensional, first order, non-homogeneous, quasi-linear PDEs

$$\frac{\partial \mathbf{u}}{\partial t} + \mathcal{A}(\mathbf{u})\frac{\partial \mathbf{u}}{\partial \mathbf{x}} + \mathbf{b}(\mathbf{u}) = \mathbf{0}, \tag{1.35}$$

where $\mathbf{u}^T(x,t) = [u_1 \dots u_n]$ is a differentiable vector, $\mathcal{A}$ is a non-singular matrix and $\mathbf{b}$ is a real-valued vector. Note that, in general, $\mathcal{A}$ and $\mathbf{b}$ may not depend on $\mathbf{u}$. Let $\mathbf{l}^k = [l_1^k \dots l_n^k]$ and λ^k be a "left" eigenvector and eigenvalue (group velocity), respectively, of the matrix $\mathcal{A}$, where the index $k \in \{1, 2 \dots, n\}$. Then, the above quasi-linear system can be written in the so-called *characteristic form*

$$\mathbf{l}^k \cdot \frac{d\mathbf{u}}{dt} + f^k(\mathbf{u}) = 0 \qquad \text{on} \qquad \frac{dx^k}{dt} = \lambda^k, \tag{1.36}$$

with the scalar function $f^k(\mathbf{u}) = \mathbf{l}^k \cdot \mathbf{b}$ and $x^k = x^k(t)$ being a parametrised characteristic curve. In linear systems, the eigenvector $\mathbf{l}^k$ does not depend on $\mathbf{u}$. In this case, it is possible to reduce the above *characteristic form* (1.36) to

$$\frac{dr^k}{dt} + f^k(\mathbf{u}) = 0 \qquad \text{on} \qquad \frac{dx^k}{dt} = \lambda^k, \tag{1.37}$$

with $r^k = \mathbf{l}^k \cdot \mathbf{u}$. On the other hand, in non-linear systems, $\mathbf{l}^k$ may depend on $\mathbf{u}$ and it is not always possible to achieve the diagonal system form (1.37). It would be necessary in this situation to find a non-zero τ for each r^k such that

$$\tau dr^k = \mathbf{l}^k \cdot d\mathbf{u} \tag{1.38}$$

to reach to the representation (1.37). This can always be attained for $n = 2$, but not necessarily possible for $n > 2$ (Pfaff's problem) [1]. Now, if $f^k = 0$, then $r^k = \mathbf{l}^k \cdot \mathbf{u}$ is called *Riemann invariant* and the system (1.37) becomes

$$\frac{\partial r^k}{\partial t} + \lambda^k \frac{\partial r^k}{\partial x} = 0 \qquad \text{on} \qquad \frac{dx^k}{dt} = \lambda^k. \tag{1.39}$$

This means that the Riemann invariant r^k is constant along the characteristic curve $x^k(t)$. If $f^k \neq 0$, then r^k is termed *Riemann variable*, so the form (1.37) represents a diagonal system of Riemann variables.

For the KdV equation, Whitham did extremely ingenious calculations which were essentially extensive algebraic manipulations on elliptic integrals, as the periodic wave solution of the KdV equation is in terms of the elliptic functions cn or dn, to reduce the modulation equations of the KdV equation to Riemann invariant form. His original paper was a seminal contribution in non-linear dispersive wave theory [83]. The subsequent major advance happened when it was justified using techniques from functional analysis that the ability to set the KdV modulation equations in Riemann invariant form was linked to the KdV equation having an inverse scattering solution [127]. This contribution demonstrated how to derive Whitham modulation equations for other non-linear dispersive wave equations having inverse scattering solutions (integrable equations). Because of this advance, DSW solutions for integrable, non-linear, dispersive wave equations such as the defocusing NLS equation [62], the focusing NLS equation (giving an unstable DSW) [128] and the Benjamin-Ono equation [129, 130, 131, 132] were found, in contrast to Whitham's work for the KdV modulation equations.

In principle, the DSW solution for any non-linear dispersive wave equation with a modulationally stable periodic wave solution can then be derived. However, most non-linear dispersive wave equations are non-integrable. While it is still difficult to determine the full DSW structure for non-integrable equations, a general method exists to find its solitary wave and linear dispersive wave edges if the DSW is of "KdV-type," that is it consists of a monotonic modulated periodic wavetrain with solitary waves at one edge and linear, dispersive waves at the other [18]. The method is coined the DSW fitting method, or El's method ascribing to Gennady El who developed this technique in his papers [133, 134]. This method is based solely on the linear dispersion relation of the equation of interest. The reason that this can be done is that for a modulationally stable, non-linear, periodic, dispersive wave, its modulation equations are degenerate at its two edges and have a standard structure which can be determined without detailed knowledge of the full modulation equations. The DSW fitting method was tested for several non-integrable equations, such as the Kawahara equation [79], the dispersive Eulerian fluid equations (dispersive Navier-Stokes equations with zero viscosity) [135], the Benjamin-Ono equation (by introducing a modified version of the DSW fitting method) [130], the magma flow equations [136], the Whitham equation [137], the non-linear ion-acoustic wave equations in collisionless plasma [134], etc. Excellent agreements were found with numerical solutions for these equations. This method will be examined for nematic DSWs in Chapter 5. Of interest in this thesis is the Kawahara

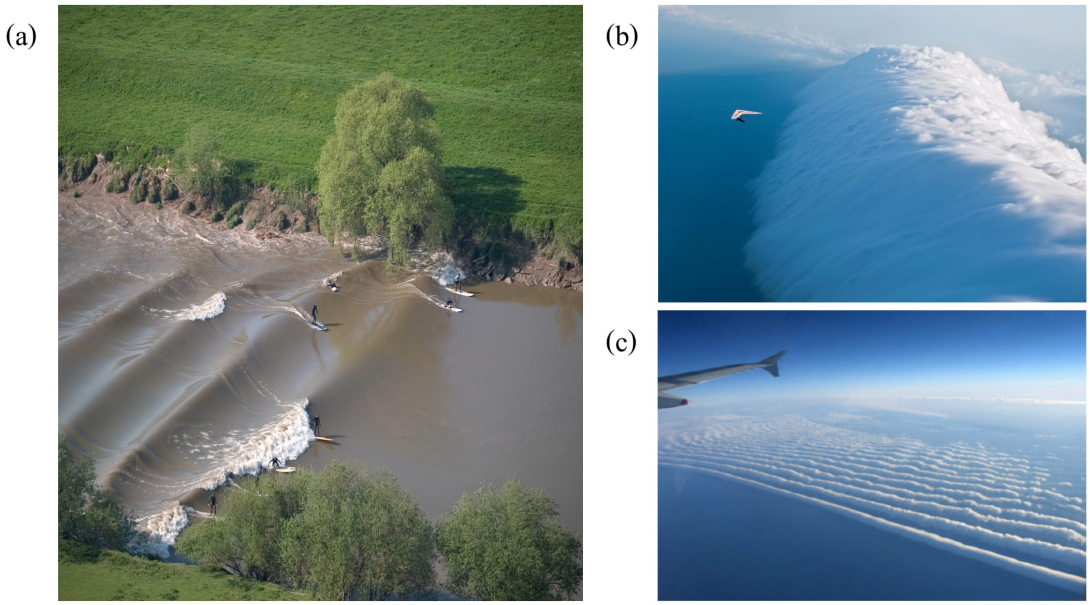

Figure 1.9: DSWs in shallow water and atmosphere. (a) DSW (undular bore) on the Severn river near Gloucester, England, taken in 2007. Courtesy of Mark Humpage, this image was retrieved from his website: www.markhumpage.com. (b) Hang glider in front of a morning glory cloud (DSW) over the Gulf of Carpentaria, Northern Australia. This image was taken from [172]. (c) Panoramic view of morning glory clouds. Courtesy of the COMET® Program.

equation,

$$\frac{\partial u}{\partial t} + 6u\frac{\partial u}{\partial x} + \mu_d \frac{\partial^3 u}{\partial x^3} + \frac{\partial^5 u}{\partial x^5} = 0; \ \mu_d 0, \tag{1.40}$$

where the μ_d parameter denotes the dispersion strength. This is the KdV equation with the next higher order, fifth order, dispersion included [79]. In the context of fluid mechanics, the Kahawara equation arises when surface tension effects in water waves are incorporated in the weakly non-linear, long wave asymptotic expansion of the water wave equations (Serre equations)[138], resulting in the extended, generalised Serre equations [**?**]. For positive dispersion, $\mu_d \geq 0$, we shall see in Section 5.1 why we require μ_d to be positive here rather than negative, Kawahara DSWs take the form of non-classical DSWs, in the sense that the DSWs are attached to a small-amplitude resonant wavetrain [79, 80]. This non-standard structure of the DSW is termed radiating DSWs [61]. At a critical value of μ_d, the KdV-type DSW structure disappears and new types of DSWs are generated as μ_d evolves beyond this critical value. One of these new DSW types is a radiating DSW and the others are known as crossover and travelling DSWs [79, 61]. For detailed descriptions of these non-classical DSWs, see Section 3.2.1. There is an analogy, to some extent, between the Kawahara and nematic DSWs.

The topic of this thesis is focused on DSWs governed by the defocusing nematic equations (2.19) and (2.20). This is a non-integrable system of equations and lacks a known exact non-linear periodic wave solution. For these reasons, Whitham modulation equations are not reachable for the nematic equations. Therefore, we seek a weakly non-linear, dispersive, periodic, wavetrain (Stokes wave) solution of the nematic equations and apply Whitham's averaging theory to this periodic wavetrain. This will be dealt

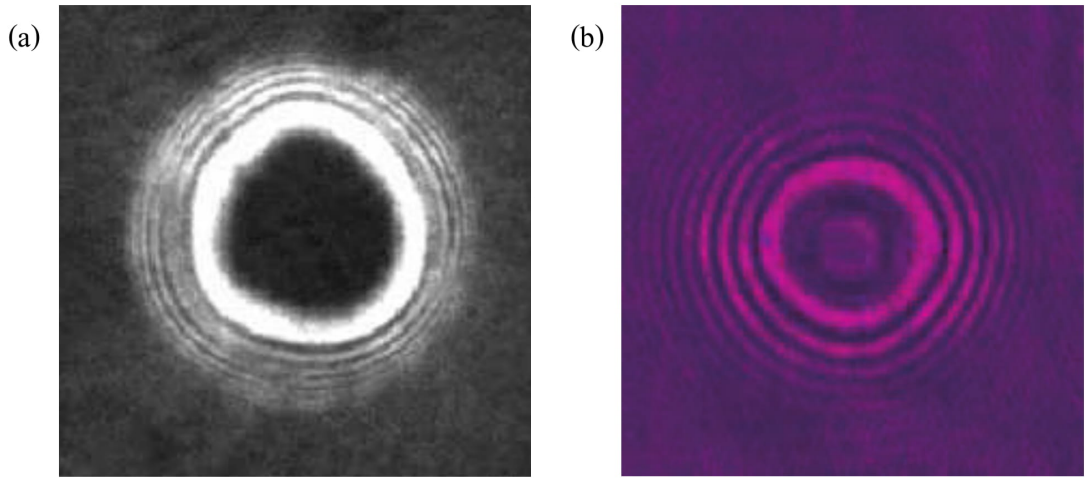

Figure 1.10: Experimental pictures of DSWs. (a) A blast pulse of a laser beam propagating through the centre of a static Bose-Einstein condensate. This pulse rapidly pushes atoms from the centre of the superfluid radially outward, resulting in the formation of fluid density concentric rings (quantum DSWs). Courtesy of Eric Cornell et al. [20]. (b) Oscillatory fronts (optical DSWs) created by a Gaussian laser beam travelling through a photorefractive crystal. Courtesy of Wenjie Wan et al. [112].

with in Chapter 4.

DSWs' occurrences in nature are utterly ubiquitous. We mention some of them here. The typical example of DSWs is tidal bores which take place in coastal areas of strong tidal flow and appropriate coastal topography to enhance the flow, for instance, the Severn Estuary in England, the Bay of Frundy in Canada and the Pororoca tidal bore on the Amazon River in Brazil. DSWs can also be found in a broad array of physical systems, including meteorology, an example being the morning glory clouds which are rare phenomena that occur in Australia and elsewhere [139, 140, 141], oceanography [123, 142], water waves [123, 143], geophysics (magma flow) [136, 144, 145, 146], photorefractive crystals [111, 112, 113, 114], non-linear optical fibers [115, 116], non-linear thermal optical media [117, 118] and colloidal media [147, 148]. Moreover, DSWs have been observed in quantum media acting as BECs [20] and Fermionic fluids [150]. See [18] for a summary of these applications. Figures 1.9 and 1.10 present some demonstrated and experimental snapshots of DSWs occurring in different physical media.

1.5 Thesis Organisation

This thesis is organised as follows. In Chapter 2, a dispersive hydrodynamic model that governs the optical propagation of a linearly polarised light wave through a nematic liquid crystal doped with an azo-dye is given. Then, the research aims of the thesis will be discussed. Chapter 3 presents an efficient numerical scheme that solves the defocusing nematic equations subject to the initial jump condition in the optical field amplitude (2.29) and the resulting initial step condition in the director angle (2.31). The numerical scheme section will be followed by a section that presents distinct numerical solutions and discusses each of the obtained non-dispersive and dispersive hydrodynamic regimes in detail. In Chapter 4, a Stokes wave solution will be derived from the nematic dispersive hydrodynamic system as the nematic equations have no known general non-linear,

periodic wave solution that can be used in Whitham's averaging theory. Modulation theory will then be developed based on a slowly varying nematic Stokes wave to deduce the nematic modulation equations and study the modulational stability of the Stokes wave. Chapter 5 presents a thorough theoretical analysis of the nematic non-dispersive and dispersive hydrodynamic regimes using various perturbation methods. In Chapter 6, theoretical results will be compared with numerical solutions and discussed. In general, the agreement between the theory and numerical solutions is found to vary from very good, with an error bound $\mathcal{O}(0.05)$, to excellent, with an error bound $\mathcal{O}(10^{-3})$. Lastly, Chapter 7 outlines the main research results and approximate methods used in this thesis and concludes with a list of potential research projects that are under our current investigation.

Chapter 2

Dispersive Hydrodynamic Model and Research Objectives

In this chapter, we present a mathematical model that governs the evolution of a linearly polarised light wave propagating in a cell filled with a defocusing nematic liquid crystal and the response of the nematic molecules. This model represents the mathematics behind the physics experiment which was discussed in Section 1.3. This model will be first non-dimensionalised and then written in a dispersive hydrodynamic form. The research objectives of this thesis will be outlined at the end of the chapter.

2.1 Mathematical Model

Let $\mathbf{U} = U\hat{e}_X$ be the electric vector field of a polarised light beam that propagates in the middle of the defocusing nematic liquid crystal cell along the Z direction with a wave vector $\mathbf{k} = k\hat{e}_Z$. W assume that the applied static electric field $\mathbf{E} = E\hat{e}_X$ determines the molecular director pre-tilt angle θ_0 in the XZ dimensional propagation plane, so that it overcomes the Fréedericksz threshold. Recall that Fréedericksz threshold is the minimum amount of the electric field required to initiate this rotation θ_0 and overcome the elastic intermolecular forces in the nematic. We take E and θ to be invariants in the Y direction. The rate of change of ϕ in the Z direction is very small due to the paraxial approximation (small-angle approximation). The bias E is assumed to be unaffected by the optical perturbation of the director $\hat{n}$. The mathematical model that governs the complex-valued, slowly varying envelope of the optical beam's electric field U and the total angular rotation $\phi = \theta + \theta_0$, which is due to the optical and static electric fields, consists of two coupled PDEs. In dimensional form, they are [6, 7]:

$$2ik_0 n_e \frac{\partial U}{\partial Z} + \frac{\partial^2 U}{\partial X^2} - \left\{\sin^2\phi - \sin^2\theta_0\right\} k_0^2 \varepsilon_a U = 0 \tag{2.1}$$

and

$$4K\frac{\partial^2 \phi}{\partial X^2} + \left\{2\Delta\varepsilon_{RF}E^2 + \varepsilon_0\varepsilon_a|U|^2\right\}\sin 2\phi = 0. \tag{2.2}$$

The first equation (2.1) is an NLS-type equation, while the second equation (2.2) is a non-linear elliptic PDE. Here, the constant K is the single, elastic, molecular response constant approximation in which the elastic constants for splay, bend and twist are all assumed to be equal, $\Delta\varepsilon_{RF}$ is the dielectric anisotropy at radio frequencies (1 kHz) normally used for biasing the cell, k_0 is the input wavenumber of the beam in free space, n_e is the extraordinary refractive index (1.4) and $\varepsilon_a = n_\parallel^2 - n_\perp^2$ is the optical

anisotropy. When the nematic liquid crystal is of focusing type, that is to say it does not contain an azo dye, so a bright solitary wave is generated rather than a dark one, the governing equations will be exactly the same, except that the coefficient of $k_0^2\varepsilon_a U$ in the NLS-type equation (2.1) will come with a positive sign instead of a negative one. From now on, we will call the system (2.1)–(2.2) the "defocusing nematic equations."

Note that the above underlying equations (2.1)–(2.2) are in terms of several physical variables and parameters which have distinct units. To be able to study these equations with mathematical methods, especially numerical and perturbation methods, it is best to convert this system to non-dimensional form. Otherwise, when it comes to, for example, comparing two or more physical quantities in a single equation and decide which one is small or large, the comparison is obviously meaningless without reference values. The key process to remove units from an equation(s) involving physical quantities and parameters is known as scaling or non-dimensionalisation. This is a standard method in applied mathematics and it is at the heart of mathematical modelling.

In general, to derive the non-dimensional counterpart of a dimensional system of equations, the independent and dependent dimensional physical variables involved in that system need to be re-scaled to dimensionless mathematical quantities. This is done, for instance, by dividing those variables by specific scales whose units are the same as the physical variables. These scales are often called characteristic scales and they are commonly deduced from the physics behind our mathematical model of interest. Having this in mind, for the defocusing nematic equations, consider the following dimensionless quantities:

$$u = \frac{U}{U_0}, \quad x = \frac{X}{W_0}, \quad z = \frac{Z}{D}, \tag{2.3}$$

where U_0, W_0 and D are some characteristic scales. We will see how to select these scales from the physics of our experimental set-up shortly. Substituting (2.3) into the system of equations (2.1) and (2.2) gives

$$i\frac{\partial u}{\partial z} + \frac{1}{2}\frac{D}{k_0 n_e {W_0}^2}\frac{\partial^2 u}{\partial x^2} - \frac{Dk_0\varepsilon_a}{2n_e}\left\{\sin^2\phi - \sin^2\theta_0\right\}u = 0 \tag{2.4}$$

and

$$\frac{8K}{W_0^2|U_0|^2\varepsilon_0\varepsilon_a}\frac{\partial^2\phi}{\partial x^2} + \left\{\frac{4\Delta\varepsilon_{RF}E^2}{|U_0|^2\varepsilon_0\varepsilon_a} + 2|u|^2\right\}\sin 2\phi = 0. \tag{2.5}$$

Let us assume that the extra induced rotation θ of the director, beyond the imposed pre-tilt angle θ_0, much less than the pre-tilt angle, that is to say $|\theta| \ll \theta_0$. Note that this assumption is in agreement with experiments [6]. Then, the trigonometric coefficient in equation (2.4) can be asymptotically simplified as

$$\sin^2\phi - \sin^2\theta_0 = \frac{1}{2}\left\{1 - \cos 2\theta\right\}\cos 2\theta_0 + \sin\theta_0\cos\theta_0\sin 2\theta \sim \theta\sin 2\theta_0. \tag{2.6}$$

Therefore, equations (2.4) and (2.5) become

$$i\frac{\partial u}{\partial z} + \frac{1}{2}\left\{\frac{D}{k_0 n_e W_0^2}\right\}\frac{\partial^2 u}{\partial x^2} - \left\{\frac{Dk_0\varepsilon_a\sin 2\theta_0}{4n_e}\right\}2\theta u = 0 \tag{2.7}$$

and

$$\frac{8K}{W_0^2|U_0|^2\varepsilon_0\varepsilon_a}\frac{\partial^2\phi}{\partial x^2} + \left\{\frac{4\Delta\varepsilon_{RF}E^2}{|U_0|^2\varepsilon_0\varepsilon_a} + 2|u|^2\right\}\sin 2\phi = 0. \tag{2.8}$$

Now, we observe that when we set the terms between the curly brackets in equation

(2.7) equal to 1, we obtain

$$W_0 = \frac{2}{k_0\sqrt{\varepsilon_a \sin 2\theta_0}} \tag{2.9}$$

and

$$D = \frac{4n_e}{k_0\varepsilon_a \sin 2\theta_0}, \tag{2.10}$$

which are well-known expressions for laser beam waist and diffraction length, respectively, in non-linear optical physics [6, 9]. This offers us a good scale choice, based on physics, of the characteristic scales for x and z in (2.3). As for the electric field U, the natural choice to make u in (2.3) a non-dimensional dependent variable is to choose U_0 to be the complex electric field amplitude at the origin of the nematic cell. For simplicity, let us denote

$$\alpha = \frac{8K}{W_0^2|U_0|^2\varepsilon_0\varepsilon_a} \quad \text{and} \quad \beta = \frac{4\Delta\varepsilon_{RF}E^2}{|U_0|^2\varepsilon_0\varepsilon_a}, \tag{2.11}$$

so we have

$$i\frac{\partial u}{\partial z} + \frac{1}{2}\frac{\partial^2 u}{\partial x^2} - 2\theta u = 0 \tag{2.12}$$

and

$$\alpha\frac{\partial^2\phi}{\partial x^2} + \left\{\beta + 2|u|^2\right\}\sin 2\phi = 0. \tag{2.13}$$

In the absence of the optical beam, i.e., no additional molecular rotation θ due to the optical field, we have

$$\alpha\frac{\partial^2\theta_0}{\partial x^2} = -\beta \sin 2\theta_0. \tag{2.14}$$

Substituting equation (2.14) into (2.13) gives

$$\alpha\frac{\partial^2\theta}{\partial x^2} + \beta\left\{\cos 2\theta_0 \sin 2\theta + (\cos 2\theta - 1)\sin 2\theta_0\right\} + 2|u|^2 \sin\left(2\theta_0 + 2\theta\right) = 0. \tag{2.15}$$

With the experimental approximation $|\theta| \ll \theta_0$ and the small enough limit of θ so that the first terms in the Taylor series of $\sin 2\theta$ and $\cos 2\theta$ can be taken, the above equation (2.15) becomes

$$\nu\frac{\partial^2\theta}{\partial x^2} + 2q\theta + 2\,|u|^2 = 0, \tag{2.16}$$

where the non-dimensional parameters ν and q satisfy

$$\nu = \frac{\alpha}{\sin 2\theta_0} = \frac{8K}{W_0^2|U_0|^2\varepsilon_0\varepsilon_a \sin 2\theta_0} \tag{2.17}$$

and

$$q = \frac{\beta}{\tan 2\theta_0} = \frac{4\Delta\varepsilon_{RF}E^2}{|U_0|^2\varepsilon_0\varepsilon_a \tan 2\theta_0}. \tag{2.18}$$

However, in real optics experiments, the Fréedericksz transition does not take place unless the nematic molecules are pre-tilted at an angle more than or close to $\pi/4$, which implies that $\cos(2\theta_0) < 0$ [11]. Therefore, the correct dimensionless nematic equations are

$$i\frac{\partial u}{\partial z} + \frac{1}{2}\frac{\partial^2 u}{\partial x^2} - 2\theta u = 0 \tag{2.19}$$

and

$$\nu\frac{\partial^2\theta}{\partial x^2} - 2q\theta + 2\left|u\right|^2 = 0, \tag{2.20}$$

with

$$q = \frac{\beta}{\left|\tan 2\theta_0\right|} = \frac{4\Delta\varepsilon_{RF}}{\left|U_0\right|^2\varepsilon_0\varepsilon_a\left|\tan 2\theta_0\right|}E^2. \tag{2.21}$$

The parameter ν is termed the non-locality parameter and experimentally it has been found that its value is large; $\nu = \mathcal{O}(200)$ [5, 6]. With this large non-local limit, the molecular director perturbation θ becomes wider than the optical intensity $|u|^2$ profile of the laser beam [5, 6, 7, 8]. In this regard, the nematic reorientational response is non-local. This non-local response and large value of ν play a dominating role in nematic DSW structures. The parameter q, for typical experimental conditions, is of order $\mathcal{O}(1)$ [5, 6, 60, 61]. We note that in the so-called local limit $\nu \to 0$, the defocusing nematic equations (2.19) and (2.20) reduce to the defocusing NLS equation

$$i\frac{\partial u}{\partial z} + \frac{1}{2}\frac{\partial^2 u}{\partial x^2} - \frac{2}{q}|u|^2 u = 0 \tag{2.22}$$

whose DSW theoretical solution is known [62] and numerical solution is given in Figure 1.8(b). While the nematic system takes the form of an NLS-type system, its DSW more resembles a KdV DSW ($p = 1, d = 1$) [60, 61] than an NLS DSW ($p = -1, d = -1$) [62] due to the large non-locality ν, as is observed from the numerical solutions in Chapter 3.

While the system of equations (2.19) and (2.20) has been presented in the context of the non-linear optics of nematic liquid crystals, they are more general than this. The same system of equations arises in the optics of non-linear thermal optical media [64, 65], for example lead glasses [66, 67, 68], and certain photorefractive crystals [69]. A similar system of equations also arises in simplified models of fluid turbulence [70] and in quantum gravity as the Schödinger-Newton equations [71, 72, 73].

The defocusing nematicon system of equations (2.19) and (2.20) can be written in a dispersive hydrodynamic form (1.23) by the use of the so-called Madelung transformation [18]. Within the framework of the nematic equations in this thesis, the Madelung transformation is a polar coordinate representation of the complex, optical, electrical field u propagating through the cell filled with (azo-doped) nematic liquid crystals, expressly,

$$u = \sqrt{\rho}e^{i\phi}, \;\; v = \phi_x. \tag{2.23}$$

Here, the variable ϕ is the full nematic phase, ρ is the squared light wave intensity ($\rho = |u|^2$) and v is the change in the nematic phase ϕ. This transformation leads to the following dispersive hydrodynamic system

$$\underbrace{\frac{\partial\rho}{\partial z} + \rho\frac{\partial v}{\partial x} + v\frac{\partial\rho}{\partial x}}_{\text{Non-dispersive}} = 0, \tag{2.24}$$

$$\underbrace{\frac{\partial v}{\partial z} + v\frac{\partial v}{\partial x} + 2\frac{\partial\theta}{\partial x}}_{\text{Non-dispersive}} = \underbrace{\frac{\partial}{\partial x}\left(\frac{\rho_{xx}}{4\rho} - \frac{\rho_x^2}{8\rho^2}\right)}_{\text{Dispersive}}, \tag{2.25}$$

$$\underbrace{2\rho - 2q\theta}_{\text{Non-dispersive}} = \underbrace{-\nu\frac{\partial^2\theta}{\partial x^2}}_{\text{Dispersive}}. \tag{2.26}$$

We call the above system the "nematic dispersive hydrodynamics." If the dispersive terms in (2.24)–(2.26) are ignored, we recover Euler equations for compressible gas dynamics, or shallow water wave equations with different parameter roles, which are Navier-Stokes equations with zero viscosity and zero external force on a fluid [77]. Because of this analogy, we term the above system nematic dispersive hydrodynamics. In the local limit, $\nu \to 0$, the nematic dispersive hydrodynamics becomes the defocusing NLS dispersive hydrodynamics [62], namely, with $q = 2$,

$$\frac{\partial \rho}{\partial z} + \rho \frac{\partial v}{\partial x} + v \frac{\partial \rho}{\partial x} = 0, \tag{2.27}$$

$$\frac{\partial v}{\partial z} + v \frac{\partial v}{\partial x} + \frac{\partial \rho}{\partial x} = \frac{\partial}{\partial x}\left(\frac{\rho_{xx}}{4\rho} - \frac{\rho_x^2}{8\rho^2} \right). \tag{2.28}$$

It is important to remark that the criterion of having odd derivatives as dispersive terms and even derivatives as non-dispersive terms does not hold for the nematic dispersive hydrodynamics. This criterion is only valid for hydrodynamic systems arises in the context of fluid mechanics, as previously stated in Section 1.4. Instead, we follow the general criterion demonstrated in El's paper [133]. We scale the variables x and z by slow variables, say, $X' = \varepsilon x$ and $Z' = \varepsilon z$, where $0 < \varepsilon \ll 1$. Then, the non-dispersive terms are those of order $\mathcal{O}(1)$ and the rest are the dispersive ones. From this point onwards, we label equation (2.24) the "mass equation" and equation (2.25) the "momentum equation" due to their analogy with the mass and the momentum equations which emerge in shallow water wave theory [1, 77]. There is a much stronger motivation behind adopting these tags which pertains to Nöther's Theorem. We will come back to this in more detail in Section 4.2.

2.2 Research Objectives

The research in this thesis studies various kinds of standard and non-standard DSWs which arise from the defocusing nematic equations (2.19) and (2.20), which govern an optical beam propagating in the non-linear optical medium of a nematic liquid crystal [6, 74, 75].

To generate a DSW for our underlying physical system, we impose a step initial condition that represents an abrupt change in the intensity/power of the optical electric field u at $z = 0$, the input position of the beam into the nematic cell is

$$u(x,0) = \begin{cases} u_- e^{i\phi_-}, & x < 0 \\ u_+ e^{i\phi_+}, & x > 0, \end{cases} \tag{2.29}$$

where the initial nematic phases ϕ_- and ϕ_+ are

$$\phi_- = v_- x \quad \text{and} \quad \phi_+ = v_+ x. \tag{2.30}$$

The constants v_- and v_+ in the expressions (2.30) play the role of initial wavenumbers. The nematic molecular response equation (2.20) shows that the consistent initial condition for the resulting director angle θ is

$$\theta(x,0) = \begin{cases} \frac{u_-^2}{q}, & x < 0 \\ \frac{u_+^2}{q}, & x > 0. \end{cases} \tag{2.31}$$

Unfortunately, the nematic equations form a non-integrable system and a general exact theoretical solution has not been found in literature. The nematic response equation (2.20) is a damped, linear, elliptic PDE (forced Helmholtz-like equation) with constant coefficients. Hence, its solution can be expressed in terms of a Green's function. However, when this Green's function is substituted ino the electric field equation (2.19), the result is an involved non-linear, non-local, dispersive wave equation which is not integrable and has no known general exact solution, see e.g. [76]. Therefore, to obtain an insight into the nematic DSW solution, we shall solve the problem using numerical methods. Numerical solutions show that there are several non-dispersive and dispersive hydrodynamic regimes, depending significantly upon the optical intensity difference $|u_- - u_+|$ and the values of the initial phases ϕ_- and ϕ_+. In most of the numerical solutions, nematic DSWs were found to be resonant DSWs, that for which there is a resonance between the waves of the DSW and linear dispersive radiation. This is not a standard form of a DSW as it is not the classical KdV or NLS DSWs. The observed resonance has a major effect on the DSW structure as the resonant radiation leaks mass and energy from it. The effect of the resonant radiation on the nematic DSW structure will be discussed in detail in this thesis.

There have been a number of studies of nematic DSWs recently [60, 61]. However, several disagreements between theoretical and numerical solutions over the full range of the initial intensity strengths $|u_- - u_+|$ were found. The reasons why there was not satisfactory agreement in [60] were that the nematic DSW was assumed to be a KdV-type DSW and a reductive third order nematic KdV equation was used to study the nematic DSW theoretically, rather than using the full reductive nematic Kawahara (fifth order KdV) equation [78], especially when the initial jump $|u_- - u_+|$ is small. On the other hand, when the initial jump $|u_- - u_+|$ is large, it was assumed in [61] that the DSW has a gas dynamic shock jump condition rather than a "Whitham shock" jump condition [81, 85]. These assumptions do not hold over the full range of initial jumps in the optical intensity, as is found in this thesis. The main objective of this thesis is to develop a comprehensive analytical treatment which covers all regimes for the nematic DSW and in agreement with numerical solutions.

Chapter 3

Numerical Method and Simulations

In this chapter, we present an efficient numerical method that solves the governing defocusing nematic equations (2.19)–(2.20) subject to the initial jump condition (2.29) and the resulting one (2.31). As discussed in Chapter 2, this mathematical model is a non-integrable system. It is helpful then to implement a numerical method that solves this model and allows us to identify what form a nematic DSW evolves to. We utilise a numerical approach similar to the efficient one developed by Fornberg and Whitham [86, 89] to solve non-linear dispersive wave equations typified by the KdV equation and its generalisations. They used Fourier (spectral) and leap-frog (centred-difference) methods to calculate the spatial and temporal coordinates of the equations, respectively. Here, instead of using a leap-frog numerical scheme, we deploy the method of 4^{th} order Runge-Kutta (RK4) as it is faster and its numerical accuracy is higher. To improve the stability of our numerical scheme, the method of integrating factors will be used, as explained in [87, 88, 89]. In principle, the mathematical formations of DSWs are unrelated to spatial boundaries, so they do not require specific/complicated boundary conditions, only an initial condition in a form of step is needed, resulting in a periodic boundary condition. For this reason, the use of spectral methods is the best option for the computation of DSWs. This is in addition to the undefeated speed of algorithms with $\mathcal{O}(N \ln N)$, where N is the number of spatial grids [90].

3.1 Pseudo-spectral Method

We start by applying the continuous Fourier transform to the NLS-type equation (2.19)

$$\frac{d}{dz}\mathcal{F}\{u(x,z);f\} + \frac{if^2}{2}\mathcal{F}\{u(x,z);f\} + i\mathcal{F}\{2\theta(x,z)u(x,z);f\} = 0, \tag{3.1}$$

where $f \in \mathbb{R}$ represents the frequency. Here, the adopted definitions of the continuous Fourier transform and its inverse transform are

$$\mathcal{F}\{u(x,z);f\} = \hat{u}(f,z) = \int_{-\infty}^{\infty} u(x,z)e^{2\pi i x f}\,dx, \tag{3.2}$$

$$\mathcal{F}^{-1}\{\hat{u}(f,z);x\} = u(x,z) = \int_{-\infty}^{\infty} \hat{u}(f,z)e^{-2\pi i x f}\,df, \tag{3.3}$$

respectively. Equation (3.1) is an ODE equation in the time-like variable z. Since we aim to solve this problem numerically, then we have to discretise the spatial, frequency and temporal-like domains. Assume that we are interested in the spatial computational domain

$$x \in \left[-\frac{L}{2}, \frac{L}{2}\right], \tag{3.4}$$

and we want to discretise it into $N-$equidistant samples (grids) such that N satisfies $N = 2^j$ for some $j \in \mathbb{N}$. Such choice of N is necessary when it comes to applying the fast Fourier transform method (FFT) [89, 90, 91]. Then a discretisation of the variable x reads

$$x_n = n\Delta x; \quad n \in \left\{-\frac{N}{2}+1, ..., \frac{N}{2}\right\}, \tag{3.5}$$

where the sampling rate is $\Delta x = L/N$. The frequency domain is discretised so that the aliasing phenomenon does not occur [89, 91]. Aliasing is a computational phenomenon by which undesired low frequency waves can take on the appearance or the identity of high frequency waves due to discretisation and discrete sampling of a continuous wave. To be specific, we have to restrict the range of the frequencies values to be

$$f_k = k\Delta f; \quad k \in \left\{-\frac{N}{2}+1, ..., \frac{N}{2}\right\}, \tag{3.6}$$

where the frequency resolution satisfies $\Delta f = 2\pi/N\Delta x = 2\pi/L$ [89, 91]. Therefore, equation (3.1) takes the following discretised form

$$\frac{d}{dz}\hat{u}_k(z) + \frac{i}{2}f_k^2\hat{u}_k(z) + i\mathcal{F}\left\{2\theta_n(z)u_n(z); k\right\} = 0. \tag{3.7}$$

The time-like variable z will be dealt with shortly. With the discretisation of the variables x and u, the continuous Fourier transforms (3.2)–(3.3) must be discretised as well. The discrete version of the Fourier transform is merely the Riemann sum of its integral. Thus, the discrete Fourier transform (DFT) is defined as

$$\hat{u}_k(z) = \sum_{n=-N/2+1}^{N/2} u_n(z)e^{2\pi ink/N}, \tag{3.8}$$

while the inverse discrete Fourier transform (IDFT) is given by

$$u_n(z) = \frac{1}{N}\sum_{k=-N/2+1}^{N/2} \hat{u}_k(z)e^{-2\pi ink/N}. \tag{3.9}$$

The parameter Δx in the above Riemann summations (3.8) and (3.9) is neglected because the discrete Fourier transform basically maps the complex functions $u_n(z)$ into the complex functions $\hat{u}_k(z)$ without a necessary dependence on the sampling rate [91].

There is a "stiffness" problem arising in this numerical scheme and is due to the term u_{xx} in the electric field equation (2.19). This term involves high frequencies, f_k^2, in the discretised electric field equation (3.7) which can delay numerical stabilities. Including such a stiff term in the numerical scheme requires the use of a very small sampling rate to achieve stability, so it is expensive. To overcome this problem and suppress instabilities at high frequencies, we use the method of integrating factors [87, 88, 89]. Following this approach, we multiply the ODE (3.7) by the integrating factor $e^{if_k^2 z/2}$

which yields

$$\frac{d}{dz}\left\{e^{if_k^2 z/2}\hat{u}_k(z)\right\} = -i\mathcal{F}\left\{2\theta_n(z)u_n(z);k\right\}e^{if_k^2 z/2}. \tag{3.10}$$

The director angle $\theta_n(z)$ is determined from the director equation (2.20). When we apply the DFT to the director equation, we obtain

$$\hat{\theta}_k(z) = \frac{2\widehat{u_k^2}(z)}{\nu f_k^2 + 2q}, \tag{3.11}$$

which gives $\theta_n(z)$ through the application of the IDFT, i.e.,

$$\theta_n(z) = \mathcal{F}^{-1}\left\{\frac{2\widehat{u_k^2}(z)}{\nu f_k^2 + 2q}; n\right\}. \tag{3.12}$$

Another possible and fast way, but might affect the spectral accuracy of the numerical scheme, to find $\theta_n(z)$ is by using a Fourier transform based on a finite difference method. This is commonly used for Poisson or Helmholtz boundary value problems, refer to [91]. The basic idea is to discretise the spatial second order derivative in (2.20) by, for example, a leap-frog scheme, which leads to

$$\frac{\nu}{\Delta x^2}\left\{\theta_{n+1}(z) - 2\theta_n(z) + \theta_{n-1}(z)\right\} - 2q\theta_n(z) + 2|u_n|^2(z) = 0, \tag{3.13}$$

and then use the IDFTs of the functions $\theta_n(z)$ and $u_n(z)$, following the definition (3.9), so that we end up with the expression

$$\hat{\theta}_k(z) = \frac{\widehat{u_k^2}(z)}{q - \frac{\nu}{\Delta x^2}\left\{\cos\left(\frac{2\pi k}{N}\right) - 1\right\}}. \tag{3.14}$$

This enables us to deduce $\theta_n(z)$ via applying the IDFT. In a real experimental set-up [6, 92], the molecular angle θ is fixed at the boundaries of a nematic cell as the molecules are anchored by polymer films, as discussed in Section 1.3. However, we are not looking at the full nematic cell as the wave propagation takes place in the middle of the cell, which is far from the boundaries. We can now substitute either the formula (3.12) or the IDFT of (3.14) into the electric field equation (3.10) and solve the ODE problem by employing the RK4 method.

Now let us consider the following z computational domain

$$z \in [0, T] \tag{3.15}$$

to be discretised. We divide this into M-equispaced grid points for which

$$z_m = m\Delta z; \quad m \in \{0, ..., M-1\}, \tag{3.16}$$

and the temporal-like step is $\Delta z = T/M$. Let us denote

$$R\left(\hat{u}_k^m, z_m\right) = -i\mathcal{F}\left\{2\mathcal{F}^{-1}\left\{\hat{\theta}_k^m; n\right\}\mathcal{F}^{-1}\left\{\hat{u}_k^m; n\right\}; k\right\}. \tag{3.17}$$

Hence, the solution of the discretised electric field equation (3.10) from the RK4 procedure [93] reads

$$\hat{u}_k^{m+1} = \hat{u}_k^m + \frac{1}{6}\left\{r_1 + 2r_2 + 2r_3 + r_4\right\}, \tag{3.18}$$

with

$$r_1 = \Delta z R\left(\hat{u}_k^m, z_m\right), \tag{3.19}$$

$$r_2 = \Delta z R\left(\hat{u}_k^m + \frac{1}{2}r_1, z_m + \frac{1}{2}\Delta z\right), \tag{3.20}$$

$$r_3 = \Delta z R\left(\hat{u}_k^m + \frac{1}{2}r_2, z_m + \frac{1}{2}\Delta z\right), \tag{3.21}$$

$$r_4 = \Delta z R\left(\hat{u}_k^m + r_3, z_m + \Delta z\right). \tag{3.22}$$

Finally, the solutions u_n^m are calculated by applying the DFT to (3.18). The computation of the Fourier coefficients $\hat{u}_k^m$ and u_n^m in the DFT and IDFT is performed by the FFT and inverse fast Fourier transform (IFFT) methods [89, 90, 91], in the order given.

The final thing that we need to deal with is the fitting of an initial step into the Fourier spectral method that generates a periodic solution. We can impose periodicity in our computational domain by taking an initial condition as a "top hat" joining the initial levels u_- and u_+, but which has a jump down to u_+ to enforce periodicity, as illustrated in Figure 3.1. From this figure, moreover, we recognise that the numerical solution at the initial jump from u_- to u_+ is symmetric to the one in the opposite direction. Therefore, we only focus on the right hand side initial jump here. The theoretical sharp discontinuities at the both jumps must be smoothed to ensure that Gibbs' phenomenon [99] will not take place. This can be done by using hyperbolic tangent functions. To be mathematically specific, this is smoothing given by

$$u(x_n, 0) = \left\{\frac{1}{2}\left(u_- - u_+\right)\left(\tanh\frac{x_n + D}{W} - \tanh\frac{x_n}{W}\right) + u_+\right\} e^{i\phi(x_n,0)}, \tag{3.23}$$

with $\phi(x_n, 0) = v(x_n, 0)x_n$ smoothed in a similar fashion, namely,

$$v(x_n, 0) = \frac{1}{2}\left\{v_- - v_+\right\}\left\{\tanh\frac{x_n + D}{W} - \tanh\frac{x_n}{W}\right\} + v_+. \tag{3.24}$$

The width W was chosen to be large enough to stop instabilities, but small enough to well approximate a step. In practice, $W = 1$ was found suitable. The distance D at which the initial condition goes back to the level u_+ was chosen large enough so that the waves generated from the step at $x = 0$ do not interact with the step down, with $D = 10000$ found suitable.

As for the change in the phase v, it is calculated through differentiating the Madelung transformation (2.23):

$$u_x = \left\{|u|_x + i|u|\phi_x\right\} e^{i\phi} \quad \Longrightarrow \quad \phi_x = v = \mathrm{Im}\left(\frac{u_x}{u}\right). \tag{3.25}$$

Then, it is computed numerically by discretising the derivative term u_x by a leap-frog scheme, as its accuracy is of order 2. We then acquire

$$v_n^m = \mathrm{Im}\left(\frac{u_{n+1}^m - u_{n-1}^m}{2\Delta x^2 u_n^m}\right). \tag{3.26}$$

Finally, to achieve numerical stability and have the scheme robust, suitable number of Fourier modes were found to be $N = 2^{17} = 131072$, with a z step $\Delta z = 0.005$ and domain range $L = 32768$. All the comparisons with numerical solutions will be for the

parameter choices $q = 2$ and $\nu = 200$. In particular, the value of the non-locality ν depends on the beam power and wavelength, but $\nu = 200$ is typical for near-infrared beams of milliwatt powers [101, 102, 103, 104].

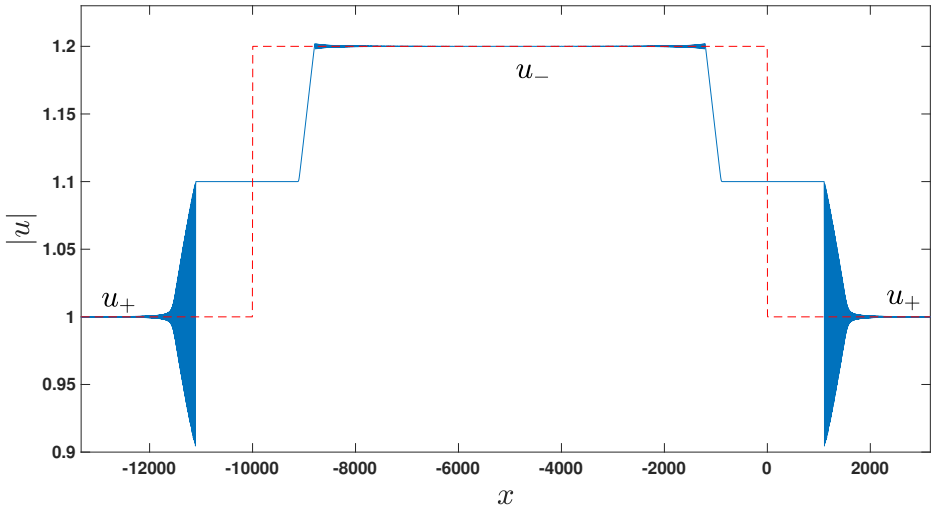

Figure 3.1: The initial top hat (3.23); red (dashed) line. A nematic numerical solution, computed from (3.18), is symmetric at the right and left initial jumps due to the periodicity of Fourier spectral method; blue (solid) line. Here, $z = 1000$, $u_- = 1.2$, $u_+ = 1.0$, $\nu = 0.2$ and $q = 2$. (Online version in colour.)

3.2 Results and Discussions

3.2.1 Zero Initial Phase Jumps

Consider first the numerical solution of the nematic equations (2.19) and (2.20) with the initial discontinuities (2.29) and (2.31) for no jump in the phase; $\phi_- = \phi_+ = 0$. The solution depends critically on the initial jump height $u_- - u_+$, with five various DSW regimes, plus one dispersionless regime possible. Figures 3.2 to 3.7 show these hydrodynamic structures. Four of these DSW types are similar to some extent to those for the Kawahara equation (1.40) [79, 80]. The other two are related to the existence of the vacuum cases with $u = 0$ at some point. These solutions will be for the particular values $u_- = 1$, with varying u_+, with $\nu = 200$ and $q = 2$.

- **Regime 1. Perturbed dispersive shock wave (PDSW):**

  This regime is numerically identified for $0.76 < u_+ < 1.0$ and is shown in Figure 3.2. The nematic DSW of this type resembles the standard KdV DSW ($p = 1, d = 1$) [86, 105], with a monotonic modulated wavetrain consisting of bright solitary waves at the leading edge and linear waves at the trailing edge. There is no resonant wavetrain ahead of the DSW as there is no resonance between the phase velocity of a possible resonant wavetrain and the DSW [60, 61]. As the nematic equations (2.19) and (2.20) are bi-directional, there is also a backwards propagating expansion wave, as for the compressible flow shock tube problem [1, 106], which links the level behind u_- and an intermediate shelf of height $|u| = u_i$ behind the DSW. The DSW takes the place of the shock in the Sod

shock tube problem. Thus, this DSW structure is the dispersive analogue of the Sod shock tube problem. The solution for this DSW type will be found as a perturbation of the KdV DSW ($p = 1, d = 1$).

- **Regime 2. Radiating dispersive shock wave (RDSW):**

  This structure takes place in the interval $0.70 < u_+ < 0.76$. When the jump height reaches the critical value being $u_- - u_+ < 0.24$, resonance can exist between the DSW and diffractive waves (dispersive waves), so that a resonant wavetrain ahead of the DSW is generated, as shown in Figure 3.3. The DSW itself resembles a KdV DSW ($p = 1, d = 1$), but with an attached resonant wavetrain. This case resembles the equivalent RDSW type for the Kawahara equation [79]. The DSW itself will be found to be a perturbed KdV DSW ($p = 1, d = 1$), as for the PDSW regime.

- **Regime 3. Crossover dispersive shock wave (CDSW):**

  This type occurs in the range $0.44 < u_+ < 0.70$. With increasing jump height, the DSW becomes unstable, as does its resonant wavetrain, as seen in Figure 3.4. The DSW loses its rank ordered structure and the resonant wavetrain has a highly modulated amplitude. Again, this DSW structure is similar to its equivalent for the Kawahara equation [79].

- **Regime 4. Travelling dispersive shock wave (TDSW):**

  This nematic DSW structure exists for $0.22 < u_+ < 0.44$. Here, the DSW itself disappears, leaving just a resonant wavetrain, as shown in Figure 3.5. This solution form is similar to the travelling DSW (TDSW) found for the Kawahara equation (1.40) [79]. A remnant of the DSW is left in the form of a negative polarity solitary wave (termed Whitham shock) which links the resonant wavetrain to the intermediate level. It is further seen that the resonant wavetrain is of higher amplitude than in the CDSW case and has stabilised.

- **Regime 5. Vacuum dispersive shock wave (VDSW):**

  This regime arises for $0 < u_+ < 0.22$. As u_+ decreases, the jump height increases, and the amplitude of the resonant wavetrain grows, so that the minimum of its oscillation eventually hits the vacuum point $u = 0$, at which point there is a phase singularity and the DSW solution changes form, as illustrated in Figure 3.6. A constant amplitude resonant wavetrain now propagates on a varying mean level. Behind this, there is a resonant wavetrain on a constant mean level, which is linked to the intermediate level by a negative polarity wave, as for the TDSW. A similar vacuum point solution occurs for the defocusing NLS equation [62, 63], but without the accompanying resonant wavetrain.

- **Regime 6. Dam break problem:**

  When the initial level ahead $u_+ = 0$, the numerical solution becomes essentially non-diffractive, namely, non-dispersive, as depicted in Figure 3.7. This solution is referred to as the dam break solution because it is a simple wave solution of the shallow water wave equations and emerges as a solution for the flow generated by a breaking dam [1]. Note that there are some small wiggles near the corner where the simple wave solution meets the initial level ahead. This is because of the discontinuity in derivatives being smoothed by the effect of dispersion [86].

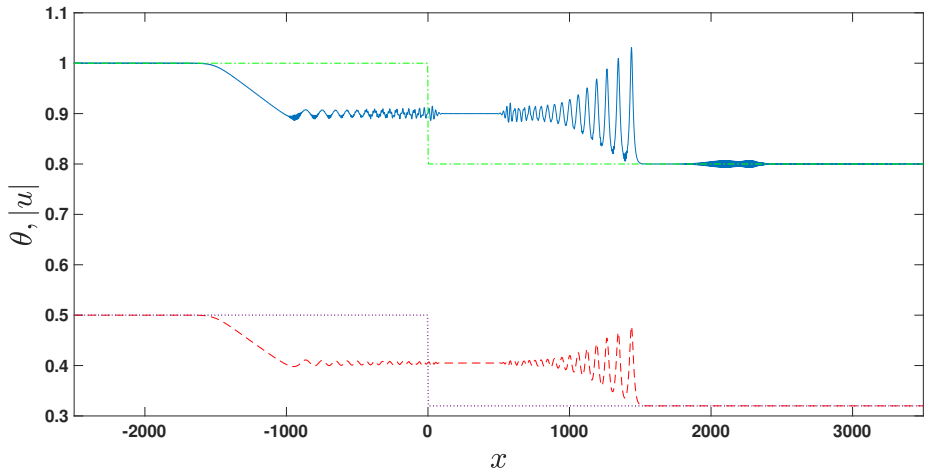

Figure 3.2: Regime 1, PDSW regime. Numerical solutions of the nematic equations (2.19) and (2.20) for the initial conditions (2.29) and (2.31). Blue (solid) line: $|u|$ at $z = 1500$; red (dashed) line θ at $z = 1500$; green (dash-dot) line: $|u|$ at $z = 0$ and violet (dotted) line θ at $z = 0$. Here, $u_- = 1.0$, $u_+ = 0.8$, $\nu = 200$ and $q = 2$. (Online version in colour.)

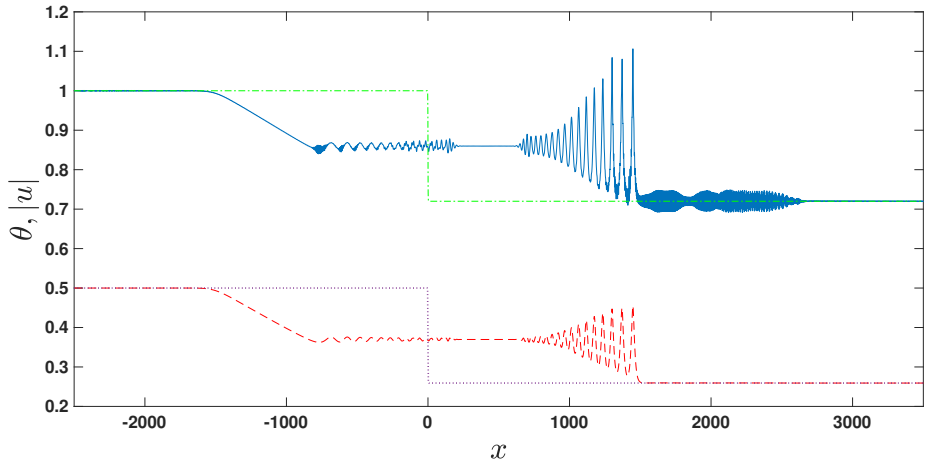

Figure 3.3: Regime 2, RDSW regime. Numerical solutions of the nematic equations (2.19) and (2.20) for the initial conditions (2.29) and (2.31). Blue (solid) line: $|u|$ at $z = 1500$; red (dashed) line θ at $z = 1500$; green (dash-dot) line: $|u|$ at $z = 0$ and violet (dotted) line θ at $z = 0$. Here, $u_- = 1.0$, $u_+ = 0.72$, $\nu = 200$ and $q = 2$. (Online version in colour.)

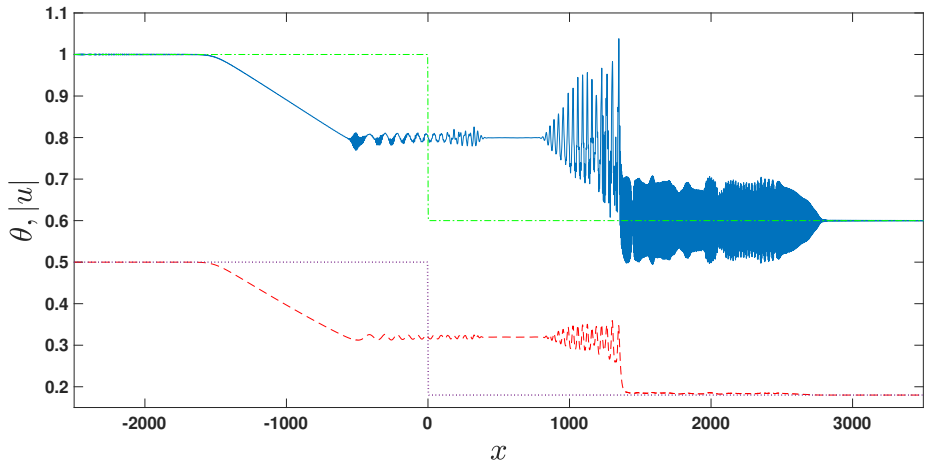

Figure 3.4: Regime 3, CDSW regime. Numerical solutions of the nematic equations (2.19) and (2.20) for the initial conditions (2.29) and (2.31). Blue (solid) line: $|u|$ at $z = 1500$; red (dashed) line θ at $z = 1500$; green (dash-dot) line: $|u|$ at $z = 0$ and violet (dotted) line θ at $z = 0$. Here, $u_- = 1.0$, $u_+ = 0.6$, $\nu = 200$ and $q = 2$. (Online version in colour.)

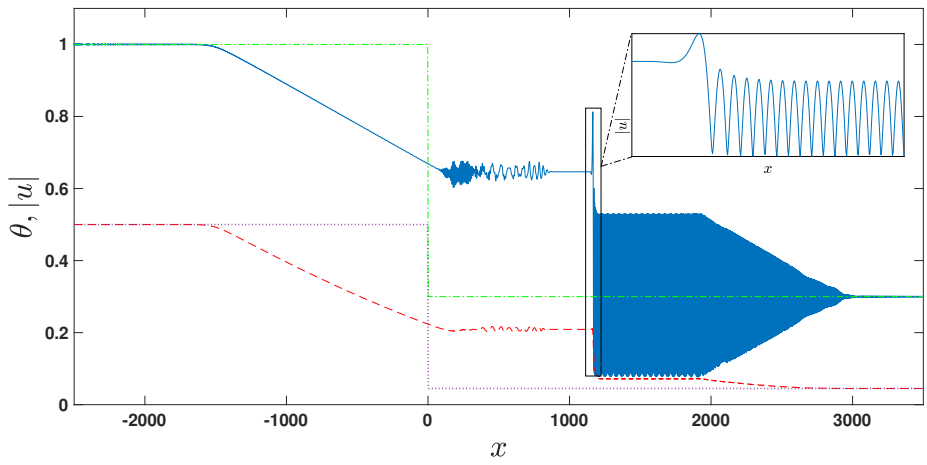

Figure 3.5: Regime 4, TDSW regime. Numerical solutions of the nematic equations (2.19) and (2.20) for the initial conditions (2.29) and (2.31). Blue (solid) line: $|u|$ at $z = 1500$; red (dashed) line θ at $z = 1500$; green (dash-dot) line: $|u|$ at $z = 0$ and violet (dotted) line θ at $z = 0$. Here, $u_- = 1.0$, $u_+ = 0.3$, $\nu = 200$ and $q = 2$. (Online version in colour.)

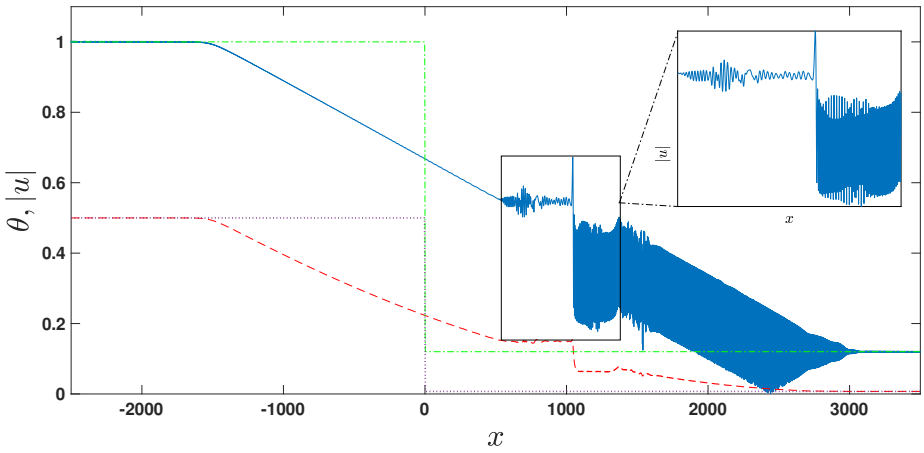

Figure 3.6: Regime 5, VDSW regime. Numerical solutions of the nematic equations (2.19) and (2.20) for the initial conditions (2.29) and (2.31). Blue (solid) line: $|u|$ at $z = 1500$; red (dashed) line θ at $z = 1500$; green (dash-dot) line: $|u|$ at $z = 0$ and violet (dotted) line θ at $z = 0$. Here, $u_- = 1.0$, $u_+ = 0.12$, $\nu = 200$ and $q = 2$. (Online version in colour.)

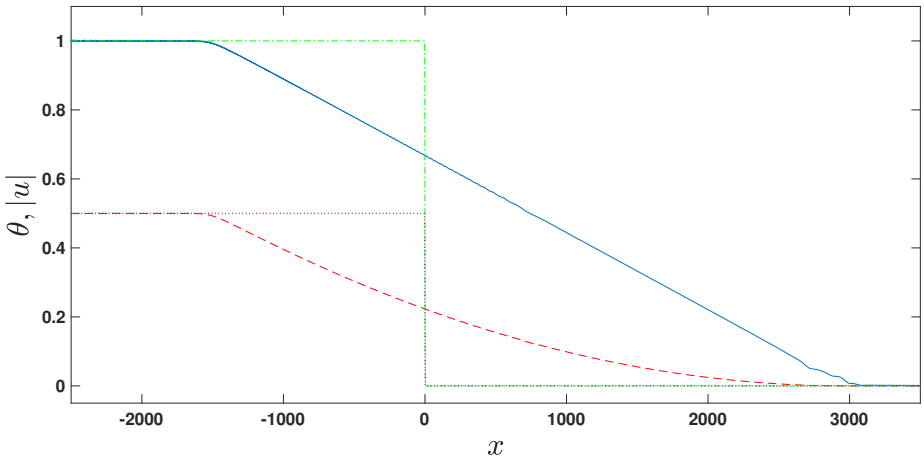

Figure 3.7: Regime 6, dam break problem. Numerical solutions of the nematic equations (2.19) and (2.20) for the initial conditions (2.29) and (2.31). Blue (solid) line: $|u|$ at $z = 1500$; red (dashed) line θ at $z = 1500$; green (dash-dot) line: $|u|$ at $z = 0$ and violet (dotted) line θ at $z = 0$. Here, $u_- = 1.0$, $u_+ = 0.0$, $\nu = 200$ and $q = 2$. (Online version in colour.)

3.2.2 Non-zero Initial Phase Jumps

Let us consider next the solution of the nematic equations (2.19) and (2.20) with the initial discontinuities (2.29) and (2.31) for non-zero jumps in the phase, in other words, $\phi_-,\ \phi_+ \neq 0$. These new DSW types involve combinations of resonant DSWs and rarefaction waves identified for v_- and v_+. These numerical solutions are slightly similar to those for Calogero-Sutherland (CS) dispersive hydrodynamics [107] and the defocusing NLS equation [62]. However, the nematic solutions are much more complicated. This is due to the strong effect of the non-locality and possible resonant radiations making the nematic solutions different than those that were mentioned above. The way to classify the new solutions in this section is via specifying particular inequalities which are derived from Riemann invariants of the nematic dispersive hydrodynamics (2.24)–(2.26) in the dispersionless limit. These Riemann invariants will be derived in Chapter 5. The inequalities are given in the expressions (3.27)–(3.32) below. They will be stated here and verified in Section 5.2. Based on the numerical simulations depicted in Figures 3.8 to 3.13, we provide the following descriptions:

- **Case 1. Slow simple wave and fast DSW:**

  The solution for this case is merely that outlined previously for $v_- = v_+ = 0$. It is one of the hydrodynamic regimes in the previous subsection based on the jump height at $z = 0$. We have an expansion fan, propagating in the upstream (left) direction and a DSW travelling in the opposite direction, both of which are joined by an intermediate shelf $u_i,\ v_i$. Any of Figures 3.2 to 3.7 is an example for this case. The existence region for this case, in terms of the nematic Riemann invariants, is

  $$v_- - 2\sqrt{\frac{2}{q}}u_- \leq v_+ - 2\sqrt{\frac{2}{q}}u_+ \quad \text{and} \quad v_- + 2\sqrt{\frac{2}{q}}u_- \geq v_+ + 2\sqrt{\frac{2}{q}}u_+. \tag{3.27}$$

- **Case 2. A pair of DSWs connected by a steady level:**

  In this case, no expansion wave exists and we are left with two DSWs of crossover type, unlike the NLS and CS dispersive hydrodynamics where the DSWs are of NLS and KdV-type, respectively [62, 107]. We have one DSW which propagates to the right and another one which travels to the left. They are both linked by an intermediate shelf $u_i,\ v_i$ that rises above both the rear $u_-,\ v_-$ and the front $u_+,\ v_+$ levels. The existence region for this case, in terms of the nematic Riemann invariants, is

  $$v_- - 2\sqrt{\frac{2}{q}}u_- > v_+ - 2\sqrt{\frac{2}{q}}u_+ \quad \text{and} \quad v_- - 2\sqrt{\frac{2}{q}}u_- \leq v_+ + 2\sqrt{\frac{2}{q}}u_+. \tag{3.28}$$

  A numerical solution for this case is illustrated in Figure 3.8 and a suitable selection of the parameters $u_+,\ u_-,\ v_+$ and v_- is captioned in the figure.

- **Case 3. Fast simple wave and slow DSW:**

  When the orientation of the initial jump in Case 1 is reversed, i.e., $u_- < u_+$, then the DSW and the expansion fan flip around, with $u_- < u_i < u_+$. Thus, the solution in this case consists of an expansion fan moving in the downstream (right) direction which connects the initial levels $u_+,\ v_+$ ahead to an intermediate shelf $u_i,\ v_i$. The solution is then taken from this intermediate shelf to the upstream initial levels $u_-,\ v_-$. Obviously, the theoretical solution of this case is going to

be similar to Case 1, the sole distinction is the waves' propagation direction. The existence region for this case, in terms of the nematic Riemann invariants, is

$$v_- - 2\sqrt{\frac{2}{q}}u_- > v_+ - 2\sqrt{\frac{2}{q}}u_+ \quad \text{and} \quad v_- + 2\sqrt{\frac{2}{q}}u_- < v_+ + 2\sqrt{\frac{2}{q}}u_+. \tag{3.29}$$

A numerical solution for this case is shown in Figure 3.9 and an appropriate choice of the parameters $u_+,\ u_-,\ v_+$ and v_- is captioned in the figure.

- **Case 4. Two simple waves linked by a constant plateau:**

  Here, the solution is composed of two expansion waves travelling in opposite directions with their lower edges anchored at an intermediate shelf $u_i,\ v_i$. This shelf sits below the front and rear initial levels, that is to say $u_- < u_i < u_+$. Looking at Figure 3.10 or 3.11, we can see that this solution forms a hybrid solution between the expansion fans in Case 1 and Case 3. An additional observation is that as the time-like variable z evolves, two small modulated wavetrains are created on the shelf. This is because two small jumps in the centre of the intermediate level are generated, which create small DSWs. As the DSWs are resonant, resonant dispersive waves are also produced. The existence region for this case, in terms of the nematic Riemann invariants, is

$$v_- + 2\sqrt{\frac{2}{q}}u_- < v_+ + 2\sqrt{\frac{2}{q}}u_+ \quad \text{and} \quad v_- + 2\sqrt{\frac{2}{q}}u_- \geq v_+ - 2\sqrt{\frac{2}{q}}u_+. \tag{3.30}$$

  A numerical solution for this case is shown in Figures 3.10 and 3.11 at different z for a suitable selection of the parameters $u_+,\ u_-,\ v_+$ and v_- as captioned in the figures.

- **Case 5. Two simple waves and a vacuum region:**

  This solution is shown in Figure 3.12. This is similar to the previous case, but with the intermediate level u_i approaching the vacuum $u = 0$ as z advances, as occurs for the defocusing NLS DSW [62, 63] and the CS DSW [107]. The existence region for this case, in terms of the nematic Riemann invariants, is

$$v_- + 2\sqrt{\frac{2}{q}}u_- < v_+ - 2\sqrt{\frac{2}{q}}u_+. \tag{3.31}$$

  A suitable choice of the parameters $u_+,\ u_-,\ v_+$ and v_- is captioned in the figure.

- **Case 6. A pair of fast and slow interacting DSWs:**

  The solution for this case occurs when two DSWs collide and interact with each other, analogous to the NLS and CS dispersive hydrodynamics [107, 108]. The solution for this structure is then a two phase wavetrain, which is difficult to analyse without the full Whitham modulation equations. The solution of Figure 3.13 shows two interacting TDSWs. There are two partial DSWs on either side of the central wavetrain, which is (almost) a uniform resonant wavetrain. In essence, the interaction has destroyed the intermediate shelf so that the two individual TDSWs can join with each other. The existence region for this case, in terms of the nematic Riemann invariants, is

$$v_- - 2\sqrt{\frac{2}{q}}u_- > v_+ + 2\sqrt{\frac{2}{q}}u_+. \tag{3.32}$$

An appropriate choice of the parameters u_+, u_-, v_+ and v_- is captioned in the figure.

Expressions (3.27)–(3.32) comprise four arbitrary parameters u_-, u_+, v_- and v_+. To construct a simple geometrical visualisation of the classification of these new cases, we set $u_+ = 1$, $v_+ = 0$ and plot a classification diagram in the coordinate system (u_-, v_-), as shown in Figure 3.14. Note that changing the parameter values of u_+ and v_+ does not affect the classification.

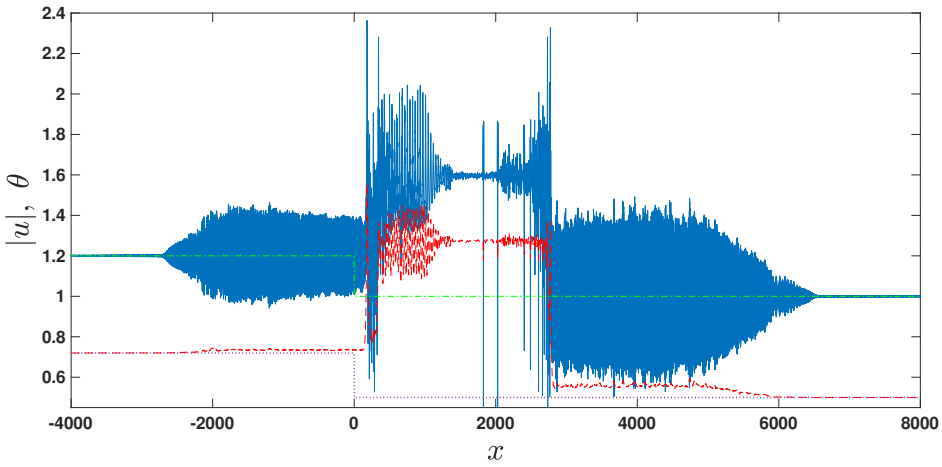

Figure 3.8: Case 2, a pair of DSWs connected by a steady level. Numerical solutions of the nematic equations (2.19) and (2.20) for the initial conditions (2.29) and (2.31). Blue (solid) line: $|u|$ at $z = 1500$; red (dashed) line θ at $z = 1500$; green (dash-dot) line: $|u|$ at $z = 0$ and violet (dotted) line θ at $z = 0$. Here, $u_- = 1.2$, $u_+ = 1.0$, $v_- = 2$, $v_+ = 0$ and $q = 2$. (Online version in colour.)

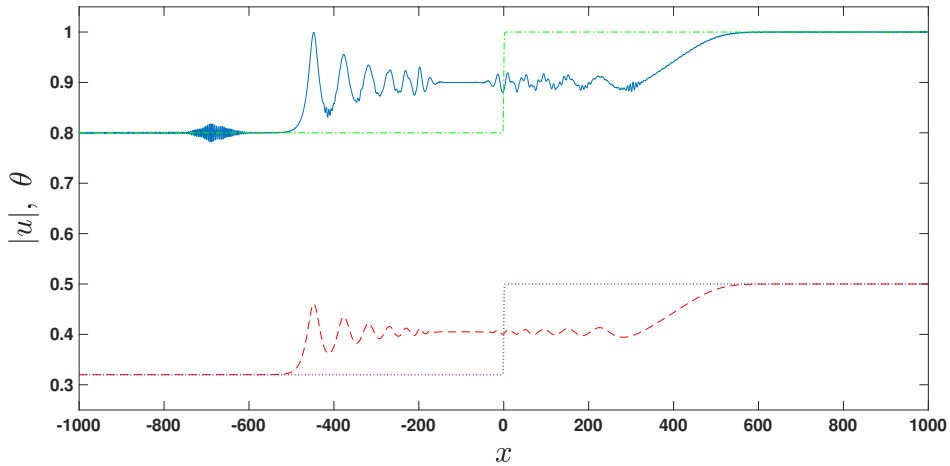

Figure 3.9: Case 3, fast simple wave and slow DSW. Numerical solutions of the nematic equations (2.19) and (2.20) for the initial conditions (2.29) and (2.31). Blue (solid) line: $|u|$ at $z = 500$; red (dashed) line θ at $z = 500$; green (dash-dot) line: $|u|$ at $z = 0$ and violet (dotted) line θ at $z = 0$. Here, $u_- = 0.8$, $u_+ = 1.0$, $v_- = 0$, $v_+ = 0$ and $q = 2$. (Online version in colour.)

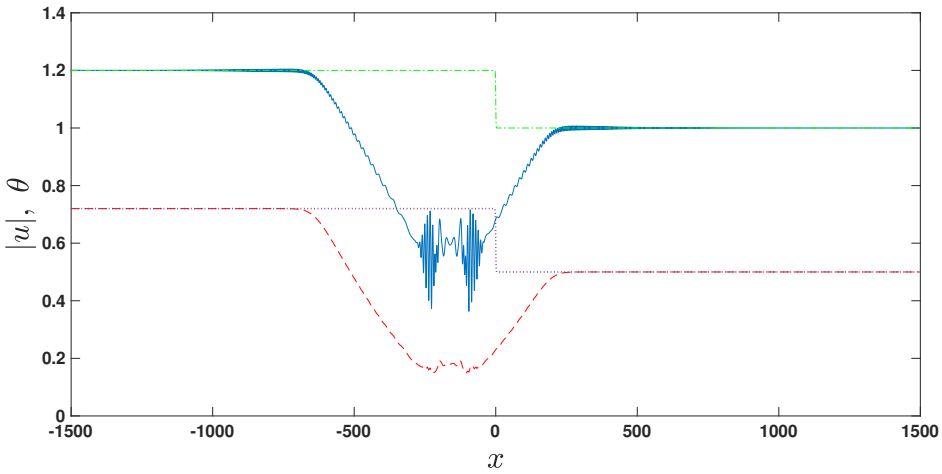

Figure 3.10: Case 4, two simple waves linked by a constant plateau. Numerical solutions of the nematic equations (2.19) and (2.20) for the initial conditions (2.29) and (2.31). Blue (solid) line: $|u|$ at $z = 200$; red (dashed) line θ at $z = 200$; green (dash-dot) line: $|u|$ at $z = 0$ and violet (dotted) line θ at $z = 0$. Here, $u_- = 1.2$, $u_+ = 1.0$, $v_- = -2$, $v_+ = 0$ and $q = 2$. (Online version in colour.)

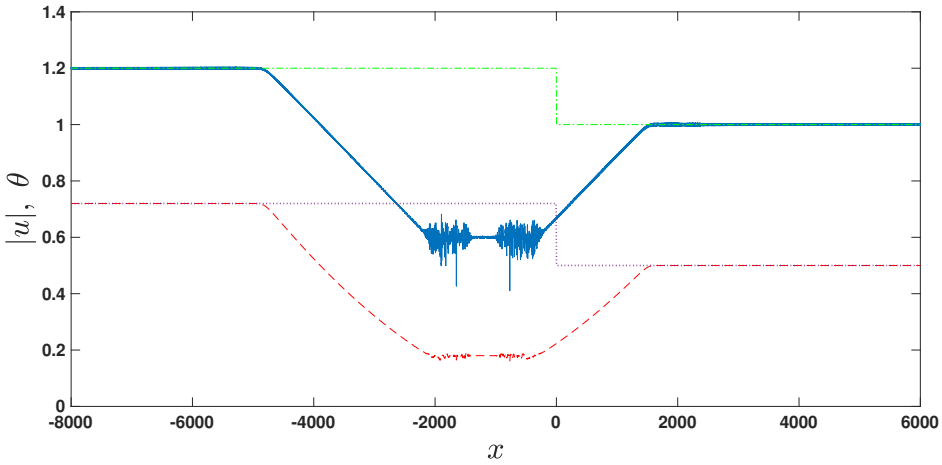

Figure 3.11: Case 4, two simple waves linked by a constant plateau. Numerical solutions of the nematic equations (2.19) and (2.20) for the initial conditions (2.29) and (2.31). Blue (solid) line: $|u|$ at $z = 1500$; red (dashed) line θ at $z = 1500$; green (dash-dot) line: $|u|$ at $z = 0$ and violet (dotted) line θ at $z = 0$. Here, $u_- = 1.2$, $u_+ = 1.0$, $v_- = -2$, $v_+ = 0$ and $q = 2$. (Online version in colour.)

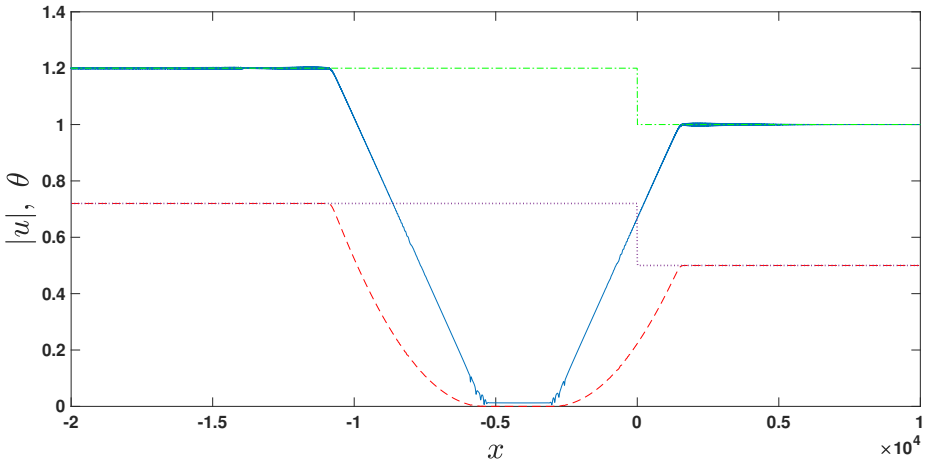

Figure 3.12: Case 5, two simple waves and a near-vacuum region. Numerical solutions of the nematic equations (2.19) and (2.20) for the initial conditions (2.29) and (2.31). Blue (solid) line: $|u|$ at $z = 1500$; red (dashed) line θ at $z = 1500$; green (dash-dot) line: $|u|$ at $z = 0$ and violet (dotted) line θ at $z = 0$. Here, $u_- = 1.2$, $u_+ = 1.0$, $v_- = -6$, $v_+ = 0$ and $q = 2$. (Online version in colour.)

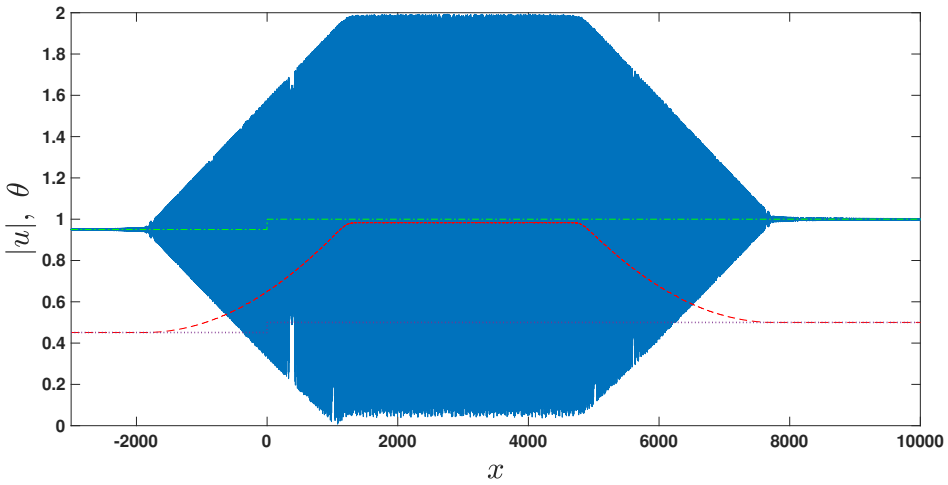

Figure 3.13: Case 6, a couple of fast and slow interacting DSWs. Numerical solutions of the nematic equations (2.19) and (2.20) for the initial conditions (2.29) and (2.31). Blue (solid) line: $|u|$ at $z = 1000$; red (dashed) line θ at $z = 1000$; green (dash-dot) line: $|u|$ at $z = 0$ and violet (dotted) line θ at $z = 0$. Here, $u_- = 0.95$, $u_+ = 1.0$, $v_- = 6$, $v_+ = 0$ and $q = 2$. (Online version in colour.)

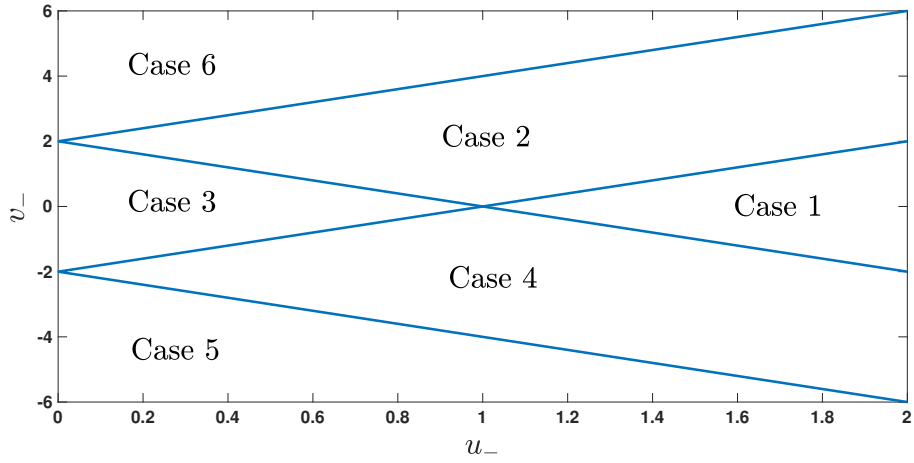

Figure 3.14: Geometrical classification of the six cases in the (u_-, v_-) Cartesian plane when the initial phases in (2.29) and (2.31) are not both zeroes. Here, $u_+ = 1$, $v_+ = 0$ and $q = 2$. (Online version in colour.)

3.3 Conclusions

A pseudo-spectral method based on the numerical method developed by Whitham and Forenberg [86, 89] was used to solve the Riemann problem of the defocusing nematic equations (2.19) and (2.20). Fourier spectral and RK4 methods were used to discretise and solve the spatial and temporal-like dimensions, respectively. It has been found that the resulting numerical solutions depend critically upon two things: the magnitude/strength of the initial jump condition in the optical field $|u_- - u_+|$ and the initial jump values of the optical field phases ϕ_- and ϕ_+.

For $u_- > u_+$ ($u_- \neq 0$) and zero initial phases ($\phi_- = \phi_+ = 0$), the initial discontinuity evolves into six distinct hydrodynamic regimes. One regime is fully non-dispersive and the other regimes are made of non-dispersive and dispersive regions. The non-dispersive regions in these regimes are given by rarefaction wave solutions, similar to dam break solutions in shallow water wave theory, whilst the dispersive regions are featured by various (resonant) DSW solutions. These DSWs are resonant in the sense that there is a resonant radiation propagating ahead of them. The form of these DSWs varies from classical to non-classical as the difference $u_- - u_+$ changes from small to large. The nematic dispersive shock and rarefaction wave solutions are joined by a non-zero intermediate level acting as a mean of u_- and u_+.

On the other hand, for non-zero initial phases (ϕ_-, $\phi_+ \neq 0$), the initial jump breaks into five new different non-dispersive/dispersive hydrodynamic regimes and one more regime that is identical to one of the regimes that were discussed above. These new regimes are combinations of various rarefaction waves and resonant DSWs.

Chapter 4

Modulational Stability of Nematic Wavetrains

In this chapter, we apply Whitham's averaging theory to understand the behaviour and the structure of a non-linear periodic wave solution governed by the defocusing nematic equations. This periodic wave is related to the resonant radiation generated by a nematic DSW. This approach will generate modulation equations that govern the slowly varying wave parameters of the nematic periodic wave solution. As discussed in Section 1.4, the main ingredient in this method is the need for an exact periodic wave solution. Unfortunately, the nematic equations (2.19) and (2.20) possess no known exact general solution, in particular a periodic travelling wave solution. However, if we assume that the resonant wavetrain has a small amplitude, known in non-linear wave theory as "weakly" non-linear wavetrain, then a periodic wave solution can be found as a Stokes expansion. This was similarly done for the Kawahara equation in [79], the KdV5 equation (Kawahara equation (1.40) with $\mu_d = 0$) in [80] and the fluid conduit equation in [151]. We start this chapter by deriving a nematic Stokes wave and then conclude it with deriving weakly non-linear modulation equations. These modulation equations will help us to study the modulational stability of the nematic resonant radiation and to analyse the structures of the nematic TDSW and VDSW regimes. Here, we focus only on the modulational stability part and defer the analysis of the TDSW and VDSW structures through modulation theory until the next chapter.

4.1 Nematic Uniform Stokes waves

We seek a Stokes expansion solution for the nematic dispersive hydrodynamic equations (2.24)–(2.26). This can be done by adopting perturbation expansions in the small parameter a ($0 < a \ll 1$), where a is the amplitude of the wavetrain, for the variables ρ, v, θ and ω about mean levels $\bar{\rho}$, $\bar{v}$, $\bar{\theta}$ and linear angular frequency ω_0, respectively. They are

$$\rho = \bar{\rho} + a\rho_1 \cos\varphi + a^2\rho_2 \cos 2\varphi + a^3\rho_3 \cos 3\varphi + o(a^3), \tag{4.1}$$
$$v = \bar{v} + av_1 \cos\varphi + a^2 v_2 \cos 2\varphi + a^3 v_3 \cos 3\varphi + o(a^3), \tag{4.2}$$
$$\theta = \bar{\theta} + a\theta_1 \cos\varphi + a^2\theta_2 \cos 2\varphi + a^3\theta_3 \cos 3\varphi + o(a^3), \tag{4.3}$$
$$\omega = \omega_0 + a\omega_1 + a^2\omega_2 + o(a^2), \tag{4.4}$$

where

$$\varphi = kx - \omega z \tag{4.5}$$

is the uniform wavetrain phase. Our task is to determine the coefficients ρ_1, ρ_2, v_1, v_2, θ_1, θ_2, ω_1, ω_2 and the linear dispersion relation ω_0. This can be achieved by substituting the above Stokes expansions into the nematic dispersive hydrodynamic system.

Originally, the general form of Stokes expansions are in terms of general unknown functions, for instance, $f_n(\varphi)$, where $n \in \mathbb{N}$, used instead of the Fourier modes $\cos(n\varphi)$ in the expansions (4.1)–(4.3) [1, 153]. The substitution of these general Stokes expansions into the governing system of interest results in a system of ODEs in the functions $f_n(\varphi)$. It is well-known in non-linear dispersive wave theory that Stokes' approach in the weakly non-linear limit yields functions that are proportional to Fourier modes [1, 153], namely,

$$f_n(\varphi) \propto \cos(n\varphi). \tag{4.6}$$

Because of this, it is possible and equivalent to use directly the Fourier modes $\cos(n\varphi)$ in place of the general functions $f_n(\varphi)$ in the nematic Stokes expansions. This adoption helps us to determine the weakly non-linear, periodic wavetrain without the necessity of solving differential equations.

Now, the substitution of the above nematic Stokes expansions into the mass equation (2.24) gives

$$\begin{aligned}
\mathcal{O}(a) &: \quad k\bar{v}\rho_1 - \omega_0\rho_1 + k\bar{\rho}v_1 = 0, && (4.7)\\
\mathcal{O}(a^2) &: \quad \omega_1\rho_1 \sin\varphi - \{kv_1\rho_1 + 2k\bar{v}\rho_2 - 2\omega_0\rho_2 + 2k\bar{\rho}v_2\}\sin 2\varphi = 0, && (4.8)\\
\mathcal{O}(a^3) &: \quad 2\omega_2\rho_1 - kv_2\rho_1 - kv_1\rho_2 = 0. && (4.9)
\end{aligned}$$

In equation (4.8), we notice coefficients of two distinct harmonic modes. It is standard in perturbation theory that terms which are proportional to the Fourier modes $\sin\varphi$ and $\cos\varphi$ are secular terms which lead to unbounded growth in the solution in φ. This can be more clear in the framework of using the general functions $f_n(\varphi)$ for the Stokes expansions, as these secular terms appear as one of the damping terms in the obtained differential equations and resonate with the differential operator [1]. The secular terms must be discarded [1, 152]. Here, we only have one secular term in (4.8) and we can eliminate it by setting

$$\omega_1 = 0, \tag{4.10}$$

so that we have a periodic and bounded wavetrain. Expanding the angular frequency ω in a power series is vital in weakly non-linear dispersive wave theory, as secular terms can be eliminated. This was one of the Stokes' remarkable discoveries in 1847 [153].

The substitution of the above Stokes series into the momentum equation (2.25), eliminating secular terms again, provides

$$\begin{aligned}
\mathcal{O}(a) &: \quad k^3\rho_1 + 4\bar{\rho}\bar{v}kv_1 - 4\omega_0\bar{\rho}v_1 + 8\bar{\rho}k\theta_1 = 0, && (4.11)\\
\mathcal{O}(a^2) &: \quad 3k^3\rho_1^2 - 4k\bar{\rho}^2v_1^2 - 16k^3\bar{\rho}\rho_2 - 16k\bar{v}\bar{\rho}^2v_2 \\
&\qquad + 16\omega_0\bar{\rho}^2v_2 - 32k\bar{\rho}^2\theta_2 = 0, && (4.12)
\end{aligned}$$

while the substitution into the director equation (2.26) gives

$$\begin{aligned}
\mathcal{O}(1) &: \quad \bar{\theta}q - \bar{\rho} = 0, && (4.13)\\
\mathcal{O}(a) &: \quad 2\rho_1 - \nu k^2\theta_1 - 2q\theta_1 = 0, && (4.14)\\
\mathcal{O}(a^2) &: \quad 4\nu k^2\theta_2 + 2q\theta_2 - 2\rho_2 = 0. && (4.15)
\end{aligned}$$

There is no need to additionally consider the terms of order $\mathcal{O}(a^3)$ in the momentum

and director equations as we are able to find an expression for ω_2 by (4.9) only,

$$\omega_2 = \frac{k}{2\rho_1}\left\{v_1\rho_2 + v_2\rho_1\right\}. \tag{4.16}$$

Therefore, the overall hierarchy now reads

$$\begin{aligned}
\mathcal{O}(1) \quad &: \quad \bar{\theta} = \frac{\bar{\rho}}{q}, && (4.17)\\
\mathcal{O}(a) \quad &: \quad \left\{k\bar{v} - \omega_0\right\}\rho_1 + k\bar{\rho}v_1 = 0, && (4.18)\\
&: \quad k^3\rho_1 + \left\{4\bar{\rho}\bar{v}k - 4\omega_0\bar{\rho}\right\}v_1 + 8\bar{\rho}k\theta_1 = 0, && (4.19)\\
&: \quad 2\rho_1 - \left\{\nu k^2 + 2q\right\}\theta_1 = 0, && (4.20)\\
\mathcal{O}(a^2) \quad &: \quad k\rho_1 v_1 + 2k\bar{v}\rho_2 - 2\omega_0\rho_2 + 2k\bar{\rho}v_2 = 0, && (4.21)\\
&: \quad 3k^3\rho_1^2 - 4k\bar{\rho}^2 v_1^2 - 16k^3\bar{\rho}\rho_2 \\
&\qquad\qquad + \left\{16\omega_0\bar{\rho}^2 - 16k\bar{v}\bar{\rho}^2\right\}v_2 - 32k\bar{\rho}^2\theta_2 = 0, && (4.22)\\
&: \quad 2\rho_2 - \left\{4\nu k^2 + 2q\right\}\theta_2 = 0, && (4.23)\\
\mathcal{O}(a^3) \quad &: \quad \omega_2 = \frac{k}{2\rho_1}\left\{v_1\rho_2 + v_2\rho_1\right\}. && (4.24)
\end{aligned}$$

We notice from equation (4.17) that the mean level of the nematic director profile $\bar{\theta}$ is relative to the optical intensity mean level $\overline{|u|}$. This matches the numerical simulations of the nematic resonant wavetrains, as shown in Chapter 3.

Remark 2. *It is clear that the correct notation to express the mean level of the optical intensity should be given by* $\overline{|u|}$*. However, for the purpose of simplicity in mathematical expressions presented in this thesis, we shall start using the notation* $\bar{u}$ *instead. Thus, we will assume here that* $\bar{u} \equiv \overline{|u|}$*.*

Numerically, it has been found that the mean level of the resonant wavetrain $\bar{u}$ is indeed very close to the value $\bar{u} = \sqrt{q\bar{\theta}}$ rather than u_+, especially when the jump from u_- to u_+ is large as in the TDSW and VDSW regimes. The root cause for this is the non-linear interactions between the nematic DSWs and the resonant wavetrain, resulting in an uplift in the resonant mean level from u_+ to $\sqrt{q\bar{\theta}}$. Then, the resonant wavetrain does not oscillate on the mean level $\bar{u} = u_+$, as assumed in previous work [60, 61].

Let us now determine the Stokes coefficients. To determine the linear dispersion relation ω_0, we note that the $\mathcal{O}(a)$ equations (4.18)–(4.20) have a solution of

$$\begin{vmatrix} k\bar{v} - \omega_0 & k\bar{\rho} & 0 \\ k^3 & 4\bar{\rho}\bar{v}k - 4\omega 0\bar{\rho} & 8\bar{\rho}k \\ 2 & 0 & -\nu k^2 - 2q \end{vmatrix} = 0, \tag{4.25}$$

which provides

$$\omega_0 = k\bar{v} + \frac{\sqrt{k\bar{\rho}}}{\sqrt{\nu k^2 + 2q}}\sqrt{4k + \frac{k^3}{4\bar{\rho}}(\nu k^2 + 2q)}. \tag{4.26}$$

When we insert the above linear dispersion relation into equation (4.18), we obtain

$$v_1 = \frac{1}{\sqrt{k\bar{\rho}(\nu k^2 + 2q)}}\sqrt{4k + \frac{k^3}{4\bar{\rho}}(\nu k^2 + 2q)}. \tag{4.27}$$

Equation (4.8) then gives

$$\theta_1 = \frac{2\rho_1}{2q + \nu k^2}. \tag{4.28}$$

All the Stokes corrections of order $\mathcal{O}(a)$ have been found, except ρ_1. We can choose

$$\rho_1 = 1, \tag{4.29}$$

as this then sets the amplitude parameter a. As for the remainder of the nematic Stokes coefficients to $\mathcal{O}(a^2)$, they are calculated through solving the system of equations (4.21)–(4.24) on using the above expressions (4.26)–(4.29). After many simplifications carried out in Maple software, we find

$$\rho_2 = \frac{-(8\,k^2\nu + 4\,q)}{k^2\,(2\,k^4\nu^2 + 5\,k^2\nu\,q - 8\,\nu\,\bar{\rho} + 2\,q^2)}, \tag{4.30}$$

$$v_2 = -\left\{\frac{k^4\nu + 2\,k^2 q + 16\,\bar{\rho}}{\nu\,k^2 + 2\,q}\right\}^{\frac{1}{2}} \times \tag{4.31}$$

$$\frac{(3\,k^6\nu^2 + 15k^4\nu\,q/2 + 12\,k^2\nu\,\bar{\rho} + 3\,k^2q^2 + 12\,q\bar{\rho})}{12\bar{\rho}^2k^2\,(k^4\nu^2 + 5k^2\nu\,q/2 + q^2 - 4\,\nu\,\bar{\rho})}, \tag{4.32}$$

$$\theta_2 = \frac{-4}{k^2\,(2\,k^4\nu^2 + 5\,k^2\nu\,q - 8\,\nu\,\bar{\rho} + 2\,q^2)}, \tag{4.33}$$

$$\omega_2 = -\left\{\frac{k^4\nu + 2\,k^2 q + 16\,\bar{\rho}}{\nu\,k^2 + 2\,q}\right\}^{\frac{1}{2}} \times$$

$$\frac{(k^6\nu^2 + 5k^4\nu\,q/2 + 12\,k^2\nu\,\bar{\rho} + k^2q^2 + 8\,q\bar{\rho})}{8\bar{\rho}^2k\,(k^4\nu^2 + 5k^2\nu\,q/2 + q^2 - 4\,\nu\,\bar{\rho})}. \tag{4.34}$$

As we can see, however, the expressions for the Stokes coefficients are complicated and not really useful to derive amenable modulation equations. Fortunately, the resonant wavetrain is a wave of short wavelength, namely, $k = \mathcal{O}(1)$, relative to the nematic DSW, which is a long wave with wavenumber range $0 < k < 0.15$, and the non-local limit of ν large can be taken as it is the physical limit in experiments [6, 92]. Taking then the nematic non-locality effect into account and after non-trivial algebra carried out in Maple software, we have the following asymptotic results:

$$\omega_0 = k\bar{v} + \frac{k^2}{2} + \frac{4\bar{\rho}}{\nu k^2} - \frac{8\bar{\rho}q}{\nu^2k^4} - \frac{16\bar{\rho}^2}{\nu^2k^6} + o\left(\frac{1}{\nu^2k^6}\right), \tag{4.35}$$

$$v_1 = \frac{k}{2\bar{\rho}} + \frac{4}{\nu\,k^3} - \frac{8q}{\nu^2k^5} - \frac{16\bar{\rho}}{\nu^2k^7} + o\left(\frac{1}{\nu^2k^7}\right), \tag{4.36}$$

$$\theta_1 = \frac{2}{\nu k^2} - \frac{4q}{\nu^2k^4} + o\left(\frac{1}{\nu^2k^4}\right), \tag{4.37}$$

$$\rho_2 = -\frac{4}{\nu k^4} + \frac{8q}{\nu^2k^6} - \frac{16\bar{\rho}}{\nu^2k^8} + o\left(\frac{1}{\nu^2k^8}\right), \tag{4.38}$$

$$v_2 = -\frac{k}{4\bar{\rho}^2} - \frac{4}{\bar{\rho}\nu k^3} + \frac{8q}{\bar{\rho}\nu^2k^5} - \frac{16}{\nu^2k^7} + o\left(\frac{1}{\nu^2k^7}\right), \tag{4.39}$$

$$\theta_2 = -\frac{2}{\nu^2k^6} + o\left(\frac{1}{\nu^2k^6}\right), \tag{4.40}$$

$$\omega_2 = -\frac{k^2}{8\bar{\rho}^2} - \frac{3}{\bar{\rho}\nu k^2} + \frac{6q}{\bar{\rho}\nu^2k^4} - \frac{20}{\nu^2k^6} + o\left(\frac{1}{\nu^2k^6}\right). \tag{4.41}$$

It is important to mention that the above nematic linear dispersion relation ω_0 for the resonant wavetrain is in terms of the wave phase which satisfies $\phi_x = v$, instead of the original phase ϕ in the Madelung transformation (2.23). To obtain the dispersion relation for the original phase ϕ, we need to add the phase shift term which is omitted on differentiating the phase ϕ. This can be seen by looking for the dispersion relation for a wave in u on a constant background $\bar{\theta}$. This results in a linear Schrödinger equation in the complex electric field u

$$i\frac{\partial u}{\partial z} + \frac{1}{2}\frac{\partial^2 u}{\partial x^2} - 2\theta u = 0, \tag{4.42}$$

with the asymptotic limit

$$\theta \sim \bar{\theta} = \frac{\bar{u}^2}{q}. \tag{4.43}$$

In other words, in finding the phase ϕ from v, with $\phi_x = v$, a function of z must be determined which is in fact $2\bar{\rho}/q$ to match with waves on a constant mean/background. The asymptotic assumption (4.43) is in fair agreement with numerical solutions for the director θ in the resonant wavetrain region, see Chapter 3. The reason why the profile of the director is nearly constant and has the averaged value given by (4.43) is that the non-locality effect smooths out the response of the director to the electric field, resulting in the director essentially reacting to the mean of the rapid oscillation of $|u|$, as has been found previously [60, 59, 154]. The above linear Schrödinger equation (4.42) possesses a dispersion relation, for right-propagating waves that captures the phase shift,

$$\omega = \frac{k^2}{2} + 2\bar{\theta} = \frac{k^2}{2} + \frac{2\bar{\rho}}{q}. \tag{4.44}$$

This linear dispersion relation matches (4.35) at $\mathcal{O}(1)$, with $\bar{v} = 0$ and the phase shift term $2\bar{\rho}/q$ added. For the resonance, at first (linear) approximation, the mean level of v is

$$\bar{v} = 2\sqrt{\frac{2}{q}}\left(\bar{u} - u_+\right), \tag{4.45}$$

we will verify this in Chapter 5. The approximation of the linear Schrödinger equation (4.42) assumes that the resonance oscillates about the mean level $\bar{u} = u_+$, rather than $\bar{u} = \sqrt{q\bar{\theta}}$, hence, $\bar{v} = 0$. Although this is not precisely true for the resonance, this approximation gives an excellent prediction of the phase shift. Another way to determine the phase shift $2\bar{\rho}/q$ without the above argument is by implementing the above Stokes' approach with a perturbation expansion in ϕ instead of a perturbation in v (4.2), as this involves no differentiation with respect to x. The resonant mean level $\bar{u}$ will be determined theoretically when we study Whitham modulation jump conditions in Chapter 5. The linear nematic dispersion relation (4.35) now becomes

$$\omega_0 = k\bar{v} + \frac{k^2}{2} + \frac{2\bar{\rho}}{q} + \frac{4\bar{\rho}}{\nu k^2} - \frac{8\bar{\rho}q}{\nu^2 k^4} - \frac{16\bar{\rho}^2}{\nu^2 k^6} + o\left(\frac{1}{\nu^2 k^6}\right). \tag{4.46}$$

Lastly, the nematic Stokes expansions are

$$\rho = \bar{\rho} + a\cos\varphi - \frac{4a^2}{\nu k^4}\cos 2\varphi + o\left(\frac{a^2}{\nu k^4}\right), \tag{4.47}$$

$$v = \bar{v} + \frac{ka}{2\bar{\rho}}\cos\varphi - \frac{ka^2}{4\bar{\rho}^2}\cos 2\varphi + o\left(a^2\right), \tag{4.48}$$

$$\theta = \frac{\bar{\rho}}{q} + \frac{2a}{\nu k^2}\cos\varphi - \frac{2a^2}{\nu^2 k^6}\cos 2\varphi + o\left(\frac{a^2}{\nu^2 k^6}\right), \tag{4.49}$$

$$\omega = k\bar{v} + \frac{k^2}{2} + \frac{2\bar{\rho}}{q} - \frac{k^2 a^2}{8\bar{\rho}^2} + o\left(a^2\right), \tag{4.50}$$

where only the leading order terms are taken in the Stokes coefficients. Higher order terms are not necessary for the calculation of the resonant wavetrain in the next section.

4.2 Nematic Slowly Varying Stokes Waves and Modulational Stability

We now move to the derivation of the nematic Whitham modulation equations in the weakly non-linear limit by employing the above calculated Stokes expansions. There are several approaches to formulate these modulation equations. One way is by averaging the Lagrangian formulation of the equations and another way is through averaging the conservation laws for the governing equations, or a combination of both. In this study, it has been found that the method of averaged Lagrangians provides us with conservation laws of mass, wave action and waves. For a full set of the modulation equations, two additional conservation laws are needed. These conservation laws are conservation of energy and momentum. To procure them, we use Nöther's Theorem and average the resulting energy and momentum conservation laws over the fast oscillations, as was done by Whitham to derive the modulation equations for the KdV equation [1, 83]. In this sense, a mixture of the methods of averaged Lagrangians and conservation laws is optimal.

Let us commence with the method of averaged Lagrangians. The Lagrangian for the nematic equations (2.19) and (2.20) is [154]

$$L = i\left(u^* u_z - u u_z^*\right) - |u_x|^2 - 4\theta|u|^2 + \nu\theta_x^2 + 2q\theta^2. \tag{4.51}$$

However, what we really need is the Lagrangian for the nematic equations in the shallow water wave form (2.24)–(2.26). To obtain this, we apply the Madelung transformation (2.23) to the above Lagrangian (4.51). This results in

$$L = -2\rho\phi_z - \frac{\rho_x^2}{4\rho} - \rho\phi_x^2 - 4\rho\theta + \nu\theta_x^2 + 2q\theta^2. \tag{4.52}$$

For many non-linear dispersive wave equations, such as the KdV5 equation [80], the KdV equation and the Klein-Gordon equation [1], it is typical that a slowly varying wave parameter appears in governing Lagrangians in terms of derivatives only, namely, in terms of potentials. This demands that we introduce the so-called pseudo-phase ψ for the mean flow $\bar{v}$, with

$$\gamma = -\psi_z \quad \text{and} \quad \bar{v} = \psi_x. \tag{4.53}$$

This is a standard step in Whitham's averaging theory [1]. In other words, we seek a slowly varying Stokes wave for the variable ϕ as

$$\phi = \psi + \Phi(\varphi), \tag{4.54}$$

with the wave parameters, the amplitude a, wavenumber k, angular frequency ω and mean height $\bar{v}$, slowly varying functions of x and z. The quantities γ and $\bar{v}$ are given the names pseudo-frequency and pseudo-wavenumber [1], respectively. Their combination

as $\psi = \bar{v}x - \gamma z$ represents a pseudo-phase for a uniform wavetrain. These quantities have important physical meanings in water wave theory, as they represent mean fluid velocity and mean height [1]. The function Φ represents a wavetrain with zero mean level and the function ψ gives the mean level variation for this wavetrain, given by (4.53). The slowly varying wavenumber and angular frequency are defined from the (slowly varying) phase φ by

$$k = \varphi_x \quad \text{and} \quad \omega = -\varphi_z. \tag{4.55}$$

With the use of

$$\phi_x = \bar{v} + k\Phi_\varphi \tag{4.56}$$

and

$$\phi_z = -\gamma - \omega\Phi_\varphi, \tag{4.57}$$

the Lagrangian (4.52) becomes

$$L = 2\rho\gamma + 2\rho\omega\Phi_\varphi - \frac{k^2\rho_\varphi^2}{4\rho} - \rho\bar{v}^2 - 2k\bar{v}\rho\Phi_\varphi - k^2\rho\Phi_\varphi^2 - 4\theta\rho + \nu k^2\theta_\varphi^2 + 2q\theta^2. \tag{4.58}$$

We approximate the ratio in the third term in (4.58) by Taylor series based on the Stokes expansion (4.1) and select the leading order term only,

$$\frac{\rho_\varphi^2}{\rho} \sim \frac{a^2\sin^2\varphi}{\bar{\rho}} + o(a^2), \tag{4.59}$$

as higher order terms are beyond the calculated order. Then, the Lagrangian is expressed as

$$L = 2\rho\gamma + 2\rho\omega\Phi_\varphi - \frac{k^2a^2}{4\bar{\rho}}\sin^2\varphi - \rho\bar{v}^2 - 2k\bar{v}\rho\Phi_\varphi - k^2\rho\Phi_\varphi^2 - 4\theta\rho + \nu k^2\theta_\varphi^2 + 2q\theta^2. \tag{4.60}$$

The function Φ is deduced from equations (4.2) and (4.56), which gives

$$\Phi(\varphi) = a\Phi_1\sin\varphi + a^2\Phi_2\sin 2\varphi = \frac{av_1}{k}\sin\varphi + \frac{a^2v_2}{2k}\sin 2\varphi. \tag{4.61}$$

Substituting the slowly varying Stokes waves (4.47)–(4.50) and the expression (4.61) into the Lagrangian (4.60), and then averaging over the fast scale variable φ by integrating from 0 to 2π, yields the averaged Lagrangian in terms of the slow-scale variables

$$\begin{aligned}
\mathcal{L} &= \frac{1}{2\pi}\int_0^{2\pi} L d\varphi = \mathcal{L}\left(\bar{\rho}, \varphi_x, \varphi_z, \psi_x, \psi_z, a\right) \\
&= \left\{2\bar{\rho}\gamma - \bar{\rho}\bar{v}^2 - \frac{2\bar{\rho}^2}{q}\right\} \\
&\qquad + a^2\left\{\frac{k^2\theta_1^2\nu}{2} - \bar{v}v_1\rho_1 + q\theta_1^2 - \frac{v_1^2\bar{\rho}}{2} + \frac{v_1\rho_1\omega}{k} - \frac{k^2\rho_1}{8\bar{\rho}} - 2\theta_1\rho_1\right\} + o(a^2) \\
&= \left\{2\bar{\rho}\gamma - \frac{2\bar{\rho}^2}{q} - \bar{\rho}\bar{v}^2\right\} + a^2\left\{\frac{\omega}{2\bar{\rho}} - \frac{k^2}{4\bar{\rho}} - \frac{\bar{v}k}{2\bar{\rho}}\right\} + o(a^2).
\end{aligned} \tag{4.62}$$

Note that the higher order terms of order $\mathcal{O}\left(\frac{1}{\nu}\right)$ have been neglected as they are not needed to determine the resonant wavetrain at leading order. We have four slowly

varying functions $(\bar{\rho}, \varphi, \psi, a)$, so we need four modulation equations, which are Euler-Lagrange equations of the averaged Lagrangian. Taking the variations of the averaged Lagrangian (4.62) with respect to the amplitude a,

$$\delta a : \quad \mathcal{L}_a = 0, \tag{4.63}$$

gives the non-linear dispersion relation

$$\omega = \omega_0 + \mathcal{O}(a^2). \tag{4.64}$$

To obtain the Stokes dispersion relation (4.50) to $\mathcal{O}(a^2)$ by taking variations with respect to a, the averaged Lagrangian is needed to $\mathcal{O}(a^4)$. However, this dispersion relation is known via (4.50), so these $\mathcal{O}(a^4)$ terms in the averaged Lagrangian are not necessary here. Taking variations of the averaged Lagrangian (4.62) with respect to the pseudo-phase ψ,

$$\delta\psi \quad : \quad \frac{\partial}{\partial z}\frac{\partial \mathcal{L}}{\partial \gamma} - \frac{\partial}{\partial x}\frac{\partial \mathcal{L}}{\partial \bar{v}} = 0, \tag{4.65}$$

gives

$$\frac{\partial}{\partial z}\{\bar{\rho}\} + \frac{\partial}{\partial x}\left\{\bar{\rho}\bar{v} + \frac{a^2 v_1 \rho_1}{2}\right\} = 0, \tag{4.66}$$

which results in the averaged mass conservation equation

$$\frac{\partial \bar{\rho}}{\partial z} + \frac{\partial}{\partial x}\left\{\bar{\rho}\bar{v} + \frac{k a^2}{4\bar{\rho}}\right\} = 0, \tag{4.67}$$

on using (4.48). Taking variations with respect to the phase φ,

$$\delta\varphi \quad : \quad \frac{\partial}{\partial z}\frac{\partial \mathcal{L}}{\partial \omega} - \frac{\partial}{\partial x}\frac{\partial \mathcal{L}}{\partial k} = 0, \tag{4.68}$$

gives

$$\frac{\partial}{\partial z}\left\{\frac{a^2 \rho_1 v_1}{k}\right\} + \frac{\partial}{\partial x}\left\{k\theta_1^2 \nu a^2 - \frac{v_1 \rho_1 \omega a^2}{k^2} - \frac{k\rho_1 a^2}{4\bar{\rho}}\right\} = 0, \tag{4.69}$$

which results in the conservation law of wave action equation

$$\frac{\partial}{\partial z}\left\{\frac{a^2}{\bar{\rho}}\right\} + \frac{\partial}{\partial x}\left\{\frac{\bar{v}a^2}{\bar{\rho}} + \frac{k a^2}{\bar{\rho}}\right\} = 0, \tag{4.70}$$

on using (4.47)–(4.50). As usual in non-linear dispersive wave problems, a set of modulation equations is concluded with the conservation of waves equation. This is derived from the wavenumber and frequency expressions (4.55) as a consistency relation, expressly,

$$\frac{\partial k}{\partial z} + \frac{\partial \omega}{\partial x} = 0. \tag{4.71}$$

Another name that is commonly given for the conservation of waves equation in modulation theory is the consistency equation [1, 19]. There is another consistency equation, analogous to the waves conservation (4.71), which follows from the expressions (4.53) for the pseudo-phase, that is,

$$\frac{\partial \bar{v}}{\partial z} + \frac{\partial \gamma}{\partial x} = 0. \tag{4.72}$$

Although this consistency equation will not be used for nematic modulations, it will show up automatically in the middle of our work. So far we have three modulation equations, and we lack one more equation to close the modulation system. To proceed, we use Nöther's Theorem on the Lagrangian (4.52). Only conservation laws that arise from this theorem are acceptable in modulation theory, as was pointed out in Section 1.4. The theorem says that if a Lagrangian possesses a continuous symmetry, i.e., it is invariant under continuous transformations or translations, then conservation laws can be deduced from these symmetries. Mathematically speaking, the theorem is formulated as [155]:

Nöether's Theorem. *Let us assume that the functional*

$$J[\boldsymbol{r}] = \int_{\mathbb{R}^n} F\left(\boldsymbol{x}, \boldsymbol{r}, \nabla \boldsymbol{r}\right) d\boldsymbol{x} \tag{4.73}$$

is invariant under the family of transformations

$$x_i^* = x_i + \alpha h_i\left(x_i, r_j, r_{x_j}\right); \quad (i = 1, 2, 3, \ldots, n), \tag{4.74}$$

$$r_j^* = r_j + \alpha w_j\left(x_i, r_j, r_{x_j}\right); \quad (j = 1, 2, 3, \ldots, m), \tag{4.75}$$

for an arbitrary region $\mathbb{R}^n$ such that α is a small constant, $\boldsymbol{x} = \langle x_1, \ldots, x_n\rangle$ and $\boldsymbol{r} = \langle r_1, \ldots, r_m\rangle$, h_i and w_j are continuously differentiable functions. Then

$$\sum_{i=1}^{n} \frac{\partial}{\partial x_i}\left\{\sum_{j=1}^{m} \frac{\partial F}{\partial\left(\frac{\partial r_j}{\partial x_i}\right)} \bar{w}_j + F h_i\right\} = 0 \tag{4.76}$$

on each extremal surface of $J[r]$, which are conservation laws for the underlying equation(s), where

$$\bar{w}_j = w_j - \sum_{i=1}^{n} \frac{\partial r_j}{\partial x_i} h_i. \tag{4.77}$$

The Lagrangian (4.52), $L = L\left(\rho, \theta, \nabla\rho, \nabla\phi, \nabla\theta\right)$, is invariant under the following three collections of translations. First, it is invariant under a translation with respect to ϕ, that is, $\phi^* = \phi + \alpha$, which gives the mass conservation law

$$\frac{\partial}{\partial z}\frac{\partial L}{\partial \phi_z} + \frac{\partial}{\partial x}\frac{\partial L}{\partial \phi_x} = 0. \tag{4.78}$$

Second, it is invariant under a translation with respect to x, namely, $x^* = x + \alpha$, which leads to the momentum conservation law

$$\frac{\partial}{\partial z}\left\{\frac{\partial L}{\partial \rho_z}\frac{\partial \rho}{\partial x} + \frac{\partial L}{\partial \phi_z}\frac{\partial \phi}{\partial x} + \frac{\partial L}{\partial \theta_z}\frac{\partial \theta}{\partial x}\right\} + \frac{\partial}{\partial x}\left\{\frac{\partial L}{\partial \rho_x}\frac{\partial \rho}{\partial x} + \frac{\partial L}{\partial \phi_x}\frac{\partial \phi}{\partial x} + \frac{\partial L}{\partial \theta_x}\frac{\partial \theta}{\partial x} - L\right\} = 0. \tag{4.79}$$

Third, it is invariant under a translation with respect to z, $z^* = z + \alpha$, which yields the energy conservation law

$$\frac{\partial}{\partial z}\left\{\frac{\partial L}{\partial \rho_z}\frac{\partial \rho}{\partial z} + \frac{\partial L}{\partial \phi_z}\frac{\partial \phi}{\partial z} + \frac{\partial L}{\partial \theta_z}\frac{\partial \theta}{\partial z} - L\right\} + \frac{\partial}{\partial x}\left\{\frac{\partial L}{\partial \rho_x}\frac{\partial \rho}{\partial z} + \frac{\partial L}{\partial \phi_x}\frac{\partial \phi}{\partial z} + \frac{\partial L}{\partial \theta_x}\frac{\partial \theta}{\partial z}\right\} = 0. \tag{4.80}$$

The terms mass, momentum and energy are used in this thesis in the sense of the invariances of a Lagrangian and how they arise in water wave theory and classical

mechanics [1, 156]. While these terms will be used here, in optics they have different interpretations. For example, mass conservation equation is conservation of optical power. Substituting the expression for the nematic Lagrangian (4.52) into (4.78)–(4.80), we have the mass, momentum and energy conservation equations

$$\begin{aligned}
\frac{\partial \rho}{\partial z}+\frac{\partial}{\partial x}\left\{\rho v\right\}&=0,\\
\frac{\partial}{\partial z}\left\{\rho v\right\}+\frac{\partial}{\partial x}\left\{\rho v^2+\frac{\rho_x^2}{4\rho}+q\theta^2-\frac{\nu\theta_x^2}{2}-\frac{\rho_{xx}}{4}\right\}&=0,\\
\frac{\partial}{\partial z}\left\{\frac{\rho_x^2}{4\rho}+\rho v^2+4\theta\rho-\nu\theta_x^2-2q\theta^2\right\}+\frac{\partial}{\partial x}\left\{\frac{3v\rho_x^2}{4\rho}+\frac{\rho_x v_x}{2}+\rho v^3-\frac{v\rho_{xx}}{2}\right.&\\
\left.+4\rho\theta v+2\nu\theta_x\theta_z\right\}&=0,
\end{aligned}\tag{4.81}$$

respectively. Although the first and second formulae in (4.81) are merely the first two equations in the nematic dispersive hydrodynamic system (2.24)–(2.26), after some algebraic manipulations, Nöther's approach has to be undertaken to make sure that these are the correct conservation laws that eliminate the secular terms in the multi-scales method of modulation theory. This was the motive behind using the titles mass and momentum equations for (2.24) and (2.25), respectively, from the start. By using the Stokes expansions (4.1)–(4.4) and averaging over the phase φ from 0 to 2π, we obtain the averaged mass, momentum and energy conservation laws

$$\begin{aligned}
\frac{\partial \bar{\rho}}{\partial z}+\frac{\partial}{\partial x}\left\{\bar{\rho}\bar{v}+\frac{v_1\rho_1 a^2}{2}\right\}&=0,\\
\frac{\partial}{\partial z}\left\{\bar{\rho}\bar{v}+\frac{v_1\rho_1 a^2}{2}\right\}+\frac{\partial}{\partial x}\left\{\frac{\bar{\rho}^2}{q}+\bar{v}^2\bar{\rho}+\frac{q\theta_1^2a^2}{2}+\frac{k^2\rho_1^2a^2}{8\bar{\rho}}+\frac{v_1^2\bar{\rho}a^2}{2}+\bar{v}v_1\rho_1a^2\right.&\\
\left.-\frac{k^2\theta_1^2\nu a^2}{4}\right\}&=0,\\
\frac{\partial}{\partial z}\left\{\frac{2\bar{\rho}^2}{q}+\bar{v}^2\bar{\rho}+2\theta_1\rho_1a^2-q\theta_1^2a^2+\frac{k^2\rho_1^2a^2}{8\bar{\rho}}+\frac{v_1^2\bar{\rho}a^2}{2}+\bar{v}v_1\rho_1a^2-\frac{k^2\theta_1^2\nu a^2}{2}\right\}&\\
+\frac{\partial}{\partial x}\left\{\bar{\rho}\bar{v}^3+\frac{4\bar{v}\bar{\rho}^2}{q}+\frac{3\bar{v}\bar{\rho}v_1^2a^2}{2}+\frac{3\bar{v}^2v_1\rho_1a^2}{2}+\frac{2\bar{\rho}v_1\rho_1a^2}{q}+2\bar{\rho}v_1\theta_1a^2+2\bar{v}\rho_1\theta_1a^2\right.&\\
\left.+\frac{k^2v_1\rho_1a^2}{2}+\frac{3\bar{v}k^2\rho_1^2a^2}{8\bar{\rho}}-k\omega_0\nu\theta_1^2a^2\right\}&=0,
\end{aligned}\tag{4.82}$$

respectively. When the Stokes expansions (4.47)–(4.50) are used in the above equations, we obtain the averaged mass, momentum and energy conservation laws as, in order,

$$\begin{aligned}
\frac{\partial \bar{\rho}}{\partial z}+\frac{\partial}{\partial x}\left\{\bar{\rho}\bar{v}+\frac{ka^2}{4\bar{\rho}}\right\}&=0,\\
\frac{\partial}{\partial z}\left\{\bar{\rho}\bar{v}+\frac{ka^2}{4\bar{\rho}}\right\}+\frac{\partial}{\partial x}\left\{\frac{\bar{\rho}^2}{q}+\bar{\rho}\bar{v}^2+\frac{k^2a^2}{4\bar{\rho}}+\frac{\bar{v}ka^2}{2\bar{\rho}}\right\}&=0,\\
\frac{\partial}{\partial z}\left\{\bar{\rho}\bar{v}^2+\frac{2\bar{\rho}^2}{q}+\frac{k^2a^2}{4\bar{\rho}}+\frac{k\bar{v}a^2}{2\bar{\rho}}\right\}+\frac{\partial}{\partial x}\left\{\bar{\rho}\bar{v}^3+\frac{4\bar{v}\bar{\rho}^2}{q}+\frac{ka^2}{q}+\frac{k^3a^2}{4\bar{\rho}}\right.&\\
\left.+\frac{3\bar{v}k^2a^2}{4\bar{\rho}}+\frac{3\bar{v}^2ka^2}{4\bar{\rho}}\right\}&=0,
\end{aligned}\tag{4.83}$$

The averaged mass conservation law in (4.83) is in conformity with (4.67), which is expected.

Now, the set of the modulation equations for the nematic Stokes wave that enables us to deduce the "structure" of the resonant wavetrain generated by the DSW (to be specific, TDSW and VDSW) is

$$\begin{aligned}
\frac{\partial \bar{\rho}}{\partial z}+\frac{\partial}{\partial x}\left\{\bar{\rho}\bar{v}+\frac{kA}{4\bar{\rho}}\right\}&=0,\\
\frac{\partial k}{\partial z}+\frac{\partial}{\partial x}\left\{k\bar{v}+\frac{k^2}{2}+\frac{2\bar{\rho}}{q}-\frac{k^2A}{8\bar{\rho}^2}\right\}&=0,\\
\frac{\partial}{\partial z}\left\{\bar{\rho}\bar{v}+\frac{kA}{4\bar{\rho}}\right\}+\frac{\partial}{\partial x}\left\{\frac{\bar{\rho}^2}{q}+\bar{\rho}\bar{v}^2+\frac{k^2A}{4\bar{\rho}}+\frac{\bar{v}kA}{2\bar{\rho}}\right\}&=0,\\
\frac{\partial}{\partial z}\left\{\bar{\rho}\bar{v}^2+\frac{2\bar{\rho}^2}{q}+\frac{k^2A}{4\bar{\rho}}+\frac{k\bar{v}A}{2\bar{\rho}}\right\}+\frac{\partial}{\partial x}\left\{\bar{\rho}\bar{v}^3+\frac{4\bar{v}\bar{\rho}^2}{q}+\frac{kA}{q}+\frac{k^3A}{4\bar{\rho}}+\frac{3\bar{v}k^2A}{4\bar{\rho}}\right.&\\
\left.+\frac{3\bar{v}^2kA}{4\bar{\rho}}\right\}&=0,
\end{aligned}\tag{4.84}$$

where $A=a^2$, this will be dealt with in Sections 5.5 and 5.6. On the other hand, the family of the modulation equations that allows us to understand the "modulational stability" of the resonant wavetrain generated by the nematic DSWs can be summarised as

$$\begin{aligned}
\frac{\partial \bar{\rho}}{\partial z}+\frac{\partial}{\partial x}\left\{\bar{\rho}\bar{v}+\frac{kA}{4\bar{\rho}}\right\}&=0,\\
\frac{\partial}{\partial z}\left\{\frac{A}{\bar{\rho}}\right\}+\frac{\partial}{\partial x}\left\{\frac{\bar{v}A}{\bar{\rho}}+\frac{kA}{\bar{\rho}}\right\}&=0,\\
\frac{\partial k}{\partial z}+\frac{\partial}{\partial x}\left\{k\bar{v}+\frac{k^2}{2}+\frac{2\bar{\rho}}{q}-\frac{k^2A}{8\bar{\rho}^2}\right\}&=0,\\
\frac{\partial}{\partial z}\left\{\bar{\rho}\bar{v}+\frac{kA}{4\bar{\rho}}\right\}+\frac{\partial}{\partial x}\left\{\bar{\rho}\bar{v}^2+\frac{\bar{\rho}^2}{q}+\frac{k^2A}{4\bar{\rho}}+\frac{\bar{v}kA}{2\bar{\rho}}\right\}&=0.
\end{aligned}\tag{4.85}$$

Here, the notation $A=a^2$ is adopted as it simplifies the subsequent calculations, especially in the modulational stability calculations of the nematic Stokes wave. In this chapter, we concentrate on addressing the modulational stability of the Stokes wave based on the modulation equations (4.85). Methods to find the TDSW and VDSW solutions by the means of the modulation equations (4.84) will be presented in the next chapter, based on Whitham modulation jump conditions [81, 85].

To determine the modulational stability of the nematic Stokes wave, the modulation equations (4.85) need to be set in the characteristic form (1.36) [1]. In general, if the size of a system of PDEs is at most second order, then one can always set the system in Riemann invariant form (1.39) by using a standard method that reduces it to a scalar ODE with an integrating factor that can always be found. For systems of PDEs of higher order, however, it may or may not be possible to set them in Riemann invariant form. An example of a third order system of coupled PDEs for which an integrating factor can be found is Euler's equations of perfect gas dynamics, see e.g. [1]. Another example of a third order system is the weakly non-linear modulation equations for the KdV5 equation which have been derived and put in Riemann invariant form [80]. The weakly non-linear nematic modulation system (4.85) is a fourth order system. We have not been able to set them in an exact Riemann invariant form. However, we can set them in characteristic form asymptotically using "eigenvalue perturbation method."

This method seeks asymptotic expressions, in a form of a perturbation series, for the eigenvalues and the eigenvectors of a matrix, see a rigorous discussion of this method in [157].

Differentiating term by term the fluxes and the densities in the modulation equations (4.85) and collecting terms with common coefficients gives

$$\begin{aligned}
\bar{\rho}_z + \left\{\bar{v} - \frac{kA}{4\bar{\rho}^2}\right\}\bar{\rho}_x + \frac{A}{4\bar{\rho}}k_x + \frac{k}{4\bar{\rho}}A_x + \bar{\rho}\bar{v}_x = 0,\\
k_z + \left\{\frac{2}{q} + \frac{Ak^2}{4\bar{\rho}^3}\right\}\bar{\rho}_x + \left\{\bar{v} + k - \frac{kA}{4\bar{\rho}^2}\right\}k_x - \frac{k^2}{8\bar{\rho}^2}A_x + k\bar{v}_x = 0,\\
A_z - \frac{kA}{\bar{\rho}}\bar{\rho}_x + Ak_x + \left\{\bar{v} + k + \frac{kA}{4\bar{\rho}^2}\right\}A_x + 2A\bar{v}_x = 0,\\
\bar{v}_z + \left\{\frac{2}{q} - \frac{A}{2\bar{\rho}^2 q}\right\}\bar{\rho}_x + \frac{Ak^2}{32\bar{\rho}^4}A_x + \bar{v}\bar{v}_x = 0,
\end{aligned} \tag{4.86}$$

which can be expressed in the matrix form

$$\boldsymbol{G}_z + \mathcal{B}(\boldsymbol{G})\boldsymbol{G}_x = \boldsymbol{0}, \tag{4.87}$$

where $\boldsymbol{G}^T = [\bar{\rho}\ k\ A\ \bar{v}]$ and

$$\mathcal{B} = \begin{bmatrix}
\bar{v} - \frac{kA}{4\bar{\rho}^2} & \frac{A}{4\bar{\rho}} & \frac{k}{4\bar{\rho}} & \bar{\rho}\\
\frac{2}{q} + \frac{Ak^2}{4\bar{\rho}^3} & \bar{v} + k - \frac{kA}{4\bar{\rho}^2} & -\frac{k^2}{8\bar{\rho}^2} & k\\
-\frac{kA}{\bar{\rho}} & A & \bar{v} + k + \frac{kA}{4\bar{\rho}^2} & 2\,A\\
\frac{2}{q} - \frac{A}{2\bar{\rho}^2 q} & 0 & \frac{Ak^2}{32\bar{\rho}^4} & \bar{v}
\end{bmatrix}. \tag{4.88}$$

Notice that the last equation in (4.86) represents the consistency equation (4.72) after differentiating the function γ which can be obtained by taking the mass conservation out of the momentum conservation. Let us denote the perturbed eigenvalues and eigenvectors, of the matrix system (4.87) by

$$\begin{aligned}
\lambda_1 &= \lambda_{1,0} + \sqrt{A}\lambda_{1,1} + \mathcal{O}\left(A\right),\\
\lambda_2 &= \lambda_{2,0} + \sqrt{A}\lambda_{2,1} + \mathcal{O}\left(A\right),\\
\lambda_3 &= \lambda_{3,0} + A\lambda_{3,1} + \mathcal{O}\left(A^2\right),\\
\lambda_4 &= \lambda_{4,0} + A\lambda_{4,1} + \mathcal{O}\left(A^2\right),
\end{aligned} \tag{4.89}$$

and

$$\begin{aligned}
\boldsymbol{\chi_1} &= \boldsymbol{\chi_{1,0}} + \sqrt{A}\boldsymbol{\chi_{1,1}} + \mathcal{O}\left(A\right),\\
\boldsymbol{\chi_2} &= \boldsymbol{\chi_{2,0}} + \sqrt{A}\boldsymbol{\chi_{2,1}} + \mathcal{O}\left(A\right),\\
\boldsymbol{\chi_3} &= \boldsymbol{\chi_{3,0}} + A\boldsymbol{\chi_{3,1}} + \mathcal{O}\left(A^2\right),\\
\boldsymbol{\chi_4} &= \boldsymbol{\chi_{4,0}} + A\boldsymbol{\chi_{4,1}} + \mathcal{O}\left(A^2\right).
\end{aligned} \tag{4.90}$$

The eigenvalues λ_1 and λ_2 are constructed as perturbation series in powers of $\sqrt{A}$, while the others are calculated as perturbation series in powers of A. This is important. Otherwise, we will encounter asymptotic inconsistency in determining higher order corrections such as $\lambda_{1,1}$ and $\lambda_{2,1}$. In detailed explanation, when the λ_1 and λ_2 expressions (4.89) are substituted into (4.87), we find that $\lambda_{1,1}$ and $\lambda_{1,2}$ are only pos-

sible to be determined at the asymptotic order $\mathcal{O}\left(A^2\right)$, which is beyond the calculated asymptotic order, hence, the lack of consistency in the asymptotics. This is due to one characteristic being double at leading order (repeated eigenvalues).

To proceed, we first find the eigenvalues and the "left" eigenvectors of the above matrix system (4.87) with $A = 0$, that is, the eigenvalues and the eigenvectors of order $\mathcal{O}(1)$. After a standard linear algebra calculation, we find that the eigenvalues are

$$\lambda_{1,0} = \lambda_{2,0} = \bar{v} + k, \quad \lambda_{3,0} = \bar{v} + \sqrt{\frac{2\bar{\rho}}{q}}, \quad \lambda_{4,0} = \bar{v} - \sqrt{\frac{2\bar{\rho}}{q}}, \tag{4.91}$$

and the left eigenvectors are

$$\boldsymbol{\chi_{1,0}} = \begin{bmatrix} 0 \\ 0 \\ 1 \\ 0 \end{bmatrix}, \ \boldsymbol{\chi_{2,0}} = \begin{bmatrix} 0 \\ 0 \\ -1 \\ 0 \end{bmatrix}, \ \boldsymbol{\chi_{3,0}} = \begin{bmatrix} \sqrt{\frac{2}{q\bar{\rho}}} \\ 0 \\ \frac{\sqrt{2q\bar{\rho}}k}{4\bar{\rho}^2\left(\sqrt{2\bar{\rho}q}-kq\right)} \\ 1 \end{bmatrix}, \ \boldsymbol{\chi_{4,0}} = \begin{bmatrix} -\sqrt{\frac{2}{q\bar{\rho}}} \\ 0 \\ \frac{\sqrt{2q\bar{\rho}}k}{4\bar{\rho}^2\left(\sqrt{2\bar{\rho}q}+kq\right)} \\ 1 \end{bmatrix}. \tag{4.92}$$

Next, we substitute the perturbed expressions (4.89) and (4.90), on using (4.91) and (4.92), into the weakly non-linear system (4.87) and gather the terms whose asymptotic orders are identical, i.e., $\mathcal{O}\left(\sqrt{A}\right)$ and $\mathcal{O}\left(A\right)$. After extensive algebraic manipulations carried out in Maple software, we end up with the perturbed eigenvalues (characteristics)

$$\begin{aligned}
\lambda_1 &= \{\bar{v} + k\} + \sqrt{A}\left\{\frac{k}{4\bar{\rho}}\sqrt{\frac{20\,\bar{\rho} - 2k^2q}{k^2q - 2\,\bar{\rho}}}\right\}, \\
\lambda_2 &= \{\bar{v} + k\} - \sqrt{A}\left\{\frac{k}{4\bar{\rho}}\sqrt{\frac{20\,\bar{\rho} - 2k^2q}{k^2q - 2\,\bar{\rho}}}\right\}, \\
\lambda_3 &= \left\{\bar{v} + \sqrt{\frac{2\bar{\rho}}{q}}\right\} + A\left\{\frac{k}{2\bar{\rho}}\frac{\left(2\sqrt{2\bar{\rho}} - k\sqrt{q}\right)}{\left(\sqrt{2\bar{\rho}}\left(k^2q + 2\,\bar{\rho}\right) - 4\,k\bar{\rho}\sqrt{q}\right)}\right\}, \\
\lambda_4 &= \left\{\bar{v} - \sqrt{\frac{2\bar{\rho}}{q}}\right\} + A\left\{\frac{k}{2\bar{\rho}}\frac{\left(2\sqrt{2\bar{\rho}} + k\sqrt{q}\right)}{\left(\sqrt{2\bar{\rho}}\left(k^2q + 2\,\bar{\rho}\right) + 4\,k\bar{\rho}\sqrt{q}\right)}\right\},
\end{aligned} \tag{4.93}$$

associated with the perturbed left eigenvectors

$$\begin{aligned}
\boldsymbol{\chi_1} &= \begin{bmatrix} 0 \\ 0 \\ 1 \\ 0 \end{bmatrix} + \sqrt{A}\begin{bmatrix} \frac{-32\lambda_1\,\bar{\rho}^2}{k(k^2q-10\,\bar{\rho})} \\ \frac{-8\lambda_1\,\bar{\rho}^2\left(k^2q-2\,\bar{\rho}\right)}{k^2(k^2q-10\,\bar{\rho})} \\ 0 \\ \frac{-8\lambda_1\,\bar{\rho}^2\left(k^2q+2\,\bar{\rho}\right)}{k^2(k^2q-10\,\bar{\rho})} \end{bmatrix}, \\
\boldsymbol{\chi_2} &= \begin{bmatrix} 0 \\ 0 \\ 1 \\ 0 \end{bmatrix} + \sqrt{A}\begin{bmatrix} \frac{32\lambda_1\,\bar{\rho}^2}{k(k^2q-10\,\bar{\rho})} \\ \frac{8\lambda_1\,\bar{\rho}^2\left(k^2q-2\,\bar{\rho}\right)}{k^2(k^2q-10\,\bar{\rho})} \\ 0 \\ \frac{8\lambda_1\,\bar{\rho}^2\left(k^2q+2\,\bar{\rho}\right)}{k^2(k^2q-10\,\bar{\rho})}, \end{bmatrix},
\end{aligned} \tag{4.94}$$

$$\boldsymbol{\chi}_3 = \begin{bmatrix} \sqrt{\frac{2}{q\bar{\rho}}} \\ 0 \\ \frac{\sqrt{2q\bar{\rho}}\,k}{4\bar{\rho}^2\left(\sqrt{2q\bar{\rho}}-kq\right)} \\ 1 \end{bmatrix} + A \begin{bmatrix} 0 \\ \frac{1}{4\,\bar{\rho}^2+2\,\bar{\rho}\,k^2q-4\,\bar{\rho}\,k\sqrt{2q\bar{\rho}}} \\ 0 \\ 0 \end{bmatrix},$$
$$\boldsymbol{\chi}_4 = \begin{bmatrix} -\sqrt{\frac{2}{q\bar{\rho}}} \\ 0 \\ \frac{\sqrt{2q\bar{\rho}}\,k}{4\bar{\rho}^2\left(\sqrt{2q\bar{\rho}}+kq\right)} \\ 1 \end{bmatrix} + A \begin{bmatrix} 0 \\ \frac{1}{4\,\bar{\rho}^2+2\,\bar{\rho}\,k^2q+4\,\bar{\rho}\,k\sqrt{2q\bar{\rho}}} \\ 0 \\ 0 \end{bmatrix}. \tag{4.95}$$

The above perturbed eigenvectors are calculated up to the first non-trivial asymptotic order. In calculating the Riemann variables, only the first non-trivial terms in the expansions in terms of $\mathcal{O}(\sqrt{A})$ and $\mathcal{O}(A)$ were retained for simplicity and to yield amenable expressions. A similar asymptotic approach was done for the KdV5 equation [80] and excellent agreement with numerical solutions was found. In summary, the characteristic form of the modulation equations (4.85) is

$$-\frac{32\lambda_1\bar{\rho}^2a}{k\left(qk^2-10\bar{\rho}\right)}\frac{d\bar{\rho}}{dz}-\frac{8\lambda_1\bar{\rho}^2\left(qk^2-2\bar{\rho}\right)a}{k^2\left(qk^2-10\bar{\rho}\right)}\frac{dk}{dz}+\frac{da^2}{dz}-\frac{8\lambda_1\bar{\rho}^2\left(qk^2+2\bar{\rho}\right)a}{k^2\left(qk^2-10\bar{\rho}\right)}\frac{d\bar{v}}{dz}=0$$
$$\text{on}\quad \frac{dx}{dz}=\lambda_1=\bar{v}+k+\frac{ka}{4\bar{\rho}}\sqrt{\frac{20\,\bar{\rho}-2k^2q}{qk^2-2\,\bar{\rho}}}, \tag{4.96}$$
$$\frac{32\lambda_1\bar{\rho}^2a}{k\left(qk^2-10\bar{\rho}\right)}\frac{d\bar{\rho}}{dz}+\frac{8\lambda_1\bar{\rho}^2\left(qk^2-2\bar{\rho}\right)a}{k^2\left(qk^2-10\bar{\rho}\right)}\frac{dk}{dz}+\frac{da^2}{dz}+\frac{8\lambda_1\bar{\rho}^2\left(qk^2+2\bar{\rho}\right)a}{k^2\left(qk^2-10\bar{\rho}\right)}\frac{d\bar{v}}{dz}=0$$
$$\text{on}\quad \frac{dx}{dz}=\lambda_2=\bar{v}+k-\frac{ka}{4\bar{\rho}}\sqrt{\frac{20\,\bar{\rho}-2k^2q}{qk^2-2\,\bar{\rho}}}, \tag{4.97}$$
$$\sqrt{\frac{2}{q}}\frac{1}{\sqrt{\bar{\rho}}}\frac{d\bar{\rho}}{dz}+\frac{a^2}{4\bar{\rho}^2+2qk^2\bar{\rho}-4\sqrt{2q}k\bar{\rho}^{3/2}}\frac{dk}{dz}+\frac{\sqrt{2q}k}{4\bar{\rho}^{3/2}\left(\sqrt{2q}\sqrt{\bar{\rho}}-qk\right)}\frac{da^2}{dz}+\frac{d\bar{v}}{dz}=0$$
$$\text{on}\quad \frac{dx}{dz}=\lambda_3=\bar{v}+\sqrt{\frac{2}{q}}\sqrt{\bar{\rho}}+\frac{ka^2}{2\bar{\rho}}\frac{2\sqrt{2\bar{\rho}}-\sqrt{q}k}{\sqrt{2\bar{\rho}}\left(qk^2+2\,\bar{\rho}\right)-4\sqrt{q}\,k\bar{\rho}}, \tag{4.98}$$
$$-\sqrt{\frac{2}{q}}\frac{1}{\sqrt{\bar{\rho}}}\frac{d\bar{\rho}}{dz}+\frac{a^2}{4\bar{\rho}^2+2qk^2\bar{\rho}+4\sqrt{2q}k\bar{\rho}^{3/2}}\frac{dk}{dz}+\frac{\sqrt{2q}k}{4\bar{\rho}^{3/2}\left(\sqrt{2q}\sqrt{\bar{\rho}}+qk\right)}\frac{da^2}{dz}+\frac{d\bar{v}}{dz}=0$$
$$\text{on}\quad \frac{dx}{dz}=\lambda_4=\bar{v}-\sqrt{\frac{2}{q}}\sqrt{\bar{\rho}}+\frac{ka^2}{2\bar{\rho}}\frac{2\sqrt{2\bar{\rho}}+\sqrt{q}k}{\sqrt{2\bar{\rho}}\left(qk^2+2\,\bar{\rho}\right)+4\sqrt{q}\,k\bar{\rho}}, \tag{4.99}$$

to $\mathcal{O}(a^2)$. Unfortunately, it was not possible to set the characteristic form (4.96)–(4.99) into Riemann invariant form; a basic manifestation of Pfaff's problem [1]. Note that at leading order, with $a=0$, the two characteristics (4.98) and (4.99) are those for the shallow water wave equations [1], which must be the case. The system (4.96)–(4.99) is hyperbolic if the wavenumber k falls within the restricted range

$$\bar{u}<\sqrt{\frac{q}{2}}\,k<\sqrt{5}\,\bar{u}, \tag{4.100}$$

as $\bar{u}=\sqrt{\bar{\rho}}$. The Stokes wavetrain is then modulationally stable for k in the range

(4.100) and unstable otherwise. The restricted range of the wavenumber for stability leads to the resonant wavetrain generated by the DSW being unstable over the majority of the range of its existence. Outside the range (4.100), the system (4.96)–(4.99) is a mixed elliptic-hyperbolic system since the characteristics (4.98) and (4.99), which are those for the shallow water equations at leading order, are always real. This is important as in the following chapter the Riemann variables on these characteristics are used to construct the solutions in the TDSW and VDSW regimes. The rest of the characteristics, which are (4.96) and (4.97), represent the non-linear generalisation of the linear nematic group velocity in the short-wavelength approximation. The leading terms in these characteristics are the linear group velocities and these velocities are perturbed by two identical corrections with opposite signs. Such double splitting of characteristic velocities, under the effect of the non-linearity, is standard in non-linear dispersive wave theory [1]. Our study and discussion of the nematic modulational stability will be extended with further details in the next chapter, to be specific, in Sections 5.4 and 5.5.

4.3 Conclusions

A Stokes wave solution as an alternative to an exact non-linear periodic wave solution for the non-integrable defocusing nematic equations was derived. Weakly non-linear Whitham's modulation theory was then employed on a slowly varying nematic Stokes wave to derive two sets of modulation equations. These modulation equations are obtained by a mixture of the methods of averaged Lagrangians and averaged conservation laws. The set of modulation equations obtained from the method of averaged Lagrangians was used to study the modulational stability of nematic resonant radiation, whilst the other one obtained from the method of averaged conservation laws will be used in Chapter 5 to analyse the structures of the nematic TDSW and VDSW regimes. The reason behind these two different utilisations of modulation equations is the energy conservation law which is needed in the physical theory of shock waves instead of the wave action conservation law, more details will be given in Section 5.5. The nematic modulation equations is a system of size 4×4, and it was impossible to us to find integrating factors that set this modulation system in Riemann invariant form (Pfaff's problem). It has been found that when the value of the resonant wavenumber lies within the range $k^2 \in (2\bar{u}/q, 10\bar{u}/q)$, the nematic modulation system becomes fully hyperbolic, otherwise, it is half elliptic half hyperbolic.

Chapter 5

Full Analysis of Nematic Hydrodynamics

In this chapter, we derive theoretical solutions for nematic non-dispersive and dispersive hydrodynamic regimes. These solutions are obtained by using the method characteristics and various perturbation techniques that are base directly or indirectly on Whitham's averaging theory. The theoretical results will be compared with numerical solutions and discussed further in the next chapter.

5.1 Non-convex Dispersive Hydrodynamics

Non-convex dispersive hydrodynamics is a dispersive hydrodynamic equation or system of equations whose linear dispersion relation ω is a non-convex function over the domain of the wavenumber k. The nematic dispersive hydrodynamic system (2.24)–(2.26) is an example of non-convex dispersive hydrodynamics. Indeed, the profile of its linear dispersion relation has an inflection point at $k = 0.281$, as depicted in Figure 5.3. In essence, the loss of convexity for the linear dispersion relation leads to a potential resonance between low and high frequency waves [61, 79]. This is consistent with what is seen in Figures 3.3 and 3.4. These figures show that the nematic (resonant) DSWs are made of two different wave structures based on two distinct frequency scales. First, a KdV-type DSW ($p = 1, d = 1$) which consists of modulated waves of low frequencies (long-wavelengths; $0 < k < 0.15$) lies at the leading edge of the intermediate level. Second, there is a linear resonant wavetrain, located in the front of the DSW, which is composed of waves of relatively high frequencies (short-wavelengths), actually $k = \mathcal{O}(1)$. The resonance acts as a damping force on the nematic DSW and this results in a leak in energy and mass from the DSW. This is the underlying reason for why the nematic DSW in, for example, Figure 3.4, resembles an unstable modulated wavetrain. The effect of the resonance on the DSW form is significant when the difference between u_- and u_+ is large. However, it is negligible when this difference is small. Note that there is another branch of non-convex dispersive hydrodynamics in which hyperbolic fluxes are non-convex, as in the modified KdV equation [18, 171]. This source of non-convexity in dispersive hydrodynamics gives rise to undercompressive shock waves and shock-rarefactions in the theory of hyperbolic systems. This kind of non-convex dispersive hydrodynamics is outside the scope of this thesis, however, so it will not be discussed further.

In general, the existence of a resonance in non-linear dispersive wave equations is typical when higher order dispersive effects are taken into account. For instance,

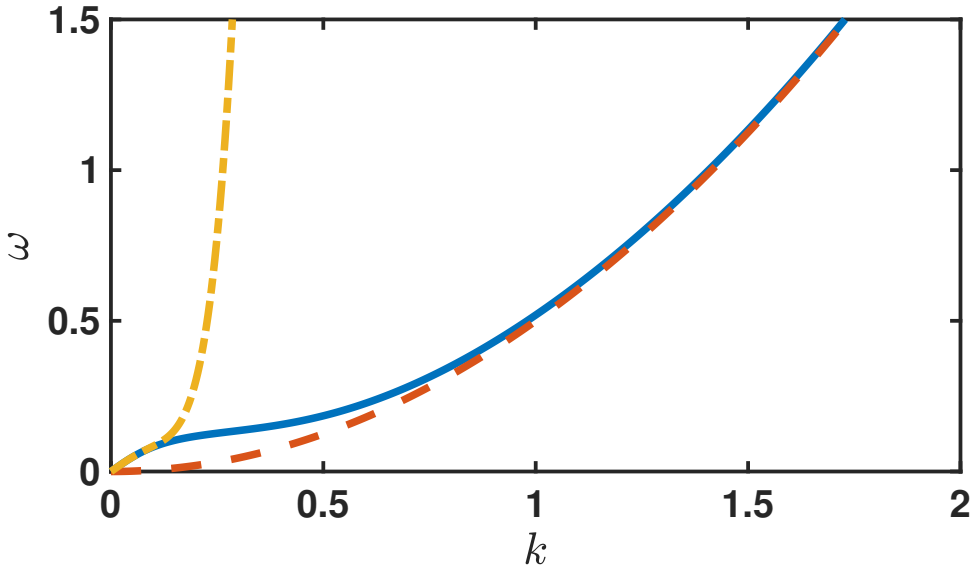

Figure 5.1: Full dispersion relation (blue; solid line), long wave dispersion relation (yellow; dash-dot) and short wave dispersion relation (orange; dashed line). Here, $\nu = 200$, $q = 2$, $\bar{\rho} = 1$ and $\bar{v} = 0$. (Online version in colour.)

resonant DSWs have been observed experimentally in the context of non-linear optics, for which the governing equations is the NLS equation with higher order dispersive terms added [158, 159, 160, 161] and also have been studied in the context of fluid mechanics when fifth order dispersion is added to the KdV equation (water wave theory) [79, 80, 81]. Similarly, resonant radiation is possible to exist as part of solitary wave solutions of non-linear dispersive wave equations when higher order dispersive terms are added. The effect of the linear resonant radiation generation by solitary wave solutions of these equations is well-known in the framework of non-linear optics [163, 164] and gravity-capillary water waves [165, 166, 167, 168]. A simple example of a non-convex dispersive hydrodynamic equation, that is related to the work of this thesis and has been well studied recently, is the Kawahara equation (1.40) [79, 80, 81]. The linear dispersion relation for the Kawahara equation (1.40) about an initial state (a background) $\bar{u}$ is

$$\omega = 6\bar{u}k - \mu_d k^3 + k^5. \tag{5.1}$$

When the dispersion parameter μ_d is positive ($\mu_d > 0$), the linear dispersion relation becomes a non-convex function over the range of the wavenumber k. Then, linear radiation can propagate at a phase velocity V_p that equals the velocity of the lead solitary wave V_s of the Kawahara DSW, yielding a propagating resonance ahead of the DSW whose front is given by the group velocity of the linear radiations [61, 79, 80]. Solitary waves are then unstable and leak away to radiation. Figure 5.2 shows a resonant DSW governed by the non-convex Kawahara equation (1.40). The analogy between this figure and Figure 3.3 is illuminating. When the dispersion parameter is negative ($\mu_d < 0$), the linear dispersion relation becomes convex, thus, the Kawahara equation does not exhibit a resonant DSW in this case. The resulting DSW is similar to the DSW given by the classical third-order KdV equation (1.10) which has the linear dispersion relation

$$\omega = 6\bar{u}k - \mu_d k^3. \tag{5.2}$$

Independent of whether the sign of the dispersion is positive or negative in the third-order KdV equation, the solitary waves at the leading edge of the KdV DSW ($p = 1, d = 1$) do not shed radiation ahead of it due to the convexity or the concavity of the linear dispersion relation (5.2), as can be seen in Figures 1.7 and 1.8(a). Thus, the change in the curvature from negative (concavity) to positive (convexity) in the non-convex linear dispersion relation corresponds to radical transformations in the form of the Kawahara DSWs as k increases [79]. Now let us discuss the non-convexity of

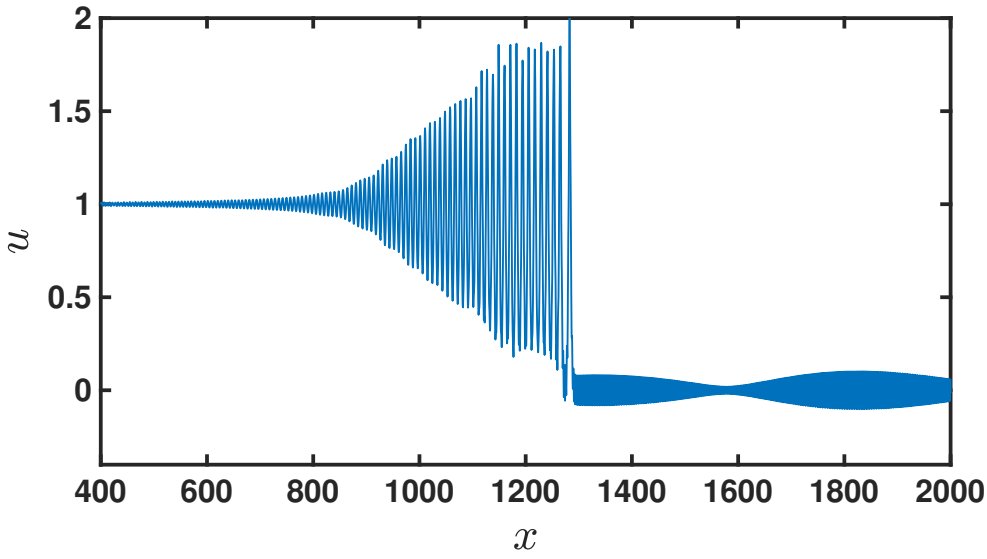

Figure 5.2: A resonant DSW governed by the Kawahara equation (1.40). Here, $\mu_d = 7.0$, $u_- = 1$, $u_+ = 0$ and $t = 50$

the nematic dispersive hydrodynamics (2.24)–(2.26). To analyse mathematically the two generic oscillatory structures existing for the nematic resonant DSWs, we need to seek long- and short-wavelength approximations of the full linear dispersion relation (4.26). The short-wavelength approximation of the full linear dispersion relation has been already derived in Section 4.1 and we recall it here. With the asymptotic limits $\nu \gg 1$ and $\nu k^2 \gg 1$, the dispersion relation is

$$\omega = k\bar{v} + \frac{k^2}{2} + \frac{2\bar{\rho}}{q} + \mathcal{O}\left(\frac{1}{\nu k^2}\right). \tag{5.3}$$

In contrast, the long-wavelength approximation of the full linear dispersion relation, with the asymptotic limits $k \ll 1$ and $\nu k^2 \ll 1$, is

$$\omega = k\left\{U + \bar{v}\right\} - \frac{U}{4}\left\{\frac{\nu}{q} - \frac{q}{4\bar{\rho}}\right\}k^3 + \frac{U}{32}\left\{\frac{3\nu^2}{q^2} + \frac{\nu}{2\bar{\rho}} - \frac{q^2}{16\bar{\rho}^2}\right\}k^5 + o(k^5), \tag{5.4}$$

with

$$U = \sqrt{\frac{2}{q}}\sqrt{\bar{\rho}}. \tag{5.5}$$

This long-wavelength approximation is analogous to the Kawahara linear dispersion relation (5.1). Although we have assumed that $\nu k^2 \ll 1$, this does not hold always true for reasonably small wavenumber due to the very large value of the non-locality ν. However, we shall see that this long wave approximation captures key qualitative

characteristics of the nematic dispersion relation (4.26). From the short wave asymptotic expression (5.3), we can see that the dispersion is convex for large wavenumbers ($\omega_{kk} > 0$), whereas the asymptotic formula (5.4) shows that the dispersion is concave for small wavenumbers ($\omega_{kk} < 0$). Hence, we see the non-convexity of the full linear dispersion relation (4.26) over the whole range of the wavenumber. A comparison between the approximations (5.3) and (5.4) and the nematic full linear dispersion relation (4.26) is given in Figure 5.3. It can be seen that the expressions (5.3) and (5.4) coincide with the profile of the full nematic dispersion relation in the limits of low and high wavenumber, respectively, which is to be expected. Yet, because of the large coefficient of the k^5 term in the asymptotic dispersion relation (5.4), the short-wavelength approximation expansion rapidly diverges from the exact nematic linear dispersion relation as k increases. Nonetheless, it qualitatively captures the basic property of the non-convexity of the full nematic linear dispersion relation, so it can be used for qualitative predictions of the effects of the non-locality on the nematic DSW behaviour. In Figure **??**, we can see that the full nematic phase velocity V_p is a non-monotonic function and has an inflection point at a particular wavenumber, $k = 0.099$. This is also qualitatively captured by the long-wavelength approximation. The change in the behaviour of the full phase velocity from decreasing to increasing indicates that the solitary waves' velocity in the nematic KdV-type DSW regime, that takes place in the low wavenumber limit, changes to be equal to the phase velocity of the linear radiation in the high wavenumber limit, namely, $V_s = V_p$, hence the observed resonance.

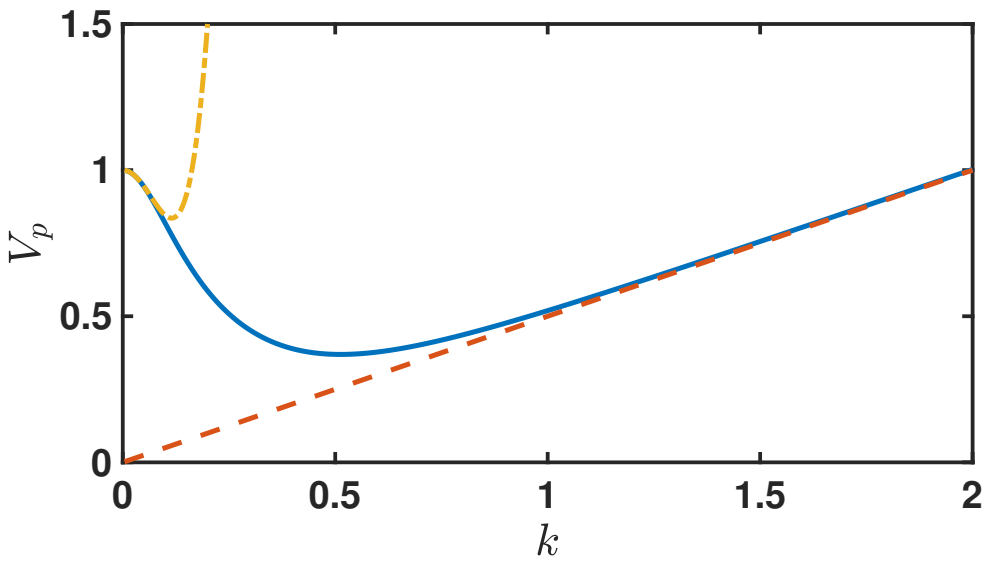

Figure 5.3: Full dispersion relation (blue; solid line), long wave dispersion relation (yellow; dash-dot) and short wave dispersion relation (orange; dashed line). Here, $\nu = 200$, $q = 2$, $\bar{\rho} = 1$ and $\bar{v} = 0$. (Online version in colour.)

5.2 Nematic Non-dispersive Hydrodynamics

In this section, we derive theoretical solutions of the defocusing nematic equations (2.19) and (2.20) in the dispersionless limit. These solutions will be derived in both cases for which the initial phases in the condition (2.29) are both trivial, $\phi_- = \phi_+ = 0$, and when at least one of the initial phases is not so, ϕ_- and/or $\phi_+ \neq 0$. As shown in

Chapter 3, the majority of the numerical nematic hydrodynamic solutions feature two distinct wave structures that can be easily distinguished by the influence of dispersion. These solutions have expansion waves followed by DSWs with a shelf in between, or the other way around, as in Case 1, see Subsection 3.2.2. Other hydrodynamic regimes are either fully non-dispersive, such as the dam break solution [1], a combination of rarefaction waves, or completely dispersive for which DSWs are interacting with each other. Theoretically, the non-dispersive and dispersive regions existing in the numerical solutions can be analysed separately by using the polar coordinate transformation, the Madelung transformation (2.23). The nematic hydrodynamics in the dispersionless limit then takes the form of, on using (2.24)–(2.26),

$$\begin{aligned} \frac{\partial \rho}{\partial z} + \rho \frac{\partial v}{\partial x} + v \frac{\partial \rho}{\partial x} &= 0, & (5.6)\\ \frac{\partial v}{\partial z} + v \frac{\partial v}{\partial x} + 2 \frac{\partial \theta}{\partial x} &= 0, & (5.7)\\ 2\rho - 2q\theta &= 0, & (5.8) \end{aligned}$$

which yields the following second order system

$$\begin{aligned} \frac{\partial \rho}{\partial z} + v \frac{\partial \rho}{\partial x} + \rho \frac{\partial v}{\partial x} &= 0, & (5.9)\\ \frac{\partial v}{\partial z} + \frac{2}{q} \frac{\partial \rho}{\partial x} + v \frac{\partial v}{\partial x} &= 0, & (5.10) \end{aligned}$$

The variables ρ and v play the roles of the fluid depth and the fluid velocity in the shallow water wave equations [1], respectively. To calculate the nematic non-dispersive solutions, the above dispersionless equations (5.9) and (5.10) need to be set in Riemann invariant form. Clearly, the associated matrix system of this dispersionless system is

$$\begin{bmatrix} \rho \\ v \end{bmatrix}_z + \begin{bmatrix} v & \rho \\ 2/q & v \end{bmatrix} \begin{bmatrix} \rho \\ v \end{bmatrix}_x = \begin{bmatrix} 0 \\ 0 \end{bmatrix}. \tag{5.11}$$

This matrix has eigenvalues (characteristics)

$$\lambda_+ = v + \sqrt{\frac{2}{q}}\sqrt{\rho} \quad \text{and} \quad \lambda_- = v - \sqrt{\frac{2}{q}}\sqrt{\rho}, \tag{5.12}$$

and "left" eigenvectors

$$\boldsymbol{\chi}_+^T = \begin{bmatrix} \sqrt{\frac{2}{q}}\frac{1}{\sqrt{\rho}} \\ 1 \end{bmatrix} \quad \text{and} \quad \boldsymbol{\chi}_-^T = \begin{bmatrix} -\sqrt{\frac{2}{q}}\frac{1}{\sqrt{\rho}} \\ 1 \end{bmatrix}. \tag{5.13}$$

Therefore, we find the characteristic form of the nematic dispersionless hydrodynamics (5.6)–(5.8),

$$\begin{aligned} dv + \sqrt{\frac{2}{q}}\frac{1}{\sqrt{\rho}} d\rho = 0 \quad &\text{on} \quad C_+ : \frac{dx}{dz} = v + \sqrt{\frac{2}{q}}\sqrt{\rho}, & (5.14)\\ dv - \sqrt{\frac{2}{q}}\frac{1}{\sqrt{\rho}} d\rho = 0 \quad &\text{on} \quad C_- : \frac{dx}{dz} = v - \sqrt{\frac{2}{q}}\sqrt{\rho}. & (5.15) \end{aligned}$$

Since this is a second order system, it can be set in Riemann invariant form as integrating factors always exist [1]. The Riemann invariant form of the non-dispersive system

(5.6)–(5.8) is

$$v + 2\sqrt{\frac{2}{q}}\sqrt{\rho} = R_+ \qquad \text{on} \qquad C_+ : \frac{dx}{dz} = v + \sqrt{\frac{2}{q}}\sqrt{\rho}, \tag{5.16}$$

$$v - 2\sqrt{\frac{2}{q}}\sqrt{\rho} = R_- \qquad \text{on} \qquad C_- : \frac{dx}{dz} = v - \sqrt{\frac{2}{q}}\sqrt{\rho}, \tag{5.17}$$

with $\theta = \rho/q$. These Riemann invariants and characteristics are the keys to deduce the dam break and simple wave solutions existing in the nematic regimes, as we shall see shortly. Because there are many types of non-dispersive wave solutions that can be observed from the numerical solutions presented in Chapter 3, these solutions will be classified into three classes: Rarefaction Wave Classes I, II and III. Our classification is mainly based upon the orientation of the rarefaction wave and the existence of more than one rarefaction wave in one hydrodynamic regime. Detailed descriptions of these rarefaction waves will be given in the subsequent subsections, as well as providing theoretical solutions for them. The analytical solutions will be compared with numerical solutions in Chapter 6 and excellent agreement is found. Note that these theoretical solutions are also valid as non-dispersive solutions for the defocusing NLS equation (1.17). This is because the nematic dispersive hydrodynamics is an NLS-type system and reduces to the NLS dispersive hydrodynamics in the limit $\nu \to 0$.

5.2.1 Rarefaction Wave Class I

This is a simple wave solution that exists when the initial level behind is non-zero ($u_- \neq 0$), the initial phases are both trivial ($\phi_- = \phi_+ = 0$) and $u_- > u_+$. This class of non-dispersive solution is divided into two non-dispersive subclasses. One subclass is a pure expansion fan with a zero initial level ahead, $u_+ = 0$. This is the counterpart of the dam break solution that occurs in shallow water wave theory [1]. The another subclass is an expansion fan with a shelf $u_i \neq 0$, as the level ahead of u_-, separating the simple wave from the nematic DSW. These types of dispersionless waves are demonstrated in Figures 3.2–3.7.

Let us commence with the first dispersionless subclass, for which $u_+ = 0$. Generally speaking, we need to determine the right Riemann invariant and the characteristic, from (5.16) and (5.17), which are associated with this class of rarefaction wave. Clearly, there are four pair of options: (R_+, C_+), (R_+, C_-), (R_-, C_+) and (R_-, C_-). The valid choice that corresponds to this rarefaction wave is found to be (R_+, C_-). The other options give invalid trailing or leading edge velocities for the rarefaction wave. The Riemann invariant on the C_+ characteristics, R_+, is determined by the initial condition (2.29). This gives

$$v + 2\sqrt{\frac{2}{q}}\sqrt{\rho} = R_+ = 2\sqrt{\frac{2}{q}}\sqrt{\rho_-}. \tag{5.18}$$

Hence, the phase gradient v and the characteristic curves C_- become, respectively,

$$v = 2\sqrt{\frac{2}{q}}\left\{\sqrt{\rho_-} - \sqrt{\rho}\right\} \quad \text{and} \quad \frac{x}{z} = v - \sqrt{\frac{2\rho}{q}}, \tag{5.19}$$

where the constant of integration obtained by integrating the characteristics C_- equals zero as the expansion fan starts at $x = 0$ at the initial value $z = 0$. From equation (5.19), we deduce that the trailing and leading edge velocities of the dam break solution

are, in the order given,

$$\frac{x_-}{z} = -\sqrt{\frac{2}{q}}\sqrt{\rho_-} \quad \text{and} \quad \frac{x_+}{z} = 2\sqrt{\frac{2}{q}}\sqrt{\rho_-}. \tag{5.20}$$

The analytical expressions for the derivative of the phase v and the optical intensity $|u| = \sqrt{\rho}$ as functions of the independent variables x and z are, on solving equations (5.19),

$$v = \frac{2}{3}\frac{x}{z} + \frac{2}{3}\sqrt{\frac{2}{q}}u_- \quad \text{and} \quad |u| = \frac{1}{3}\sqrt{\frac{q}{2}}\left\{2\sqrt{\frac{2}{q}}u_- - \frac{x}{z}\right\}. \tag{5.21}$$

The final solution for the dam break problem is then

$$|u| = \begin{cases} u_-, & \frac{x}{z} < -\sqrt{\frac{2}{q}}u_- \\ \frac{1}{3}\sqrt{\frac{q}{2}}\left\{2\sqrt{\frac{2}{q}}u_- - \frac{x}{z}\right\}, & -\sqrt{\frac{2}{q}}u_- \le \frac{x}{z} \le 2\sqrt{\frac{2}{q}}u_- \\ 0, & 2\sqrt{\frac{2}{q}}u_- < \frac{x}{z} \end{cases} \tag{5.22}$$

and

$$v = \begin{cases} 0, & \frac{x}{z} < -\sqrt{\frac{2}{q}}u_- \\ \frac{2}{3}\left\{\sqrt{\frac{2}{q}}u_- + \frac{x}{z}\right\}, & -\sqrt{\frac{2}{q}}u_- \le \frac{x}{z} \le 2\sqrt{\frac{2}{q}}u_- \\ 2\sqrt{\frac{2}{q}}u_-, & 2\sqrt{\frac{2}{q}}u_- < \frac{x}{z}. \end{cases} \tag{5.23}$$

Next, we solve the second dispersionless subclass for which the level ahead of u_- is the shelf $u_i \neq 0$. The main differences between the previous dam break solution and this dispersionless solution are the velocity of the leading edge of the rarefaction wave and the value of the phase derivative on the intermediate level u_i. As the leading edge of the simple wave is connected to the intermediate level, then it follows from (5.19) that the derivative of the phase and the leading edge velocity at the shelf are, respectively,

$$v_i = 2\sqrt{\frac{2}{q}}\left\{u_- - u_i\right\} \quad \text{and} \quad \frac{x_i}{z} = \sqrt{\frac{2}{q}}\left\{2u_- - 3u_i\right\}. \tag{5.24}$$

Therefore, the overall solution for the non-dispersive wave is

$$|u| = \begin{cases} u_-, & \frac{x}{z} < -\sqrt{\frac{2}{q}}u_- \\ \frac{1}{3}\sqrt{\frac{q}{2}}\left\{2\sqrt{\frac{2}{q}}u_- - \frac{x}{z}\right\}, & -\sqrt{\frac{2}{q}}u_- \le \frac{x}{z} \le \sqrt{\frac{2}{q}}\left\{2u_- - 3u_i\right\} \\ u_i, & \sqrt{\frac{2}{q}}\left\{2u_- - 3u_i\right\} < \frac{x}{z} \le s_- \end{cases} \tag{5.25}$$

and

$$v = \begin{cases} 0, & \frac{x}{z} < -\sqrt{\frac{2}{q}}u_- \\ \frac{2}{3}\left\{\sqrt{\frac{2}{q}}u_- + \frac{x}{z}\right\}, & -\sqrt{\frac{2}{q}}u_- \le \frac{x}{z} \le \sqrt{\frac{2}{q}}\left\{2u_- - 3u_i\right\} \\ v_i, & \sqrt{\frac{2}{q}}\left\{2u_- - 3u_i\right\} < \frac{x}{z} \le s_-. \end{cases} \tag{5.26}$$

The value of the velocity s_- of the leading edge of the shelf u_i depends on the nematic DSW regimes. In the PDSW, RDSW and CDSW regimes, s_- denotes the group velocity of the trailing edge of the DSW, whilst in the TDSW and VDSW regimes, it is the Whitham shock velocity. These velocities will be calculated in Sections 5.3, 5.5 and 5.6. Now, the remaining thing is to determine analytically the shelf u_i analytically. This

quantity can be determined by the requirement that the Riemann invariant along the characteristics C_-, that is, R_-, is conserved across the nematic DSW. This was shown to be true for the defocusing NLS DSW by using modulation theory [18, 133, 134, 162] and we here generalise it to the nematic DSWs as the electric field equation in the defocusing nematic system is a defocusing NLS-type equation. Thus, we have

$$v_i - 2\sqrt{\frac{2}{q}}\sqrt{\rho_i} = R_- = -2\sqrt{\frac{2}{q}}\sqrt{\rho_+}, \tag{5.27}$$

which then yields, on using (5.24),

$$u_i = \frac{1}{2}\{u_- + u_+\}. \tag{5.28}$$

Equation (5.28) means that the shelf height is simply the average value of the initial levels ahead u_+ and behind u_-, which is in agreement with numerical solutions of Chapter 3. The corresponding director solution is given by $\theta = |u|^2/q$. This finishes the analytical discussion of Rarefaction Wave Class I.

5.2.2 Rarefaction Wave Class II

This simple wave solution exists when the initial level ahead is non-zero ($u_+ \neq 0$), at least one of the initial phases is non-trivial (ϕ_- and/or $\phi_+ \neq 0$) and the initial phases satisfy the inequalities (3.29) with $u_- < u_+$. There are two different non-dispersive subclasses here. The first subclass is a pure expansion fan with a trivial initial level ($u_- = 0$), while the second one is an expansion fan with a shelf $u_i \neq 0$ as the level separating the simple wave from the nematic DSW. It is clear that this class is opposite to the previous one. This class of non-dispersive wave is presented in Subsection 3.2.2 as Case 3, see Figure 3.9.

Contrary to Rarefaction Wave Class I, the simple wave solution in this class corresponds to the Riemann invariant and characteristic pair (R_-, C_+). The calculation is similar to the one of the previous section, but with the initial wavenumbers v_- and v_+ accounted for now. We start with the dam break solution that takes place when $u_- = 0$. From the initial condition (2.29), the Riemann invariant along the characteristics C_- satisfies

$$v - 2\sqrt{\frac{2}{q}}\sqrt{\rho} = R_- = v_+ - 2\sqrt{\frac{2}{q}}\sqrt{\rho_+}. \tag{5.29}$$

Then, the phase gradient v and the characteristic curves C_+ are, successively,

$$v = v_+ + 2\sqrt{\frac{2}{q}}\{\sqrt{\rho} - \sqrt{\rho_+}\} \quad \text{and} \quad \frac{x}{z} = v + \sqrt{\frac{2}{q}}\sqrt{\rho}. \tag{5.30}$$

and

$$v = v_+ + 2\sqrt{\frac{2}{q}}\{\sqrt{\rho} - \sqrt{\rho_+}\} \quad \text{and} \quad \frac{x}{z} = v + \sqrt{\frac{2}{q}}\sqrt{\rho}. \tag{5.31}$$

Consequently, the trailing and leading edge velocities of the dam break solution are, in the order given,

$$\frac{x_-}{z} = v_+ - 2\sqrt{\frac{2}{q}}\sqrt{\rho_+} \tag{5.32}$$

and

$$\frac{x_+}{z} = v_+ + \sqrt{\frac{2}{q}}\sqrt{\rho_+}. \tag{5.33}$$

The theoretical expressions for the phase derivative v and the optical intensity $|u| = \sqrt{\rho}$ as functions of the independent variables x and z are, on using equations (5.31),

$$v = \frac{2}{3}\frac{x}{z} - \frac{2}{3}\sqrt{\frac{2}{q}}\sqrt{\rho_+} + \frac{v_+}{3} \quad \text{and} \quad |u| = \frac{1}{3}\sqrt{\frac{q}{2}}\left\{\frac{x}{z} + 2\sqrt{\frac{2}{q}}\sqrt{\rho_+} - v_+\right\}. \tag{5.34}$$

Therefore, the solution of the dam break problem for this case is

$$|u| = \begin{cases} 0, & \frac{x}{z} < v_+ - 2\sqrt{\frac{2}{q}}u_+ \\ \frac{1}{3}\sqrt{\frac{q}{2}}\left\{\frac{x}{z} + 2\sqrt{\frac{2}{q}}u_+ - v_+\right\}, & v_+ - 2\sqrt{\frac{2}{q}}u_+ \le \frac{x}{z} \le v_+ + \sqrt{\frac{2}{q}}u_+ \\ u_+, & v_+ + \sqrt{\frac{2}{q}}u_+ < \frac{x}{z} \end{cases} \tag{5.35}$$

and

$$v = \begin{cases} 0, & \frac{x}{z} < v_+ - 2\sqrt{\frac{2}{q}}u_+ \\ \frac{2}{3}\frac{x}{z} - \frac{2}{3}\sqrt{\frac{2}{q}}u_+ + \frac{v_+}{3}, & v_+ - 2\sqrt{\frac{2}{q}}u_+ \le \frac{x}{z} \le v_+ + \sqrt{\frac{2}{q}}u_+ \\ v_+, & v_+ + \sqrt{\frac{2}{q}}u_+ < \frac{x}{z}. \end{cases} \tag{5.36}$$

As for the case for which the intermediate level $u_i \neq 0$ is located at the rear side of the simple wave separating the expansion fan from the nematic DSW. The trailing edge of the rarefaction wave now propagates with the velocity

$$\frac{x_i}{z} = v_i + \sqrt{\frac{2}{q}}\sqrt{\rho_i}, \tag{5.37}$$

for which the derivative of the phase on the intermediate height v_i is given by, on using (5.31),

$$v_i = v_+ + 2\sqrt{\frac{2}{q}}\left\{\sqrt{\rho_i} - \sqrt{\rho_+}\right\}. \tag{5.38}$$

The analytical formula for the shelf $u_i = \sqrt{\rho_i}$ in the above equations can be determined by the fact that the Riemann invariant R_- is conserved through the rarefaction wave and R_+ is conserved across the nematic DSW. The first conservation result is already given in equation (5.38), whereas the latter conservation result at $\rho = \rho_i$ and $v = v_i$ is

$$v_i + 2\sqrt{\frac{2}{q}}\sqrt{\rho_i} = R_+ = v_- + 2\sqrt{\frac{2}{q}}\sqrt{\rho_-}. \tag{5.39}$$

Solving equations (5.38) and (5.39) gives

$$u_i = \sqrt{\rho_i} = \frac{1}{4}\sqrt{\frac{q}{2}}\left\{v_- - v_+\right\} + \frac{1}{2}\left\{\sqrt{\rho_-} + \sqrt{\rho_+}\right\} \tag{5.40}$$

and

$$v_i = \frac{1}{2}\left\{v_- + v_+\right\} + \sqrt{\frac{2}{q}}\left\{u_- - u_+\right\}. \tag{5.41}$$

Therefore, the trailing edge velocity of the simple wave is

$$\frac{x_i}{z} = \frac{1}{4}\left\{3v_- + v_+\right\} + \frac{1}{2}\sqrt{\frac{2}{q}}\left\{3u_- - u_+\right\}. \tag{5.42}$$

Hence, we finally have the theoretical solution for the second subclass of Rarefaction Wave Class II:

$$|u| = \begin{cases} u_i, & s_- \leq \frac{x}{z} < \frac{1}{4}\{3v_- + v_+\} + \frac{1}{2}\sqrt{\frac{2}{q}}\{3u_- - u_+\} \\ \frac{1}{3}\sqrt{\frac{q}{2}}\left\{\frac{x}{z} + 2\sqrt{\frac{2}{q}}u_+ - v_+\right\}, & \frac{1}{4}\{3v_- + v_+\} + \frac{1}{2}\sqrt{\frac{2}{q}}\{3u_- - u_+\} \leq \frac{x}{z} \\ & \leq v_+ + \sqrt{\frac{2}{q}}u_+ \\ u_+, & v_+ + \sqrt{\frac{2}{q}}u_+ < \frac{x}{z} \end{cases} \tag{5.43}$$

and

$$v = \begin{cases} v_i, & s_- \leq \frac{x}{z} < \frac{1}{4}\{3v_- + v_+\} + \frac{1}{2}\sqrt{\frac{2}{q}}\{3u_- - u_+\} \\ \frac{2}{3}\frac{x}{z} - \frac{2}{3}\sqrt{\frac{2}{q}}u_+ + \frac{v_+}{3}, & \frac{1}{4}\{3v_- + v_+\} + \frac{1}{2}\sqrt{\frac{2}{q}}\{3u_- - u_+\} \leq \frac{x}{z} \\ & \leq v_+ + \sqrt{\frac{2}{q}}u_+ \\ v_+, & v_+ + \sqrt{\frac{2}{q}}u_+ < \frac{x}{z}. \end{cases} \tag{5.44}$$

The associated director solution is given by $\theta = |u|^2/q$. This completes the analytical investigation of Rarefaction Wave Class II.

5.2.3 Rarefaction Wave Class III

This wave is a combination of two distinct simple waves. However, these waves are similar to the ones belonging to the classes of Rarefaction Wave I and II, with a shelf u_i separating them from each other. This is found when the initial levels u_-, u_+ and the initial wavenumbers v_-, v_+ satisfy inequalities (3.30) and (3.31). For illustrations of this class, see Figures 3.10, 3.11 and 3.12.

In this class, the downstream simple wave resembles a rarefaction wave of Class II and its solution is given by (5.43) and (5.44). The simple wave in the upstream direction, on the other hand, represents a rarefaction wave of class I, but the initial wavenumbers are now non-zero so the solution for this wave is not given in Subsection 5.2.1. Nonetheless, the derivation of the analytical solution for this simple wave, with the initial wavenumbers included, is analogous to the calculation in the previous subsection. Therefore, we only present here the final result of this derivation. The analytical solution for Rarefaction Wave Class III is

$$|u| = \begin{cases} u_-, & \frac{x}{z} < v_- - \sqrt{\frac{2}{q}}u_- \\ \frac{1}{3}\sqrt{\frac{q}{2}}\left\{v_- + 2\sqrt{\frac{2}{q}}u_- - \frac{x}{z}\right\}, & v_- - \sqrt{\frac{2}{q}}u_- \leq \frac{x}{z} \\ & \leq \frac{1}{4}\{v_- + 3v_+\} + \frac{1}{2}\sqrt{\frac{2}{q}}\{u_- - 3u_+\}, \\ u_i = \frac{1}{2}\{u_- + u_+\} + \frac{1}{4}\sqrt{\frac{q}{2}}\{v_- - v_+\}, & \frac{1}{4}\{v_- + 3v_+\} + \frac{1}{2}\sqrt{\frac{2}{q}}\{u_- - 3u_+\} < \frac{x}{z} \\ & < \frac{1}{4}\{3v_- + v_+\} + \frac{1}{2}\sqrt{\frac{2}{q}}\{3u_- - u_+\}, \\ \frac{1}{3}\sqrt{\frac{q}{2}}\left\{2\sqrt{\frac{2}{q}}u_+ - v_+ + \frac{x}{z}\right\}, & \frac{1}{4}\{3v_- + v_+\} + \frac{1}{2}\sqrt{\frac{2}{q}}\{3u_- - u_+\} \leq \frac{x}{z} \\ & \leq v_+ + \sqrt{\frac{2}{q}}u_+, \\ u_+, & v_+ + \sqrt{\frac{2}{q}}u_+ < \frac{x}{z} \end{cases} \tag{5.45}$$

and

$$v=\begin{cases} v_-, & \frac{x}{z}<v_--\sqrt{\frac{2}{q}}u_- \\ \frac{1}{3}v_-+\frac{2}{3}\sqrt{\frac{2}{q}}u_-+\frac{2}{3}\frac{x}{z}, & v_--\sqrt{\frac{2}{q}}u_-\le\frac{x}{z} \\ & \le\frac{1}{4}\{v_-+3v_+\}+\frac{1}{2}\sqrt{\frac{2}{q}}\{u_--3u_+\}, \\ v_i=\frac{1}{2}\{v_-+v_+\}+\sqrt{\frac{2}{q}}\{u_--u_+\}, & \frac{1}{4}\{v_-+3v_+\}+\frac{1}{2}\sqrt{\frac{2}{q}}\{u_--3u_+\}<\frac{x}{z} \\ & <\frac{1}{4}\{3v_-+v_+\}+\frac{1}{2}\sqrt{\frac{2}{q}}\{3u_--u_+\}, \\ \frac{1}{3}v_+-\frac{2}{3}\sqrt{\frac{2}{q}}u_++\frac{2}{3}\frac{x}{z}, & \frac{1}{4}\{3v_-+v_+\}+\frac{1}{2}\sqrt{\frac{2}{q}}\{3u_--u_+\}\le\frac{x}{z} \\ & \le v_++\sqrt{\frac{2}{q}}u_+, \\ v_+, & v_++\sqrt{\frac{2}{q}}u_+<\frac{x}{z}, \end{cases} \tag{5.46}$$

The corresponding director solution is given by $\theta=|u|^2/q$. This finishes all of our discussion pertaining to the nematic non-dispersive hydrodynamics.

5.3 Nematic Perturbed and Radiating DSWs

In this section, the analytical solution for the PDSW regime (Regime 1), as illustrated in Figure 3.2, and the RDSW regime (Regime 2), as depicted in Figure 3.3, will be derived. These theoretical solutions will be based on the ability to reduce the defocusing nematic equations (2.19) and (2.20) into a fifth order KdV equation, termed the nematic Kawahara equation, under the asymptotic limit of small jump heights u_i-u_+. This can be done by using particular multiple-scale perturbation expansions. This approach is similar to the one used to reduce the NLS equation to the KdV equation and conversely [25].

The nematic equations were first reduced to a third order KdV equation, in the small amplitude approximation $u_i-u_+\ll 1$, by Horikis [173]. This nematic third order KdV equation was utilised in [60, 61] to study nematic DSW regimes. However, the agreement with numerical solutions was poor. It is a major result of the present work that incorporating higher order dispersive effects is essential to tackle the whole range of nematic DSWs. The derivation of the nematic Kawahara equation in the case of small jump heights from the shelf u_i to the initial flow state ahead u_+ was actually accomplished by El and Smyth [61], but without using it to study the full DSW regimes. The nematic Kawahara equation does not only address the poor agreement between the analytical and numerical solutions, but it also provides a physical explanation of the presence of the resonant wavetrains seen in Figures 3.2 to 3.5 as it has been shown that for the Kawahara equation (1.40) linear dispersive waves resonate with the DSW if $\mu_d>0$ [79]. In this case, the Kawahara DSW can be a PDSW, RDSW, CDSW or TDSW, depending on the size of the dispersive parameter μ_d. The vacuum cases of Figures 3.5 and 3.6, that is, when the optical intensity can vanish $|u|=0$ in some region, cannot occur for a KdV DSW. They arise for nematic and NLS-type DSWs due to the requirement $|u|\ge 0$.

In the small amplitude limit, the defocusing nematic equations (2.19) and (2.20) can be reduced to a fifth order KdV equation on using the following perturbation expansions

$$\rho = \rho_0+\varepsilon^2P_1(\xi,\eta)+\varepsilon^4P_2(\xi,\eta)+\ldots, \tag{5.47}$$
$$v = \varepsilon^2V_1(\xi,\eta)+\varepsilon^4V_2(\xi,\eta)+\varepsilon^6V_3(\xi,\eta)+\ldots, \tag{5.48}$$

$$\theta \;=\; \frac{\rho_0}{q} + \varepsilon^2\theta_1(\xi,\eta) + \varepsilon^4\theta_2(\xi,\eta) + \varepsilon^6\theta_3(\xi,\eta) + \ldots, \tag{5.49}$$

for small deviations from the level ρ_0. This level ρ_0 points to the level from which the leading solitary wave edge of the PDSW/RDSW arises, in the (ρ, x) coordinate system at a specific z, i.e., $\rho_0 = \rho_+$, with $|\varepsilon| \ll 1$ being a measure of this deviation. Here, we choose $\varepsilon^2 = \rho_i - \rho_0$, which indicates the jump associated with the nematic KdV-type DSW existing in the (ρ, x) coordinate system. In the moving scaled coordinates

$$\xi = \varepsilon\{x - Uz\} \quad \text{and} \quad \eta = \varepsilon^3 z, \tag{5.50}$$

with

$$U = \sqrt{\frac{2}{q}}\sqrt{\rho_0} = \sqrt{\frac{2}{q}}u_0, \tag{5.51}$$

a fifth order KdV equation can be derived in the following way. We start by substituting the perturbation series (5.47) and (5.49) into the nematic molecular response equation (2.26), we then acquire

$$\mathcal{O}(\varepsilon^2) \;:\; \theta_1 = \frac{P_1}{q}, \tag{5.52}$$

$$\mathcal{O}(\varepsilon^4) \;:\; \theta_2 = \frac{\nu}{2q}\frac{\partial^2\theta_1}{\partial\xi} + \frac{P_2}{q} + \frac{\nu\varepsilon^2}{2q}\frac{\partial^2\theta_2}{\partial\xi^2}. \tag{5.53}$$

The term $\nu\varepsilon^2\partial_{\xi\xi}\theta_2/2q$ is formally of asymptotic order $\mathcal{O}(\varepsilon^2)$ and should arise at next order in the expression for θ_3, as in Horikis' work [173]. However, this implicitly presumes that $\nu = \mathcal{O}(1)$, which is not the case for experimental values of ν. Therefore, this term will be retained at order $\mathcal{O}(\varepsilon^4)$. Considering $\nu\varepsilon^2\partial_{\xi\xi}\theta_2/2q$ as a correction, equation (5.53) can be solved for θ_2 to give

$$\theta_2 = \left\{\frac{\nu}{2q}\frac{\partial^2\theta_1}{\partial\xi^2} + \frac{P_2}{q}\right\} + \frac{\varepsilon^2\nu^2}{4q^2}\frac{\partial^4\theta_1}{\partial\xi^4} + \frac{\varepsilon^2\nu}{2q^2}\frac{\partial^2 P_2}{\partial\xi^2}. \tag{5.54}$$

Note that the last term in (5.54) has to be retained as (5.53) yields that P_2 can be of order $\mathcal{O}(\nu)$, making the final term of order $\mathcal{O}(\nu^2\varepsilon^2)$. Substituting the perturbation series (5.47)–(5.49) into the mass equation (2.24) and the momentum equation (2.25), we have, respectively,

$$\mathcal{O}(\varepsilon^3) \;:\; \frac{\partial V_1}{\partial\xi} = \frac{U}{\rho_0}\frac{\partial P_1}{\partial\xi} \quad \text{and} \quad U\frac{\partial V_1}{\partial\xi} = \frac{2}{q}\frac{\partial P_1}{\partial\xi}, \tag{5.55}$$

on using (5.52) for θ_1. Compatibility between the equations in (5.55) for V_1 and P_1 then gives the coordinate velocity U (5.51). Similarly, at order $\mathcal{O}(\varepsilon^5)$ the mass equation (2.24) and the momentum equation (2.25) gives, respectively,

$$\mathcal{O}(\varepsilon^5): \quad \rho_0\frac{\partial V_2}{\partial\xi} + V_1\frac{\partial P_1}{\partial\xi} + P_1\frac{\partial V_1}{\partial\xi} + \frac{\partial P_1}{\partial\eta} - U\frac{\partial P_2}{\partial\xi} = 0 \tag{5.56}$$

and

$$\mathcal{O}(\varepsilon^5): \quad \frac{\partial V_1}{\partial\eta} - U\frac{\partial V_2}{\partial\xi} + 2\frac{\partial\theta_2}{\partial\xi} + V_1\frac{\partial V_1}{\partial\xi} - \frac{1}{4\rho_0}\frac{\partial^3 P_1}{\partial\xi^3} = 0. \tag{5.57}$$

It was shown in [60, 173] that substituting the first two leading order terms of (5.54), the terms in curly brackets, into (5.57) and combining it with (5.55) and (5.56) results

in the classical KdV equation. To extend this, we include the higher order terms of (5.54). The difficulty we have here is with calculating the last term in (5.54) as the correction P_2 cannot be calculated separately at order $\mathcal{O}(\varepsilon^5)$, leading to equations (5.56) and (5.57), and a higher order approximation is needed. To overcome this problem, we propose an appropriate ansatz for P_2 which is consistence with (5.56) and (5.57). Let us assume that

$$P_2 = \alpha\nu \frac{\partial^2 \theta_1}{\partial \xi^2} = \frac{\alpha\nu}{q} \frac{\partial^2 P_1}{\partial \xi^2}, \tag{5.58}$$

where α is a non-zero real constant to be found. Thus, on using (5.55) and substituting (5.54) and (5.58) into (5.57) we have

$$\frac{\partial V_2}{\partial \xi} = \frac{-1}{\rho_0} \left\{ \frac{\partial P_1}{\partial \eta} + \frac{2U}{\rho_0} P_1 \frac{\partial P_1}{\partial \xi} - \frac{\alpha\nu U}{q} \frac{\partial^3 P_1}{\partial \xi^3} \right\}. \tag{5.59}$$

Now, substituting (5.54), (5.58) and (5.59) into (5.56), we obtain the fifth order KdV equation in P_1

$$\frac{\partial P_1}{\partial \eta} + \frac{3}{qU} P_1 \frac{\partial P_1}{\partial \xi} + \frac{U}{4} \left(\frac{\nu}{q} - \frac{q}{4\rho_0} \right) \frac{\partial^3 P_1}{\partial \xi^3} + \frac{\nu^2 \varepsilon^2 \rho_0}{4q^3 U} (1 + 2\alpha) \frac{\partial^5 P_1}{\partial \xi^5} = 0. \tag{5.60}$$

Here, we need to choose $\alpha = -1/8$ to make the linear dispersion relation of the above equation compatible with the linear dispersion relation in the long-wavelength approximation (5.4). Hence, the correction P_1 satisfies a KdV equation with fifth order dispersion (nematic Kawahara equation)

$$\frac{\partial P_1}{\partial \eta} + \frac{3}{qU} P_1 \frac{\partial P_1}{\partial \xi} + \frac{U}{4} \left\{ \frac{\nu}{q} - \frac{q}{4\rho_0} \right\} \frac{\partial^3 P_1}{\partial \xi^3} + \varepsilon^2 \frac{3\nu^2 U}{32q^2} \frac{\partial^5 P_1}{\partial \xi^5} = 0. \tag{5.61}$$

The linear dispersion relation of the Kawahara equation (5.61), on a zero background $\bar{P}_1 = 0$, is

$$\tilde{\omega} = -\frac{U}{4} \left\{ \frac{\nu}{q} - \frac{q}{4\rho_0} \right\} \tilde{k}^3 + \varepsilon^2 \frac{3\nu^2 U}{32q^2} \tilde{k}^5, \tag{5.62}$$

where the tilde notation ($\sim$) refers to the re-scaled wave parameters in the coordinates ξ and η. The re-scaled linear dispersion relation (5.62) is consistent with the nematic linear long-wavelength dispersion relation (5.4). To be able to make a comparison between these dispersion relations and conclude their consistency, the coordinates ξ and η in (5.61) need to be transformed to the physical coordinates x and z. Let us assume then that $A(x, z) = \varepsilon^2 P_1(\xi, \eta)$. This assumption, along with the scaling relations (5.50), result in the physical coordinate counterpart of the nematic Kawahara equation (5.61) in the coordinate system (ρ, x), to be specific,

$$\frac{\partial A}{\partial z} + U \frac{\partial A}{\partial x} + \frac{3}{qU} A \frac{\partial A}{\partial x} + \frac{U}{4} \left\{ \frac{\nu}{q} - \frac{q}{4\rho_0} \right\} \frac{\partial^3 A}{\partial x^3} + \frac{3\nu^2 U}{32q^2} \frac{\partial^5 A}{\partial x^5} = 0. \tag{5.63}$$

The linear dispersion relation of equation (5.63), on a zero background $\bar{A} = 0$ as $\bar{P}_1 = 0$, is

$$\omega = Uk - \frac{U}{4} \left\{ \frac{\nu}{q} - \frac{q}{4\rho_0} \right\} k^3 + \frac{3\nu^2 U}{32q^2} k^5. \tag{5.64}$$

As can be seen, this dispersion relation is identical to (5.4), with a zero mean phase gradient level, $\bar{v} = v_+ = 0$, and the leading order term in the coefficient of k^5 being properly accounted for. The reason why the background of the phase gradient is con-

sidered zero, in the small jump height approximation, is due to the assumption that the solitary wave leading edge of the PDSW/RDSW sits on the initial level ahead $u_0 = u_+$ for which $\bar{v} = 0$, which agrees with numerical solutions. Theoretically, this can be understood from the mathematical expression for $\bar{v}$. This expression is derived from the conservation of the Riemann invariant R_- through the DSW, similar to the defocusing NLS dispersive hydrodynamics [18, 133, 134, 162]. This conservation results in

$$\bar{v} = 2\sqrt{\frac{2}{q}}\left\{\bar{u} - u_+\right\} \implies v_+ = 2\sqrt{\frac{2}{q}}\left\{u_+ - u_+\right\} = 0. \tag{5.65}$$

To derive the full coefficient of the fifth derivative in (5.61), the asymptotic expansions (5.47) to (5.49) need to be taken to $\mathcal{O}(\varepsilon^4)$ in ρ and $\mathcal{O}(\varepsilon^6)$ in v and θ [61]. Actually, extending the calculations to these next orders requires extensive calculations. It is much easier then to match the coefficient of k^5 in the dispersion relations (5.4) and (5.64) at the order $\mathcal{O}(\varepsilon^2\nu^2)$. It is easy to see from (5.50), (5.63) and (5.64) that the wavenumber and the angular frequency in the physical coordinates x and z are connected with their re-scaled counterparts through

$$k = \varepsilon\tilde{k}, \quad \omega = Uk + \varepsilon^3\tilde{\omega}. \tag{5.66}$$

These relations are important as they will be used in the perturbed and radiating DSW solutions in the next subsection and in the calculations for the CDSW regime, given in Section 5.4.

The theoretical results obtained in this thesis will be fully compared with numerical solutions for $|u|$ in the coordinate system (x, z). It is much easier then to deal with a nematic Kawahara equation in the $|u|$ variable, rather than ρ. We therefore seek a perturbation expansion in the optical intensity,

$$|u| = \sqrt{\rho} = u_0 + \varepsilon^2 u_1(\xi, \eta) + \varepsilon^4 u_2(\xi, \eta) + \ldots, \tag{5.67}$$

with u_0 the level ahead on which the solitary wave edge of the DSW sits, i.e., $u_0 = u_+$ [60, 185]. From (5.47) and (5.67), we deduce that $P_1 = 2u_0u_1$. This leads to the nematic Kawahara equation in the variable u_1

$$\frac{\partial u_1}{\partial \eta} + 3\sqrt{\frac{2}{q}}u_1\frac{\partial u_1}{\partial \xi} + \sqrt{\frac{2}{q}}\frac{u_0}{4}\left\{\frac{\nu}{q} - \frac{q}{4u_0^2}\right\}\frac{\partial^3 u_1}{\partial \xi^3} + \varepsilon^2\sqrt{\frac{2}{q}}\frac{3\nu^2 u_0}{32q^2}\frac{\partial^5 u_1}{\partial \xi^5} = 0. \tag{5.68}$$

The discontinuous jump that corresponds to the nematic perturbed and radiating DSWs governed by equation (5.68) is now $u_i - u_0$, instead of $\rho_i - \rho_0$. Because of this, it is better to re-define the small parameter ε^2, which now measures the deviation from the initial level ahead $u_0 = u_+$ to the level behind u_i. This means

$$\varepsilon^2 = \rho_i - \rho_0 = u_i^2 - u_0^2 \xrightarrow{\text{Re-definition}} \left\{u_i - u_0\right\}\left\{u_i + u_0\right\} = \varepsilon^2\left\{u_i + u_0\right\}. \tag{5.69}$$

Therefore, with $\varepsilon^2 = u_i - u_0$, we have

$$\boxed{\frac{\partial u_1}{\partial \eta} + 3\sqrt{\frac{2}{q}}u_1\frac{\partial u_1}{\partial \xi} + \sqrt{\frac{2}{q}}\frac{u_0}{4}\left\{\frac{\nu}{q} - \frac{q}{4u_0^2}\right\}\frac{\partial^3 u_1}{\partial \xi^3} + \varepsilon^2\sqrt{\frac{2}{q}}\frac{3\nu^2\left\{u_i + u_0\right\}u_0}{32q^2}\frac{\partial^5 u_1}{\partial \xi^5} = 0.} \tag{5.70}$$

From now on, when the term "nematic Kawahara equation" is mentioned, the equation which is referred to is (5.70). As there are many nematic Kawahara equations listed

above in this section and the reader may get confused with which one we will rely on throughout the thesis, the one that we are interested in has been highlighted by a box.

In the highly non-local limit $\nu \gg 1$, we notice that the coefficient of the third derivative term in (5.70) is positive, so that solitary waves are waves of elevation, which explains why the DSWs illustrated in Figures 3.2 and 3.3 are similar to KdV-type DSWs of elevation with solitary waves at the leading edge and linear diffractive waves at the trailing edge, not NLS-type DSWs, which consists of waves of depression for which the positions of the solitary waves and linear diffractive waves are reversed. The fifth derivative term is nominally of higher order, but due to the high non-locality ν the combination $\varepsilon\nu$ can be $\mathcal{O}(1)$ [61]. In the local limit $\nu \to 0$, the third order dispersive term in the nematic Kawahara equation (5.70) becomes negative and the fifth order dispersive term can be neglected as it becomes very small. This leads to a transformation in the form of the DSW from a positive polarity and positive orientation KdV-type DSW ($p = 1,\ d = 1$) to a negative polarity and negative orientation KdV-type DSW ($p = -1,\ d = -1$), similar to the DSW structure displayed in the bottom left corner of Figure 1.8. This DSW structure together with the simple wave solution in non-dispersive regions represent overall a defocusing NLS-type dispersive hydrodynamics.

The nematic Kawahara equation reduction (5.70) of the full nematic equations (2.19) and (2.20) will be used in Subsection 5.3.1 to derive the solutions for the PDSW and RDSW regimes as these cases correspond to a small jump height $u_i - u_+$. While the DSW radiates resonant waves in the RDSW regime, the effect of the loss associated with these waves is small and can be neglected to find the DSW solution, as shall be seen soon. The resonant radiation loss becomes dominant in the CDSW regime and will be dealt with in Section 5.4. In Subsection 5.3.2, a set of conditions, so-called admissibility conditions [18, 136], that test whether a DSW is in the standard form (KdV or NLS forms) or not will be discussed. The final subsection will deal with the application of the DSW fitting method [18, 133, 134] to the nematic PDSW and RDSW regimes. This method was briefly highlighted in Section 1.4. The theoretical solutions will be compared with numerical solutions in Chapter 6, with excellent agreement found.

5.3.1 The Fifth Order KdV (Kawahara) equation as a Perturbed KdV equation

It has been shown that the KdV equation with all the next higher order non-linear dispersive and non-linear-dispersive terms of asymptotic order α, such that $0 < \alpha \ll 1$, in the weakly non-linear long-wavelength expansion

$$\frac{\partial \Psi}{\partial T} + 6\psi\frac{\partial \Psi}{\partial X} + \alpha C_1 \Psi^2 \frac{\partial \Psi}{\partial X} + \frac{\partial^3 \Psi}{\partial X^3} + \alpha C_2 \frac{\partial \Psi}{\partial X}\frac{\partial^2 \Psi}{\partial X^2} + \alpha C_3 \Psi \frac{\partial^3 \Psi}{\partial X^3} + \alpha C_4 \frac{\partial^5 \Psi}{\partial X^5} = 0 \quad (5.71)$$

can be transformed by a non-local perturbation expansion to the standard KdV equation (1.10) with error $\mathcal{O}\left(\alpha^2\right)$ [125], which is of higher order than the validity of the original equation (5.71). By way of illustration, this is given by

$$\Psi(X,T) = \psi + \alpha C_5 \psi^2 + \alpha C_6 \psi_{XX} + \alpha C_7 \psi_X \int_{V_c T}^{X} \left\{\psi(\zeta, T) - \bar{\psi}\right\} d\zeta \quad (5.72)$$

and the re-scaled coordinates

$$X' = X + \alpha C_7 \bar{\psi}\left\{X - V_c T\right\} + \alpha C_7 \Lambda T, \qquad T' = T + \alpha C_4 X/3, \quad (5.73)$$

where

$$C_5 = \frac{1}{6}\left\{C_3 - C_1 + 4C_4\right\}, \qquad C_6 = \frac{1}{12}\left\{C_2 - 6C_4 - C_1\right\}, \tag{5.74}$$

$$C_7 = \frac{1}{3}\left\{8C_4 - C_3\right\}, \qquad \Lambda = V_c\psi - 3\psi^2 - \psi_{X'X'}. \tag{5.75}$$

This non-local perturbation transformation leads to the classical KdV equation

$$\frac{\partial\psi}{\partial T'} + 6\psi\frac{\partial\psi}{\partial X'} + \frac{\partial^3\psi}{\partial X'^3} = 0, \tag{5.76}$$

when asymptotic terms of order $\mathcal{O}(\alpha^2)$ are ignored. The C_i's, $i \in \{1, \ldots, 7\}$, in the above equations are real constants and their values depend on the physical model of interest. see [126] for examples of this. The variables $\bar{\psi}$ and V_c denote the mean level and phase velocity of the KdV cnoidal wave solution, in order. As for Λ, it is a real constant obtained by the first integral of the KdV equation.

The above transformation was then used to find the DSW solution of the higher order KdV equation (5.71) from that for the standard KdV equation [125]. This PDSW solution will be used to find the perturbed and radiating DSW solutions (Regimes 1 and 2) for the reduction (5.70) of the governing nematic equations. The Kawahara reduction (5.70) does not contain the higher order terms $u_1^2u_{1X}$, $u_{1X}u_{1XX}$ and u_1u_{1XXX} of the general higher order KdV equation (5.71). The reason for this can most easily be seen via the nematic dispersion relation (4.26) in the long-wave limit $k \ll 1$, giving the dispersion relation (5.4). We note that the dispersion relation (5.4) does not contain a term $\bar{u}^2k$, so that there is no higher order non-linear term $u_1^2u_{1X}$. In addition, the fifth derivative term in (5.70) was obtained by including the fifth derivative from higher order in the expansions (5.47)–(5.49) as the coefficient $\varepsilon^2\nu^2$ can be $\mathcal{O}(1)$ as ν is large. In a similar manner, the higher order non-linear/dispersive terms $u_{1X}u_{1XX}$ and u_1u_{1XXX} would be at most $\mathcal{O}(\varepsilon^2\nu)$ and so can be ignored.

For simplicity, let us express the reductive Kawahara equation (5.70) of the nematic equations as

$$\frac{\partial u_1}{\partial\eta} + B_2u_1\frac{\partial u_1}{\partial\xi} + B_3\frac{\partial^3u_1}{\partial\xi^3} + \varepsilon^2B_4\frac{\partial^5u_1}{\partial\xi^5} = 0, \tag{5.77}$$

where

$$B_2 = 3\sqrt{\frac{2}{q}}, \quad B_3 = \sqrt{\frac{2}{q}}\frac{u_+}{4}\left\{\frac{\nu}{q} - \frac{q}{4u_+^2}\right\}, \quad B_4 = \sqrt{\frac{2}{q}}\frac{3\nu^2\left\{u_- + u_+\right\}u_+}{32q^2}. \tag{5.78}$$

To solve for the nematic perturbed and radiating DSWs, we start by transforming equation (5.77) to the standard higher order form (5.71). This can be done by re-scaling the moving coordinates ξ and η into new coordinates X and T with

$$X = B_5\xi \quad \text{and} \quad T = B_6\eta. \tag{5.79}$$

This new coordinate re-scaling gives

$$\frac{\partial u_1}{\partial T} + 6\left\{\frac{B_2B_5}{6B_6}\right\}u_1\frac{\partial u_1}{\partial X} + \left\{\frac{B_3B_5^3}{B_6}\right\}\frac{\partial^3u_1}{\partial X^3} + \left\{\frac{\varepsilon^2B_4B_5^5}{B_6}\right\}\frac{\partial^5u_1}{\partial X^5} = 0. \tag{5.80}$$

Now, we want to find B_5 and B_6 such that

$$\frac{B_2B_5}{6B_6} = 1 \tag{5.81}$$

and

$$\frac{B_3 B_5^3}{B_6} = 1. \tag{5.82}$$

These equalities lead to the following expressions

$$B_5 = \sqrt{\frac{2}{u_+}} \left\{ \frac{\nu}{q} - \frac{q}{4u_+^2} \right\}^{-1/2}, \tag{5.83}$$

$$B_6 = \frac{1}{\sqrt{u_+ q}} \left\{ \frac{\nu}{q} - \frac{q}{4u_+^2} \right\}^{-1/2}, \tag{5.84}$$

$$\frac{\varepsilon^2 B_4 B_5^5}{B_6} = \varepsilon^2 \left\{ \frac{3(u_i + u_+)}{4u_+} \left(1 - \frac{q^2}{4u_+^2 \nu} \right)^{-2} \right\} = \varepsilon^2 C_4. \tag{5.85}$$

Therefore, we write the nematic Kawahara equation in the standard higher order form

$$\frac{\partial u_1}{\partial T} + 6u_1 \frac{\partial u_1}{\partial X} + \frac{\partial^3 u_1}{\partial X^3} + \varepsilon^2 C_4 \frac{\partial^5 u_1}{\partial X^5} = 0. \tag{5.86}$$

Equation (5.86) is the higher order KdV equation (5.71) with $\psi = u_1$, $C_1 = 0$, $C_2 = 0$, $C_3 = 0$ and $\alpha = \varepsilon^2 = u_i - u_+$. The results of [125] give that the modulated wave parameters of the DSW solution of the Kawahara equation (5.86), the cnoidal wave amplitude $\hat{a}$ (measured peak to trough), the wavenumber $\hat{k}$, the mean height $\hat{\bar{u}}$ and the characteristic velocity (non-linear group velocity) $\hat{\Gamma}_c = X/T$, are given by the expressions

$$\hat{a} = 2m - 2m\varepsilon^2 C_4 \left\{ m - \frac{8}{3} \right\}, \tag{5.87}$$

$$\hat{k} = \frac{\pi}{K(m)} \left\{ 1 - \frac{1}{3}\varepsilon^2 C_4 \left(8m^2 - 14m + 11 \right) \right\}, \tag{5.88}$$

$$\begin{aligned} \hat{\bar{u}} = {} & -1 + \left\{ \frac{2E(m)}{K(m)} + m \right\} + \frac{2}{9}\varepsilon^2 C_4 \left\{ 2 - 5m + 3m^2 + 2[2m-1]\frac{E(m)}{K(m)} \right\} \\ & + \frac{32}{9}\varepsilon^2 C_4 \left\{ 3\left[1 - \frac{E(m)}{K(m)} \right]^2 - 2\left[1 - \frac{E(m)}{K(m)} \right][1+m] + m \right\}, \end{aligned} \tag{5.89}$$

on

$$\begin{aligned} \hat{\Gamma}_c = \frac{X}{T} = {} & \hat{\beta}_1 - \frac{2}{3}\varepsilon^2 C_4 \hat{\beta}_2 + \frac{1}{3}\varepsilon^2 C_4 \hat{\beta}_1^2 - \frac{8}{3}\varepsilon^2 C_4 \left\{ -m^2 + 2m - 1 \right\} \\ & - \frac{8}{3}\varepsilon^2 C_4 \left\{ -1 + m + \frac{2E(m)}{K(m)} \right\} \left\{ \hat{\beta}_1 - \hat{V} \right\}, \end{aligned} \tag{5.90}$$

with

$$\hat{V} = 2\left\{ m + 1 \right\} - \frac{4}{3}\varepsilon^2 C_4 \left\{ -3m^2 + 3m - 2 \right\} \tag{5.91}$$

and

$$\hat{\beta}_1 = \hat{V} - \frac{4m\left\{1-m\right\}K(m)}{E(m) - \left\{1-m\right\}K(m)}, \quad \hat{\beta}_2 = 2\left\{1+m\right\} - \frac{4m\left\{1-m\right\}K(m)}{E(m) - \left\{1-m\right\}K(m)}. \tag{5.92}$$

Here, $K(m)$ and $E(m)$ are complete elliptic integrals of the first and second kinds of modulus m, respectively. The hat symbol ($\wedge$) in the above expressions refers to the

re-scaled wave parameters in the X and T coordinates.

The wave parameter expressions (5.87)–(5.92) are valid solutions in the re-scaled coordinate system. Hence, we need to transform these formulae back to the physical coordinates x and z to be able to make comparisons with numerical solutions. The re-scaled amplitude $\hat{a}$ and mean level $\hat{\bar{u}}$ can be transformed to the actual amplitude a and the mean level $\bar{u}$ on using the perturbation expansion (5.67). This is because the coordinate transformation from ξ and η to X and T does not affect the value of a wave parameter that is related to the height. Thus, the physical amplitude and mean level are, respectively,

$$a(x,z) = \varepsilon^2 \hat{a}(X,T) \quad \text{and} \quad \bar{u}(x,z) = \varepsilon^2 \hat{\bar{u}}(X,T). \tag{5.93}$$

On the other hand, the re-scaled wavenumber $\hat{k}$ and the characteristic velocity $\hat{\Gamma}_c = X/T$ can be transformed to their values in the physical x and z coordinates by comparing the linear dispersion relation (5.64) with the one obtained from equation (5.63) on using the scaling relations (5.50) and (5.79). We then have the wave parameter relations between the coordinates (X,T) and (x,z) are given by

$$k = \varepsilon B_5 \hat{k} \quad \text{and} \quad \Gamma_c = U + \frac{\varepsilon^2 B_6}{B_5}\hat{\Gamma}_c. \tag{5.94}$$

Finally, the PDSW solution is

$$a = 2m\{u_i - u_+\} + 2mC_4\{u_i - u_+\}^2\left\{\frac{8}{3} - m\right\}, \tag{5.95}$$

$$k = \frac{\pi\sqrt{2\{u_i - u_+\}}}{K(m)\sqrt{u_+}\sqrt{\frac{\nu}{q} - \frac{q}{4u_+^2}}}\left\{1 - \frac{1}{3}C_4\left(8m^2 - 14m + 11\right)(u_i - u_+)\right\}, \tag{5.96}$$

$$\begin{aligned}\bar{u} = {} & 2u_+ - u_i + \{u_i - u_+\}\left\{2\frac{E(m)}{K(m)} + m\right\} \\ & + \frac{32}{9}C_4\{u_i - u_+\}^2\left\{3\left[1 - \frac{E(m)}{K(m)}\right]^2 - 2\left[1 - \frac{E(m)}{K(m)}\right][1+m] + m\right\} \\ & + \frac{2}{9}C_4\{u_i - u_+\}^2\left\{2 - 5m + 3m^2 + 2[2m-1]\frac{E(m)}{K(m)}\right\}\end{aligned} \tag{5.97}$$

on

$$\begin{aligned}\Gamma_c = \frac{x}{z} = {} & \sqrt{\frac{2}{q}}\left\{u_+ + \frac{1}{2}\beta_1 - \frac{1}{3}C_4\beta_2 + \frac{1}{6}C_4\beta_1^2 - \frac{4}{3}C_4[u_i - u_+]^2[m(2-m) - 1]\right. \\ & \left. - \frac{4}{3}C_4[u_i - u_+]\left[m - 1 + \frac{2E(m)}{K(m)}\right][\beta_1 - V]\right\},\end{aligned} \tag{5.98}$$

with

$$V = 2\{u_i - u_+\}\{1+m\} - \frac{4}{3}C_4\{u_i - u_+\}^2\left\{3m - 3m^2 - 2\right\}, \tag{5.99}$$

$$\beta_1 = V - \frac{4m\{u_i - u_+\}\{1-m\}K(m)}{E(m) - \{1-m\}K(m)}, \tag{5.100}$$

and

$$\beta_2 = 2\{u_i - u_+\}^2\left\{1 + m - \frac{2m[1-m]K(m)}{E(m) - [1-m]K(m)}\right\}. \tag{5.101}$$

Note that various typographical errors in the asymptotic expressions of [125] have been corrected to obtain the expressions (5.95)–(5.101). The limit $m = 0$ corresponds to the trailing linear diffractive wave edge of the PDSW, propagating with the velocity s_i, and $m = 1$ corresponds to the leading, solitary wave edge, travelling with the velocity V_s. The DSW then lies within the region

$$\sqrt{\frac{2}{q}}\left\{4u_+ - 3u_i + \frac{64}{3}C_4(u_i - u_+)^2\right\} \leq \frac{x}{z} \leq \sqrt{\frac{2}{q}}\left\{2u_i - u_+ + \frac{4}{3}C_4(u_i - u_+)^2\right\}. \tag{5.102}$$

The amplitude a_s of the solitary wave at the leading edge of the DSW can be found from the amplitude expression (5.95) on setting $m = 1$. This gives

$$a_s = 2\{u_i - u_+\} + \frac{10}{3}C_4\{u_i - u_+\}^2, \tag{5.103}$$

so that the height H_s of the lead solitary wave of the DSW from $u = 0$ is

$$H_s = a_s + u_+ = 2u_i - u_+ + \frac{10}{3}C_4\{u_i - u_+\}^2. \tag{5.104}$$

This completes the solution for the PDSW regime.

As we are considering here a perturbed KdV DSW solution for the nematic PDSW regime, it is worth then to draw the reader's attention to recent research work that has used Whitham's averaging theory for generating perturbed modulation equations associated with the Riemann problem of a "perturbed" KdV equation. For further details, see [149]. Whether this work of A. Kamchatnov could be applied to solve the nematic PDSW problem or not is a potential study of interest, and it would be good to investigate it in the future.

As previously found [60, 61], a resonance between dispersive radiation and the DSW can occur when the phase velocity of the diffractive radiation equals the velocity V_s of the lead solitary wave of the DSW. As can be seen from Figure 3.3 this resonant radiation is short wave, $k = \mathcal{O}(1)$, relative to the DSW, $0 < k < 0.15$, so that the appropriate linear dispersion relation is (5.3). Resonance then occurs for the wavenumber k_r, with

$$V_s = \frac{\omega_r}{k_r} = k_r + \frac{2u_+^2}{qk_r} = V_{p,r}, \tag{5.105}$$

which implies

$$k_r = V_s + \sqrt{V_s^2 - \frac{4}{q}u_+^2}, \tag{5.106}$$

on taking $\bar{v} = v_+ = 0$, which is assuming that the resonant wavetrain sits on the initial level $\bar{u} = u_+$ ahead. If $V_s \leq 2u_+/\sqrt{q}$, then there is no resonant wavetrain ahead of the DSW, which is the PDSW regime illustrated in Figure 3.2. If $V_s > 2u_+/\sqrt{q}$, then the DSW sheds a resonant wavetrain ahead of it as the group velocity $c_{g,r} = \partial_{k_r}\omega_r = k_r$ of the resonant wavetrain is greater than its phase velocity ($V_s = V_{p,r} < c_{g,r}$) [60, 61], on using (5.105) and (5.102). Resonance can then occur if $V_s \geq 2u_+/\sqrt{q}$. If this resonant condition is not satisfied, then there is just a standard DSW and we have the PDSW regime.

When the resonance condition (5.105) has a solution, we have the RDSW regime for the nematic DSW, as illustrated in Figure 3.3. It was found that the RDSW regime is also well described by the perturbed KdV DSW solution (5.95)–(5.98). This is because the resonant radiation shed by the DSW is of small amplitude, as can be seen from

Figure 3.3, and the existence regime for this type is small, as seen from Table 6.1 in Chapter 6. The resonant wavetrain has a major effect in the CDSW regime, which is dealt with in the subsequent section, as the resonant wavetrain acts as a damping on the DSW and the resonant wavetrain is significant in the CDSW regime.

5.3.2 DSW Admissibility Conditions

At this point the admissibility conditions for the existence of a DSW need to be checked [18, 136]. These relate to the genuine non-linearity and hyperbolicity of the associated Whitham modulation equations upon which DSW solutions are ultimately based. See Section 1.4 for mathematical explanations of the notions of the genuine non-linearity and hyperbolicity. The breakdown of these leads to linear degeneracy in the first case and modulational instability in the second case, so that the standard DSW solution, as derived earlier, breaks down. These admissibility conditions are given in the form of partial derivatives of the trailing and leading edge velocities of the classical DSW. Strictly speaking, for a DSW with the initial levels u_- behind and u_+ ahead, we need to have the following conditions [18, 136, 137]

$$\frac{\partial s_-}{\partial u_-} \neq 0 \quad , \quad \frac{\partial V_s}{\partial u_+} \neq 0, \tag{5.107}$$

$$\frac{\partial s_-}{\partial u_+} \neq 0 \quad , \quad \frac{\partial V_s}{\partial u_-} \neq 0, \tag{5.108}$$

where s_- and V_s stand for the linear group velocity at the trailing edge and the soliton velocity at the leading edge, respectively. The trailing and leading edge velocities of a "stable" DSW are either increasing or decreasing (monotonic) functions in the variables u_- and u_+ [18]. Therefore, from a physical point of view, the requirement of the above admissibility conditions makes sense as their break down means that the edge velocities are not monotonic functions, which results in a multi-phase wavetrain.

In our case, $s_- = s_i$ as the trailing edges of the PDSW and RDSW sit on the shelf u_i. Clearly, the DSW admissibility conditions require that the partial derivatives of the velocities of the trailing edge s_i and of the leading edge V_s do not have turning points as functions of u_- and u_+. Conditions (5.107) require that the Whitham modulation equations form a genuinely non-linear system at the trailing and leading edges of the DSW, respectively. The failure of one of these conditions means that at the turning point a centred simple wave solution of the Whitham modulation equations which governs a standard DSW is not possible. In contrast, criteria (5.108) imply that the Whitham modulation equations form a strictly hyperbolic system at the trailing and leading edges of the DSW, respectively. The breakdown of one of these criteria means that the Whitham modulation equations lose hyperbolicity and become an elliptic system of equations at the turning point, resulting in compression and self-implosion in the interior structure of the DSW (unstable modulated wavetrain) [135, 136]. In our calculations, we approximate the constant C_4 in (5.85) by $C_4 = 3\{u_i + u_+\}/4u_+$ as ν is large. We also approximate the shelf u_i in (5.102) by the average value (5.28). The nematic DSW is fundamentally formed by varying u_- and u_+, and the shelf u_i is a function of both of them. This means that fixing u_i is not the same as fixing u_-. Therefore, we shall differentiate with respect to u_- instead of u_i for the trailing edge of the nematic DSW. We now have

$$\frac{\partial s_i}{\partial u_-} = \sqrt{\frac{2}{q}}\left\{\frac{6u_-^2}{u_+} + 4u_- - 10u_+ - \frac{3}{2}\right\}, \tag{5.109}$$

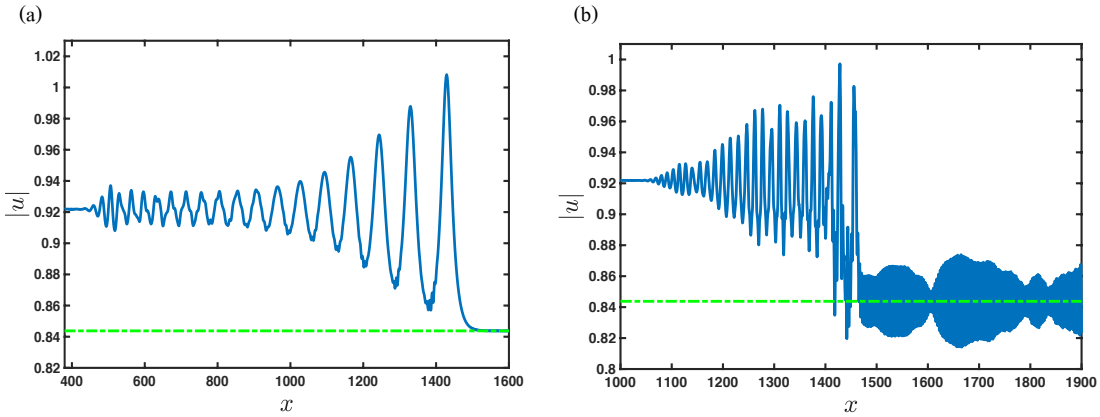

Figure 5.4: Parts of numerical solutions of the nematic equations (2.19) and (2.20) for the initial condition (2.29). Blue (solid) line: $|u|$ at $z = 1000$; green (dash-dot) line: the initial level ahead (turning point) $u_+ = 0.85369$. (a) Nematic DSW solution with $\nu = 200$, (b) nematic DSW solution with $\nu = 10$. Here $u_- = 1.0$ and $q = 2$. (Online version in colour.)

$$\frac{\partial s_i}{\partial u_+} = \sqrt{\frac{2}{q}}\left\{12u_+ - 10u_- - \frac{2u_-^3}{u_+^2} + \frac{5}{2}\right\}, \tag{5.110}$$

$$\frac{\partial V_s}{\partial u_-} = \sqrt{\frac{2}{q}}\left\{1 + \frac{3u_-^2}{8u_+} + \frac{u_-}{4} - \frac{5u_+}{8}\right\} \tag{5.111}$$

and

$$\frac{\partial V_s}{\partial u_+} = \sqrt{\frac{2}{q}}\left\{\frac{3u_+}{4} - \frac{5u_-}{8} - \frac{u_-^3}{8u_+^2}\right\}. \tag{5.112}$$

We find from the leading edge velocity expression (5.102) for V_s that the partial derivatives do not vanish at the leading edge as $u_- > u_+$, so there is no collapse of the DSW structure at the leading edge. At the linear edge, the partial derivative of s_i with respect to u_- vanishes when $u_+ = 0.90962$ for $u_- = 1$, and the partial derivative with respect to u_+ vanishes when $u_+ = 0.85369$ for $u_- = 1$.

The breakdown of these admissibility conditions is usually clearly mirrored in numerical solutions by non-standard DSW behaviour, such as the generation of a multi-phase wavetrain or wavetrain instability [136]. However, for the nematic DSW there is no clear evidence of such behaviour for values of u_+ at or around the turning points for ν large, as seen in Figures 5.4(a) and 5.5(a).

Figure 5.4(a) shows some evidence of modulational instability at the trailing edge of the DSW, but it is minor. It can be seen that there is some non-uniform modulation of the trailing edge, with a modulated wavepacket that resembles a multi-phase behaviour, but there is no distinct change in the behaviour of the DSW, as found for other DSWs for which the admissibility conditions are not satisfied, yielding a DSW implosion [18, 136]. The reason here for this is the highly non-local response of a nematic liquid crystal. It has been shown theoretically and verified experimentally that high non-locality acts to suppress modulational instability [174, 175]. This greatly delays the onset of instability, so much so that theoretically unstable nematic wavetrains show no instability over experimental propagation distances ($\sim 1mm$). Having this experimental fact in mind, the nematic DSW at the turning point $u_+ = 0.84375$ has been examined when the

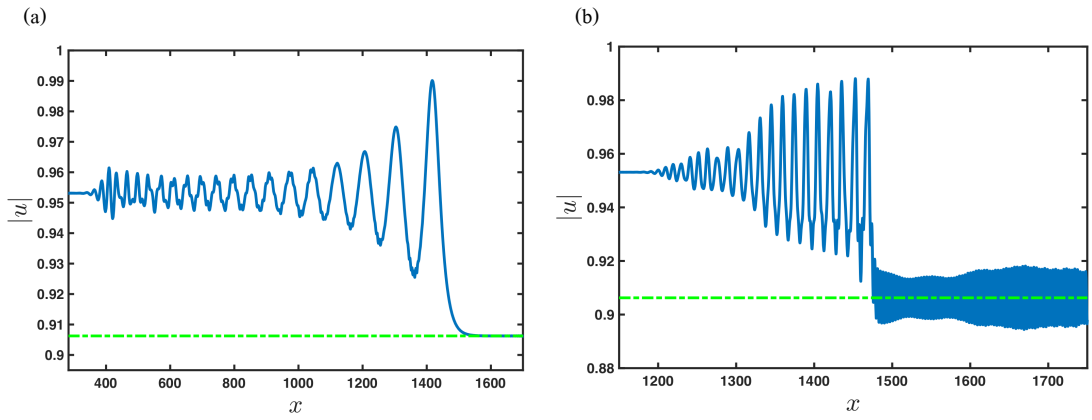

Figure 5.5: Parts of numerical solutions of the nematic equations (2.19) and (2.20) for the initial condition (2.29). Blue (solid) line: $|u|$ at $z = 1000$; green (dash-dot) line: the initial level ahead (turning point) $u_+ = 0.90962$. (a) Nematic DSW solution with $\nu = 200$, (b) nematic DSW solution with $\nu = 5$. Here $u_- = 1.0$ and $q = 2$. (Online version in colour.)

asymptotic size of ν is not large. Figure 5.4(b) illustrates the structure of the nematic DSW at the near local limit $\nu = 10$. The modulational instability at the trailing edge of the DSW is now clear from this figure.

Regarding the linear degeneracy, its existence is slightly ambiguous, either in the non-local or local regimes. It should be noted that there are no experiments that verify that the appearance of linear degeneracy is delayed by the non-locality property of the nematic response, as is the case for modulational instability. It will be speculated here that the non-locality effect hinders linear degeneracy as it is the sole reasonable and physical explanation we perceive. Figure 5.5(a) shows the DSW form at the turning point $u_+ = 0.90625$ and $\nu = 200$, while Figure 5.5(b) depicts the form at the same turning point, but with the near local limit $\nu = 5$. Unlike the modulational instability case, the choice of $\nu = 10$ was not found appropriate for linear degeneracy as the numerical solution at this value of ν does not show a notable difference when compared with Figure 5.5(a). Thus, the value of ν had to be reduced further to observe a significant difference in the DSW form, until e.g. $\nu = 5$, as given in Figure 5.5(b). Indeed, Figure 5.5(b) shows that there is an unusual behaviour at the trailing edge of the DSW. This unusual behaviour is not a numerical issue. Various (small) numerical step-sizes were checked and the same modulation was observed. Whether this is really a degeneracy of the non-linearity effect or not is a matter we are not fully certain about, however. The theoretical implication of linear degeneracy is clear, as discussed in [135]. It implies that the characteristics of the Whitham modulation equations coalesce. In other words, there is a coalescence of the non-linear group velocities [1].

5.3.3 DSW Fitting Method

The DSW fitting method, or sometimes known as El's method for DSWs [133, 134], will now be applied to determine the edge structure of the KdV-type DSWs governed by the nematic dispersive hydrodynamics (2.24)–(2.26). By the edge structure, or occasionally called the macroscopic structure [18], of a DSW we mean the boundaries/edges of the DSW which are characterised by the trailing and leading wavenumbers, velocities and positions. The determination of the amplitude parameter at the solitary wave edge of a

DSW depends upon whether there exists a known relation between the amplitude and the velocity for a solitary wave. Examples of non-linear dispersive wave equations that have explicit amplitude-velocity relations for solitary waves are the KdV equation [1], the Whitham equation [137] and the Kawahara equation (approximate relation deduced by means of perturbations) [79]. Such an explicit relation does not exist for the nematic equations (2.19)–(2.20) as an exact solitary or cnoidal wave solution is not known, so we shall focus only on the wavenumber and velocity parameters. As briefly mentioned in Section 1.4, the underlying advantage of this method is that it can be utilised for both integrable and non-integrable non-linear dispersive wave equations in the absence of the simple wave solution associated with a DSW from the Whitham modulation system for these equations. The DSW fitting method is based on the degeneracy of Whitham modulation equations in the linear and solitary wave limits. This degeneracy shows that the two edges of a DSW are governed by the linear dispersion relation for a non-linear dispersive wave equation [133, 134]. The non-dispersive form of the defocusing nematic equations is given by (5.9)–(5.10) and the linear dispersion relation is (5.4).

Following the work of El [18, 133, 134], matching the non-dispersive region behind the DSW and the trailing edge of the DSW gives that the trailing wavenumber k satisfies the following boundary value problem

$$\frac{dk}{d\bar{u}} = \frac{\partial_{\bar{u}}\omega(k;\bar{u})}{V_+(\bar{u}) - \partial_k\omega(k;\bar{u})} \quad \text{subject to} \quad k(u_+) = 0. \tag{5.113}$$

Here, $\omega(k;\bar{u})$ is the linear dispersion relation on the background level $\bar{u}$. $V_+(\bar{u})$ is the characteristic velocity of the non-linear non-dispersive wavetrain of the C_+ of the Riemann invariant of the non-dispersive equations. Here, $V_+(\bar{u}) = U + \bar{v}$, where U is (5.5), according to (5.16)–(5.17). The boundary condition $k_+ = k(u_+) = 0$, connecting the trailing edge to the leading edge, corresponds to the solitary wave edge for which the wavenumber approaches zero. The trailing edge of the DSW is consequently propagating with the group velocity

$$s_i = \frac{\partial\omega}{\partial k}\Big|_{(k;\bar{u})=(k_i;u_i)}, \tag{5.114}$$

with $k_i = k(u_i)$ at the trailing edge.

The determination of the details of the leading edge of the DSW is achieved in a similar manner, but in a less straightforward way in comparison to the trailing edge, see [18, 133, 134] for further details. This is done by introducing the concepts of "conjugate wavenumber" $\tilde{k}$ and "conjugate dispersion relation" $\tilde{\omega}(\bar{u},\tilde{k})$. These conjugate variables are related to the actual wavenumber k and the non-linear travelling wave frequency ω at the solitonic edge through the transformations

$$\tilde{k} \to -ik \quad \text{and} \quad \tilde{\omega}(\tilde{k};\bar{u}) \to -i\omega(i\tilde{k};\bar{u}). \tag{5.115}$$

Analogous to the trailing edge of the DSW, the conjugate wavenumber satisfies the boundary value problem

$$\frac{d\tilde{k}}{d\bar{u}} = \frac{\partial_{\bar{u}}\tilde{\omega}(\tilde{k};\bar{u})}{V(\bar{u}) - \partial_{\tilde{k}}\tilde{\omega}(\tilde{k};\bar{u})} \quad \text{subject to} \quad \tilde{k}(u_i) = 0, \tag{5.116}$$

linking the leading edge to the trailing edge of the DSW. The leading edge of the DSW

is then found to be travelling with the velocity

$$V_{s,+} = \frac{\tilde{w}}{\tilde{k}}\Big|_{(\tilde{k};\bar{u})=(\tilde{k}_+;u_+)}, \tag{5.117}$$

where $\tilde{k}_+ = \tilde{k}(u_+)$. The reason behind using these conjugate variables is that the fundamental periodic wave solution used in Whitham's modulation theory for KdV or KdV-type DSWs is given in the form of Jacobian elliptic functions [1, 19]. These functions have real and complex periods, which means that waves have real and complex frequencies [21]. The solitary wave solution in the real direction corresponds to a conjugate, linear, dispersive, periodic wave solution in the complex direction [18, 133, 134].

Given the above background, at the trailing edge of the DSW we have that the harmonic wavenumber $k_i = k(u_i)$, provided that u_i is (5.28), satisfies the implicit equation

$$\ln\left(\frac{u_i}{3^{\frac{5}{4}}u_+}\right) + \frac{\sqrt{17}}{34}\arctan\left(\frac{-1}{\sqrt{17}}\right) + \frac{5}{4}\ln\left(\frac{3\nu^2}{32q^2}k_i^4 - \frac{\nu}{4q}k_i^2 + 3\right) - \frac{\sqrt{17}}{34}\arctan\left(\frac{1}{\sqrt{17}}\left\{\frac{3\nu}{4q}k_i^2 - 1\right\}\right) = 0, \tag{5.118}$$

where the following integral formula was used (the constant of integration is omitted)

$$\int\left\{\frac{\alpha_1 k^2 - \alpha_2 k^4}{\alpha_3 k - \alpha_4 k^3 + \alpha_5 k^5}\right\}dk = -\frac{\alpha_2}{4\alpha_5}\ln(\alpha_5 k^4 - \alpha_4 k^2 + \alpha_3) + \frac{2\alpha_1\alpha_5 - \alpha_2\alpha_4}{2\alpha_5\sqrt{4\alpha_3\alpha_5 - \alpha_4^2}}\arctan\left(\frac{2\alpha_5 k^2 - \alpha_4}{\sqrt{4\alpha_3\alpha_5 - \alpha_4^2}}\right), \tag{5.119}$$

with $\alpha_1, \alpha_2, \alpha_3, \alpha_4$, and α_5 some valid real constants. The implicit equation (5.118) can be solved numerically for k_i by using Newton's method [93]. Then, the linear, dispersive wave edge moves with the group velocity

$$s_i = s(u_i) = \frac{\partial\omega}{\partial k}\Big|_{(k;\bar{u})=(k_i;u_i)} = -2\sqrt{\frac{2}{q}}u_+ + \sqrt{\frac{2}{q}}u_i\left\{3 - \frac{3\nu}{4q}k_i^2 + \frac{15\nu^2}{32q^2}k_i^4\right\}. \tag{5.120}$$

Similarly, at the leading solitary wave edge of the DSW, we have that the conjugate wavenumber as a function of the stationary level ahead u_+, $\tilde{k}_+ = \tilde{k}(u_+)$, satisfies the implicit equation

$$\ln\left(\frac{3^{\frac{5}{4}}u_i}{u_+}\right) + \frac{\sqrt{17}}{34}\arctan\left(\frac{1}{\sqrt{17}}\right) - \frac{5}{4}\ln\left(\frac{3\nu^2}{32q^2}\tilde{k}_{s,+}^4 + \frac{\nu}{4q}\tilde{k}_{s,+}^2 + 3\right) - \frac{\sqrt{17}}{34}\arctan\left(\frac{1}{\sqrt{17}}\left\{\frac{3\nu\tilde{k}_{s,+}^2}{4q} + 1\right\}\right) = 0. \tag{5.121}$$

The solitary wave edge then propagates with the velocity

$$V_{s,+} = V_s(u_+) = \frac{\tilde{\omega}}{\tilde{k}}\Big|_{(\tilde{k};\bar{u})=(\tilde{k}_+;u_+)} = -2\sqrt{\frac{2}{q}}u_+ + \sqrt{\frac{2}{q}}\frac{u_+}{\tilde{k}_+}\left\{3\tilde{k}_+ + \frac{\nu}{4q}\tilde{k}_+^3 + \frac{3\nu^2}{32q^2}\tilde{k}_+^5\right\}. \tag{5.122}$$

However, for $u_+ < 0.85$, the solutions of the above equations are found complex upon solving them numerically.

To get rid of this cut-off, we need to expand equations (5.118) and (5.121) in Taylor series. As the value of the wavenumber in the nematic PDSW and RDSW regimes lies within the range $0 < k < 0.15$, the arguments of the transcendental functions in equations (5.118) and (5.121) satisfy the requirement to seek Taylor expansions. Taking this into account, at the trailing edge of the DSW, we have

$$\ln\left(\frac{3\nu^2k^4}{32q^2} - \frac{\nu k^2}{4q} + 3\right) \sim \ln(3) - \frac{\nu k^2}{12q}, \tag{5.123}$$

$$\arctan\left(\frac{3\nu k^2}{4\sqrt{17}q} - \frac{1}{\sqrt{17}}\right) \sim \frac{12\sqrt{17}}{289}\frac{\nu k^2}{q} - \frac{50\sqrt{17}}{867}, \tag{5.124}$$

which lead to the trailing wavenumber asymptotic expression

$$k \sim 2\sqrt{\frac{2q}{1733\nu}}\sqrt{1734\ln\left(\frac{u_i}{9u_+}\right) + 3810}. \tag{5.125}$$

Likewise, at the leading edge of the DSW, we have

$$\ln\left(\frac{3\nu^2\tilde{k}^4}{32q^2} + \frac{\nu\tilde{k}^2}{4q} + 3\right) \sim \ln(3) + \frac{\nu\tilde{k}^2}{12q}, \tag{5.126}$$

$$\arctan\left(\frac{3\nu\tilde{k}^2}{4\sqrt{17}q} + \frac{1}{\sqrt{17}}\right) \sim \frac{12\sqrt{17}}{289}\frac{\nu\tilde{k}^2}{q} + \frac{50\sqrt{17}}{867}, \tag{5.127}$$

which yield the conjugate wavenumber asymptotic expression

$$\tilde{k} \sim 2\sqrt{\frac{q}{1733\nu}}\sqrt{3468\,\ln\left(\frac{u_i}{u_+}\right) - 0.07}. \tag{5.128}$$

Given the above asymptotics, we observe that there is no cut-off at the leading edge of the DSW and the solutions are always real. Yet, at the trailing edge of the DSW, there is a cut-off at $u_+ = 0.7$. This harmonic edge cut-off does not result because the solutions turn to complex, it actually results as the lead solitary wave velocity (5.122) becomes equal to the linear edge velocity (5.120) of the DSW, which is unphysical. The solutions of the DSW fitting method will be discussed in more detail in Chapter 6. This completes the analysis of the nematic PDSW and RDSW regimes (Regimes 1 and 2).

5.4 Nematic Crossover DSW

In this section, the solution for the nematic CDSW regime (Regime 3), as illustrated in Figure 3.4, will be derived. As can be seen from Figure 3.4, the transition towards the CDSW regime results in the KdV-type DSW existing in the PDSW and RDSW regimes becoming unstable. A large part of the CDSW structure shows that the waves which are at the leading edge have on "average" equal amplitudes and a rapid drop near the trailing edge of the DSW. It can also be noticed from Figure 3.4 that the nematic resonant wavetrain is distinctly non-uniform and has a major effect on the stability of the nematic DSW. In contrast to the CDSW regime governed by the KdV5 equation,

that is, equation (1.40) with $\mu_d = 0$, the KdV5 resonant wavetrain has "almost" a constant amplitude with a slowly varying front which takes the wavetrain down to the initial level ahead u_+ [80]. This front exemplifies a potion of a modulated solitary wavepacket [1].

We now develop an asymptotic method to solve for the nematic CDSW regime by combining two approximate methods from the work of [59, 61]. The first one is what we term in this thesis the "DSW equal amplitude approximation." This method helps us to determine the "averaged" amplitude a_s and velocity V_s of the front of the CDSW. We shall explain this method in more detail in the next subsection. The latter one is the nematic linear Wentzel-Kramers-Brillouin-Jeffreys (WKBJ) approximation which was calculated by Smyth and El [61]. Obviously, the WKBJ approximation assumes that the nematic resonant wave is a linear and high frequency wave. The assumption that this wave is a fast oscillating wave relative to the CDSW is clearly true. However, the linear assumption can be invalid as the jump height increases. In spite of the linear assumption, it has been found that the "linear" WKBJ method gives an excellent prediction for the "averaged" value of the resonant wavetrain amplitude a_r. The resonant wavenumber k_r can be calculated from the resonance condition (5.105) with V_s obtained from the DSW equal amplitude approximation.

5.4.1 DSW Equal Amplitude Approximation

When the CDSW form is compared with the (unstable) focusing NLS DSW form, as depicted in Figure 1.8(c), an illuminating analogy between each of them can be recognised, in that the DSW is composed of a train of "nearly" equal amplitude waves with a rapid decrease to the initial level behind u_- at the trailing edge. The work of [177] found that the major portion of unstable DSWs consists of a train of nearly equal amplitude waves, which justifies the approximate theory developed by Smyth and Marchant in [59] that approximates DSWs as trains of equal amplitude solitary waves, with the amplitude of the solitary waves found from conservation laws, motivated by the work of [183] on the transcritical flow of a fluid over topography.

Regardless of the integrability property of non-linear dispersive wave equations, it was found in [59] that the DSW equal amplitude method gives a theoretical prediction that ranges from very good to excellent for the averaged wave amplitude. Examples of DSWs that were studied in [59] are DSWs governed by the focusing NLS, focusing nematic and colloidal equations. Moreover, and intriguingly enough, it was found that this approximate method effectively works for stable DSWs governed by the KdV, modified KdV and Benjamin-Ono equations based on the observation that as their DSWs evolve they become dominated by solitary waves in the long term.

The DSW equal amplitude approximation can be summarised in the following steps

- Seek a solitary wave solution for the governing equation(s).
- Derive mass and energy conservation laws for these equations.
- Average these conservation laws over the spatial domain $-\infty < x < \infty$.
- Solve these averaged conservation laws for the soliton amplitude. The velocity then is determined by the amplitude-velocity relation.

This approximate method, together with the linear nematic WKBJ solution for the resonant wavetrain [61], will be utilised on the nematic Kawahara equation (5.70) in the subsequent subsection to derive the solution for the CDSW regime.

5.4.2 Implementation to the Nematic Kawahara Equation

The nematic Kawahara equation (5.77) has the "mass" (optical power) conservation equation

$$\frac{\partial}{\partial \eta} u_1 + \frac{\partial}{\partial \xi}\left\{\frac{1}{2}B_2 u_1^2 + B_3 u_{1\xi\xi} + \varepsilon^2 B_4 u_{1\xi\xi\xi\xi}\right\} = 0 \tag{5.129}$$

and the energy conservation equation

$$\frac{\partial}{\partial \eta}\left\{\frac{1}{2}u_1^2\right\} + \frac{\partial}{\partial \xi}\left\{\frac{1}{3}B_2 u_1^3 + B_3 u_1 u_{1\xi\xi} - \frac{1}{2}B_3 u_{1\xi}^2 + \varepsilon^2 B_4 u_1 u_{1\xi\xi\xi\xi} - \varepsilon^2 B_4 u_{1\xi} u_{1\xi\xi\xi} + \frac{1}{2}\varepsilon^2 B_4 u_{1\xi\xi}^2\right\} = 0. \tag{5.130}$$

These will now be used to find an approximate solution for the nematic CDSW by assuming that it consists of a uniform series of solitary waves [59], as discussed at the beginning of this section.

Let us assume that the CDSW at position (time-like) η consists of N equal solitary waves of amplitude $\tilde{a}_s$ and width $\tilde{w}_s$, where we shall use tildes to denote scaled variables in the moving and stretched coordinates (ξ, η) as considered in Section 5.3. It is also assumed that the CDSW sheds a uniform resonant wavetrain of amplitude $\tilde{a}_r$ which propagates ahead of it. Then, as $\xi \to -\infty$, $u_1 \to 1$ and as $\xi \to \infty$, $u_1 \to \tilde{a}_r \cos\left(\tilde{k}_r \xi - \tilde{\omega}_r \eta\right)$, since $|u| = u_+ + \varepsilon^2 u_1 + o\left(\varepsilon^2\right)$ with $\varepsilon^2 = u_i - u_+$. Integrating the mass and energy equations (5.129) and (5.130) over the CDSW, we have

$$N\int_{-\infty}^{\infty} u_1 \, d\xi = \left\{\frac{1}{2}B_2 - \frac{1}{4}B_2 \tilde{a}_r^2\right\}\eta, \quad N\int_{-\infty}^{\infty} \frac{1}{2}u_1^2 \, d\xi = \left\{\frac{1}{3}B_2 - \frac{1}{4}\tilde{c}_g \tilde{a}_r^2\right\}\eta. \tag{5.131}$$

In calculating the flux terms due to the resonant wavetrain on the right hand sides of (5.131), the averages of the resonant wavetrain and its square over a period have been used as the resonant wave is a high frequency wave relative to the CDSW, see Figure 3.4. Also, not averaging the resonant wavetrain terms in the right hand sides of (5.131) will make the calculations very difficult. Here, $\tilde{c}_g$ stands for the group velocity of the shed radiation in the moving and stretched (ξ, η) coordinates. In calculating the energy conservation expression (5.131), the second relation in (5.131), this group velocity is not that for the Kawahara equation (5.77), which is the group velocity for long waves in the non-local limit ν large, but that for the shed radiation, which is short wave radiation with the dispersion relation (5.3). From these conservation relations, we see that the shed radiation leaks mass and energy from the CDSW, which is the reason for the rapid decrease in its amplitude as u_+ decreases, as shall be seen in Chapter 6 when the theoretical and numerical solutions are compared with each other.

The integrals in the conservation expressions (5.131) are N times the integrals for a single solitary wave. Due to the high number of derivatives in the Kawahara equation, no exact solitary wave solutions have been derived for it. However, as for the PDSW solution in Section 5.3, the perturbation solution of [125, 182] which transforms the Kawahara equation to the standard KdV equation can be used to find a perturbed solitary wave solution of the Kawahara equation. This transformation gives that the solitary wave solution of (5.77) is

$$u_1 = \tilde{a}_s \operatorname{sech}^2 \Theta - 5\varepsilon^2 C_4 \tilde{a}_s^2 \operatorname{sech}^2 \Theta + \frac{15}{2}\varepsilon^2 C_4 \tilde{a}_s^2 \operatorname{sech}^4 \Theta, \tag{5.132}$$

with the width $\tilde{w}_s$ of the solitary wave, its phase Θ and velocity $\tilde{V}_s$ given by

$$\tilde{w}_s = \frac{\sqrt{6B_3}}{\sqrt{B_2}}\frac{\sqrt{2}}{\sqrt{\tilde{a}_s}}, \quad \Theta = \frac{\xi - \tilde{V}_s\eta}{\tilde{w}_s}, \quad \tilde{V}_s = \frac{1}{3}B_2\tilde{a}_s\left\{1 + 2\varepsilon^2 C_4\tilde{a}_s\right\}. \tag{5.133}$$

With this perturbation solution for the solitary wave, the mass and energy of a single solitary wave can be calculated as

$$\int_{-\infty}^{\infty} u_1\, d\xi = 2\tilde{a}_s\tilde{w}_s, \tag{5.134}$$

$$\int_{-\infty}^{\infty} \frac{1}{2}u_1^2\, d\xi = \frac{2}{3}\tilde{a}_s^2\tilde{w}_s + \frac{4}{3}\varepsilon^2 C_4\tilde{a}_s^3\tilde{w}_s, \tag{5.135}$$

respectively. Note that in the calculation of the energy, only terms up to $O(\varepsilon^2)$ have been retained, consistent with the order of the transformation [125, 182]. Dividing the mass and energy relations (5.131) hence gives

$$\frac{1}{3}\tilde{a}_s + \frac{2}{3}\varepsilon^2 C_4\tilde{a}_s^2 = \frac{2}{3}\frac{1 - \frac{3}{4}\frac{\tilde{c}_g\tilde{a}_r^2}{B_2}}{1 - \frac{1}{2}\tilde{a}_r^2}. \tag{5.136}$$

Equation (5.136) determines the scaled amplitude $\tilde{a}_s$ of the solitary waves of the CDSW once the scaled amplitude $\tilde{a}_r$ of the shed resonant radiation is known.

As mentioned earlier, in a former study of nematic DSWs a WKBJ solution for the shed resonant radiation was derived which was found to be in excellent agreement with numerical solutions [61]. A WKBJ solution was used as the resonant wavetrain is short wave relative to the DSW. This solution for the resonant wavetrain was given in terms of the original variables u and (x, z). Returning the amplitude relation (5.136) to the original variables can be done by using $a_s = \varepsilon^2\tilde{a}_s = \{u_i - u_+\}\tilde{a}_s$, $a_r = \varepsilon^2\tilde{a}_r = \{u_i - u_+\}\tilde{a}_r$ and (5.66). The linear resonant wavetrain solution (WKBJ solution) from the work [61] is

$$u_r = u_+ + \left\{[u_i - u_+]\left[1 + \frac{2u_+k_ra_s}{qV_s(k_r - V_s)^2}\right]^{-1}\right\}e^{i(k_rx - \omega_rz)}, \tag{5.137}$$

with ω_r given by (5.3). Therefore, the amplitude of the CDSW solitary waves is determined by

$$a_s\left\{1 + 2C_4a_s\right\} = 2\left\{u_i - u_+\right\}\frac{1 - \frac{3}{4}\frac{\left\{c_g - \sqrt{\frac{2}{q}}\,u_+\right\}a_r^2}{B_2\{u_i - u_+\}^3}}{1 - \frac{1}{2}\frac{a_r^2}{\{u_i - u_+\}^2}}, \tag{5.138}$$

with the resonant radiation's amplitude a_r given by [61]

$$a_r = \frac{u_i - u_+}{1 + \frac{2u_+k_ra_s}{qV_s\{k_r - V_s\}^2}}. \tag{5.139}$$

Here, the resonant group velocity satisfies

$$c_g = \frac{\partial\omega_r}{\partial k_r} = \frac{\partial}{\partial k_r}\left\{\frac{k_r^2}{2} + \frac{2\bar{\rho}}{q}\right\} = k_r, \tag{5.140}$$

see (5.3) wit $v_+ = 0$, has been used. On using (5.132), the height H_s of the leading solitary waves of the CDSW from $u = 0$ is

$$H_s = u_+ + a_s + \frac{5}{2} C_4 a_s^2. \tag{5.141}$$

The velocity of the solitary waves of the CDSW in the original variables is

$$V_s = \sqrt{\frac{2}{q}}\, u_+ + \frac{1}{3} B_2 a_s \left\{1 + 2C_4 a_s\right\} \tag{5.142}$$

as the ξ frame moves with velocity $u_+\sqrt{2/q}$.

Finally, the resonant wavenumber k_r is determined by the resonance condition (5.105). The reason why $v_+ = 0$ is that the resonant radiation is assumed to oscillate on the initial level ahead u_+, which agrees with numerical solutions, thus it follows from (5.65) that $v_+ = 0$. Equations (5.138) and (5.106), with (5.139), were solved numerically using Newton's method to determine the amplitude a_s and velocity V_s of the solitary waves of the CDSW and the amplitude a_r and wavenumber k_r of the resonant wavetrain. This was done by using the inbuilt function *fsolve* in MATLAB software. It was found that the resonant wave amplitude a_r is negligible for $u_+ > 0.70$. This is then the numerical upper limit of the CDSW regime, in excellent agreement with the upper CDSW regime numerical limit of Table 6.1, as given in Chapter 6, found from the above calculation. The lower limit of the CDSW regime will be discussed in the next section dealing with the TDSW regime.

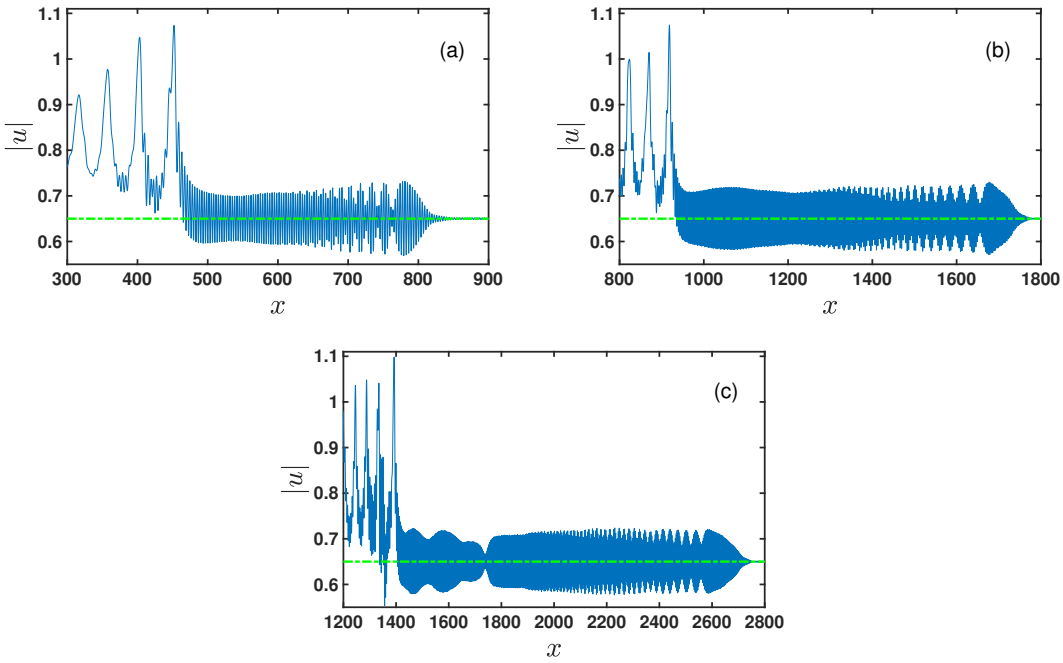

Figure 5.6: Numerical solutions of the nematic equations (2.19) and (2.20). Blue (solid) line: $|u|$; green (dash-dot) line: u_+. Solutions at (a) $z = 500$, (b) $z = 1000$, (c) $z = 1500$. Here $u_- = 1.0$, $u_+ = 0.65$, $q = 2$ and $\nu = 200$. (Online version in colour.)

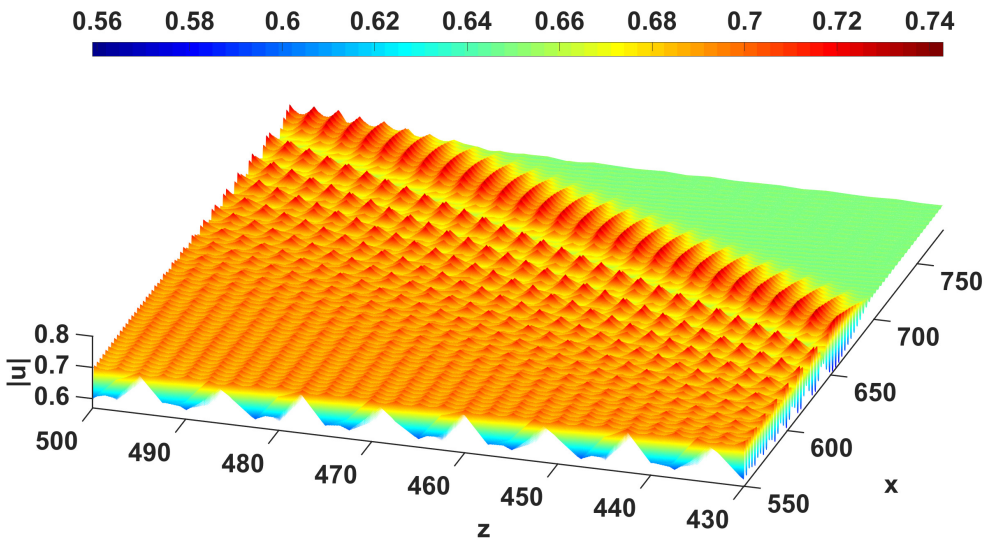

Figure 5.7: Numerical solution of the nematic equations (2.19) and (2.20) for $|u|$ showing evolution of resonant wavetrain instability. Here $u_- = 1.0$, $u_+ = 0.65$, $\nu = 200$ and $q = 2$. (Online version in colour.)

5.4.3 Resonant Wavetrain and its Modulational Stability

Let us now study further the modulational stability of the nematic resonant wavetrain ahead of the CDSW. As previously emphasised, the nematic DSW's instability structure is driven by the instability of the resonant wavetrain. Since we are assuming that the resonant wavetrain in this regime oscillates about the initial state u_+, one can rely on the Whitham modulation equations for a steady mean level $\bar{\rho} = \rho_+$ to verify that the resonant wavetrain in front of the DSW is unstable as the modulational system will be fully elliptic, see Figure 3.4. Such a modulational instability for a fixed mean level is well-known in modulation theory, see [1].

On the other hand, taking into account that the resonant mean level is slowly varying in general, the Whitham modulation equations (4.96)–(4.99) for the resonant wavetrain become half elliptic, half hyperbolic, so that Benjamin-Feir instability arises and the underlying Stokes wave solution for the resonant wavetrain becomes unstable. The Whitham modulation equations (4.96)–(4.99) for the nematic Stokes wave are fully hyperbolic for wavenumbers in the range (4.100), so that the weakly non-linear Stokes wavetrain is stable in this region. Using the resonance condition (5.105) with $k = k_r$, V_s is given by (5.102) and $\bar{u} = u_+$ with $q = 2$ and $\nu = 200$, this gives that the resonant wavetrain is unstable if $u_+ < 0.674$. However, numerical solutions show that the resonant wavetrain in the RDSW regime is unstable, see Figure 3.3 for instance, so there is a disagreement with the numerical solution in this respect.

Figure 5.6 shows this modulational instability of the resonant wavetrain for $u_+ = 0.65$. The instability of the resonant wavetrain is clear, with the breakup of the resonant wavetrain as it propagates in z now prominent. It should be noted that each wave of the DSW generates a resonant wave as a DSW is a modulated wavetrain [80]. Figure 5.6 shows that these resonant waves within the DSW are also unstable. Figure 5.7 provides further details of the evolution of the instability of the resonant wavetrain and shows a transition from a uniform wavetrain to a series of wavepackets. This detailed modulational instability evolution closely resembles experimental photographs

of Benjamin-Feir instability for water waves [176].

The Stokes wave expansions (4.1)–(4.4) and the associated Whitham modulation equations (4.96)–(4.99) are weakly non-linear and hold for relatively small amplitudes. As the amplitude of the resonant wavetrain rises it is found numerically that it restabilises, but not totally as marginal instabilities are observed in the resonant wavetrain of the TDSW regime, as shown in Figure 3.5. It can be seen that while the resonant wavetrain is not uniform, as for the fifth order KdV resonant wavetrain [80], the degree of modulation is much reduced over that of Figure 5.6. This resonant wavetrain modulational instability is significant in the CDSW regime. This completes the analysis of the nematic CDSW regime (Regime 3).

5.5 Nematic Travelling DSW

As the initial level ahead u_+ decreases in the CDSW regime, the effect of the shed resonant wavetrain grows until the DSW itself ceases to exist and there is just a large amplitude resonant wavetrain with a small amplitude wave at its trailing edge linking it to the intermediate level, as shown in Figure 3.5. This is similar to the behaviour of the DSW for the Kawahara equation (1.40) (with $\mu_d = 0$ or small enough μ_d [79, 80]) for which a standard DSW ceases to exist for large enough initial steps. The DSW is replaced by what is termed a TDSW, a travelling dispersive shock wave [79]. This previous work on the Kahawara equation shows that in the TDSW regime the DSW largely disappears, with a single remnant negative polarity solitary wave (known sometimes as an oscillatory solitary wave [78]) connecting the resonant wavetrain to the initial level behind u_-. The same structure is seen in Figure 3.5 for the nematic TDSW regime, but the remnant solitary wave now is connecting the intermediate level u_i to the resonant wavetrain.

It was shown for the Kawahara equation that in the TDSW regime the resonant wavetrain is linked to the level u_+ ahead by a partial DSW [80]. A partial DSW is a modulated wavetrain consisting of cnoidal waves for which the modulus either starts at $m = 1$ (solitary wave limit) and decreases to a value $m_o \neq 0$, or increases from $m = 0$ (linear dispersive wave limit) to $m_o \neq 1$. Therefore, it takes a uniform wavetrain down to a constant level, in contrast to a full DSW which is a modulated wavetrain that connects two uniform distinct levels [180, 181]. As stated, a negative polarity solitary wave connects the resonant wavetrain to the level u_i behind [79]. As there is no known solitary wave solution of the Kawahara equation of either polarity, in previous work [79, 80] this connection was done numerically and also by using approximate theory, see Figure 5.8. However, it has been recently realised that the determination of this connecting negative polarity solitary wave is not necessary [81]. The connection between the resonant wavetrain and the level behind can be treated as a Whitham shock, the wavetrain equivalent of a gas dynamic shock, for the Whitham modulation equations governing the resonant wavetrain, confirming speculation by Whitham when he originally developed modulation theory [1, 83]. This shock-like nature of the connection can be seen for the nematic TDSW illustrated in Figure 5.9, where the discontinuous connection between the resonant wave and the uniform level behind is clearly visible.

For the modulation equations to have a Whitham shock, they need to form a hyperbolic system. The Whitham modulation equations (4.96)–(4.99) for the Stokes wave are hyperbolic in the restricted interval (4.100). This shows that the resonant wavetrain falls outside this region over all the CDSW and all the TDSW existence intervals. However, as shown in Figure 3.5, the resonant wavetrain is stable in the TDSW regime.

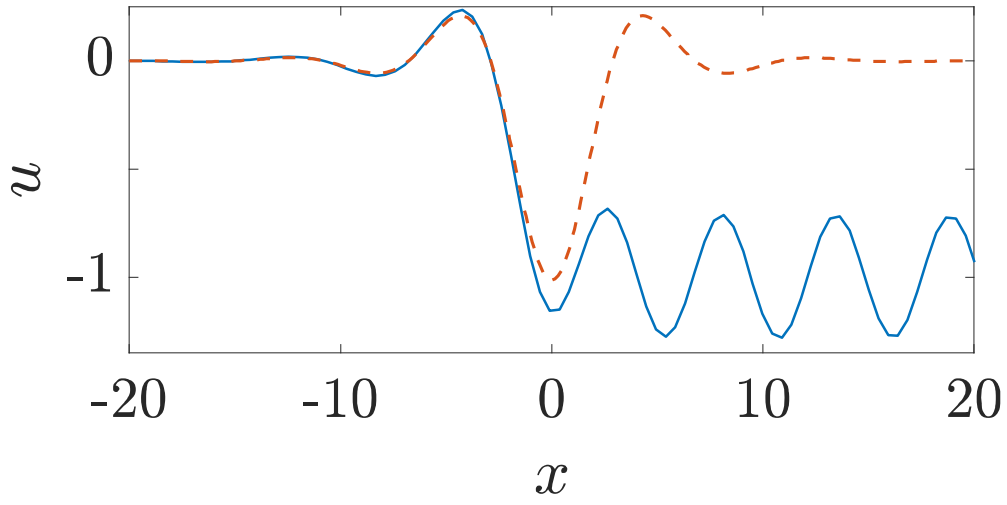

Figure 5.8: A portion of Kawahara TDSW regime. Whitham shock structure is expanded as a "partial" oscillatory solitary wave governed by the Kawahara equation (1.40). Orange (dash-dot) line: numerical full oscillatory solitary wave solution governed by the Kawahara equation with $\mu_d = 1$ (1.40). Blue (solid) line: partial oscillatory solitary wave exhibited by the Kawahara TDSW regime. Courtesy of Patrick Sprenger et al [79]. (Online version in colour.)

As discussed above, the Stokes wave modulation equations are valid in the weakly non-linear limit and the numerical results show that they do not correctly predict modulational stability for the resonant TDSW wave as it has relatively large amplitude. As the full Whitham modulation equations are not known, the Stokes' wave modulation equations will be used to find jump conditions for the connection between the intermediate level u_i and the resonant wavetrain in the TDSW regime.

5.5.1 Whitham Modulation Jump Conditions

As for the compressible gas equations, the appropriate modulation equations to determine the wave shock jump conditions are the mass, momentum and energy equations (4.84). Consistent with the TDSW structure illustrated in Figure 3.5, ahead of the Whitham shock there is the resonant wavetrain with wavenumber $k = k_r$, mean height $\bar{u} = \bar{u}_r$ ($\bar{\rho} = \bar{\rho}_r = \bar{u}_r^2$), flow $\bar{v}_r$ and amplitude $a = a_r$. Behind the Whitham shock there is no wavetrain, so the wavenumber $k = k_i = 0$, the amplitude $a = a_i = 0$ and the mean height is $\bar{u} = u_i$. Let us denote the Whitham shock velocity by U_{shock}. Then the mass, momentum and energy modulation equations (4.84) give the jump conditions

$$-\{\bar{\rho}_r - \rho_i\}\, U_{\text{shock}} + \left\{\bar{\rho}_r\bar{v}_r + \frac{k_r a_r^2}{4\bar{\rho}_r} - \rho_i v_i\right\} = 0, \tag{5.143}$$

$$-\left\{\bar{\rho}_r\bar{v}_r + \frac{a_r^2 k_r}{4\bar{\rho}_r} - \rho_i v_i\right\} U_{\text{shock}} + \left\{\frac{\bar{\rho}_r^2}{q} + \bar{v}_r^2\bar{\rho}_r + \frac{a_r^2 k_r^2}{4\bar{\rho}_r} + \frac{a_r^2\bar{v}_r k_r}{2\bar{\rho}_r} - \frac{\rho_i^2}{q} - v_i^2\rho_i\right\} = 0, \tag{5.144}$$

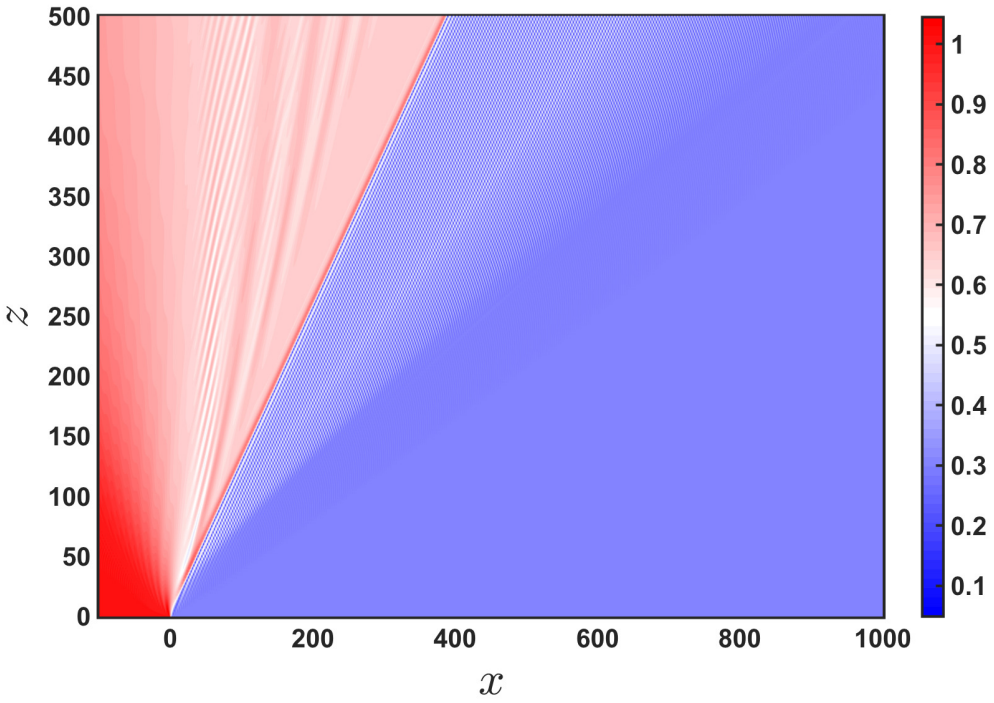

Figure 5.9: Numerical solution of the nematic equations (2.19) and (2.20) for $|u|$ in the TDSW regime showing the Whitham shock (solid red line) linking the resonant wavetrain with the intermediate shelf. Here $u_- = 1.0$, $u_+ = 0.3$, $\nu = 200$ and $q = 2$. (Online version in colour.)

and

$$-\left\{\frac{2\bar{\rho}_r^2}{q}+\bar{v}_r^2\bar{\rho}_r+\frac{a_r^2k_r^2}{4\bar{\rho}_r}+\frac{a_r^2\bar{v}_rk_r}{2\bar{\rho}_r}-\frac{2\rho_i^2}{q}-v_i^2\rho_i\right\}U_{\rm shock}+\left\{\frac{4\bar{\rho}_r^2\bar{v}_r}{q}+\right.$$
$$\left.\bar{\rho}_r\bar{v}_r^3+\frac{a_r^2k_r}{q}+\frac{3a_r^2k_r^2\bar{v}_r}{4\bar{\rho}_r}+\frac{3a_r^2\bar{v}_r^2k_r}{4\bar{\rho}_r}+\frac{a_r^2k_r^3}{4\bar{\rho}_r}-\frac{4\rho_i^2v_i}{q}-\rho_iv_i^3\right\}=0, \qquad (5.145)$$

respectively [1]. Here, v_i on the intermediate level is related to ρ_i by (5.24) for the expansion wave solution from the initial level u_- behind. In addition, there is the resonance condition obtained from the Stokes wave dispersion relation (4.4)

$$U_{\rm shock}=\bar{v}_r+\frac{1}{2}k_r+\frac{2\bar{\rho}_r}{qk_r}-\frac{k_ra_r^2}{8\bar{\rho}_r^2}. \qquad (5.146)$$

These jump conditions and the resonance condition form four equations for the six unknown parameters ρ_i, $\bar{\rho}_r$, $\bar{v}_r$, k_r, a_r and $U_{\rm shock}$. For the KdV5 equation, equation (1.40) with $\mu_d = 0$, the system was completed by matching the resonant wavetrain to the partial DSW at its leading edge, which brings the solution back to the initial level u_+. This partial DSW was found as a simple wave solution of the modulation equations of the KdV5 equation in Riemann invariant form. Even when the Stokes wave modulation equations are hyperbolic, they cannot be expressed in Riemann invariant form. To complete the solution for the TDSW regime, some assumptions based on numerical solutions will be made.

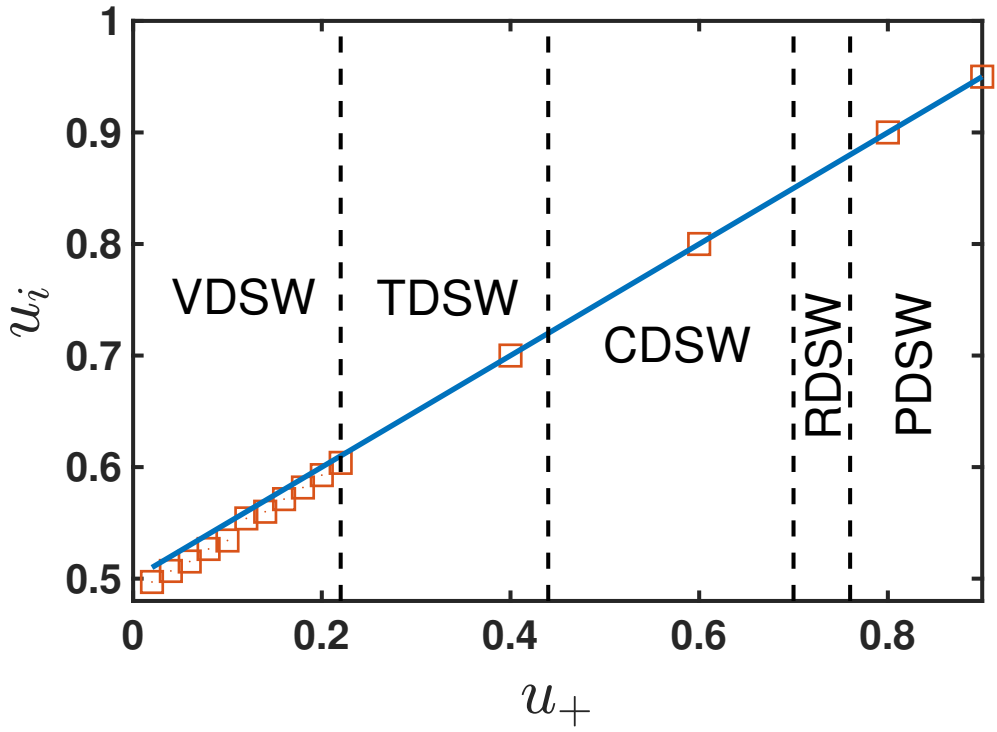

Figure 5.10: Intermediate level u_i as given by numerical solutions of the nematic equations (2.19) and (2.20) over all the nematic DSW regimes and the theoretical average expression (5.28). Numerical solution: orange boxes; theoretical values: blue (solid) line. Here $u_- = 1.0$, $\nu = 200$ and $q = 2$. (Online version in colour.)

Figure 5.10 shows the level u_i of the shelf between the expansion wave from u_- and the resonant wavetrain. It can be seen that in the TDSW regime, it is given by the average (5.28), $(1 + u_+)/2$ in this case, based on the conservation of the Riemann invariant R_- for the non-dispersive shallow water equations, given by (5.17), through the Whitham shock. The reason that this is an excellent approximation is that the Whitham shock is relatively weak, as seen from Figure 3.5, so that this Riemann invariant is conserved through the shock to leading order [1]. It will then be assumed that u_i is given by (5.28). Consistent with this, it is assumed from the shallow water Riemann invariant R_- given by (5.17) that

$$\bar{v}_r = 2\sqrt{\frac{2}{q}}\left\{\sqrt{\bar{\rho}_r} - \sqrt{\rho_+}\right\} = 2\sqrt{\frac{2}{q}}\left\{\sqrt{\bar{\rho}_r} - u_+\right\}. \tag{5.147}$$

As noted in Section 4.2 the shallow water characteristics (4.98) and (4.99) are always real, so the Riemann invariants on these can be used to propagate the solution. This assumption is based on ignoring the wave amplitude correction in the characteristic form (4.99) as this amplitude is small. With these assumptions, the jump conditions (5.143)–(5.145) were solved numerically using Newton's method. To be specific, the command function *fsolve* in MATLAB was used to solve these modulation jump conditions. It is good to mention here that, while solving the nematic modulation jump conditions numerically, the non-linear system was found extremely sensitive to given initial data, in that very slight changes in the initial data lead to significantly different results.

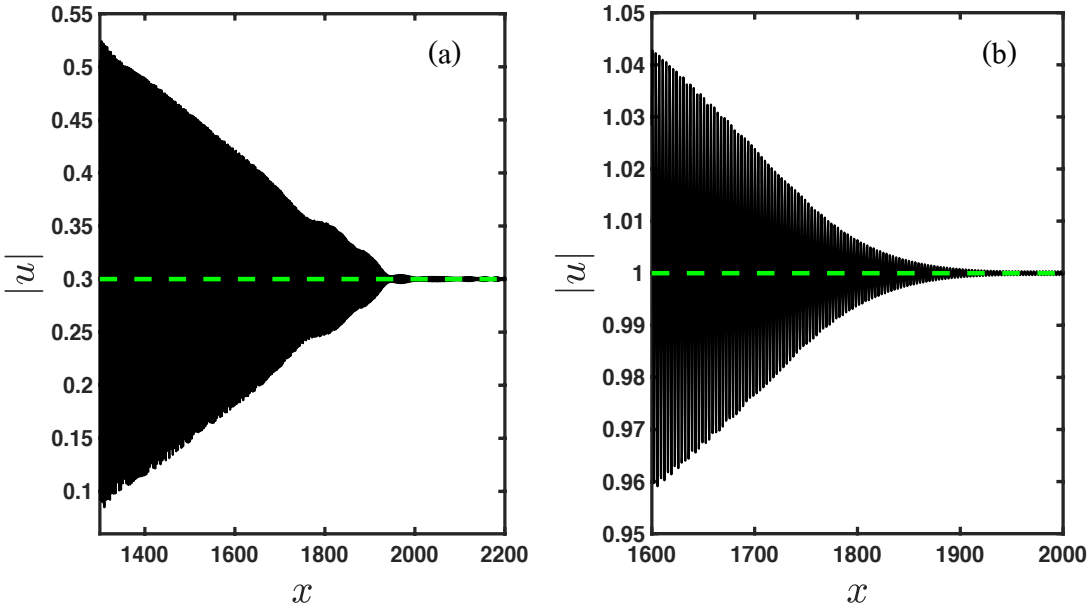

Figure 5.11: Non-local versus local partial DSWs in the nematic TDSW regime as numerical solutions of equations (2.19) and (2.20). (a) Black (solid) line: $|u|$ (non-local partial DSW); green (dash-dot) line: $u_+ = 0.3$. Here, $u_- = 1$, $q = 2$, $\nu = 200$ and $z = 1000$. (b) Black (solid) line: $|u|$ (local partial DSW); green (dash-dot) line: $u_+ = 1.0$. Here, $u_- = 1.2$, $q = 2$, $\nu = 1.5$ and $z = 1000$. (Online version in colour.)

5.5.2 Partial DSW and its Modulational Stability

As previously discussed, the resonant wavetrain in the TDSW regime is attached to a slowly varying wavetrain (partial DSW) at the front, bringing the optical intensity down to the initial flow state ahead u_+. For the KdV5 equation [80] or the Kawahara equation [79], this partial DSW is stable and weakly non-linear Whitham's modulation theory, based on a Stokes' wave approach as in Section 4.2, gave a full hyperbolic Riemann invariant system. It was then possible in previous work [80], following the work of [1, 180, 181], to determine the slowly varying amplitude, wavenumber, background (mean level), trailing and leading edge velocities of the partial DSW and excellent agreement with numerical solutions was obtained.

In this study of nematic DSWs, however, the weakly non-linear system (4.96)–(4.99) is a mixed system, half elliptic, half hyperbolic. Also, Riemann invariants cannot be found even in the hyperbolic region (4.100); known as Pfaff's problem [1]. Regrettably, this means that a solution for the nematic partial DSW is not available. Whether there is a way to deal with or solve for this nematic partial DSW is an open question.

There are further notes and comments on the nematic partial DSW and it is important to report them here. It has been found that the modulational structure of the nematic partial DSW in the TDSW regime varies depending upon the value of the non-locality parameter ν. From Figure 5.11, we notice that the non-local partial DSW, depicted in Figure 5.11(a), is notably unstable at the front, in contrast to the local counterpart, given in Figure 5.11(b). Whether the reason behind this is the fact that the nematic weakly non-linear system (4.96)–(4.99) is half elliptic, half hyperbolic and the partial DSW is unstable in the first place, rather than stable, is not clear at this stage. This instability is not a numerical issue. Several (small) numerical step-sizes were used and the same unstable behaviour was observed. Regarding the local partial

DSW, as depicted in Figure 5.11(b), it is "nearly" identical to the one governed by the KdV5 equation [80]. It is clear that it is modulationally stable. The reason why it is stable is that the nematic equations (2.19) and (2.20) approach the defocusing NLS equation (1.17), with $q = 2$, as $\nu \to 0$, so the partial DSW approaches a full stable NLS DSW, like the one shown in Figure 1.8(b). In this local limit, the nematic Kawahara equation (5.70) becomes the classical KdV equation with negative dispersion and the associated Whitham modulation equations become hyperbolic. This local partial DSW can then be found from the work of [180, 181]. This will be one of the subjects that will be studied in the future, see Section 7.2. This completes the analysis of the nematic TDSW regime (Regime 4).

5.6 Nematic Vacuum DSW

As the initial level ahead u_+ decreases in the TDSW regime, the resonant wavetrain hits the vacuum point at which $u = 0$, at which point the DSW changes form [62, 63]. When this critical level is reached, the DSW changes to the vacuum DSW (VDSW) regime, with Figure 3.6 showing a typical VDSW solution. Table 6.1 in Chapter 6 shows this critical value of u_+ for the onset of a vacuum point as given by the jump conditions (5.143)–(5.145) and by numerical solutions, with excellent agreement seen. The partial DSW of the TDSW regime which brings the resonant wavetrain down to u_+ is now on a (linearly) varying mean. As for the TDSW regime, there is a Whitham shock which links the resonant wavetrain to the intermediate level u_i. This will be

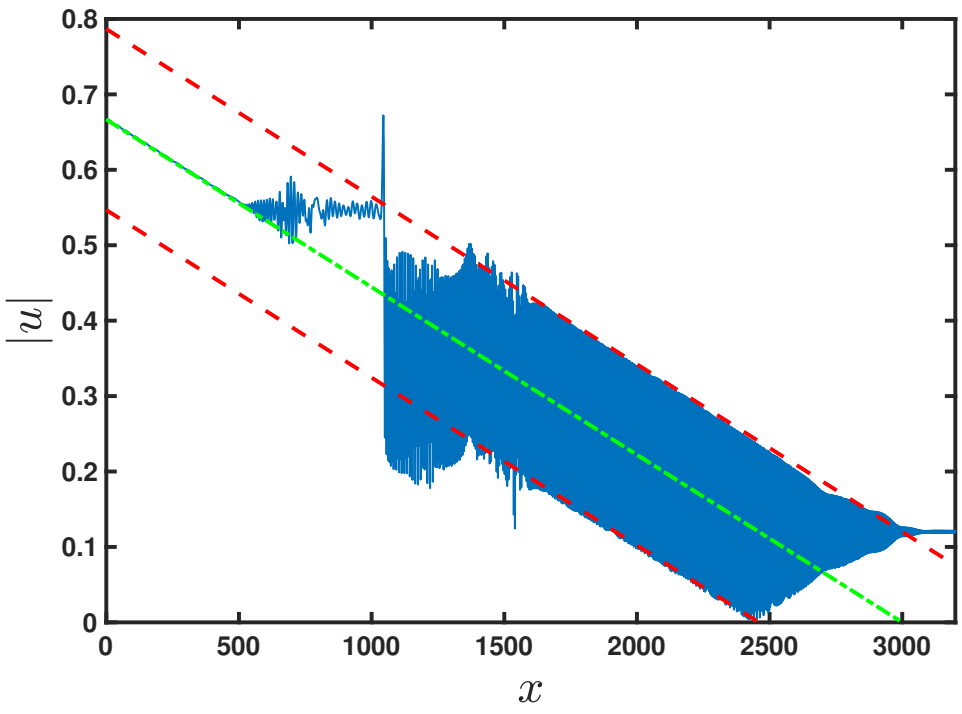

Figure 5.12: Numerical solution of the nematic equations (2.19) and (2.20) for $|u|$: blue (solid) line; expansion wave solution (5.22): green (dash-dot) line; expansion wave solution (5.22) $\pm u_+$: red (dashed) line, $+u_+$ (upper), $-u_+$ (lower). Here $u_- = 1.0$, $u_+ = 0.12$, $\nu = 200$ and $q = 2$. (Online version in colour.)

determined by the same Whitham shock jump conditions as for the TDSW regime. As for the TDSW regime, some assumptions based on numerical solutions will need to be made to derive the VDSW solution due to the lack of Whitham modulation equations in Riemann invariant form.

Figure 5.12 shows an expanded version of the VDSW solution of Figure 3.6. On the same figure the expansion wave solution (5.22) continued down to $u = 0$ and this solution with $\pm u_+$ added are shown. It can be seen that the mean and envelopes of the transition wave bringing the resonant wavetrain down to u_+ from the intermediate shelf are well approximated by this expansion wave solution. This type of wavetrain structure does not exist for the defocusing NLS DSW in the vacuum case as there is no resonance [62]. Without full Whitham modulation equations for the fully non-linear nematic equations, there is no analytical method to justify this observed structure. This structure will be assumed here, with some justification based on weak shock theory.

Figure 5.12 shows that the resonant wavetrain and its leading edge have constant amplitudes, so that $a_r = u_+$ will be assumed, which is consistent with the wave envelopes of this figure. The resonant wave amplitude is small, so that it decouples from the mean height variation in the modulation equations. As the resonant wave amplitude is small, it will be ignored in the modulation equations (4.96)–(4.99), so that the modulation equations (4.98) and (4.99) become the shallow water equations [1]. The jump conditions in the previous section then become the shallow water equation jump conditions,

$$-\{\rho_i - \rho_r\} U_{\text{shock}} + \{\rho_i v_i - \rho_r v_r\} = 0, \tag{5.148}$$

$$-\{\rho_i v_i - \rho_r v_r\} U_{\text{shock}} + \left\{ v_i^2 \rho_i + \frac{\rho_i^2}{q} - v_r^2 \rho_r - \frac{\rho_r^2}{q} \right\} = 0, \tag{5.149}$$

for which the most convenient form is [1]

$$U_{\text{shock}} = \bar{v}_r \pm \sqrt{\frac{2}{q}} \left\{ \frac{u_i^2 \left(u_i^2 + \bar{u}_r^2\right)}{2\bar{u}_r^2} \right\}^{1/2}, \quad v_i = \bar{v}_r \pm \sqrt{\frac{2}{q}} \frac{u_i^2 - \bar{u}_r^2}{u_i^2} \left\{ \frac{u_i^2 \left(u_i^2 + \bar{u}_r^2\right)}{2\bar{u}_r^2} \right\}^{1/2}. \tag{5.150}$$

The sign choice for the shallow water equations (and the compressible gas equations) is the + sign, as in [1]. However, with this choice, in the limit $u_+ \to 0$, the shock velocity approaches the front velocity of the dam break solution $2u_-\sqrt{2/q}$, from (5.22), and $u_i \to 0$. This does not accord with numerical solutions, which show that $u_i \to u_-/2$ in this limit, which is the Riemann invariant value (5.28). The correct behaviour is obtained with the − sign choice in the shallow water jump conditions (5.150). Figure 5.12 also shows that the Whitham shock is weak, meaning that the jump is small. Expanding the jump conditions (5.150) for small jump height, $u_i^2 - \bar{u}_r^2$ small, gives

$$U_{\text{shock}} = \bar{v}_r - \sqrt{\frac{2}{q}} \bar{u}_r \left\{ 1 + \frac{3}{4} \frac{u_i^2 - \bar{u}_r^2}{\bar{u}_r^2} - \frac{9}{32} \frac{\left(u_i^2 - \bar{u}_r^2\right)^2}{\bar{u}_r^4} + \ldots \right\}, \tag{5.151}$$

$$v_i = \bar{v}_r - \sqrt{\frac{2}{q}} \frac{u_i^2 - \bar{u}_r^2}{\bar{u}_r} \left\{ 1 - \frac{u_i^2 - \bar{u}_r^2}{4\bar{u}_r^2} + \ldots \right\}. \tag{5.152}$$

We see from the upper expansion wave envelope in Figure 5.12 and the expansion wave solution (5.22) that

$$u_i = \frac{\sqrt{q}}{3\sqrt{2}} \left\{ \frac{2\sqrt{2}}{\sqrt{q}} u_- - U_{\text{shock}} \right\} + u_+, \tag{5.153}$$

so that

$$U_{\text{shock}} = 2\sqrt{\frac{2}{q}}u_- + 3\sqrt{\frac{2}{q}}\left\{u_+ - u_i\right\}. \tag{5.154}$$

As for the TDSW solution, the shallow water characteristic forms (4.98) and (4.99) will be used to propagate the solution. Furthermore, as for the TDSW regime, the amplitude corrections to these Riemann variables will be neglected, so that they become the Riemann invariants (5.16) and (5.17). As the shock is weak, at leading order the Riemann invariant R_+ (5.16) is conserved through the shock, so that at first order, that is shock strength zero,

$$2\sqrt{\frac{2}{q}}u_- = \bar{v}_r + 2\sqrt{\frac{2}{q}}\bar{u}_r. \tag{5.155}$$

A measure of the shock strength is u_+ as it is small. We then seek a weak shock correction to this Riemann invariant as

$$\bar{v}_r + 2\sqrt{\frac{2}{q}}\bar{u}_r = 2\sqrt{\frac{2}{q}}\left\{u_- + \delta_1 u_+ + \delta_2 u_+^2 + \mathcal{O}(u_+^3)\right\}. \tag{5.156}$$

Substituting the Riemann invariant correction (5.156) and the shock velocity expression (5.154) into the weak shock jump conditions (5.151) and (5.152) and solving as a series in small u_+, we find $\delta_1 = \delta_2 = 0$ and

$$u_i = \bar{u}_r + 2u_+ - \frac{u_+^2}{\bar{u}_r}. \tag{5.157}$$

To $\mathcal{O}(u_+^2)$ there is then no correction to the shallow water Riemann invariant. Equation (5.154) then gives the Whitham shock velocity. As the Riemann invariant R_+ is conserved to $\mathcal{O}(u_+^2)$ through the weak Whitham shock, the intermediate level result (5.28) holds to $\mathcal{O}(u_+^2)$, as confirmed from the intermediate level comparison of Figure 5.10. Using this intermediate level expression in the shock result (5.157) gives that

$$\bar{u}_r = \frac{1}{4}u_- - \frac{3}{4}u_+ + \frac{1}{4}\sqrt{u_-^2 - 6u_+u_- + 25u_+^2} = \frac{1}{2}u_- - \frac{3}{2}u_+ + \frac{2u_+^2}{u_-} + \ldots \tag{5.158}$$

This completes the analysis of the nematic VDSW (Regime 5).

The theoretical results which are obtained in this chapter will be compared with numerical solutions and discussed in Chapter 6.

Chapter 6

Comparison with Numerical Solutions and Discussions

In this chapter, we compare the theoretical solutions for the nematic hydrodynamic regimes, which were derived in the previous chapter, with numerical solutions and discuss these results. Comparative plots are provided at the end of the chapter.

6.1 Results and Discussions

Table 6.1 gives comparisons between the existence intervals for the six nematic hydrodynamic regimes as given by numerical solutions and the analytical solutions for the parameter choices $u_- = 1$, $\nu = 200$ and $q = 2$. As can be seen, the accordance between the analytical and numerical thresholds is excellent.

DSW type	numerical existence interval	theoretical existence interval
PDSW	$0.76 \leq u_+ < 1.0$	$0.73 \leq u_+ < 1.0$
RDSW	$0.70 \leq u_+ < 0.76$	$0.70 \leq u_+ < 0.73$
CDSW	$0.44 \leq u_+ < 0.70$	$0.44 < u_+ < 0.70$
TDSW	$0.22 \leq u_+ < 0.44$	$0.24 \leq u_+ \leq 0.44$
VDSW	$0 < u_+ < 0.22$	$0 < u_+ < 0.24$
Dam break	$u_+ = 0$	$u_+ = 0$

Table 6.1: Comparisons between numerical and theoretical existence regions for the six nematic hydrodynamic regimes. Here $u_- = 1.0$, $\nu = 200$ and $q = 2$.

The comparisons shown in Figure 6.1 to Figure 6.9 will be discussed next in this order: rarefaction wave, PDSW, RDSW, CDSW, TDSW and VDSW solutions.

Let us start with the rarefaction wave solutions. Figure 6.1 shows a comparison between the nematic dam break solution (5.22) and numerical solution. It can be seen that the agreement is perfect. However, there is a slight disagreement where the rarefaction wave meets the initial levels behind u_- and ahead u_+. The reason for that is that the discontinuity in the derivatives being smoothed by the effect of dispersion [86]. Figure 6.2 shows a comparison between numerical solution and theoretical solution (5.45). This is Case 4 in Subsection 3.2.2, two rarefaction waves separated by a shelf produced when the initial phases are not zeroes. The agreement is clearly perfect.

Now, we discuss the nematic PDSW and RDSW regimes. Figures 6.3–6.5 show comparisons between numerical solutions and the perturbed and radiating KdV DSW

solutions (5.95)–(5.98) for the height $H_s = u_+ + a_s$ and the velocity V_s of the lead solitary wave of the DSW and the velocity s_i of the trailing edge of the DSW (5.102). It can be seen that there is excellent agreement for the lead solitary wave height over both the PDSW and RDSW regimes. When a resonant wavetrain is present, the amplitude of the lead wave of the DSW oscillates as resonant radiation propagates out of the DSW [60, 61, 80]. In this case, the average lead wave amplitude is taken for the numerical comparisons. Figure 6.4 shows that there is also excellent agreement for the velocity V_s of the leading edge. There is some disagreement for the lead wave height and the velocity at the transition from the RDSW regime to the CDSW regime, but this is to be expected as the DSW drastically changes form. The leading edge velocity does not show much variation from u_- in these PDSW and RDSW regimes. Setting $C_4 = 0$ in the perturbed and radiating KdV DSW solutions (5.95)–(5.98) gives the standard KdV DSW solution, for which $H_s = u_-$ and $V_s = u_-$ on using (5.28) for u_i, as found in a previous study [60], leading to poor agreement with the numerical solutions. It is then seen that the higher order dispersion in the Kawahara equation (5.70) is necessary to fully account for the lead solitary wave in the PDSW and RDSW regimes, although the additional effect is not large.

Figure 6.5 shows a comparison between numerical solutions and the perturbed KdV DSW solution for the trailing edge velocity s_i (5.102). The comparison is again very good, in particular for the turning point in the trailing edge velocity. The implications of this turning point were discussed in Subsection 5.3.2. The wavenumber of the resonant wavetrain in the RDSW regime is given by the resonance condition (5.106), which has a solution if $V_s \geq 2u_+/\sqrt{q}$. From Table 6.1, it can be seen that there is good agreement for the intervals of existence for the PDSW solution, which does not have an associated resonant wavetrain as $V_+ < 2u_+/\sqrt{q}$. There is also excellent agreement for the existence region of the RDSW, which has an associated resonant wavetrain. Note that the lower bound for the RDSW regime is connected with the existence of the CDSW regime, which will be discussed shortly.

The last thing to discuss for the PDSW and RDSW regimes is the results obtained from the DSW fitting method. As seen in Subsection 5.3.3, the given solutions in equations (5.118)–(5.122) have a cut-off at $u_+ = 0.85$, in that the DSW solutions get imaginary for $u_+ < 0.85$. A good question that one may ask here is why the perturbation method detailed in Subsection 5.3.1 remains working until $u_+ = 0.7$, but the DSW fitting method does not work below $u_+ = 0.85$? The root cause behind this is the fact that the theoretical method in Subsection 5.3.1 is based on expanding the solution in the perturbation series (5.95)–(5.98) which have real coefficients for any value of u_+, while the DSW fitting method solutions (5.118) and (5.121) are given in terms of roots of transcendental equations that become complex at particular values of u_+.

To overcome this cut-off, equations (5.118)–(5.122) have been expanded in Taylor series. Indeed, at the leading edge of the DSW, we observe no cut-off. Figure 6.4 shows that the lead solitary wave velocity solution continues until $u_+ = 0.7$, but with errors varying from 0.98% to 16% as u_+ decreases. In contrast, at the harmonic edge of the DSW, shown in Figure 6.5, there is a cut-off at $u_+ = 0.7$ which results in as the lead solitary wave edge of the DSW equals to its linear edge, namely, $V_s = s_i = 1.12$, which is physically unacceptable. Nonetheless, this cut-off is in excellent agreement with the numerical borderline between the RDSW and CDSW regimes, as provided in Table 6.1. The errors in this case vary from 0.82% to 13.8% as u_+ decreases to $u_+ = 0.72$.

Overall, the perturbation method presented in Subsection (5.3.3) is better than the DSW fitting method when they are compared with nematic numerical solutions. Pos-

sible interpretations for the disagreement between these two methods are how asymptotic terms are neglected in the methods and how wave solutions are asymptotically expanded. For instance, the DSW fitting method expands the wave solutions as Taylor series, whereas the other method expands the solutions as perturbation series resulting from a non-local transformation (5.71).

In dealing with the DSW harmonic edge, we need to mention that in general the method which is commonly used to numerically determine the trailing edge velocity of a DSW is an ad-hoc method to some degree. This is because it is difficult and not fully clear to see where "exactly" the harmonic edge of the numerical solution starts, unlike the lead solitary wave edge. An approximate method to determine this velocity is the following. First, we try to observe where the trailing amplitudes of the waves of a DSW start to descend "linearly." Second, we interpolate a polynomial of degree 1 passing through a number of linearly related crests. Third, we calculate the spatial intersection point between the interpolant and the initial level behind the DSW, that is, u_-, or in our nematic problem the shelf u_i. Fourth, we repeat the same procedure for a different z in order to calculate the velocity from two positions. Note that slight changes in the chosen linear crests can yield notable differences in the velocity. This method can always be adjusted to accord with the obtained theoretical data as much as possible. In this sense, the method is not fully rigorous and is ad-hoc, but this is the easiest way to our knowledge to determine the trailing edge velocity of a DSW from numerical data.

Next, we discuss the comparisons for the nematic CDSW regime. Figure 6.3 shows the height $H_s = u_+ + a_s + (5/2)C_4 a_s^2$ of the solitary waves of the CDSW as given by numerical solutions and the equal amplitude approximation, equations (5.138)–(5.141). It can be seen that there is excellent agreement, except near the boundary with the TDSW regime. This is expected since as the height of the jump $u_i - u_+$ grows, the KdV approximation becomes less valid. In addition, as the TDSW regime is approached, the form of the DSW changes fundamentally, with the waves of the DSW disappearing, except for one wave at the leading edge, see Figure 3.5. Figure 3.4 shows that the amplitudes of the individual waves of the CDSW have a random variation this is because the CDSW is unstable. To calculate H_s from the numerical solutions, an amplitude average was then taken over the CDSW, which is consistent with the equal amplitude approximation. Figure 6.3 shows a rapid decrease in the height of the CDSW as u_+ decreases. However, the amplitude a_r of the shed radiation grows, as can be seen from Figure 6.6 since $a_r = H_r - u_+$. The shed resonant radiation acts as a damping on the DSW and leads to its decay over the non-resonant PDSW case. As the amplitude of the resonant radiation grows, the greater the damping of the CDSW, so that its amplitude decreases.

Figure 6.4 shows comparisons for the velocity V_s of the leading edge of the CDSW from (5.142). The agreement is not as good as for the solitary wave height, but the difference between the analytical and numerical solutions is about 4%. There are no results presented for the trailing edge velocity, as for the PDSW and RDSW cases, as the equal amplitude solitary wave approximation cannot give results for the linear trailing edge.

Figure 6.6 shows comparisons between the numerical and analytical solutions for the height $H_r = u_+ + a_r$ of the resonant wavetrain, equation (5.139) with the initial level u_+ added. There is again excellent agreement, as expected as the WKBJ solution (5.137) for the resonant wavetrain was previously found to be in excellent agreement with numerical solutions [61]. It can be seen that as the RDSW regime is approached the amplitude $a_r = H_r - u_+$ of the resonant wavetrain goes to zero, as required. As

discussed in Section 5.4 the resonant wavetrain in the CDSW regime is unstable when its amplitude is low and stabilises at high enough amplitude. For the comparisons of Figure 6.6 the amplitudes and heights of low amplitude numerical resonant waves were determined before instability broke the wavetrain up. In this regard, a unit distance in the non-dimensional variable z corresponds to about 2 μm for optical beams in the near infrared [102, 103, 104]. Typical experimental nematic cell lengths are ∼1 mm, which is $z = 500$. As shown in Figure 5.6, the breakup of the resonant wavetrain in the vicinity of the CDSW occurs after $z = 1000$. This is well beyond the experimental distance at which optical solitary waves can be observed, due to their decay because of scattering losses [6, 74]. Numerical solutions show that the mean height of the resonant wavetrain is given by $\bar{u}_r = \sqrt{q\theta_r}$. As the resonant wavetrain is rapidly varying, averaging the director equation (2.20) then gives this mean height expression. The non-local response of the nematic acts to average out the oscillations of the electric field.

Figure 6.7 shows a comparison between the mean height $\bar{u}_r$ of the resonant wavetrain as given by numerical solutions and by the theoretical CDSW value $\bar{u}_r = u_+$, with excellent agreement seen. Finally, Figure 6.8 shows comparisons for the wavenumber k_r of the resonant wavetrain given by (5.106). The numerical values of k_r were determined by averaging over the resonant wavetrain. It was found that averaging 10 to 20 crests is sufficient. Unlike the resonant wave height and mean level, the comparison is poor, except in the TDSW regime where the resonant wavetrain restabilises. The reason is that the resonant wavetrain is unstable over all the CDSW regime and so does not consist of a single dominant wavenumber, as seen in Figures 5.6 and 5.7.

Now turning to the nematic TDSW regime, Figures 6.6 and 6.7 give comparisons between numerical solutions and results from the Whitham shock modulation jump conditions for the resonant wave height $H_r = a_r + \bar{u}_r$ and the resonant wave mean level $\bar{u}_r$ in the TDSW regime, equations (5.143)–(5.146) with (5.147). It can be seen that there is excellent agreement for both parameters with numerical solutions, with some deviation for the resonant wave height when it transitions to the VDSW regime. As for the equivalent transitions for the CDSW regime, this is to be expected as the resonant wave drastically changes form in the VDSW regime, as seen from Figure 3.6.

Figure 6.8 shows a comparison for the resonant wavenumber k_r and nearly perfect agreement across the TDSW regime is seen, unlike for the CDSW regime. The higher resonant wave amplitude in the TDSW regime has stabilised the wavetrain, so that the assumption of a single dominant resonant wavenumber is now valid. For $u_+ > 0.44$, the Whitham shock velocity U_{shock} from (5.146) is greater than the (linear) group velocity c_g of the resonant wavetrain, which is unphysical. This value of u_+ is then the boundary between the TDSW and CDSW regimes, in excellent agreement with numerical results, as tabulated in Table 6.1.

Figure 6.9 shows a comparison between numerical solutions and the Whitham shock jump conditions for the shock velocity U_{shock}, the velocity of the trailing edge of the resonant wavetrain, expression (5.146). Again there is near perfect agreement, except for a slight deviation near the transition to the VDSW regime. This excellent agreement for the TDSW parameters validates the assumptions (5.28) and (5.147) made above.

Finally, we now discuss the nematic VDSW regime. Figure 6.9 shows comparisons between numerical solutions for the Whitham shock velocity with the theoretical result (5.151) in the VDSW regime. It can be seen that there is excellent agreement, except near the transition to the TDSW regime where the DSW form changes. As the transition to the TDSW regime is approached, the amplitude of the resonant wavetrain increases, so that its neglect in the Riemann variables becomes less valid.

Figure 6.6 gives comparisons for the height $H_r = u_+ + \bar{u}_r$, on using (5.158), of the

resonant wavetrain with numerical values. Again, there is good agreement, except near the transition to the TDSW regime, again because the neglect of the resonant wave amplitude correction to the Riemann variables becomes less accurate. The resonant wave mean $\bar{u}_r$ comparison of Figure 6.7 is similar, with an excellent comparison seen.

Figure 5.10, given in Subsection 5.5.1, shows an excellent comparison between the numerical mean level u_i in the VDSW regime and the VDSW theoretical result (5.157), as expected as the Riemann invariant R_+ is conserved to $\mathcal{O}(u_+^2)$ through the weak Whitham shock. Figure 6.8 shows comparisons for the resonant wavenumber k_r. As for the CDSW regime, the agreement is poor, except near the boundary with the TDSW regime where the resonant wavetrain restabilises due to its increased amplitude. As stated, it was found that the Riemann invariant R_+ (5.16) is conserved to $\mathcal{O}(u_+^2)$ through the Whitham shock, which means that the intermediate level u_i is given by the mean value (5.28) to this order. It can be seen from Figure 5.10 that there is a slight deviation of 1% in u_i from the mean value in the VDSW regime which grows as u_+ decreases. Presumably, this deviation is due to higher order corrections in the Riemann invariant expansion (5.156). As this correction is small, it is not considered here.

6.2 Comparative Figures

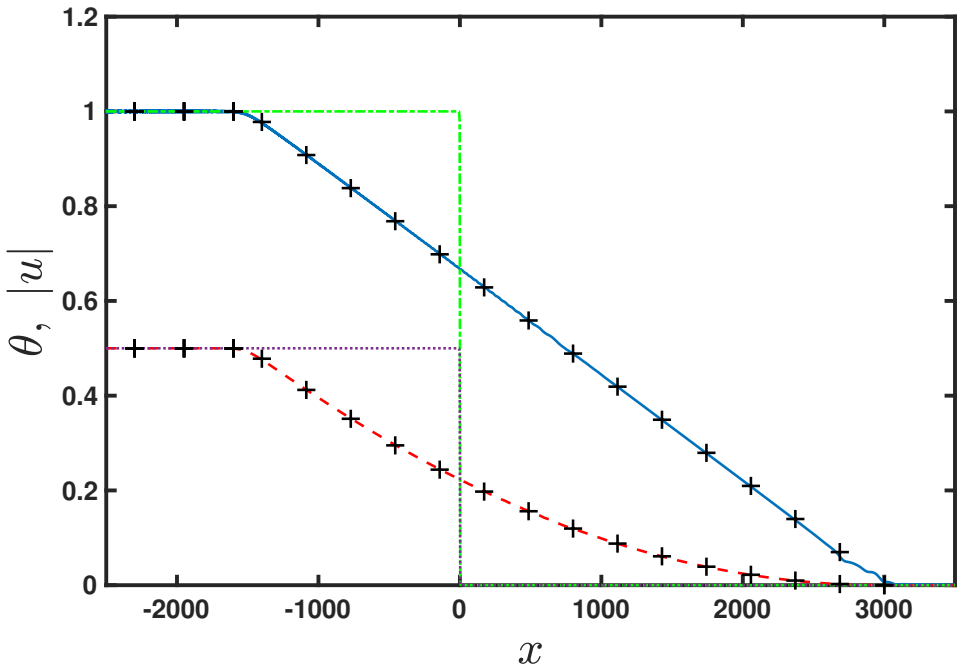

Figure 6.1: Numerical solutions of the nematic equations (2.19) and (2.20) for the initial conditions (2.29) and (2.31). Blue (solid) line: $|u|$ at $z = 1500$; red (dashed) line θ at $z = 1500$; green (dash-dot) line: $|u|$ at $z = 0$ and violet (dotted) line θ at $z = 0$; black (pluses): theoretical solution (5.22) at $z = 1500$. Here, $u_- = 1.0$, $u_+ = 0.0$, $\nu = 200$ and $q = 2$. (Online version in colour.)

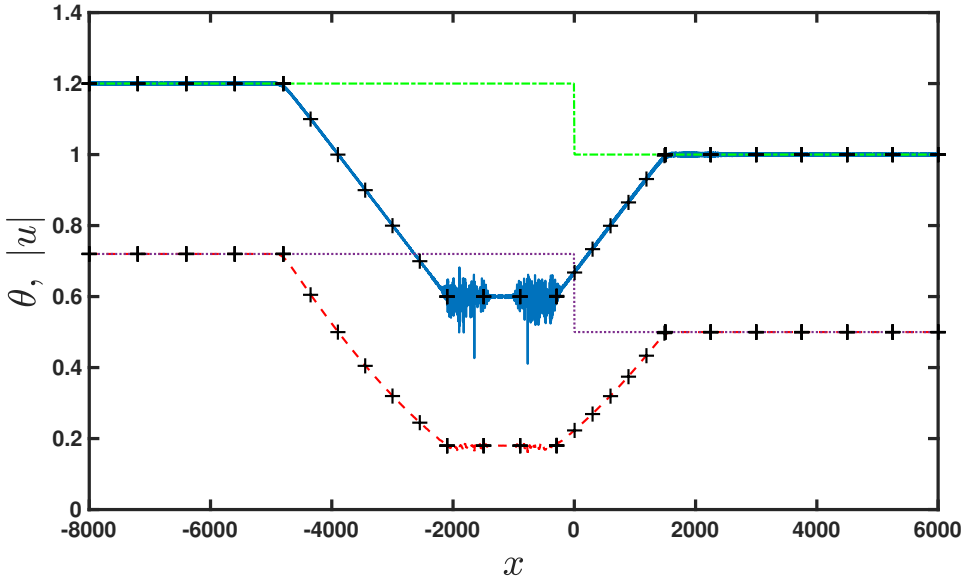

Figure 6.2: Numerical solutions of the nematic equations (2.19) and (2.20) for the initial conditions (2.29) and (2.31). Blue (solid) line: $|u|$ at $z = 1500$; red (dashed) line θ at $z = 1500$; green (dash-dot) line: $|u|$ at $z = 0$ and violet (dotted) line θ at $z = 0$; black (pluses): theoretical solution (5.45) at $z = 1500$. Here, $u_- = 1.2$, $u_+ = 1.0$, $v_- = -2$ and $v_+ = 0$. (Online version in colour.)

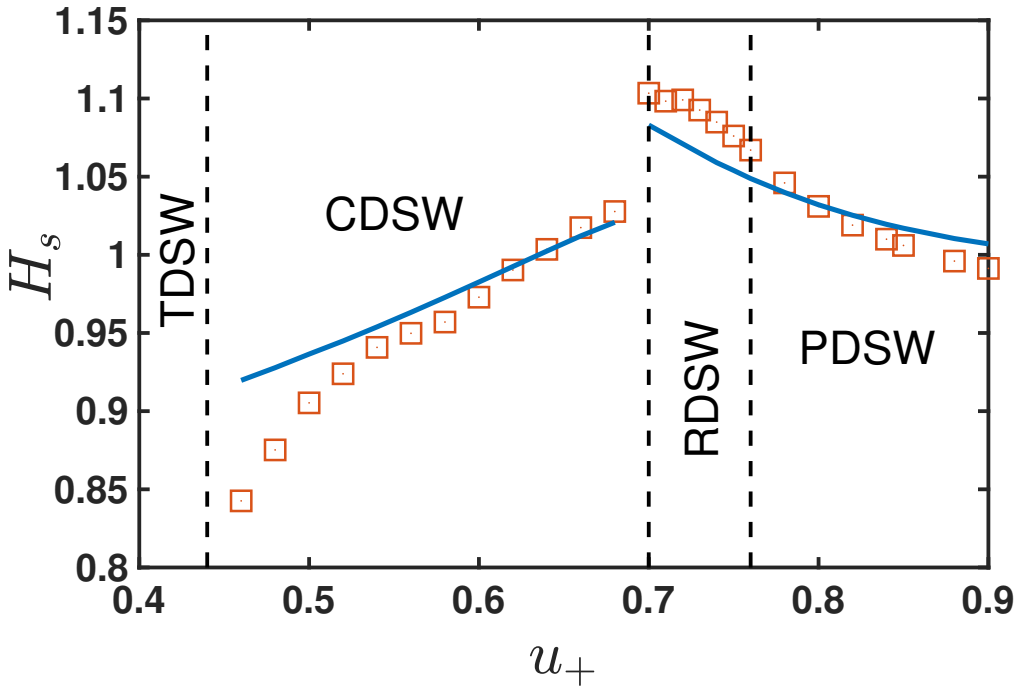

Figure 6.3: Comparisons between numerical solutions of the nematic equations (2.19) and (2.20) and the DSW solution of the lead solitary wave height H_s for the PDSW, RDSW and CDSW regimes. Numerical solution: orange boxes; analytical solution: blue (solid) line. Here, $u_- = 1.0$, $\nu = 200$ and $q = 2$. (Online version in colour.)

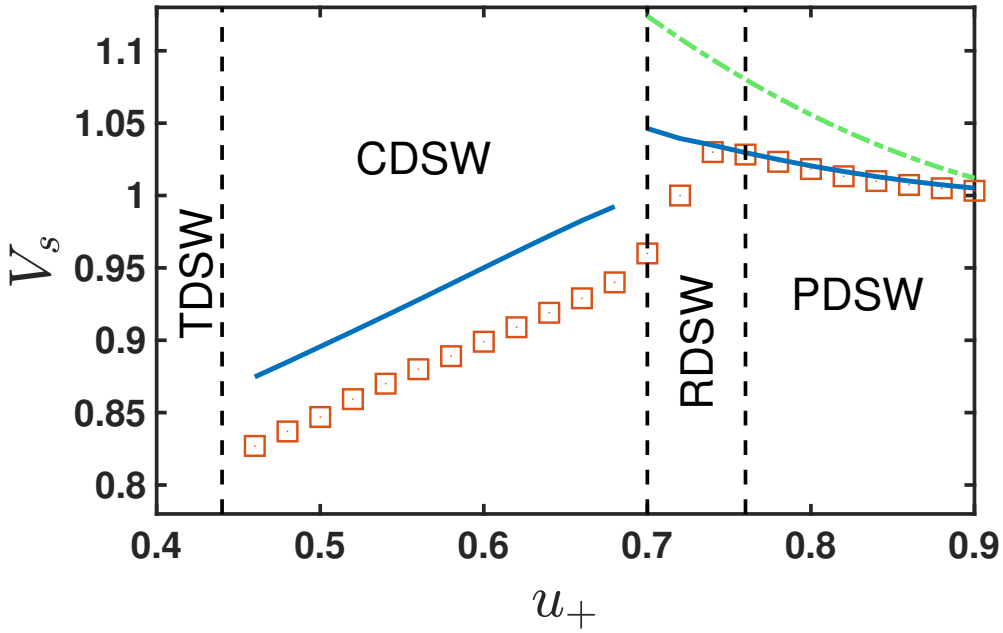

Figure 6.4: Comparisons between numerical solutions of the nematic equations and the DSW solution of the lead solitary wave velocity V_s for Regimes 1, 2 and 3. Numerical solution: orange boxes; analytical solution: blue (solid) line; DSW fitting method solutions: green (dash-dot) line. Here, $u_- = 1.0$, $\nu = 200$ and $q = 2$. (Online version in colour.)

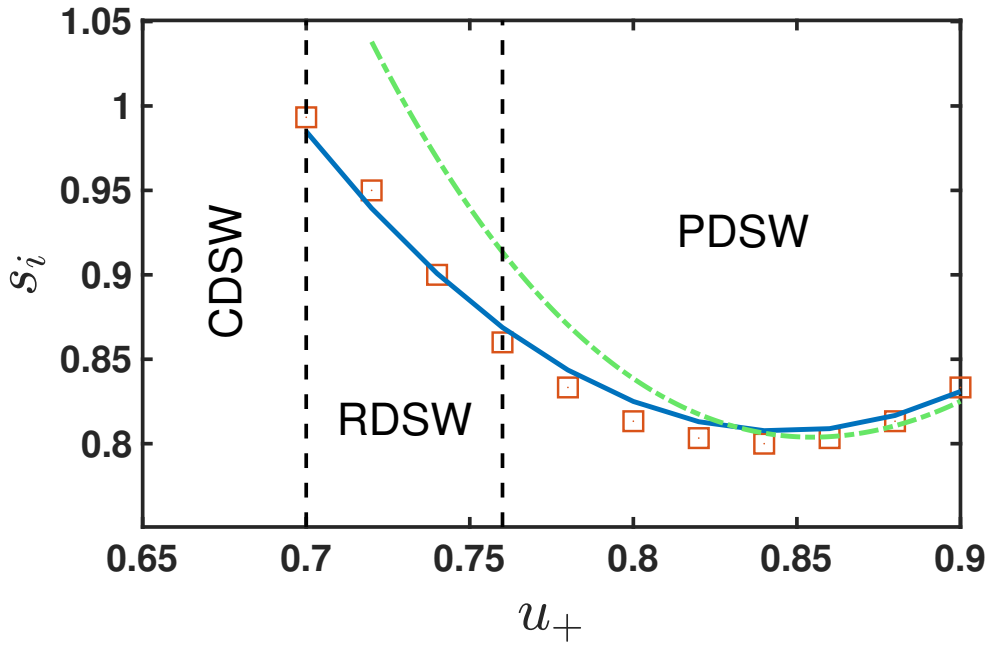

Figure 6.5: Comparisons between numerical solutions of the nematic equations and the DSW solution of the trailing edge velocity s_i for Regimes 1, 2 and 3. Numerical solution: orange boxes; analytical solution: blue (solid) line; DSW fitting method solutions: green (dash-dot) line. Here, $u_- = 1.0$, $\nu = 200$ and $q = 2$. (Online version in colour.)

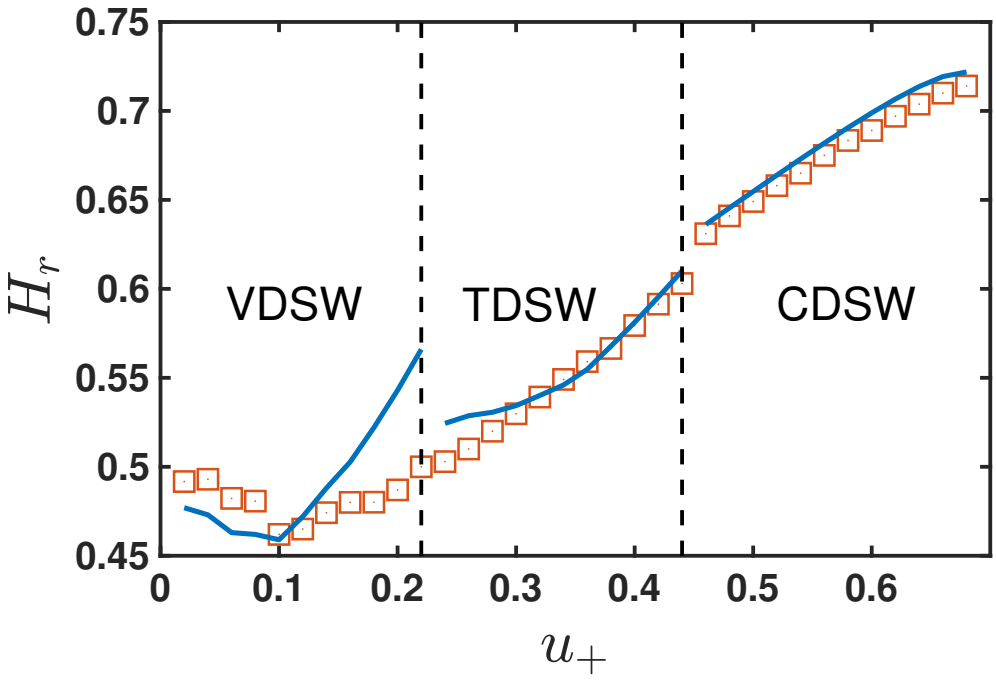

Figure 6.6: Comparisons between numerical solutions of the nematic equations (2.19) and (2.20) and the solution of the resonant wavetrain height H_r for the CDSW, TDSW and VDSW regimes. Numerical solution: orange boxes; analytical solution: blue (solid) line. Here, $u_- = 1.0$, $\nu = 200$ and $q = 2$. (Online version in colour.)

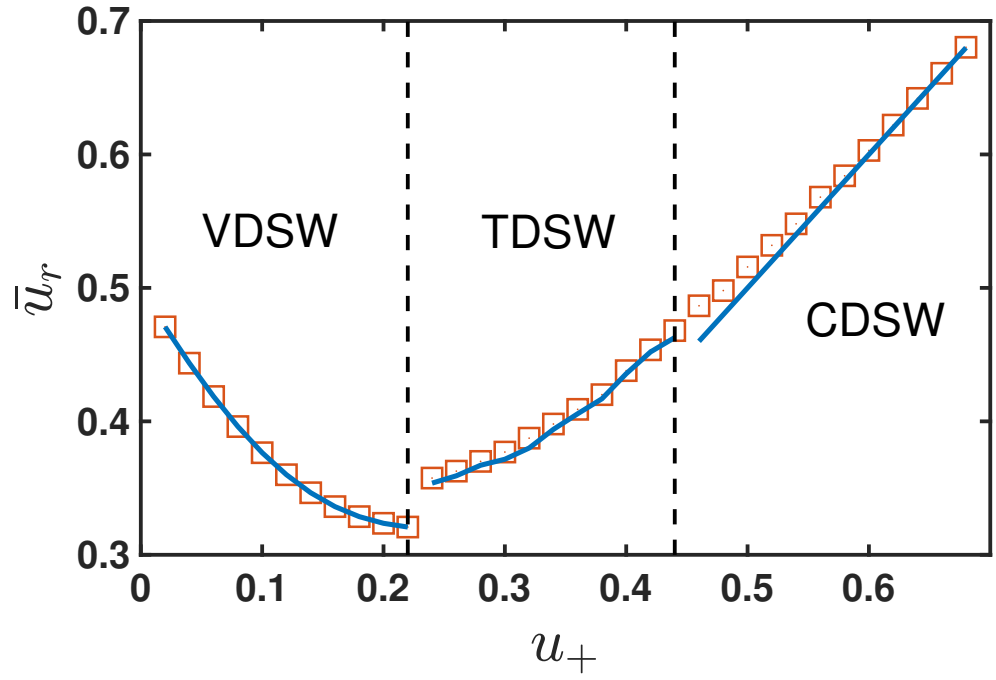

Figure 6.7: Comparisons between numerical solutions of the nematic equations (2.19) and (2.20) and the solution of the resonant wavetrain background $\bar{u}_r$ for the CDSW, TDSW and VDSW regimes. Numerical solution: orange boxes; analytical solution: blue (solid) line. Here, $u_- = 1.0$, $\nu = 200$ and $q = 2$. (Online version in colour.)

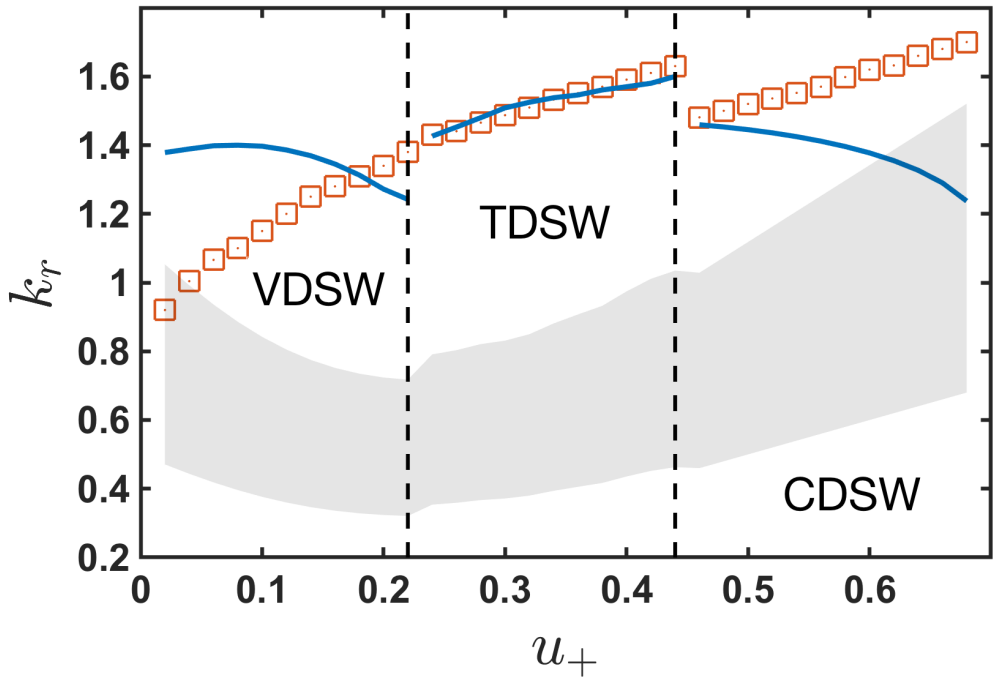

Figure 6.8: Comparisons between numerical solutions of the nematic equations (2.19) and (2.20) and the solution of the resonant wavetrain wavenumber k_r for the CDSW, TDSW and VDSW regimes. Numerical solution: orange boxes; analytical solution: blue (solid) line. The gray (shaded) region is the region (4.100) of the stability for the resonance. Here, $u_- = 1.0$, $\nu = 200$ and $q = 2$. (Online version in colour.)

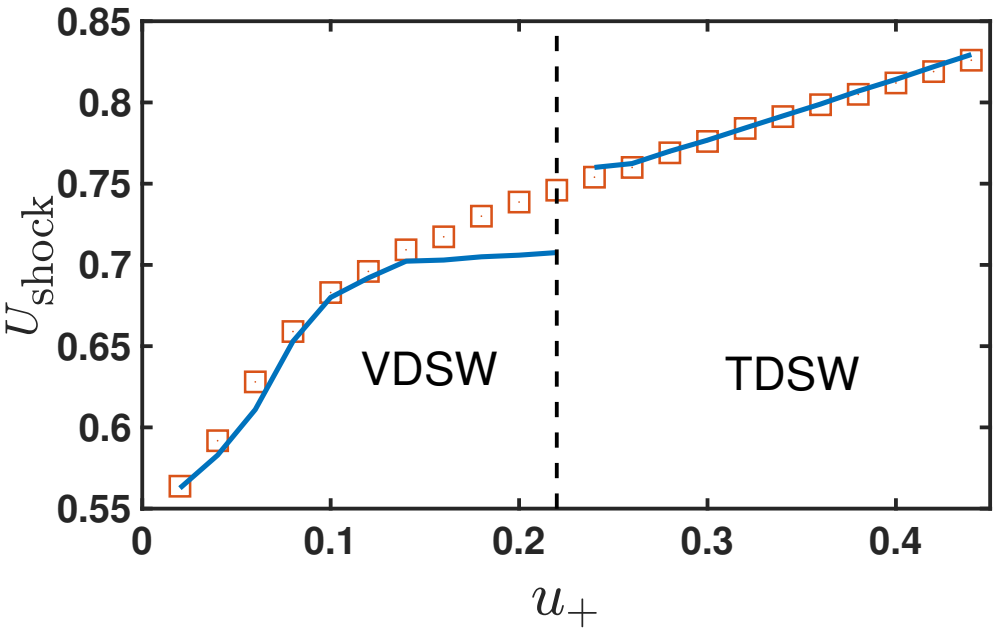

Figure 6.9: Shock velocity U_{shock} in the TDSW and VDSW regime as given by numerical solutions of the nematic equations (2.19) and (2.20) and the TDSW and VDSW regime solutions. Numerical solution: orange boxes; analytical solution: blue (solid) line. Here, $u_- = 1.0$, $\nu = 200$ and $q = 2$. (Online version in colour.)

Chapter 7

Conclusions and Future Work

7.1 Summary of Research

Dispersive shock wave (DSW) solutions of the nematic equations (2.19) and (2.20) have been found in the high non-locality limit $\nu \gg 1$, which is the experimentally relevant limit [5, 74]. It has been found that there are five distinct dispersive hydrodynamic regimes and one non-dispersive hydrodynamic regime, see Figures 3.2 to 3.7. In contrast to previous work [60, 61], the solutions in these six regimes were found based on different asymptotic and approximate techniques appropriate for each regime. The work of [60] assumed that the DSW was of KdV type in all regimes, except the dam break case, while that of [61] assumed that the DSW solution was determined by a gas dynamics type shock, except in the dam break case. The present work shows that the nematic DSW is more complicated than this, with the PDSW and RDSW regimes consisting of (perturbed) KdV-type DSWs and the TDSW and VDSW regimes being determined by Whitham shocks in the appropriate Whitham modulation equations. The CDSW regime is a transition between these two broad types. One novel feature of the present work is the use of Whitham shocks for Whitham modulation equations, as pioneered by [81], validating ideas of Whitham [1, 82] when he first developed modulation theory. The nematic DSW shows a wider range of behaviours and solution types than the equivalent resonant Kawahara DSW [79, 80]. The DSW solutions for all six regimes show excellent agreement with numerical solutions for the DSW itself (when it exists), the resonant wavetrain (when it exists) and the intermediate level linking the backwards propagating expansion wave with the DSW or Whitham shock. The only exception is for the wavenumber of the resonant wavetrain when this wavetrain is unstable, as would be expected.

As stated, the present work obtained solutions for the nematic DSW in the highly non-local limit $\nu \gg 1$. As can be seen from Figures , 5.4 and 5.5 the form of the DSW is highly dependent on the value of ν. Indeed, the nematic equations (2.19) and (2.20) reduce to the defocusing NLS equation for $\nu = 0$ and a perturbed defocusing NLS equation for ν small, for which there is no resonance. It is then of interest to study the transition from the highly non-local case to the local case with ν small. In this regard, the DSW changes from resonant to non-resonant, as indicated by the change of sign of the third derivative of the small deviation KdV reduction (5.70) of the nematic equations.

Most of the solutions for the DSW types derived here have been based to a greater or lesser degree on Whitham modulation equations for the periodic wave solution of the nematic equations. Unfortunately, this periodic wave solution is not known in general

and a weakly non-linear Stokes' wave approximation was used. While this generally gave satisfactory results, the Whitham modulation equations based on it gave incorrect modulational stability when the wave amplitude was not small. Whether these weakly non-linear modulation equations can be improved on is not clear.

The nematic system (2.19) and (2.20) is general and applies to other non-linear, non-local optical media. In particular, for optical thermal media $q = 0$ in the director equation (2.20), in which case θ is the temperature of the medium. In this limit, $|u|$ constant ceases to be a valid solution of the system, so that the step initial condition (2.29) does not result in an expansion wave and DSW being generated between constant initial levels u_- and u_+. The form of a DSW for $q = 0$ is an open question.

In summary, while the form of the DSW in the highly non-local limit has been largely resolved, there are still many open questions in regard to DSW solutions of the nematic system for general non-locality and other parameter values.

7.2 Ongoing and Future Research

One research project that is going on at the present time is the study of the transitions from non-local to local DSW regimes in a defocusing nematic liquid crystal as the non-locality ν decreases, noting that for $\nu = 0$ the nematic equations reduce to the defocusing NLS equation [186]. The objectives of this research are the following. One objective is to determine theoretically the borderlines between KdV-type nematic DSWs and NLS-type nematic DSWs in terms of the non-locality parameter ν and make comparisons with numerical borderlines. As the non-locality effect decreases, a new regime that we term a "resonant NLS DSW" appears. This is due to change in sign of the third derivative in the nematic Kawahara equation (5.70). This DSW is similar to the nematic TDSW regime, but without the Whitham shock structure (Figure 5.8) and the resonant radiation is fully stable and of short width relative to the partial DSW ahead bringing the solution down to the level ahead u_+. The next objective is to understand the structure of this new regime and this can be achieved by using Whitham's modulation theory on the nematic equations in the local limit. In the local limit, moreover, the partial DSW becomes fully stable, unlike the DSW shown in Figure 5.11(a) and more like the DSW shown in Figure 5.11(b). In this case, the coefficient of the fifth derivative in the nematic Kawahara equation (5.70) can be neglected because it becomes small as ν is not large. As a result, we have a standard KdV equation governing the resonant DSW in the small jump limit. Since the KdV equation is integrable, its Whitham modulation equations can be set in Riemann invariant form and the partial DSW problem can be found. This is another objective. This project is in collaboration with Côme Houdeville, Timothy R. Marchant and Noel F. Smyth. Another research project, which is more detailed, is the investigation of all possible regimes that could arise in the defocusing regime of a nematic liquid crystal when the initial jumps and the initial non-zero phases change simultaneously with the non-locality ν. This leads to a large number of new hydrodynamic regimes. We also plan to extend our study to two dimensional resonant nematic DSWs. These research projects are in collaboration with Noel. F. Smyth.

Appendix A

Published and In Preparation Papers

- Saleh Baqer and Noel F. Smyth. Modulation theory and resonant regimes for dispersive shock waves in nematic liquid crystals. *Physica D: Nonlinear Phenomena*, **403**, 132334 (2020). (doi:10.1016/j.physd.2020.132334)
- Saleh Baqer, Côme Houdeville, Noel F. Smyth and Timothy R. Marchant. *Nematic dispersive shock waves from nonlocal to local.* In preparation (2020).

Bibliography

[1] G. B. Whitham. *Linear and nonlinear waves.* J. Wiley and Sons, New York (1974).

[2] F. Reinitzer. Beitrge zur Kenntniss des Cholesterins. *Monatshefte Fr Chemie Und Verwandte Teile Anderer Wissenschaften*, **9**, 421–441 (1888).

[3] O. Lehmann. Über fliessende Krystalle. *Zeitschrift fr Physikalische Chemie*, **4U**, 462–472 (1889).

[4] I. C. Khoo. *Liquid Crystals: Physical Properties and Nonlinear Optical Phenomena.* J. Wiley and Sons, New York (1995).

[5] G. Assanto. *Nematicons: Spatial optical solitons in nematic liquid crystals.* J. Wiley and Sons, New York (2012).

[6] M. Peccianti and G. Assanto. *Nematicons. Physics Reports*, **516**, 147–208 (2012).

[7] G. Assanto, M. Peccianti and C. Conti. Nematicons: Optical Spatial Solitons in Nematic Liquid Crystals. *Optics and Photonics News*, **14**, 44–48 (2003).

[8] C. Conti, M. Peccianti and G. Assanto. Route to nonlocality and observation of accessible solitons. *Physical Review Letters*, **91**, 073901 (2003).

[9] G. New. *Introduction to nonlinear optics.* Cambridge University Press, England, (2011).

[10] C. Bennett. *Principles of physical optics.* J. Wiley and Sons, New York (2008).

[11] F. A. Sala, U. F. Laudyn, M. Karpierz, N. F. Smyth, A. Minzoni and G. Assanto. *Bending reorientational solitons with modulated alignment. Journal of the Optical Society of America B: Optical Physics*, **34**, 2459–2466 (2017).

[12] J. Russell. Report on waves. *Fourteenth meeting of the British Association for the Advancement of Science*, **311**, (1844).

[13] G. Airy. Tides and waves. *Encycl. Metropolitana*, **5**, 291–396 (1842).

[14] J. Boussinesq. Essai sur la théorie des eaux courantes. *Mémoires présentés par divers savants à l'Acad. des Sci. Inst. Nat. France*, **XXIII**, 1–680 (1877).

[15] L. Rayleigh. On Waves. *Phil. Mag*, **1**, 257–271 (1876).

[16] J. Miles. The Korteweg-de Vries equation: a historical essay. *Journal of Fluid Mechanics*, **106**, 131–147 (1981).

[17] D. Korteweg and G. de Vries. On the change of form of long waves advancing in a rectangular canal, and on a new type of long stationary waves. *Phil. Mag.*, **39**, 422–443 (1895).

[18] G. A. El and M. A. Hoefer. Dispersive shock waves and modulation theory. *Physica D: Nonlinear Phenomena*, **333**, 11–65 (2016).

[19] A. Kamchatnov. *Nonlinear Periodic Waves and their Modulations: An Introductory Course*. World Scientific (2000).

[20] M. A. Hoefer, M. Ablowitz, I. Coddington, E. Cornell, P. Engels and V. Schweikhard. On Dispersive and Classical Shock Waves in Bose-Einstein Condensates and Gas Dynamics. *Phys. Rev. A*, **74**, 023623 (2006).

[21] M. Abramowitz and I. Stegun. *Handbook of mathematical functions: with formulas, graphs and mathematical tables*. Dover Publications, New York (1973).

[22] N. Zabusky and M. Kruskal. Interaction of "Solitons" in a Collisionless Plasma and the Recurrence of Initial States. *Physical Review Letters*, **15**, 240–243 (1965).

[23] K. Huang. *Statistical mechanics*. J. Wiely and Sons, New York (1987).

[24] E. Fermi, S. Ulam and J. Pasta. *Studies of nonlinear problems: Part I*. Los Alamos Scientific Laboratory, U.S. Atomic Energy Commission (1955).

[25] M. Ablowitz. *Nonlinear Dispersive Waves: Asymptotic Analysis and Solitons*. Cambridge University Press, England (2011).

[26] M. Ablowitz and H. Segur. *Solitons and the inverse scattering transform* . SIAM studies in applied mathematics, Philadelphia (1985).

[27] A. Newell. *Solitons in mathematics and physics*. SIAM, Philadelphia (1985).

[28] C. Gardner, J. Greene, M. Kruskal and R. Miura. Method for Solving the Korteweg-deVries Equation. *Physical Review Letters*, **19**, 1095–1097 (1967).

[29] C. Gardner, J. Greene, M. Kruskal and R. Miura. Korteweg-de Vries equation and generalizations. VI. methods for exact solution. *Communications on Pure and Applied Mathematics*, **27**, 97–133 (1974).

[30] B. Skuse and N. F. Smyth (2008). Two-color vector-soliton interactions in nematic liquid crystals in the local response regime. *Physical Review A*, **77**, 013817 (2008).

[31] B. Skuse and N. F. Smyth. Two-colour nematicon interactions in local crystals. *IEEE/LEOS Winter Topical Meeting Series*, 125–126, (2008).

[32] B. Skuse and N. F. Smyth. Interaction of two-color solitary waves in a liquid crystal in the nonlocal regime. *Physical Review A*, **79**, 063806 (2009).

[33] N. F. Smyth and B. Tope. Beam on beam control: beyond the particle approximation. *Journal of Nonlinear Optical Physics and Materials*, **25**, 1650046 (2016).

[34] P. Kevrekidis, D. Frantzeskakis and R. Carretero-Gonzlez. *The defocusing nonlinear Schrdinger equation: From dark solitons to vortices and vortex rings*. SIAM, Philadelphia (2015).

[35] W. Kath and N. F. Smyth. Soliton evolution and radiation loss for the nonlinear Schrdinger equation. *Phys. Rev. E*, **51**, 1484–1492 (1995).

[36] V. Zakharov and A. Shabat. Exact theory of two-dimensional self-focusing and one-dimensional self-modulation of waves in nonlinear media. *Journal of Experimental and Theoretical Physics*, **34**, 62-69 (1972).

[37] G. Lamb. *Elements of soliton theory.* J. Wiely and Sons, New York (1980).

[38] A. Fokas and M. Ablowitz. The inverse scattering transform for the Benjamin-Ono equation–A pivot to multidimensional problems. *Stud. Appl. Math*, **68**, (1983).

[39] R. M. Miura, C. S. Gardner and R. M. Kruskal. Korteweg-de Vries Equation and Generalizations. II. Existence of Conservation Laws and Constants of Motion. *Journal of Mathematical Physics*, **9**, 1204–1209 (1968).

[40] T. Shingareva and C. Lizárraga-Celaya. *Solving Nonlinear Partial Differential Equations with Maple and Mathematica.* Springer (2011).

[41] Y. Kivshar and G. Agrawal. *Optical solitons from fibers to photonic crystals.* Academic Press, San Diego (2003).

[42] A. Hasegawa. *Optical solitons in fibers.* Springer, Geramny (1989).

[43] J. Moloney and A. Newell. *Nonlinear optics*, Springer (2004).

[44] Wen-Rong Sun, Bo Tian, Ya Sun, Jun Chai and Yan Jiang. Akhmediev breathers, Kuznetsov-Ma solitons and rogue waves in a dispersion varying optical fiber. *Laser Physics,* **26**, (2016).

[45] T. Benjamin and K. Hasselmann. Instability of Periodic Wavetrains in Nonlinear Dispersive Systems. *Proc. Roy. Soc. London A*, **299**, 59–76 (1967).

[46] T. Benjamin and J. Feir. The disintegration of wave trains on deep water Part I. Theory. *Journal of Fluid Mechanics*, **27**, 417–430 (1967).

[47] G. B. Whitham. Non-linear dispersion of water waves. *Journal of Fluid Mechanics*, **27**, 399–412 (1967).

[48] E. Infeld and G. Rowlands. *Nonlinear waves, solitons and chaos.* Cambridge University Press, England (2000).

[49] H. Bailung, S. Sharma and Y. Nakamura. Observation of Peregrine solitons in a multicomponent plasma with negative ions. *Physical Review Letters*, **107**, 255005 (2011).

[50] E. Gross. Structure of a quantized vortex in boson systems. *Nuovo Cimento*, 454–477 (1961).

[51] L. Pitaevskii. Vortex lines in an imperfect Bose gas. *Sov. Phys. JETP*, **13**, 451–454 (1961).

[52] L. Pitaevski and S. Stringari. *Bose-Einstein condensation.* Oxford University press, England (2003).

[53] P. Emplit, J. P. Hamaide, F. Reynaud, C.Froehly and A. Barthelemy. Picosecond steps and dark pulses through nonlinear single mode fibers. *Optics Communications*, **62**, 374–379 (1987).

[54] A. Chabchoub, O. Kimmoun, H. Branger, N. Hoffmann, D. Proment, M. Onorato and N. Akhmediev. Experimental observation of dark solitons on the surface of water. *Physical Review Letters*, **110**, 124101 (2013).

[55] K. B. Dysthe and K. Trulsen. Note on Breather Type Solutions of the NLS as Models for Freak-Waves. *Physica Scripta*, **1999**, 48–52 (1999).

[56] G. Hwang, T. R. Akylas and J. Yang. Gap solitons and their linear stability in one-dimensional periodic media. *Physica D: Nonlinear Phenomena*, **240**, 1055–1068 (2011).

[57] V. Lashkin. Two-dimensional nonlocal vortices, multipole solitons, and rotating multisolitons in dipolar Bose-Einstein condensates. *Phys. Rev. A*, **75**, 043607 (2007).

[58] A. Piccardi, A. Alberucci, N. Tabiryan and G. Assanto. Dark nematicons. *Optics Letters*, **36**, 1356–1358 (2011).

[59] T. R. Marchant and N. F. Smyth. Approximate techniques for dispersive shock waves in nonlinear media. *Journal of Nonlinear Optical Physics and Materials*, **21**, 1250035 (2012).

[60] N. F. Smyth. Dispersive shock waves in nematic liquid crystals. *Physica D: Nonlinear Phenomena*, **333**, 301–309 (2016).

[61] G. A. El and N. F. Smyth. Radiating dispersive shock waves in non-local optical media. *Proc. Roy. Soc. London A*, **472**, 20150633 (2016).

[62] G. A. El, V. V. Geogjaev, A. V. Gurevich and A. L. Krylov. Decay of an initial discontinuity in the defocusing NLS hydrodynamics. *Physica D: Nonlinear Phenomena*, **87**, 186–192 (1995).

[63] A. Moro and S. Trillo. Mechanism of wave breaking from a vacuum point in the defocusing nonlinear Schrdinger equation. *Phys. Rev. E*, **89**, 023202 (2014).

[64] E. A. Kuznetsov, A. M. Rubenchik and V. E. Zakharov. Soliton stability in plasmas and hydrodynamics. *Physics Reports*, **142**, 103–165 (1986).

[65] N. Ghofraniha, C. Conti, G. Ruocco and S. Trillo. Shocks in nonlocal media. *Physical Review Letters*, **99**, 043903 (2007).

[66] F. W. Dabby and J. R. Whinnery. Thermal self-focusing of lasers beams in lead glasses. *Applied Physics Letters*, **13**, 284–286 (1968).

[67] C. Rotschild, M. Segev, Z. Xu, Y. Kartashov, L. Torner and O. Cohen. Two-dimensional multipole solitons in nonlocal nonlinear media. *Optics Letters*, **31**, 3312–3314 (2006).

[68] C. Rotschild, B. Alfassi, O. Cohen and M. Segev. Long-range interactions between optical solitons. *Nature Physics*, **2**, 769–774 (2006).

[69] M. Segev, B. Crosignani, A. Yariv and B. Fischer. Spatial solitons in photorefractive media. *Physical Review Letters*, **68**, 923–926 (1992).

[70] A. Cheskidov, D. Holm, E. Olson and E. Titi. On a Leray-α model of turbulence. *Proceedings of the Royal Society A: Mathematical, Physical and Engineering Sciences,* **461**, 629–649 (2005).

[71] R. Penrose. On Gravity's role in Quantum State Reduction. *General Relativity and Gravitation*, **28**, 581–600 (1996).

[72] R. Penrose and P. Marcer. Quantum Computation, Entanglement and State Reduction [and Discussion]. *Philosophical Transactions: Mathematical, Physical and Engineering Sciences*, **356**, 1927–1939 (1998).

[73] R. Penrose. On the Gravitization of Quantum Mechanics 1: Quantum State Reduction. *Foundations of Physics*, **44**, 557–575 (2014).

[74] G. Assanto. Nematicons: reorientational solitons from optics to photonics. *Liquid Crystals Reviews*, **6**, 170–194 (2018).

[75] M. Peccianti, A. De Rossi, G. Assanto, A. De Luca, C. Umeton and C. I. Khoo. Electrically assisted self-confinement and waveguiding in planar nematic liquid crystal cells. *Applied Physics Letters*, **77**, 7–9 (2000).

[76] J. MacNeil. *Solitary Waves in Focussing and Defocussing Nonlinear, Nonlocal Optical Media*. PhD Thesis, University of Edinburgh (2016).

[77] H. Liepmann and A. Roshko. *Elements of gasdynamics*. Dover Publications (2001).

[78] T. Kawahara. Oscillatory Solitary Waves in Dispersive Media. *Journal of the Physical Society of Japan*, **33**, 260–264 (1972).

[79] P. Sprenger and M. A. Hoefer. Shock Waves in Dispersive Hydrodynamics with Nonconvex Dispersion. *SIAM Journal on Applied Mathematics*, **77**, 26–50 (2017).

[80] M. A. Hoefer, N. F. Smyth and P. Sprenger. Modulation theory solution for nonlinearly resonant, fifthorder Kortewegde Vries, nonclassical, traveling dispersive shock waves. *Studies in Applied Mathematics*, **142**, 219–240 (2019).

[81] P. Sprenger and M. A. Hoefer. Discontinuous shock solutions of the Whitham modulation equations as dispersionless limits of traveling waves. *Nonlinearity,* **33**, 3268–3302 (2020).

[82] G. B. Whitham. A general approach to linear and non-linear dispersive waves using a Lagrangian. *J. Fluid Mech.,* **22**, 273–283 (1965).

[83] G. B. Whitham. Non-linear dispersive waves. *Proc. Roy. Soc. London A,* **283**, 238–261 (1965).

[84] G. B. Whitham. Variational methods and applications to water waves. *Proc. Roy. Soc. London A,* **299**, 6–25 (1967).

[85] S. Gavrilyuk, B. Nkonga, K. Shyue and L. Truskinovsky. Generalized Riemann Problem for Dispersive Equations. hal-01958328 (2018).

[86] B. Fornberg and G. B. Whitham. A Numerical and Theoretical Study of Certain Nonlinear Wave Phenomena. *Proc. Roy. Soc. London A,* **289**, 373–404 (1978).

[87] T. Chan and T. Kerkhoven. Fourier Methods with Extended Stability Intervals for the Kortewegde Vries Equation. *SIAM Journal on Numerical Analysis*, **22**, 441–454 (1985).

[88] P. Milewski and E. Tabak. A PseudoSpectral Procedure for the Solution of Nonlinear Wave Equations with Examples from Free-Surface Flows. *SIAM Journal on Scientific Computing*, **21**, 1102–1114 (1999).

[89] L. Trefethen. *Spectral methods in MATLAB*. SIAM, Philadelphia (2000).

[90] J. W. Cooley and J. W. Tukey. An algorithm for the machine calculation of complex Fourier series. *Mathematics of Computation*, **19**, 297–301 (1965).

[91] W. Press, B. Flannery, S. Teukolsky and W. Vetterling. *Numerical recipes in FORTRAN : The art of scientific computing*. Cambridge University Press, England (1992).

[92] N. F. Smyth and Gaetano Assanto. Self-confined light waves in nematic liquid crystals. *Physica D: Nonlinear Phenomena*, **402**, 132182 (2019).

[93] R. Burden and J. Faires. *Numerical analysis*. Brooks Cole (1997).

[94] M. Lighthill and G. B. Whitham. On Kinematic Waves. II. A Theory of Traffic Flow on Long Crowded Roads. *Proc. Roy. Soc. London A,* **229**, 317–345 (1955).

[95] M. Flynn, A. Kasimov, J. Nave, R. Rosales and B. Seibold. Self-sustained nonlinear waves in traffic flow. *Phys. Rev. E*, **79**, 056113 (2009).

[96] B. Seibold, M. Flynn, A. Kasimov and R. Rosales. Constructing set-valued fundamental diagrams from jamiton solutions in second order traffic models. *Networks and Heterogeneous Media*, **8**, 745–772 (2013).

[97] M. Flynn, A. Kasimov, J. Nave, R. Rosales and B. Seibold. Self-sustained nonlinear waves in traffic flow. *Phys. Rev. E*, **79**, 056113 (2009).

[98] J. Luke. Mathematical Models for Landform Evolution. *Journal of Geophysical Research*, **77**, 2460–2464 (1972).

[99] R. Haberman. *Elementary applied partial differential equations with Fourier series and boundary value problems*. Prentice Hall, New Jersey (1998).

[100] H. Liepmann and G. Laguna. Nonlinear Interactions in the Fluid Mechanics of Helium II. *Annual Review of Fluid Mechanics*, **16**, 139–177 (1984).

[101] G. Assanto, A. Minzoni, M. Peccianti and N. F. Smyth. Optical solitary waves escaping a wide trapping potential in nematic liquid crystals: Modulation theory. *Phys. Rev. A*, **79**, 033837 (2009).

[102] U. Laudyn, M. Kwaśny, F. Sala, M. Karpierz, N. F. Smyth and G. Assanto. Curved optical solitons subject to transverse acceleration in reorientational soft matter. *Sci. Rep.*, **7** 12385 (2017).

[103] F. A. Sala, N. F. Smyth, U. A. Laudyn, M. A. Karpierz, A. A. Minzoni and G. Assanto. Bending reorientational solitons with modulated alignment. *Journal of the Optical Society of America A*, **34**, 2459–2466 (2017).

[104] U. Laudyn, M. Kwany, M. Karpierz, N. F. Smyth and G. Assanto. Accelerated optical solitons in reorientational media with transverse invariance and longitudinally modulated birefringence. *Phys. Rev. A*, **98**, 023810 (2018).

[105] A. Gurevich and L. Pitaevskii. Nonstationary structure of a collisionless shock wave. *Sov. Phys. JETP*, **33**, 291–297 (1974).

[106] G. Sod. A survey of several finite difference methods for systems of nonlinear hyperbolic conservation laws. *Journal of Computational Physics*, **27**, 1–31 (1978).

[107] G. A. El, L. Nguyen and N. F. Smyth. Dispersive shock waves in systems with nonlocal dispersion of BenjaminOno type. *Nonlinearity*, **31**, 1392–1416 (2018).

[108] R. Bikbaev. Finite-gap attractors and transition processes of the shock-wave type in integrable systems. *Journal of Mathematical Sciences*, **77**, 3033–3041 (1995).

[109] W. Ziniu, X. Yizhe, W. Wenbin and H. Ruifeng. Review of shock wave detection method in CFD post-processing. *Chinese Journal of Aeronautics*, **26**, 501–513 (2013).

[110] NASA Captures First Air-to-Air Images of Supersonic Shockwave Interaction in Flight. (2019, March 5). Retrieved October 2, 2015, from https://www.nasa.gov/centers/armstrong/features/supersonic-shockwave-interaction.html

[111] C. Barsi, W. Wan, C. Sun and J. Fleischer. Dispersive shock waves with nonlocal nonlinearity. *Optics Letters*, **32**, 2930–2932 (2007).

[112] W. Wan, S. Jia and J. Fleischer. Dispersive superfluid-like shock waves in nonlinear optics. *Nature Physics*, **3**, 46–51 (2006).

[113] G. A. El, A. Gammal, E. Khamis, R. Kraenkel and A. Kamchatnov. Theory of optical dispersive shock waves in photorefractive media. *Phys. Rev. A*, **76**, 053813 (2007).

[114] W. Wan, D. Dylov, C. Barsi and J. Fleischer. Diffraction from an edge in a self-focusing medium. *Optics Letters*, **35**, 2819–2821 (2010).

[115] G. Xu, A. Mussot, A. Kudlinski, S. Trillo, F. Copie and M. Conforti. Shock wave generation triggered by a weak background in optical fibers. *Optics Letters*, **41**, 2656–2659 (2016).

[116] J. Fatome, C. Finot, G. Millot, A. Armaroli and S. Trillo. Observation of Optical Undular Bores in Multiple Four-Wave Mixing. *Physical Review X*, **4**, 021022 (2014).

[117] N. Ghofraniha, C. Conti, G. Ruocco and S. Trillo. Shocks in nonlocal media. *Physical Review Letters*, **99**, 043903 (2007).

[118] J. Wang, D. Lu, Q. Guo, W. Hu and J. Li. Observation of surface dispersive shock waves in a self-defocusing medium. *Phys. Rev. A*, **91**, 063819 (2015).

[119] G. A. El, A. Kamchatnov, V. Khodorovskii, E. Annibale and A. Gammal. Two-dimensional supersonic nonlinear Schrodinger flow past an extended obstacle. *Phys. Rev. E*, **80**, 046317 (2009).

[120] D. Durran. *Numerical methods for fluid dynamics with applications to geophysics*. Springer, New York (2010).

[121] P. Niyogi, S. K. Chakrabartty and M. K. Laha. *Introduction to Computational Fluid Dynamics*. Pearson Education Canada (2009).

[122] A. LoggKent, Kent-Andre Mardal and Garth Wells. *Automated Solution of Differential Equations by the Finite Element Method*. Springer (2012).

[123] P. Baines. *Topographic effects in stratified flows*. Cambridge University Press, England (1998).

[124] R. Johnson. A non-linear equation incorporating damping and dispersion. *Journal of Fluid Mechanics*, **42**, 49–60 (1970).

[125] T. R. Marchant and N. F. Smyth (2006). An undular bore solution for the higher-order Kortewegde Vries equation. *Journal of Physics A: Mathematical and General*, **39**, 563–569 (2006).

[126] J. Yang. Dynamics of Embedded Solitons in the Extended Kortewegde Vries Equations. *Studies in Applied Mathematics*, **39**, 337–365 (2001).

[127] H. Flaschka, M. Forest and D. McLaughlin. Multiphase averaging and the inverse spectral solution of the Kortewegde Vries equation. *Communications on Pure and Applied Mathematics*, **33**, 739–784 (1980).

[128] G. A. El, A. Gurevich, V. Khodorovskiĭ and A. Krylov. Modulational instability and formation of a nonlinear oscillatory structure in a "focusing" medium. *Physics Letters A*, **177**, 357–361 (1993).

[129] S. Dobrokhotov and Y. Krichever (1991). Multi-phase solutions of the Benjamin-Ono equation and their averaging. *Mathematical Notes of the Academy of Sciences of the USSR*, 49, 583–594 (1991).

[130] M. C. Jorge, A. A. Minzoni and N. F. Smyth. Modulation solutions for the BenjaminOno equation. *Physica D: Nonlinear Phenomena*, **132**, 1–18 (1999).

[131] Y. Matsuno. The Small Dispersion Limit of the Benjamin-Ono Equation and the Evolution of a Step Initial Condition. *Journal of the Physical Society of Japan*, **67**, 1814–1817 (1998).

[132] Y. Matsuno. Nonlinear modulation of periodic waves in the small dispersion limit of the Benjamin-Ono equation. *Phys. Rev. E*, **58**, 7934–7940 (1998).

[133] G. A. El, V. Khodorovskiĭ and A. Tyurina. Determination of boundaries of unsteady oscillatory zone in asymptotic solutions of non-integrable dispersive wave equations. *Physics Letters A*, **318**, 526–536 (2003).

[134] G. A. El. Resolution of a shock in hyperbolic systems modified by weak dispersion. *Chaos: An Interdisciplinary Journal of Nonlinear Science*, **15**, 37103 (2005).

[135] M. A. Hoefer. Shock Waves in Dispersive Eulerian Fluids. *Journal of Nonlinear Science*, **24**, 525–577 (2014).

[136] N. Lowman and M. A. Hoefer. Dispersive shock waves in viscously deformable media. *Journal of Fluid Mechanics*, **718**, 524–557 (2013).

[137] X. An, T. R. Marchant and N. F. Smyth. Dispersive shock waves governed by the Whitham equation and their stability. *Proc. Roy. Soc. London A*, **474**, 20180278 (2018).

[138] F. Dias and P. Milewski. On the fully-nonlinear shallow-water generalized Serre equations. *Physics Letters A*, **374**, 1049–1053 (2010).
serre2 Y. Matsuno. Hamiltonian formulation of the extended Green-Naghdi equations. *Physica D: Nonlinear Phenomena*, **301–302**, 1–7 (2015).

[139] D. Christie. Long Nonlinear Waves in the Lower Atmosphere. *Journal of the Atmospheric Sciences*, **46**, 1462–1491 (1989).

[140] R. Clarke, R. Smith and D. Reid. The Morning Glory of the Gulf of Carpentaria: An Atmospheric Undular Bore. *Monthly Weather Review*, **109**, 1726–1750 (1981).

[141] A. Porter and N. F. Smyth. Modelling the morning glory of the Gulf of Carpentaria. *Journal of Fluid Mechanics*, **454**, 1–20 (2002).

[142] N. F. Smyth and P. Holloway. Hydraulic Jump and Undular Bore Formation on a Shelf Break. *Journal of Physical Oceanography*, **18**, 947–962 (1988).

[143] J. Esler and J. Pearce. Dispersive dam-break and lock-exchange flows in a two-layer fluid. *Journal of Fluid Mechanics*, **667**, 555–585 (2011).

[144] D. Scott and D. Stevenson. Magma solitons. *Eos, Transactions, American Geophysical Union*, **65**, 1087–1088 (1984).

[145] D. Scott and D. Stevenson. Magma ascent by porous flow. *Journal of Geophysical Research*, **91**, 9283–9296 (1986).

[146] T. R. Marchant and N. F. Smyth. Approximate solutions for magmon propagation from a reservoir. *Ima Journal Of Applied Mathematics*, **70**, 796–813 (2005).

[147] X. An, T. R. Marchant and N. F. Smyth. Optical dispersive shock waves in defocusing colloidal media. *Physica D: Nonlinear Phenomena*, **342**, 45–56 (2017).

[148] T. R. Marchant and N. F. Smyth. Semi-analytical solutions for dispersive shock waves in colloidal media. *Journal of Physics B: Atomic, Molecular and Optical Physics*, **45**, 145401 (2012).

[149] A. M. Kamchatnov. Whitham theory for perturbed Korteweg-de Vries equation. *Phsyica D: Nonlinear Phenomena,* **333**, 99–106 (2016).

[150] N. Lowman and M. A. Hoefer. Fermionic shock waves: Distinguishing dissipative versus dispersive regularizations. *Phys. Rev. A*, **88**, 013605 (2013).

[151] M. Maiden and M. A. Hoefer. Modulations of viscous fluid conduit periodic waves. *Proc. Roy. Soc. London A*, **472**, 20160533 (2016).

[152] M. Holmes. *Introduction to Perturbation Methods.* Springer, New York (2013).

[153] G. G. Stokes. On the theory of oscillatory waves. *Math. Phys. Pap.*, **8**, 197–229 (1847).

[154] G. Assanto, T. R. Marchant and N. F. Smyth. Collisionless shock resolution in nematic liquid crystals. *Phys. Rev. A*, **78**, 063808 (2008).

[155] I. M. Gelfand and S. V. Fomin. *Calculus of variations*. Revised and translated by R. A. Silverman. Dover books on mathematics (2000).

[156] C. Lanczos. *The variational principles of mechanics*. Dover Books on Physics and Chemistry (1949).

[157] J. P. Keener. *Principles of applied mathematics: Transformation and approximation*. CRC Press (1995).

[158] M. Conforti and S. Trillo. Dispersive wave emission from wave breaking. *Opt. Lett.,* **38**, 3815–3818 (2013).

[159] M. Conforti and S. Trillo. Radiative effects driven by shock waves in cavity-less four-wave mixing combs. *Opt. Lett.,* **39**, 5760–5763 (2014).

[160] M. Conforti, S. Trillo, A. Mussot and A. Kudlinski. Parametric excitation of multiple resonant radiations from localized wavepackets. *Sci. Rep.,* **5**, 1–5 (2015).

[161] S. Malaguti, M. Conforti and S. Trillo. Dispersive radiation induced by shock waves in passive resonators. *Opt. Lett.,* **39**, 5626–5629 (2014).

[162] M. Conforti, F. Baronio and S. Trillo. Resonant radiation shed by dispersive shock waves. *Phys. Rev. A*, **89**, 013807 (2014).

[163] Dmitry V. Skryabin and Andrey V. Gorbach. Colloquium: Looking at a soliton through the prism of optical supercontinuum. *Reviews of Modern Physics*, **82** 1287–1299 (2010).

[164] V. Afanasjev, Y. Kivshar and C. Menyuk. Effect of third-order dispersion on dark solitons. *Optics Letters*, **21**, 1975–1977 (1996).

[165] J. Boyd. Weakly non-local solitons for capillary-gravity waves: Fifth-degree Korteweg-de Vries equation. *Physica D: Nonlinear Phenomena*, **48**, 129–146 (1991).

[166] R. Grimshaw and N. Joshi. Weakly Nonlocal Solitary Waves in a Singularly Perturbed Korteweg-De Vries Equation. *SIAM Journal on Applied Mathematics*, **55**, 124–135 (1995).

[167] R. Grimshaw, B. Malomed and E. S. Benilov. Solitary waves with damped oscillatory tails: an analysis of the fifth-order Korteweg-de Vries equation. *Physica D: Nonlinear Phenomena*, **77**, 473–485 (1994).

[168] V. Karpman. Radiation by weakly nonlinear shallow-water solitons due to higher-order dispersion. *Phys. Rev. E*, **58**, 5070–5080 (1998).

[169] D. Bourgault, P. Galbraith, C. Chavanne and P. Eyraud. Generation of internal solitary waves by frontally forced intrusions in geophysical flows. *Nature Communications*, **7**, 13606 (2016).

[170] M. Ablowitz and D. Baldwin. Nonlinear shallow ocean-wave soliton interactions on flat beaches. *Phys. Rev. E*, **86**, 036305 (2012).

[171] G. A. El, M. A. Hoefer and M. Shearer. Dispersive and diffusive-dispersive shock waves for non-convex conservation laws. *SIAM Review*, **59**, 3–61 (2016).

[172] Surfing atmospheric waves – the Morning Glory phenomenon. (2016, October 13). Retrieved October 2, 2015, from https://www.scisnack.com/2016/10/13/surfing-atmospheric-waves-the-morning-glory-phenomenon.

[173] T. P. Horikis. Small-amplitude defocusing nematicons. *J. Phys. A,* **48**, 02FT01 (2015).

[174] M. Peccianti, C. Conti and G. Assanto. Optical modulational instability in a nonlocal medium. *Phys. Rev. E,* **68**, 025602(R) (2003).

[175] G. Assanto, M. Peccianti and C. Conti. One dimensional transverse modulational instability in nonlocal media with a reorientational nonlinearity. *IEEE J. Sel. Top. Quantum Electron.,* **10**, 862–869 (2003).

[176] M. Van Dyke, *An Album of Fluid Motion,* Parabolic Press, Stanford, California (1982).

[177] G. A. El, E. G. Khamis and A. Tovbis. Dam break problem for the focusing nonlinear Schrödinger equation and the generation of rogue waves. *Nonlinearity,* **29**, 2798–2836 (2016).

[178] J. Pitt, C. Zoppou and S. Roberts. Behaviour of the Serre equations in the presence of steep gradients revisited. *Wave Motion*, **76**, 61–77 (2018).

[179] N. F. Smyth. Modulation Theory Solution for Resonant Flow Over Topography. *Proc. Roy. Soc. London A*, **409** 79–97 (1987).

[180] T. R. Marchant and N. F. Smyth. Initial-boundary value problems for the Korteweg-de Vries equation. *IMA J. Appl. Math.,* **47**, 247–264 (1991).

[181] T. R. Marchant and N. F. Smyth. The initial-boundary problem for the Korteweg-de Vries equation on the negative quarter-plane. *Proc. Roy. Soc. London A,* **458**, 857–871 (2002).

[182] T. R. Marchant. Asymptotic solitons of the extended Kortewegde Vries equation. *Phys. Rev. E*, **59**, 3745–3748 (1999).

[183] R. Grimshaw and N. F. Smyth. Resonant flow of a stratified fluid over topography. *Journal of Fluid Mechanics*, **169** 429–464 (1986).

[184] E. M. de Jager. On the origin of the Korteweg-de Vries equation. *Forum der Berliner Mathematischen Gesellschaft Dezember*, **19**, 171–195 (2011).

[185] Saleh Baqer and N. F. Smyth. Modulation theory and resonant regimes for dispersive shock waves in nematic liquid crystals. *Physica D: Nonlinear Phenomena*, **403**, 132334 (2020).

[186] Saleh Baqer, Côme Houdeville, Noel F. Smyth and Timothy R. Marchant. *Nematic dispersive shock waves from nonlocal to local.* In preparation (2020).